Non-linear Overload Behaviour and Ductility of Reinforced Concrete Flexural Members Containing 500MPa Grade Steel Reinforcement

By

REBECCA JANE GRAVINA

B.E. Civil (Hons)

A Thesis Submitted for the Degree of Doctor of Philosophy

Department of Civil and Environmental Engineering

Adelaide University

Australia

January 2002

CORRIGENDA

Page No. V: In paragraph 2, line number 6, replace 'Centre for Construction and Industrial Design' with 'Centre for Construction Technology and Research'.

Page No. 43: Replace the second paragraph with the following two paragraphs,

Beams subjected to variable moment gradients are considered, and hence a shear force will be present in these regions. Nevertheless, the influence of shear and shear cracks is ignored since the shear force is minimal compared to the bending moment gradient in beam sections where bending is dominant.

Sectional forces at the boundaries of each discrete block are determined from the moments acting in these sections. As a simplifying approximation it is assumed that strains are linearly distributed at the cracked section as in the uncracked section (Figure 4.12). In the cracked section profile it is assumed that the crack tip is located on the neutral axis since the concrete in tension between the crack tip and the neutral axis is ignored. The concrete tensile stress is considered to be negligible in comparison to the steel tensile stress. The sectional stresses and strains are then calculated by applying the equations governing the sectional equilibrium, together with the material laws for concrete and steel.

Page No. 58: After the second paragraph of Section 4.3.4, include the following paragraph:

In the analysis procedure steel fracture is defined as the stage when the local tensile steel strain at the section of maximum moment reaches the uniform elongation at peak stress. Concrete softening is defined to occur when the local concrete compressive strain at the section of maximum moment reaches 0.008 to ensure that the load deformation behaviour is in the post-ultimate unloading stage. At this stage the steel has not fractured and hence the failure is by concrete.

Page No. 60: In Figure 4.44 replace distrubution with distribution

Page No. 66: In paragraph 1, replace both citings of Figure 4.30 with Figure 4.31

Page No. 67: In Section 6.2.1 first paragraph, replace Section 4.3.5 with Section 4.3.3

Page No. 97: In Figure 6.2 on the left hand side f_{sy}/f_{sy} should read f_{su}/f_{su}

ABSTRACT

The design approaches in the Australian concrete structures standard, AS 3600, require a certain amount of plastic deformation capacity of reinforced concrete members to satisfy ductility requirements. Among the various structural design issues to consider, ductility is required for structural analysis procedures to provide safe designs, and ensure warning of failure of statically determinate and indeterminate structures by large deflections; and to supply resistance against imposed deformations due to temperature effects, shrinkage, creep and foundation movements.

The constant demand to provide the construction industry with cost effective materials has resulted in a growing trend towards the use of higher strength concrete and steel reinforcement. Unfortunately, structural ductility has been recognised to decrease in reinforced concrete beams constructed with the recently introduced high-strength 500MPa grade Australian reinforcing steels.

The aim of this research is to investigate the overload behaviour and modes of collapse of reinforced concrete flexural members containing 500MPa grade reinforcing steels. A further objective is to evaluate the adequacy of current ductility requirements for design according to AS 3600 to ensure strength and safety.

A local deformation model has been developed that can predict the available rotation capacity of critical high moment regions in reinforced concrete beams, taking into account the progressive formation of flexural cracks, the bond-slip behaviour between the steel and surrounding concrete, and the ductility level of the reinforcing steel. The model has been used to develop a method of analysis of indeterminate beams to simulate the full range of behaviour and deals with failures both by steel fracture and concrete softening.

Comparisons made with published beam test data and analytic predictions show both the local deformation model and the indeterminate beam analysis are reasonably accurate, and can be used to determine local deformations at high overload, as well as the overall system behaviour.

A parametric study investigating the factors influencing rotation capacity in plastic hinge regions of flexural members has been undertaken. The main parameters investigated were the uniform elongation and strain-hardening ratio of the steel, the effective depth of the section, the span to depth ratio of the member and the concrete compressive strength.

The continuous beam analysis developed was used in a numerical study of moment redistribution in a range of fixed end beams and propped cantilevers. It was found that more moment redistribution can occur in an indeterminate beam as the strain-hardening ratio of the steel increases while the uniform elongation remains constant.

Considering the effect of the uniform elongation of the steel, for beams with steel reinforcement ratios such that failure is by steel fracture, the degree of possible moment redistribution increases as the steel uniform elongation increases, while the strain-hardening ratio remains constant. However, for beams with steel reinforcement ratios such that failure is by concrete, a decrease in the uniform elongation at constant strain-hardening ratio causes a reduction in the available degree of moment redistribution.

The investigation of the effect of the uniform elongation and strain-hardening ratio of the steel on the degree of moment redistribution, have highlighted if changes are made to steel manufacturing techniques in order to increase the uniform elongation of the reinforcing steel, then it is important also to simultaneously increase the strain-hardening ratio.

In dealing with moment redistribution, designers need to be aware that a size effect exists. The degree of moment redistribution available effectively decreases as the effective depth of the member increases, at constant slenderness ratio.

The numerical study has revealed several inadequacies in the current design clauses in AS 3600 for ductility and moment redistribution. In relation to continuous beams constructed with Class N steel, unsafe designs are likely to result if 30 per cent design

moment redistribution is used together with a neutral axis parameter less than or equal to 0.2. Specifically, premature failure is likely to occur, with a loss of strength of as much as 10 per cent. In relation to continuous beams constructed with Class L steel, the present AS 3600 clauses can lead to over conservative results because no moment redistribution at all is allowed. Numerical calculations in fact show that moment redistribution of up to 10 per cent can be achieved in certain circumstances without premature failure and loss of strength.

Modifications to several current design clauses in AS 3600 relating to moment redistribution and minimum ductility requirements are suggested. The recommendations are specific to Clauses 7.6.8.2 and 7.6.8.3 that deal with the simplified procedure of linear elastic analysis with moment redistribution for beams reinforced with Class N steel and Class L steel respectively. A new clause that could be added to the commentary of AS 3600 giving details of a first principles approach to design for moment redistribution is also suggested. The approach requires the calculation of the available rotation capacity and the required rotation capacity in critical region of continuous beams, to ensure the former is larger than the latter. The method for calculating the available and required rotation capacity could be similar to those described in this thesis.

STATEMENT OF ORIGINALITY

This thesis contains no material which has been accepted for the award of any other degree or diploma at any university or other tertiary institution, and to the best of my knowledge and belief this thesis contains no material previously published or written by another person, except where due reference is made in the thesis text.

I give consent to this copy of my thesis, when deposited in the University Library, being made available for loan and photocopying.

Signed: **Date:** 22-01-02

Rebecca J. Gravina

ACKNOWLEDGEMENTS

The work described in this thesis was carried out at Adelaide University in the Department of Civil and Environmental Engineering under the supervision of Professor Robert F. Warner. The funding for this project was provided through an Australian Postgraduate Award Scholarship for Industry as well as contributions from the Steel Reinforcement Industry of Australia and is gratefully acknowledged.

I would like to express my deepest gratitude to Professor Robert Warner for his patient and critical guidance throughout the duration of this project, and also for his excellent contributions to the review of this thesis. I wish to also thank Associate Professor Mike Griffith and my colleagues from the Structures Group at Adelaide University for beneficial contributions at our weekly meetings and valuable discussions and ideas. I would also like to acknowledge the industry support provided by Mr Mark Turner of the Steel Reinforcement Industry of Australia and Dr Mark Patrick of the Centre for Construction and Industrial Design, University of Western Sydney.

To my parents, I am eternally grateful for their continual support, love and guidance. Finally, to my beloved husband Michael, for his optimism and encouragement, which has provided me with the motivation and strength to complete this work.

LIST OF PUBLICATIONS

The following papers have been published as a result of this research:

Gravina, R.J. and Warner, R.F. (1999), Modelling of High-moment Plastification Regions in Concrete Structures, *Proceedings of the 16th Australasian Conference on the Mechanics of Structures and Materials*, Sydney, NSW, 8-10 December, p103-107.

Gravina, R.J. and Warner, R.F. (2001), Available Rotation Capacity in Reinforced Concrete Beams and Slabs Constructed with Class L and Class N Reinforcing Steels, *Proceedings of the Australian Structural Engineering Conference*, Gold Coast, Queensland, 29 April to 2 May, p391-398.

Gravina, R.J. and Warner, R.F. (2001), Moment Redistribution in Indeterminate Reinforced Concrete Beams and Slabs Constructed with 500MPa Grade, Class L and Class N Reinforcing Steels, *Proceedings of the 20th Biennial Conference of the Concrete Institute of Australia*, 11-14 September, Perth, Western Australia, p613-618.

TABLES OF CONTENTS

LIST OF FIGURES

LIST OF TABLES

PRINCIPAL NOTATIONS

A_c = cross section area of compressive concrete

A_{ct} = cross section area of tensile concrete

A_{st} = cross section area of tensile reinforcing steel

A_{sc} = cross section area of compressive reinforcement

B = width of rectangular section

D = overall depth of section

d = effective depth of section

$d_{c.g}$ = depth to centre of gravity of section

d_b = nominal diameter of bar or wire

d_{sc} = depth to compressive steel

d_{st} = depth to tensile steel

E_s = modulus of elasticity of steel

E_{sh} = steel strain-hardening slope

f_{cm} = average strength of concrete in compression

f_{ct} = concrete tensile strength

f_{sy} = yield strength of reinforcing steel

f_{su} = ultimate tensile strength of reinforcing steel

f'_c = characteristic strength of concrete in compression

I_{cr} = second moment of area of a cracked section

I_{eff} = effective second moment of area

I_g = second moment of area of the gross cross section

k_u = neutral axis depth

L = centre-to-centre distance between supports of a flexural member

l_p = plastic hinge length

l_{tr} = bond transfer length

M_{cr} = flexural cracking bending moment

M = bending moment

M_{sup} = moment in support region

M_{sp} = moment in span region

M^- = maximum moment in support region without load pad effect

M^+ = maximum moment in span region without load pad effect

P = point load

P_{cr} = cracking load

s = local slip

s_{rm} = average crack spacing

w = uniformly distributed load

w_{cr} = maximum crack width

α = moment reduction factor due to load pad, determinate beam

a_{sup} = moment reduction factor due to support pad, indeterminate beam

a_{sp} = moment reduction factor due to load pad at span, indeterminate beam

β = design moment redistribution degree

γ = ratio between moment resistance at the support and in the span

Δ = deflection

δ = static moment, M_0 multiplying factor

ε_{omax} = concrete compressive strain at zero compressive stress

ε_o = top compressive fibre strain

ε_s = tensile steel strain

θ_{pl} = rotation capacity

θ_{max} = total rotation at max load

θ_{req} = required rotation capacity

θ_y = total rotation at yield

ρ = percentage of tensile reinforcement, A_{st}/bd

ρ' = percentage of compressive reinforcement, A_{sc}/bd

σ_c = concrete compressive stress

σ_{ct} = concrete tensile stress

σ_{sc} = steel compressive stress

σ_{st} = steel tensile stress

τ = local bond stress

1

INTRODUCTION

1.1 RESEARCH BACKGROUND

System ductility is an important property which must be considered in the design of concrete structures. In a ductile structure, large deformations occur at overload prior to collapse providing adequate warning of impending failure. The ductility of the structure must be sufficient for internal actions induced at overload, to be transferred through the structure to regions less highly stressed. This redistribution enables full plastic capacity of the system to be achieved.

With the present demand to provide the construction industry with cost effective materials, there is a growing trend towards the use of higher strength concrete and steel reinforcement. Unfortunately, as recognised by the Australian Standards Committee BD/2/1, structural ductility has decreased in beams constructed with high strength 500MPa grade Australian reinforcing steels.

Tests undertaken by Patrick *et al.* (1997) revealed that indeterminate reinforced concrete beams containing high-strength low elongation steel reinforcement, such as cold-worked wire used in welded wire fabric, can fail suddenly by steel fracture, even when designed in full accordance with the requirements of the then current version of the Australian concrete structures standard AS 3600 (Standards Australia, 1994). In Europe, research has also pointed to problems of brittle steel fracture when fabric, with ductility properties similar to Australian fabrics, is used in flexural members (Eligehausen and Langer, 1987; Beeby, 1996).

The design approaches in the latest version of the Australian reinforced concrete code, AS 3600 (Standards Australia, 2001), have been reconsidered to take into account

possible loss of ductility of the reinforced concrete system due to the reduced material ductility. However, further research is needed to identify the factors that influence the ductility of the structure, and determine whether the requirements for ductility in design according to AS 3600 (Standards Australia, 2001) are adequate to ensure strength and safety, and provide new codified procedures for ductility if required.

1.2 SCOPE OF THESIS

In this thesis, an investigation is undertaken into the ductility and non-linear, overload behaviour of reinforced concrete flexural members, in particular, members containing 500MPa grade steel reinforcement. The study consists of the following:

- Development of a local deformation model that can predict the flexural behaviour of reinforced concrete beams under increasing load, including the progressive formation of flexural cracks, crack spacing, crack widths, local deformations, the bond-slip behaviour between the steel and surrounding concrete, and the final plastic deformations at failure. The model also predicts the mode of flexural failure, whether by steel fracture or concrete softening, and allows the rotation capacity and ductility of critical regions to be investigated.

- Extension of the analysis to indeterminate beams, whereby the local deformation model is applied simultaneously to negative and positive moment regions. The full range of behaviour of the indeterminate structure is predicted, starting with progressive cracking in the peak moment regions, followed by further moment redistribution as the load increases up to failure either by steel fracture or concrete softening.

- Study of the overload behaviour of reinforced concrete beams via two parametric studies to investigate, a) the factors that influence the rotation capacity in a plastic hinge region, and b) the redistribution of moment at overload in continuous beams.

The scope of this research is limited to reinforced concrete beams subjected predominately to flexure under short-term loading. Time-dependent effects such as creep and shrinkage have not been considered. The development of a computer model to carry out the analysis forms a major component of this work. The program was developed using Fortran 90.

The overall objective of the investigation was to identify minimum ductility limits needed for design according to AS 3600 to ensure strength and safety, and to evaluate the adequacy of current design clauses.

1.3 CONTENTS

Chapter 2 provides a definition of ductility, and the limits characterising the ductility level of reinforcing steels produced in Australia and overseas. Structural design clauses according to AS 3600 are reviewed, and aspects regarding the design for ductility are noted. Comparisons are also made with current ductility approaches in overseas design standards.

A review of models developed by previous researchers to determine the local deformations and rotation capacity in plastic hinge regions is given in Chapter 3. The main aspects of the procedures are presented and results from several studies into the factors affecting the rotation capacity and moment redistribution in reinforced concrete members are discussed.

Chapter 4 gives details of a new local deformation model that extends current approaches. The analysis predicts progressive formation of tensile cracks, initial yielding of the tensile steel, and subsequent spread of the yielded region to create a plastic hinge. The full range of behaviour is predicted, including failure either by steel fracture or concrete softening.

In Chapter 5 previously published beam test data is used to demonstrate the accuracy of the local deformation model introduced in Chapter 4. Factors that influence the rotation capacity in plastic hinge regions are investigated via a parametric study in Chapter 6.

Application of the procedure simultaneously to peak moment regions in indeterminate structures is described in Chapter 7. The accuracy of the extension of the model to indeterminate beam cases is demonstrated also using published test beam data.

In Chapter 8, a method whereby the available rotation capacity is compared to the required rotation capacity in critical high moment regions of a continuous beam to determine the available degree of moment redistribution that can be adopted in design is described. In addition, a study of the factors that influence the moment redistribution in

continuous beams is presented. The numerical study is used to check the adequacy of the structural design method of linear elastic analysis with moment redistribution according to AS 3600.

In Chapter 9, the research carried out in the present investigation is summarised and recommendations for design and further work are suggested.

2

DUCTILITY

2.1 DEFINITION OF DUCTILITY

Ductility is the ability of a structural system, a component of a system, or a structural material to sustain plastic deformations prior to collapse, without substantial loss of resistance. The design approaches in the Australian reinforced concrete standard, AS 3600 (Standards Australia, 2001) require a certain amount of plastic deformation capacity of reinforced concrete members. Among the various structural design issues to consider, ductility is required for structural analysis procedures to provide safe designs, and ensure warning of failure of statically determinate and indeterminate structures by large deflections; and to supply resistance against imposed deformations due to temperature effects, shrinkage, creep and foundation movements.

At the material level, the ductility of reinforcing steels depends upon the extent of the plastic deformation region. Examples of stress–strain curves obtained from tensile tests on some Australian reinforcing steel are shown in Figure 2.1. The larger the extent of the plastic deformation region, the more ductile the steel. In Figure 2.1, 'RF' and 'F' represent welded reinforcing mesh, and 'Tempcore' refers to hot-rolled reinforcing bars. In AS 3600 the ductility of the reinforcing steel is characterised by the ratio between the stress at yield, f_{sy}, and maximum stress, f_{su} and the uniform elongation at peak stress, ε_{su}.

Although the ductility of concrete is minimal compared to steel, the strain softening characteristics of concrete allow it to deform well beyond the peak strength under decreasing levels of stress. The post-peak behaviour of concrete gives an indication of the ductility. The less gradient on the softening curve, the more ductile the concrete.

The ductile response of the concrete can be improved with confining effects (Figure 2.2).

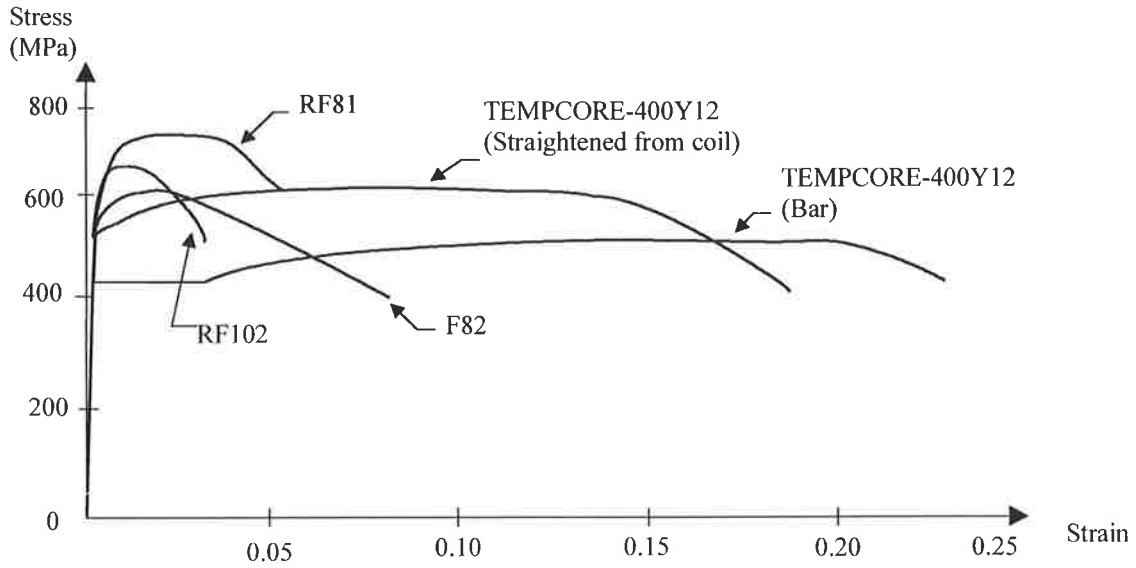

Figure 2.1 Tensile testing of Australian reinforcing steel, according to Patrick *et al.* (1997)

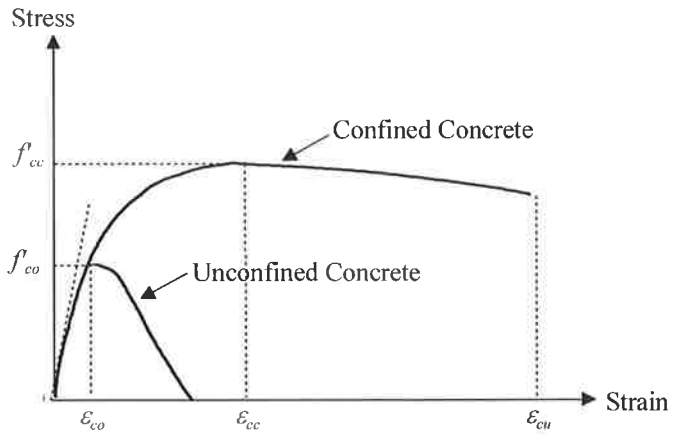

Figure 2.2 Stress-strain characteristics for confined and unconfined concrete, according to Mander *et al.* (1988)

For a flexural member, the sectional or member ductility can be determined from the moment-curvature relation. The member is ductile if it undergoes large plastic deformations prior to failure. Material ductility influences the ductile response of the member but in addition, sectional properties such as the tensile reinforcement ratio play a vital role. Figure 2.3 shows that with an increase in the reinforcement ratio the maximum moment increases but the plastic plateau decreases.

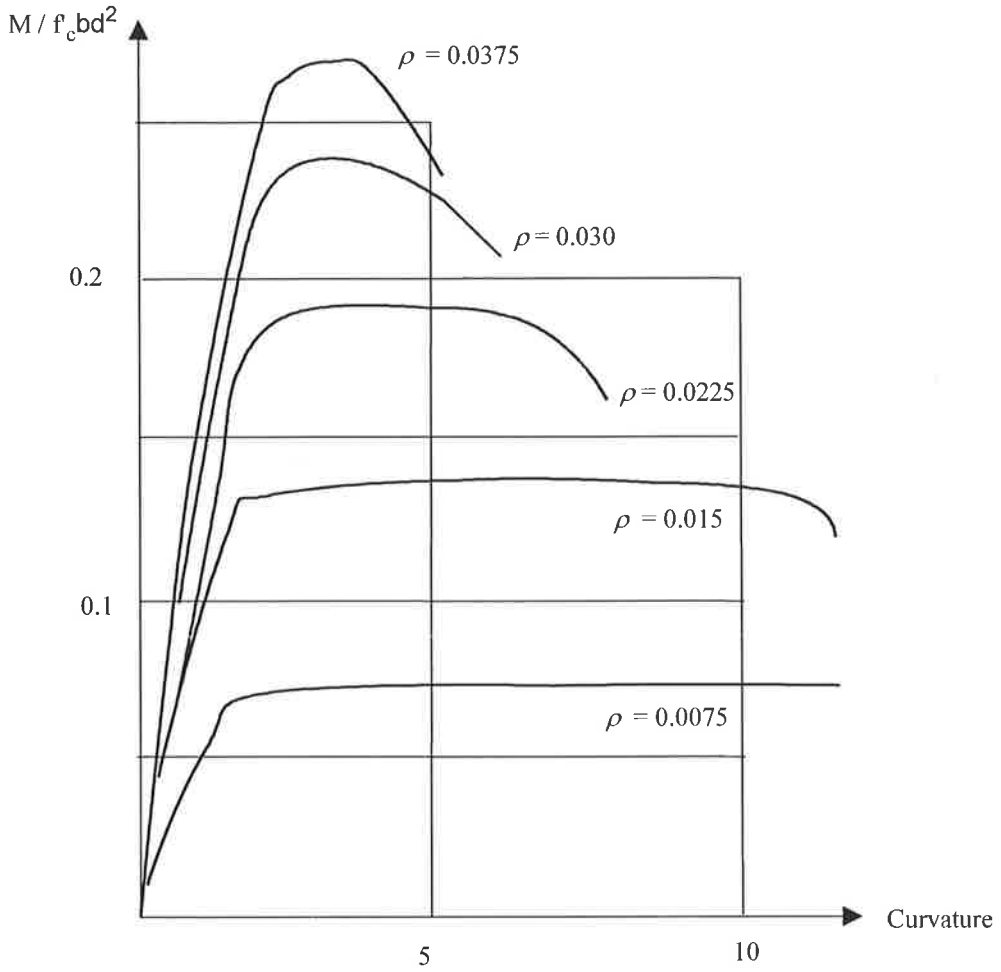

Figure 2.3 Moment-curvature relations, effect of the tensile reinforcement ratio, according to Warner *et al.* (1998)

An indicator of the sectional ductility used in design is the neutral axis parameter k_u. The neutral axis parameter k_u is defined as the ratio d_n/d when the ultimate moment acts. In AS 3600 the rectangular stress block theory is used to calculate k_u based on the ultimate moment capacity. According to AS 3600, k_u is calculated according to Equation 2.1 assuming the extreme concrete fibre strain ε_o is equal to 0.003:

$$k_u = \frac{1}{0.85\gamma}\frac{f_{sy}}{f'_c}\frac{A_{st}}{Bd} \tag{2.1}$$

where

$$\gamma = 0.85 - 0.007(f'_c - 28) \tag{2.2}$$

Equation 2.2 is valid for concrete strengths in the range of 28MPa to 65MPa.

Structural system ductility ensures that large plastic deformations form prior to collapse providing plenty of warning of imminent failure. The deformation can be represented as the rotation over a plastic hinge region or the global deflection of the structural member.

Reinforcing steels produced in Australia have undergone much change over the last few years, which has seen the introduction of high-strength reinforcement. However with the higher strength steel, the material ductility has decreased. The decrease in material ductility can lead to lower system ductility of reinforced concrete members.

The design approaches in AS 3600 have been reconsidered to take into account that in some cases, sufficient ductility of the reinforced concrete system may not be inherent due to the reduced material ductility. However, further work is needed to determine whether the requirements for ductility in design, are adequate to ensure strength and safety of reinforced concrete members, and to provide new and improved design clauses if needed.

2.2 AUSTRALIAN REINFORCING STEELS

The types of reinforcing steels currently produced in Australia include welded wire mesh (fabric) and deformed reinforcing bar. Reinforcing fabric is manufactured from cold-worked deformed wire. The deformed bars are produced by two different processes, resulting in either 'quenched and tempered' or 'hot-rolled' bars. The 1994 version of AS 3600 required all longitudinal reinforcing steel to be either grade 400Y deformed bars or 450F fabric complying with either AS 1302 (Standards Australia, 1991a) and AS 1304 (Standards Australia, 1991c). However, a nominal yield stress of 500MPa has recently been adopted as a standard for the production of Australian reinforcing steels. This has come about in the interests of harmonising with international practice. In Europe, a move to adopt a uniform grade of 500MPa for all reinforcing steels has already been undertaken with relevant adjustments to codes of practice. Currently, the relevant Australian reinforcing Standards AS 1302, AS 1303 and AS 1304 are being combined into a single standard for reinforcing steels soon to be published jointly by Standards Australia and Standards New Zealand.

It has been recognised that cold-worked wire used in welded wire fabric is much less ductile than hot-rolled deformed bars (Figure 2.1). An experimental program

undertaken by Patrick *et al.* (1997) revealed that indeterminate reinforced concrete beams constructed with high-strength low elongation steel reinforcement such as cold-worked wire, can fail suddenly by steel fracture, even when designed in full accordance with the requirements of AS 3600 based on the 1994 code version.

Two amendments have been made to AS 3600. Amendment No.1 restricted the use of cold-worked bar and mesh in flexural elements in situations where significant amounts of moment redistribution can occur. Amendment No.2 issued in early 2000 contains details on the use of main reinforcement with different ductility classes. This amendment deals with the methods of structural analysis, in particular moment redistribution and rigorous analysis instructing designers of the need to check for ductility. Until recently, the Australian concrete standard and the reinforcing standards, made no distinction between the use of hot-rolled bars and welded wire fabric in situations where steel ductility is important. The amendments have now been incorporated into the 2001 version of AS 3600 (Standards Australia, 2001).

2.2.1 Ductility Classes

Two ductility classes for reinforcing steel are now defined in AS 3600 (Standards Australia, 2001). The corresponding categories are Class N for 'normal ductility' steel and Class L for 'low ductility' steel. The classification of ductility is based on two parameters, namely, the strain-hardening ratio, f_{su}/f_{sy}, and the ultimate uniform elongation, ε_{su}, of the reinforcing steel. The limiting values of the parameters that define the grade of steel according to its ductility class are:

Class N steel 'normal ductility'	$(f_{su}/f_{sy})_k \leq 1.08$ and $\varepsilon_{su,k} \leq 5\%$
Class L steel 'low ductility'	$(f_{su}/f_{sy})_k \leq 1.03$ and $\varepsilon_{su,k} \leq 1.5\%$

This is somewhat different to the CEB-FIP (1993) Model Code in which three reinforcing steel ductility classes are distinguished:

Steel type S (seismic regions)	$(f_{su}/f_{sy})_k \leq 1.15$ and $\varepsilon_{su,k} \leq 6\%$
Steel type A (normal ductility)	$(f_{su}/f_{sy})_k \leq 1.08$ and $\varepsilon_{su,k} \leq 5\%$
Steel type B (low ductility)	$(f_{su}/f_{sy})_k \leq 1.05$ and $\varepsilon_{su,k} \leq 2.5\%$

However, Eurocode No.2 (1990) classifies two steel ductility classes:

Steel type H (normal ductility)	$(f_{su}/f_{sy})_k \leq 1.08$ and $\varepsilon_{su,k} \leq 5\%$
Steel type N (low ductility)	$(f_{su}/f_{sy})_k \leq 1.05$ and $\varepsilon_{su,k} \leq 2.5\%$

2.3 Ductility Requirements Relating to Structural Analysis Methods According to the Australian Concrete Structures Code AS 3600

According to AS 3600 (Standards Australia, 2001), various methods of structural analysis can be used as the basis for the design of concrete structures. These include simplified methods of analysis, linear elastic analysis, and linear elastic analysis with moment redistribution, plastic analysis and rigorous analysis. While each of these methods requires a minimum level of ductility in the entire structure, and in local regions, the required minimum ductility level can vary significantly according to the analysis method used. Unfortunately AS 3600 does not always specify clearly the levels of ductility that are required for each method.

The rigorous method of analysis consists of non-linear analysis taking into account realistic material properties and geometric effects by suitable incremental and/or iterative numerical methods. Material and system ductility is catered for automatically.

Simplified methods are based partly on empirical studies and rely on moment redistribution. General clauses exist in AS 3600 and among the more simplified approaches the linear elastic methods of analysis are most commonly used. Linear elastic analysis provides the ultimate load carrying capacity of a critical reinforced concrete section. The ductility of the section is provided by the maximum curvature in the section when the ultimate moment acts. Limits are placed on the neutral axis depth parameter, k_u, to ensure adequate ductility. The linear elastic analysis does not allow for the redistribution of internal forces at overload.

The plastic method of analysis allows for the redistribution of internal stresses and the formation of plastic hinges at overload. The plastic method of analysis assumes the deformation capacities of the plastic hinges are sufficient for a plastic hinge collapse mechanism to occur. To check the deformation capacity, the required rotation capacity,

θ_{req}, is compared to the plastic rotation capacity, θ_{pl}, and the following design requirement applies:

$$\theta_{req} \leq \theta_{pl} \tag{2.3}$$

AS 3600 (Standards Australia, 2001) currently does not provide a method to calculate the plastic rotation capacity.

However, methods to determine the plastic rotations can be found in CEB-FIP Model Code (1993) and in Eurocode No.2 (1990). In the CEB-FIP Model Code (1993) the plastic rotation capacity can be calculated using to the following equation:

$$\theta_{pl} = \int_0^{l_p} \frac{\delta}{d-c}\left(1-\frac{\sigma_{sr1}}{f_{yk}}\right).\left(\varepsilon_{s2}-\varepsilon_{sy}\right)dx \tag{2.4}$$

where

l_p = plastic hinge length

δ = the coefficient for taking into account the form of the stress-strain curve of the reinforcement in the inelastic range (δ=0.8)

c = the depth of compression zone

σ_{sr1} = the steel stress in the crack when the first crack forms as the characteristic concrete tensile strength is reached

ε_{s2} = the strain of the cracked section

ε_{sy} = the strain at yield stress

f_{yk} = the characteristic yield stress

With this simplified approach, the plastic rotation capacity can be estimated by Figure 2.4 based on the ductility of the steel classified in Section 2.2.1. This figure is valid for a slenderness ratio of l*/d = 6. (l* denotes the distance between two consecutive zero moment points on both sides of the support). For other values of l*/d, the rotation capacity may be multiplied by the factor $\sqrt{(l^*/(6*d))}$. In Figure 2.4, *x/d* represents the normalised neutral axis depth according to CEB-FIP Model Code (1993).

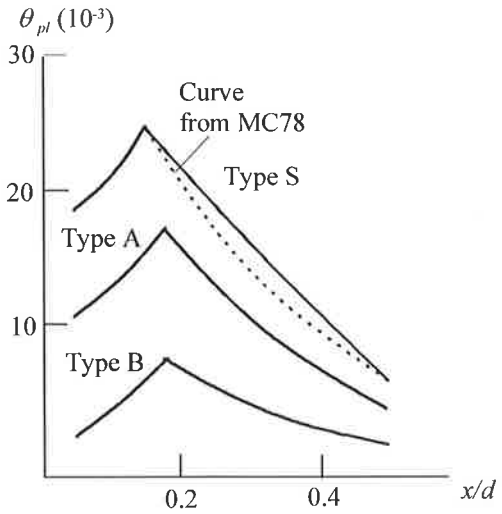

Figure 2.4 CEB-FIP Model Code (1993) provision for plastic rotation capacity

Dependent upon the ductility class of the steel, as defined in Eurocode No.2 (1990), the plastic rotation capacity can be taken from Figure 2.5. It can be seen that the plastic rotation for x/d ≤ 0.16 is limited for H steel to $\theta_{pl} = 20\text{x}10^{-3}$radians and for N steel to $\theta_{pl} = 10\text{x}10^{-3}$radians.

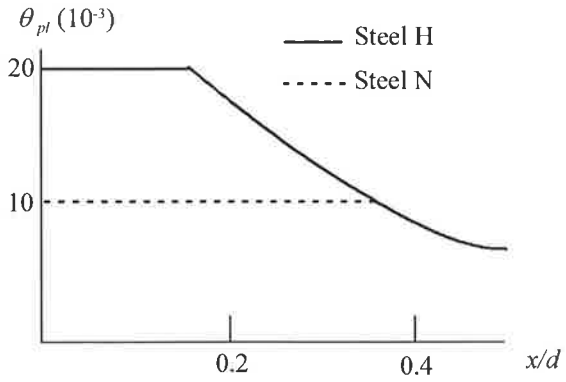

Figure 2.5 Eurocode No.2 (1990) Code provision plastic rotation capacity

The plastic rotation capacity can be expressed by the following equations:

$$\theta_{pl} = 20 \qquad \frac{x}{d} \le 0.16 \tag{2.5}$$

$$\theta_{pl} = \left[5.8 + \left(6.22 - 11.5\frac{x}{d}\right)\right]^{1.8} \qquad 0.16 \le \frac{x}{d} \le 0.5 \tag{2.6}$$

A simplified design approach, which takes into account the redistribution of stress resultants in a structure resulting from plastic hinge formations, is the method of linear elastic analysis with moment redistribution. This method takes advantage of the non-linear behaviour of reinforced concrete members by redistributing the elastically determined bending moment. For example, in a continuous beam the elastically determined bending moment over a support may be reduced, or increased provided the moment in the span region is adjusted accordingly to maintain equilibrium. The degree of moment redistribution β is defined as the ratio between the moment over the support after redistribution, M_{sup}, and the value calculated elastically for a given load, $M_{sup,el}$.

$$\beta = \frac{M_{\text{sup}}}{M_{\text{sup},el}} \text{ x } 100\% \tag{2.7}$$

Currently the design moment redistribution allowed by AS 3600 in beams with Class N steel depends upon the neutral axis parameter, k_u, in the critical regions. At the upper limits on k_u of 0.4, no moment redistribution is allowed in design, but with a k_u value of 0.2, the design moment redistribution can be up to 30 per cent. For Class L steel no moment redistribution is allowed (Figure 2.6)

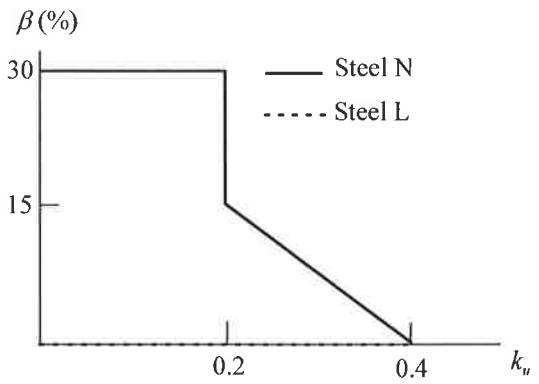

Figure 2.6 AS 3600 Code provision for allowable degree of moment redistribution

In comparison to the design moment redistribution degree given in AS 3600, various other codes adopt a similar model (CEB-FIP Model Code, 1993, Eurocode No.2, 1990, ACI Committee 318, 1999). The models give different criteria also based upon the neutral axis parameter, *x/d*, and steel ductility, however an exception to this is the moment redistribution provisions given in ACI Committee 318 (1999). The design

moment redistribution degree for some selected concrete structures codes are given below.

The CEB-FIP Model Code (1993) distinguishes between three ductility classes as introduced in Section 2.2.1, steel type S, steel type A and steel type B. The requirements for the reduction coefficient $\delta = 1 - \beta/100$ are specified as follows;

For steel type S and A:

For concrete grades C12 to C35: $\delta \geq 0.44 + 1.25\, x/d$ (2.8)

For concrete grades C40 to C60: $\delta \geq 0.56 + 1.25\, x/d$ (2.9)

and

For continuous beams: $0.75 \leq \delta \leq 1.00$

For non-sway frames: $0.75 \leq \delta \leq 1.00$

For sway frames: $0.90 \leq \delta \leq 1.00$

For steel type B:

for concrete grades C12 to C60: $\delta \geq 0.75 + 1.25\, x/d$ (2.10)

and: $0.90 \leq \delta \leq 1.00$

The European standard for the design of concrete structures Eurocode No.2 (1990) classifies two steel ductility classes, steel class H and steel class N, see Section 2.2.1. The requirements for the reduction coefficient $\delta = 1 - \beta/100$ are similar to the CEB-FIP Model Code (1993) and are specified as follows:

For concrete grades C12 to C35: $\delta \geq 0.44 + 1.25\, x/d$ (2.11)

For concrete grades C40 to C60: $\delta \geq 0.56 + 1.25\, x/d$ (2.12)

and

For steel H: $0.70 \leq \delta \leq 1.00$

For steel N: $0.85 \leq \delta \leq 1.00$

The ACI Committee 318 (1999) structural concrete code specifies the degree of moment distribution based on the percentage of steel in the critical section as follows:

$$\beta = 20\left(1 - \frac{\rho - \rho'}{\rho_b}\right) x100\% \tag{2.13}$$

where ρ_b is the reinforcement ratio producing balanced strain conditions and is calculated as follows:

$$\rho_b = \frac{0.85\beta_1 f'_c}{f_{sy}} \frac{87{,}000}{87{,}000 + f_{sy}} \tag{2.14}$$

In Figures 2.7 and 2.8 a comparison is given of the allowable degree of moment redistribution in the codes introduced above, for normal ductility and low ductility steels respectively. ACI Committee 318 (1999) does not distinguish between the steel ductility classes.

For normal ductility steels there is broad agreement between the various codes. However ACI proves to be the most conservative. The European codes are more liberal (CEB, EC2), however, they do provide a reduction in the allowable degree of moment redistribution with higher strength concrete.

For low ductility steels the code provisions vary significantly. In this case, AS 3600 is demonstrated to be ultra conservative as no redistribution is permitted. Eurocode No.2 (EC2) is also on the safer side.

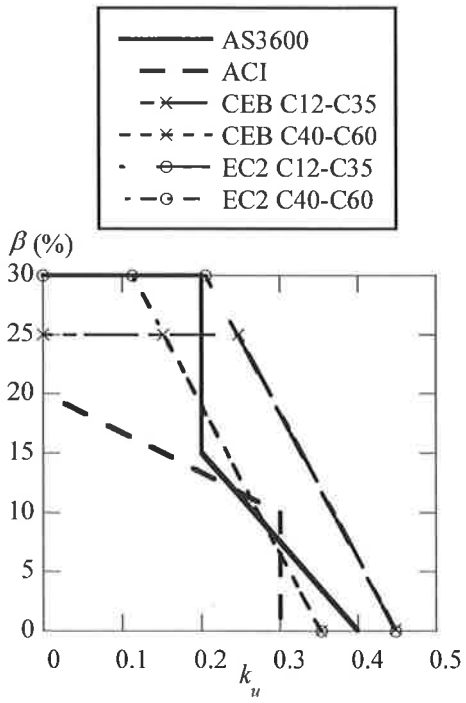

Figure 2.7 **Allowable degree of moment redistribution in various codes for normal ductility steel**

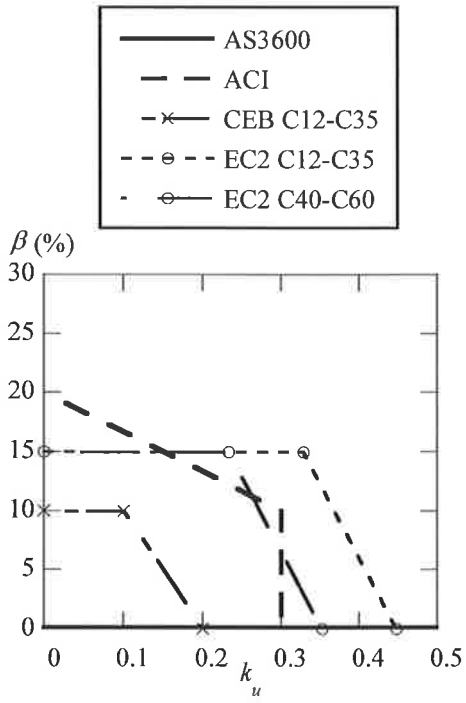

Figure 2.8 **Allowable degree of moment redistribution in various codes for low ductility steel**

2.4 SUMMARY

Structural design clauses in AS 3600 (Standards Australia, 2001), need to be reconsidered to take into account the factors influencing the ductility and rotation capacity of the plastic hinge region, in particular the ductility level of the reinforcing steels. Several steps have been taken to address this issue, notably through Amendment No.1 in 1997 and Amendment No.2 in 2000, however more work is needed. One of the main objectives of this work is to check current design limits of allowable degrees of moment redistribution for the structural analysis method of linear elastic analysis with moment redistribution, and provide new and improved design ductility limits.

To be able to accurately predict the overload behaviour of reinforced concrete structural members, methods of analysis need to be able to simulate the local deformations and available rotation capacity in critical plastic hinge regions. The next chapter reviews recently developed models for determining local flexural deformations and rotation capacity of plastic hinge regions.

3

PREVIOUS STUDIES OF LOCAL FLEXURAL DEFORMATIONS AND ROTATION CAPACITY

In this chapter, previous analytical studies of local deformations and rotation capacity in plastic hinge regions are reviewed. Relevant factors affecting the rotation capacity and the related moment redistribution in reinforced concrete beams are also investigated.

3.1 INTRODUCTION

To account for local deformations and cracking in non-linear methods of analysis, models considering the tension stiffening effect between flexural cracks have been developed. The tension stiffening effect in flexural members can be defined as the additional stiffness provided by the tensile stress in the concrete between cracks, as compared with the fully cracked elastic analysis.

Tension stiffening has been applied in various ways in non-linear analysis. On a sectional level as a modified stiffness approach, using smeared moment-curvature relationships (Branson, 1963; Beeby, 1968; CEB-FIP Model Code, 1993), or treating tension stiffening as properties of either the steel or concrete (Lin and Scordelis, 1975; Gilbert and Warner, 1978; Bazant and Oh, 1984; Gupta and Maestrini, 1990) and on a regional level, referred to in the literature as 'block models' (Bachmann, 1967; Langer, 1987; Graubner, 1987; Li, 1995; Cosenza *et al.*, 1991a; Sigrist, 1995; Bigaj, 1999; Westergaard, 1933; Maldague, 1965; Priestly *et al.*, 1971; Giuriani, 1979; Bridge and Smith, 1982; Birkenmaier, 1983; Cohn and Riva, 1987; Creazza and Di Marco, 1993; Sato *et al.*, 1992; Vasiliev and Belov, 1993; Ferretti, 1995).

The block models are of particular interest because they have moved attention away from elements represented by average deformations, to blocks delimited by two consecutive flexural cracks, and the intermediate local deformations. The assumption that perfect bond exists between the steel and concrete in reinforced concrete elements can be relaxed in the block models, and the phenomenon of slip between the steel and the concrete at sections between the cracks can be considered in the post-cracking phase. Suitable bond-slip relationships are introduced and simplified strain profiles in the cross sections are adopted.

By assuming both the stress-strain relationships of steel and concrete to be known, the models impose requirements of strain compatibility and equilibrium of forces in sections of the block, obtaining a system of differential equations. Through suitable boundary conditions, the solution to the system makes it possible to determine, for the acting moment, the distribution of stress, strain, slip, and bond stress along the block element.

The block models have been specifically formulated either as calculation models for local deformations and rotation capacity of plastic hinges (Bachmann, 1967; Langer, 1987; Graubner, 1987; Li, 1995; Cosenza *et al.,* 1991a; Sigrist, 1995; Bigaj, 1999), or developed with the aim of providing a better representation of moment-curvature-rotation relationship for pre-generated expressions (Westergaard, 1933; Maldague, 1965; Priestly *et al.*, 1971; Giuriani, 1979; Bridge and Smith, 1982; Birkenmaier, 1983; Cohn and Riva, 1987; Creazza and Di Marco, 1993; Sato *et al.*, 1992; Vasiliev and Belov, 1993; Ferretti, 1995).

The local deformation and rotation capacity models to be reviewed have evolved from the early work undertaken by Baker and Amarakone (1965), Mattock (1965) and Corley (1966). These early approaches calculated the plastic rotation capacity by multiplying the plastic part of the moment-curvature diagram with the assumed length of plastic hinge. The weakness of the models developed was that only the bending moment influence was considered and the rotation capacity was related to the curvature of a single section. Dilger (1966) further developed the procedure to calculate the deformation capacity of reinforced concrete members by considering inclined shear cracking.

3.2 Local Deformation and Rotation Capacity Models that Utilise Block Elements

Attention in this section is concentrated on block models. From the earlier approaches, Bachmann (1967) then improved the modelling of the rotation capacity of reinforced concrete members by a refined method of discretisation of the hinge region allowing for the tension stiffening between cracks. The plastic rotation is computed as the sum of the rotations of the cracked elements within the plastic hinge region. The crack element rotations are calculated by integrating the deformations along the member axis. The model developed by Bachmann (1967) also recognised that bending and shear crack hinges develop under different conditions and included a shear crack hinge model (Figure 3.1).

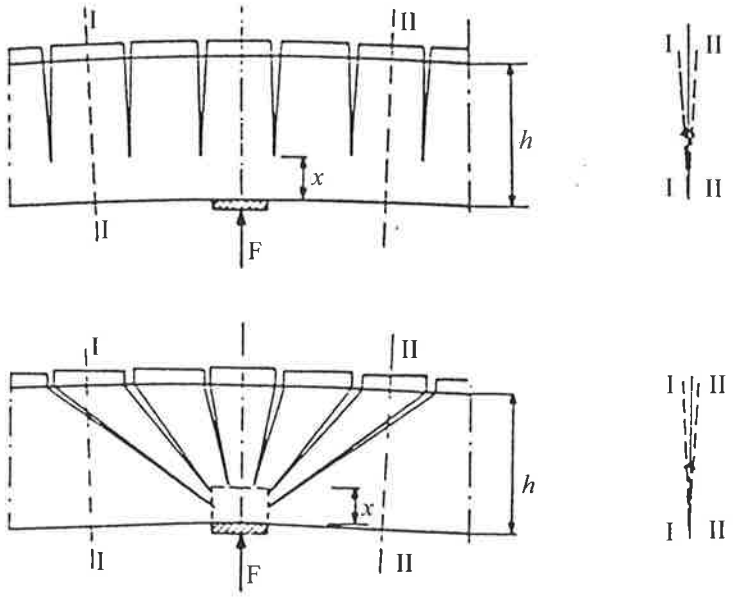

Figure 3.1 Flexural (top) and shear crack hinge (bottom), according to Bachmann (1967)

In recent work, computer-based models have been developed that consider realistic material relations for the steel and concrete and bond-slip law. The methods have further progressed, to improve the simulation of local deformations and rotation capacity to take into consideration, failure of reinforced concrete structures may occur due to rupture of the steel well below plastic rotation limits.

3.2.1 Recent Local Deformation Models

The initial work by Langer (1987) and Eligehausen and Langer (1987), involved the development of a procedure whereby the moment-curvature relationships are based on the given dimensions of the cross-section, the adopted stress-strain relationship of the reinforcing steel and concrete, and the bond-slip law (Figure 3.2). At the cracked section a linear strain profile is assumed. The distribution of moments along the beam is determined taking into account the width of the loading pad. The analysis is taken up to the ultimate moment capacity previously calculated. To represent the support region of an indeterminate beam, a statically determinate beam with the length equal to the distance between adjacent points of zero moment is used. If shear cracks are expected, the shifting of the tensile force compared to the moment-lever arm line is undertaken assuming an angle of the inclined compression struts according to Dilger (1966). The curvature in the cracked sections is calculated from the moment curvature relation or the tensile force curvature relation in the case of shear cracks. A crack spacing according to Kreller (1989) is assumed.

The contribution of concrete between cracks is calculated for every crack element by means of an iterative solution of the differential equation of bond, using a modified version of the program described in Eligehausen *et al.* (1981). The bond behaviour is represented by the bond-slip relation according to Eligehausen *et al.* (1983) and modified by Kreller (1989) to include the reduction of bond stress near the crack position. On the basis of the calculated steel strain distribution, the distribution of curvature between the cracks is derived using the distance of the tensile reinforcement to the neutral axis. Integration of these curvatures over the beam length yields the total rotation of the beam. The model has also been developed for prestressed concrete (Li, 1995; Eligehausen and Li, 1992). In this case the determination of the rotation is the result of the sum of the crack angles.

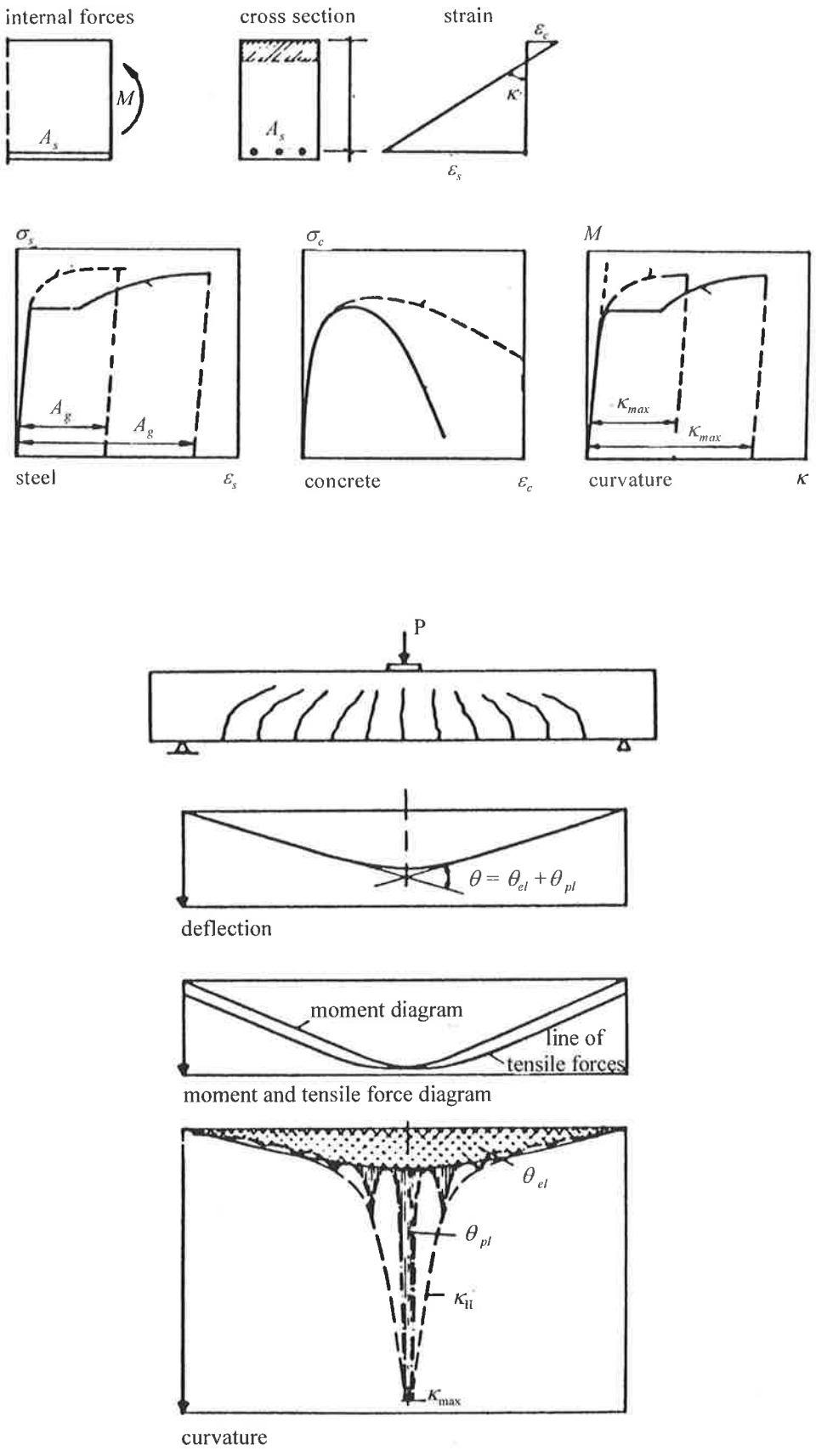

Figure 3.2 Rotation capacity model, according to Langer (1987)

Graubner (1987) simplified the iterative bond procedure to account for the tension stiffening effect, by adopting the work of Langer (1987) that provided relationships between the average steel strain between two consecutive cracks, and the peak steel strain at the crack, for the correction of steel strains in the cracked section. The approach was used in a finite element method for the analysis of section forces and deformations in three span continuous beams considering realistic material laws. Again an assumed crack spacing is adopted and influence of shear and the load pad are considered in the distribution of forces and moments along the beam.

In a model similar to the method by Langer (1987) to determine local deformations and the rotation capacity in plastic hinge regions, Cosenza *et al.* (1991a) also assume a crack spacing. The shear and load pad influences are once more considered in the distribution of forces and moments along the beam. The differing aspect is that stress transferred from the steel to the surrounding concrete acts on an effective concrete area and the strain of the concrete in tension is assumed to be constant.

In contrast to the three approaches mentioned above, the model by Sigrist (1995) uses an original tension chord model applied with a discontinuous stress field analysis to study deformations in structural concrete members (Figure 3.3). The tension chord model is intended to describe in a simple manner, the response of tension elements up to failure of the reinforcing steel. Analytical expressions for the average strain given in the tension chord model are used as a basis for the non-linear analysis of the members.

Assuming a bilinear stress-strain diagram for the reinforcing steel, along with a stepped rigid-perfectly plastic bond stress-slip relationship, and neglecting the deformations of the concrete, the distribution of bond stresses, steel stresses and strains are found. By adopting a crack spacing and applying the tension chord model to a structural element, the crack widths results from the integration of the tensile steel strains over each crack element and the elementary rotations can be calculated. The total rotation is equal to the sum of the elementary rotations. The tension cord model has also been extended for prestressed concrete tension chords.

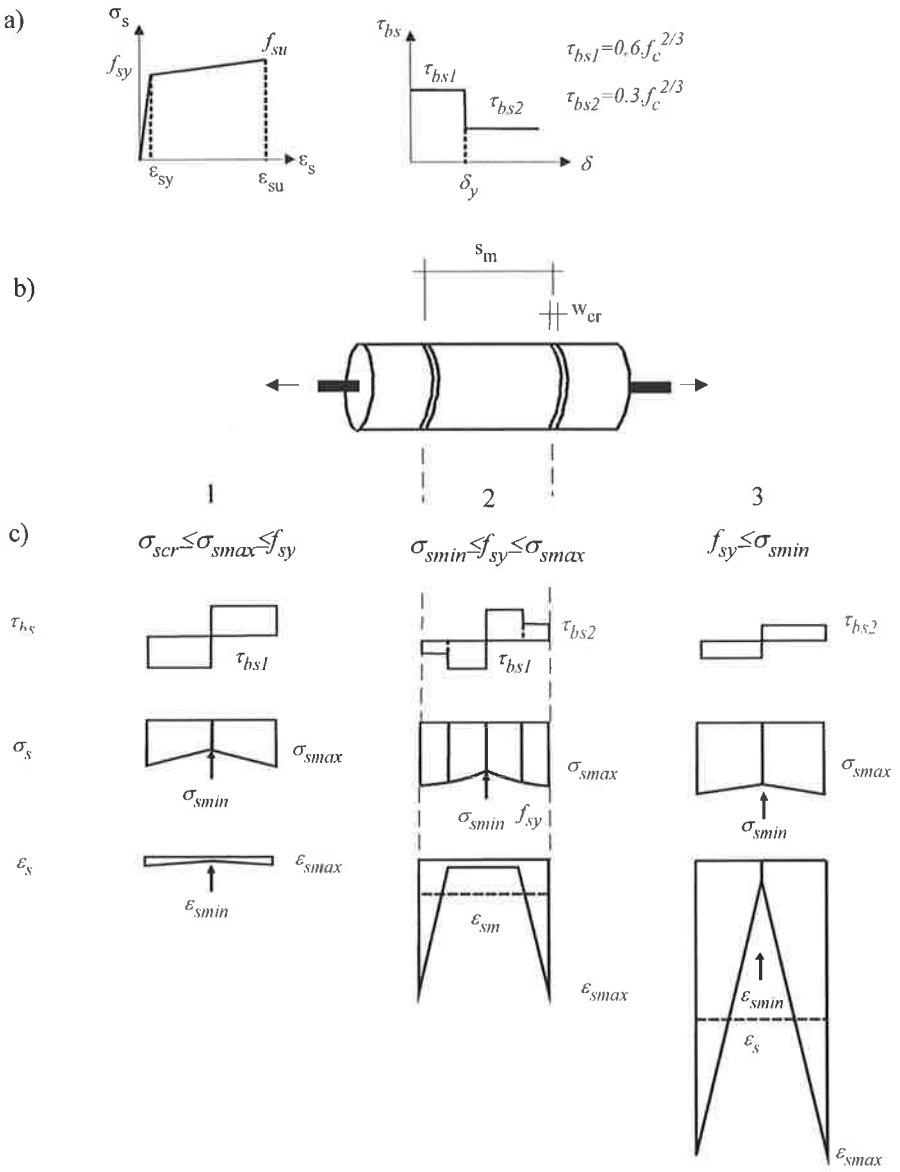

a) assumed steel stress-strain and bond-slip relationship

b) symmetrically loaded crack element

c) stresses and strains for different load stages

Figure 3.3 Tension chord model, according to Sigrist (1995)

To account for the effect of steel yielding on the bond-slip relation for ribbed bars, Bigaj (1999) developed a bond model based on the partially cracked elastic ring concept of Tepfers (1979). The bond model is applied to the method to calculate the rotation capacity of reinforced concrete members. The procedure is also similar to the model by Langer (1987), however the material relations are chosen so that the effect of strain localisation and size effect is incorporated. The member is yet again discretised assuming an average crack spacing. The elementary rotations are obtained using

calculated strains in the reinforcement, and in the upper fibre of the member compression zone integrated over each element length. The summation of the elementary rotations gives the total rotation. The calculation of elementary rotations differs to the model by Langer (1987), in which case the distribution of curvature between the cracks is derived using the distance of the tensile reinforcement to the neutral axis.

Although the method by Ferretti (1995) was developed to investigate the flexural deformability of reinforced concrete beams in the short-term load of behaviour to provide a better representation of the moment-curvature, the model is interesting since it uses a unique method for the treatment of crack spacing. The overall approach is similar to previous block models in that compatibility and equilibrium requirements are met at the section of each crack and also between cracks. However, the block models previously mentioned assume a suitable length of the block (ie. crack spacing) rather than obtaining it as a solution to the problem. In the method by Ferretti (1995), a pre-determined crack spacing is not required and the blocks are delimited by cracks that start forming when the cracking moment, M_{cr}, is attained.

The methods reviewed, excluding the model by Ferretti (1995), but including the recent work by Eligehausen *et al.* (1997) and Beeby (1998), have investigated the factors influencing the rotation capacity in plastic hinges at overload stages of behaviour and to provide a more accurate evaluation of the available ductility. Various models have taken their investigations further to investigate moment redistribution in continuous beams (Langer, 1987; Graubner, 1987; Sigrist, 1995; Bigaj, 1999). Several results from studies investigating the parameters that affect the rotation capacity are now presented.

3.3 Previous Studies on Factors Influencing Rotation Capacity of Plastic Hinge Regions

The rotation capacity in hinging regions and the extent to which moment redistribution can occur, are influenced by the ductility inherent in the structure. Many factors of material and structural type influence the available rotation capacity of plastic hinges in reinforced concrete members. These parameters can be grouped into the following categories (Cohn, 1979):

- Material parameters
  - Properties of concrete
  - Properties of steel
  - Bond properties
- Member parameters
  - Section geometry and dimensions
  - Member slenderness
  - Percentage of longitudinal reinforcement
  - Percentage of transverse reinforcement
  - Detailing of reinforcement (bar diameter and spacing)
- Statical system parameters
  - Statical system and dimensions
  - Shear effects
  - Loading type
  - Load application
  - Load repetition and cycling

From investigating the shear effect on the deformations in a plastic hinge, a number of experimental and theoretical studies (Dilger, 1966; Bachmann, 1970; Langer, 1987; Sigrist *et al.*, 1995) concluded that, depending upon the amount of shear force two quite different types of plastic hinges can develop. Flexural crack hinges which occur in the beam zone mainly affected by bending moment, and only producing flexural cracks perpendicular to the beam axis. Also shear crack hinges that occur in the beam zone which, in addition to a bending moment, are affected by a considerable shear force and exhibit inclined flexure-shear cracks. These types of hinges affect the type of failure that occurs in reinforced concrete members.

Bachmann (1970) noticed that in a flexural crack hinge, plastic deformations may be concentrated to a single or only a few flexural cracks, resulting in a reduction of rotation capacity. In the case of inclined flexural shear cracks, the rotation capacity is significantly increased since the plastic deformations extend over a relatively wide zone. Graubner (1987) also showed that the truss action, due to shear cracks, provides increased rotation capacity compared to calculations without regard to shear cracks (Figure 3.4).

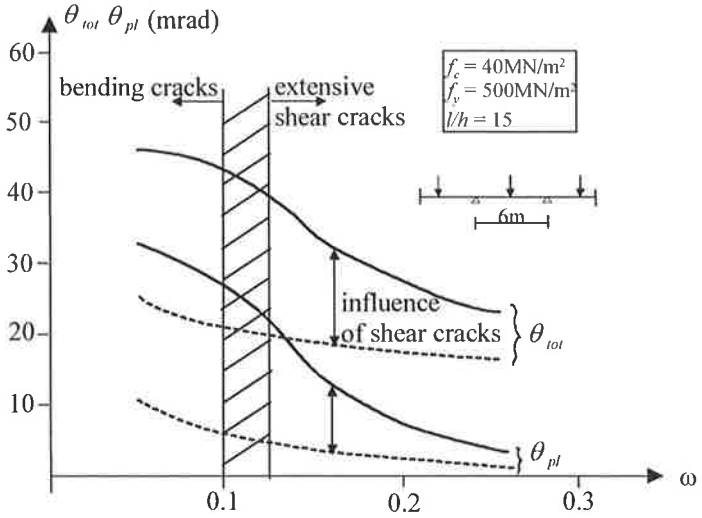

Figure 3.4 Influence of shear cracks on rotation capacity, according to Graubner (1987)

Langer (1987) and Graubner (1987) demonstrated the effect of member slenderness on the development of shear cracks in the hinge region and the available rotation capacity. For shear and flexural crack regions, an increase of the rotation capacity with increase of member slenderness was found. However in the transition zone from the shear to flexural crack hinge, a drop in the rotation capacity was observed (Figure 3.5).

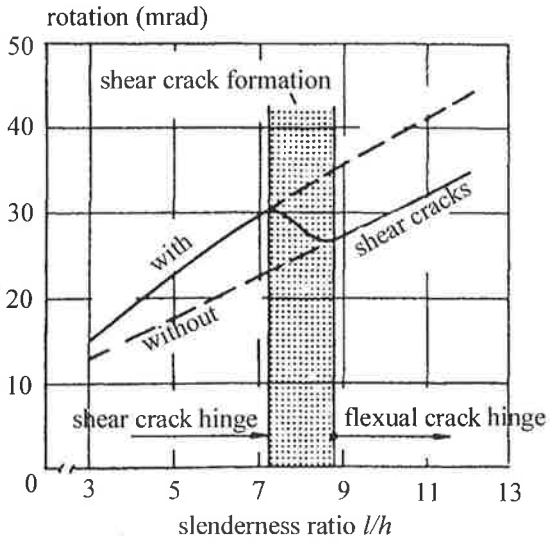

Figure 3.5 Rotation capacity as a function of member slenderness ratio – simulations of a member in three point bending with 1% tensile reinforcement, according to Langer (1987)

Another system parameter investigated by Graubner (1987) was the influence of the loading type on the rotation capacity. Under uniformly distributed loads the rotation capacity is higher in the mid-span region than in the support region due to the smaller gradient of the moment curve.

Sigrist (1995) has numerically demonstrated the effect of the section geometry on the deformation capacity of reinforced concrete members. It was shown that for values of the mechanical reinforcement ratio, ω, in the range where rupture of the reinforcement prevails, the box girder possesses higher plastic rotations than the slab with rectangular cross-section (Figure 3.6). This is mainly attributed to the effect of the ratio between member height and crack spacing, and the inclination of the compression field struts used in analysis by Sigrist (1995).

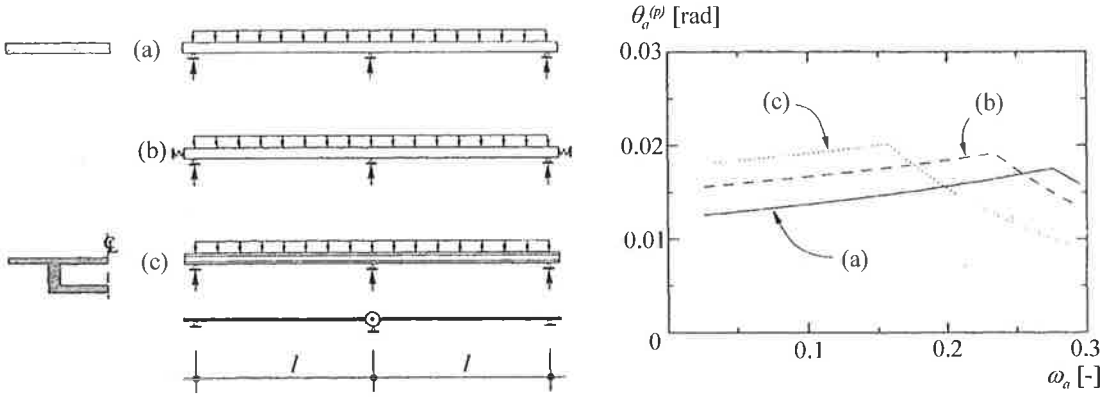

Figure 3.6 Influence of cross-section geometry on plastic rotation capacity (simulations for steel B according to MC90), according to Sigrist (1995)

Bigaj (1999) has shown a distinct size effect on the rotation capacity in plastic hinges. It was recognised that members with smaller dimensions displayed a much more ductile response to the load in comparison to members with larger dimensions, independent upon the percentage of reinforcement in the section.

The percentage of reinforcement also has an influence on the rotation capacity and the type of failure that may occur. For example, failure of a reinforced concrete member may take place due to rupture of the reinforcement, or if the deformation capacity of the steel is high, as a result of concrete crushing. Langer (1987) reported that in the range of failure of the reinforcement, rotation capacity decreases with decreasing reinforcement

percentage, as fewer cracks are formed in the region of the plastic hinge. For the case of failure of the compression zone, the maximum steel strain values at peak load decreases with increasing reinforcement percentage, resulting in a reduction of the rotation capacity (Figure 3.7).

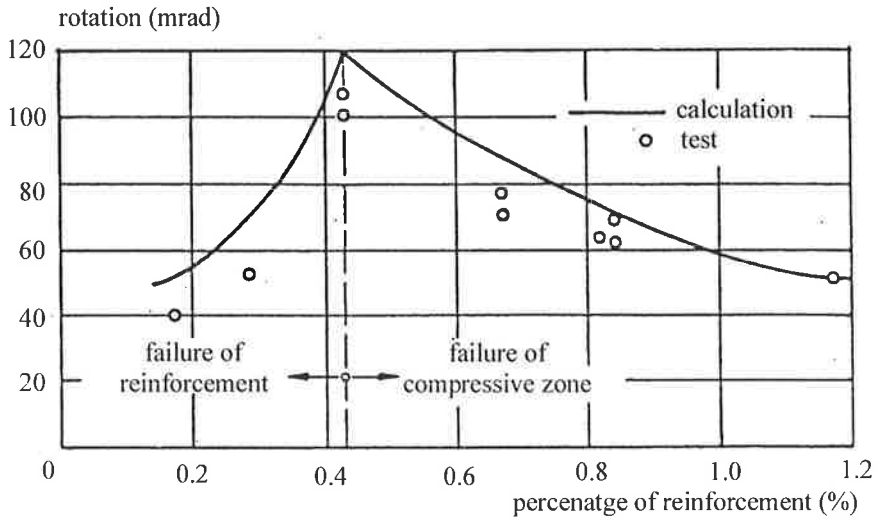

Figure 3.7 Influence of percentage of reinforcement on the rotation capacity of reinforced concrete beams, according to Langer (1987)

Having considered the parameters effecting the type of failure that can occur, another influential factor is the evaluation of the material influence on the rotation capacity. The influence of the stress-strain relationship of the reinforcing steel has been investigated by various researchers (Langer, 1987; Sigrist, 1995; Bigaj, 1999). It has been demonstrated that both high strain-hardening ratio and uniform elongation are required to produce high rotation capacity in the plastic region of the reinforced concrete members (Beeby, 1998).

The bond between the steel and the surrounding concrete contributes to the amount of tension stiffening between cracks. Eligehausen *et al.* (1997) have investigated the contribution of concrete between cracks at inelastic steel strain, and concluded the contribution of concrete between cracks significantly reduces the rotation capacity of plastic hinges. The influence of the bond between bars and concrete has also been investigated by Langer (1987), by considering no bond between the cracks and the tension stiffening due to the contribution of concrete between cracks. It was found that plastic rotation capacity is much reduced due to bond, compared to the no bond case.

The main factors that influence the rotation capacity carried out via analytical and experimental studies have been reviewed here. Further discussion on the factors influencing rotation capacity can be found in CEB-FIP Bulletin d'Information No.242 (1998).

Additional studies (Langer, 1987; Graubner, 1987; Sigrist, 1995; Bigaj, 1999) have investigated the effect of various parameters, such as the ductility class of the reinforcing steel on the allowable degree of moment redistribution. In these studies the allowable degree of moment redistribution is achieved from the evaluation of available and required rotation capacity in the hinge regions. The approaches by Langer (1987) and Bigaj (1999) represent an indeterminate beam, by a determinate beam cut out of the real system with a length equal to the distance between the inflection points over an interior support region. Real indeterminate beam cases are considered by Graubner (1987) and Sigrist (1995).

More work is still needed to investigate the ductility properties specific to Australian reinforcing steel on the available rotation capacity, and the allowable degrees of moment redistribution. Additional factors such as the effect of the slenderness ratio and effective depth also need to be reconsidered, since in some of the previous studies the slenderness ratio of the indeterminate beam may not have been considered accurately if a determinate beam was adopted to represent the structural element.

Most of the studies have been based on the deformation capacity and do not consider the strength capacity implications. The investigation presented in Chapter 8 considers the strength implications and is able to do so since real indeterminate beam configurations are considered in the analysis.

3.4 SUMMARY

The calculation models presented in this chapter consider the local bond-slip behaviour between the steel and concrete interface and are able to determine the local distribution of deformations, for example the local tensile steel strain distribution along the length of the structural element. The models have been proven to be capable of simulating available rotation capacity of critical post-yield regions. However there are some simplifying assumptions. For example, the calculations assume an average crack

spacing, except in the case of the model by Ferretti (1995) in which the crack spacing is obtained as a solution to the problem. Determinate structural elements are mainly considered, indeterminate structural elements are simulated by cutting out of the real beam, a simply supported beam corresponding to points of zero moment.

The proposed local deformation model to be introduced in the next chapter aims at improving the simplifying assumptions previously mentioned, by not assuming a crack spacing. The local deformation model follows the development of each crack through the load history of the beam. In comparison to the model by Ferretti (1995), the proposed model differs in that the analysis extends past the serviceability range of behaviour, to model peak and post-peak behaviour.

In Chapter 7, the model is extended to analyse indeterminate structural elements. If the phenomenon of moment redistribution is to be fully considered, accurate modelling of indeterminate structural elements is essential.

4

LOCAL DEFORMATION MODEL

This chapter provides details of a local deformation model that has been developed for the purpose of calculating the available rotation capacity of critical post-yield plastification regions. The analysis predicts progressive formation of tensile cracks, initial yielding of the tensile steel and subsequent spread of the yielded region to create a plastic hinge. Local flexural deformations can be traced up to the peak moment capacity. The method extends current approaches since an average crack spacing is not assumed, and the procedure is applied simultaneously to the different peak moment regions in a continuous or fixed end beam.

4.1 PROGRESSIVE CRACK FORMATION AND LOCAL DEFORMATIONS

The development of crack patterns and consequently crack locations greatly affects the plastic deformation of critical post-yield, plastification regions in reinforced concrete members.

Depending upon the magnitude of the shear force in the critical region of a reinforced concrete member, two significantly different types of plastic hinges with varying crack pattern can develop (Dilger, 1966; Bachmann, 1967; Sigrist *et al.*, 1995), that is, the flexural crack hinge and the shear crack hinge (Figure 4.1).

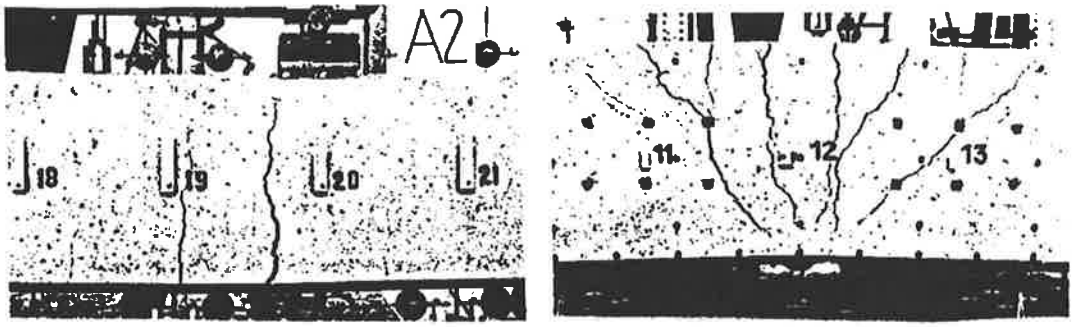

Flexural crack hinge shear crack hinge

Figure 4.1 Flexural and shear cracks, after Bachmann (1970)

Other researchers (Beeby, 1997; Bigaj, 1992) have also revealed that, depending upon the position of the cracks in the presence of a moment gradient, the extent of localised plastic deformations along the reinforcing steel length may significantly differ. Beeby (1997) has even made the distinction between two flexural failure modes, that is, the single crack hinge where the plastic strain is localised over a very small length of bar, and the multiple crack hinge where plastic deformations are dispersed over a larger length of bar.

The local deformation model developed here considers the progressive formation of flexural cracks, and the distribution of local deformations of beams subjected to variable moment gradients. The single crack hinge and multiple crack hinge defined by Beeby (1997) can be taken into account since the dispersion of plastic deformations along the length of bar can be calculated and the ductility properties of the steel are considered.

To explain the formation of flexural cracking and the distribution of local deformations, consider the reinforced concrete beam in Figure 4.2 subjected to a point load applied at mid-span. The first flexural crack is assumed to form in the section of maximum moment when the tensile stress in the concrete exceeds the tensile strength. At this stage the corresponding cracking moment, M_{cr}, can be calculated according to the following expression for a rectangular cross-section:

$$M_{cr} = bD^2 f_{ct}/6 \tag{4.1}$$

where b is equal to the section width, D overall section depth and f_{ct} is the concrete tensile strength taken here to be equal to $0.6\sqrt{f_c}$.

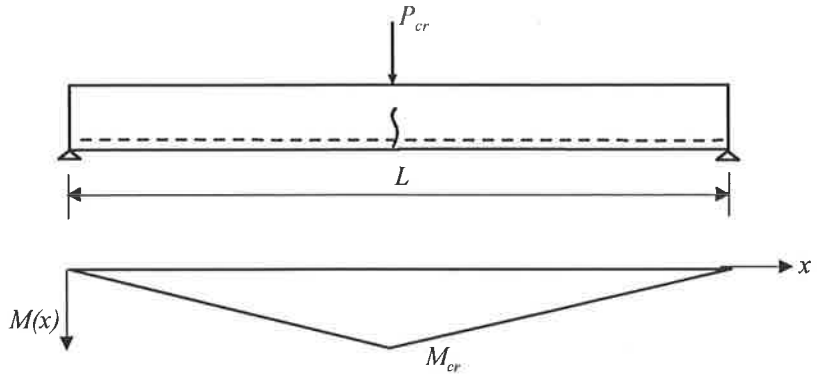

Figure 4.2 Formation first primary crack

At the section of the crack, the tensile force is carried by the reinforcing steel, which causes a sudden increase in tensile steel strain from the pre-cracked to post-cracked state (Figure 4.3). A 'disturbed region' extends on either side of the crack in which the stresses in the concrete and reinforcing steel are influenced by the initiation of the crack. In the disturbed region the tensile force in the reinforcing steel is transmitted to the surrounding concrete by the bond stress. Slip between the concrete and steel is present and varies from a maximum slip value at the crack, to a point of zero slip some distance, l_{tr}, away from the initial crack. This point of zero slip defines the extremity of the disturbed region. The distance within the disturbed region from the crack to the point of zero slip is referred to as the transfer length l_{tr}. Outside the disturbed region, there is no slip between the concrete and steel since perfect bond exists (Figure 4.3).

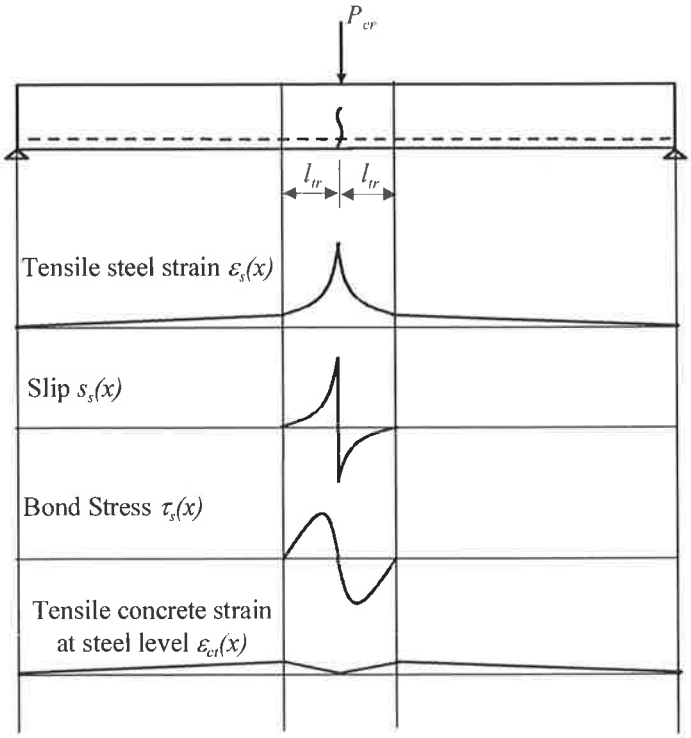

Figure 4.3 Distribution of local deformations at formation of first primary crack

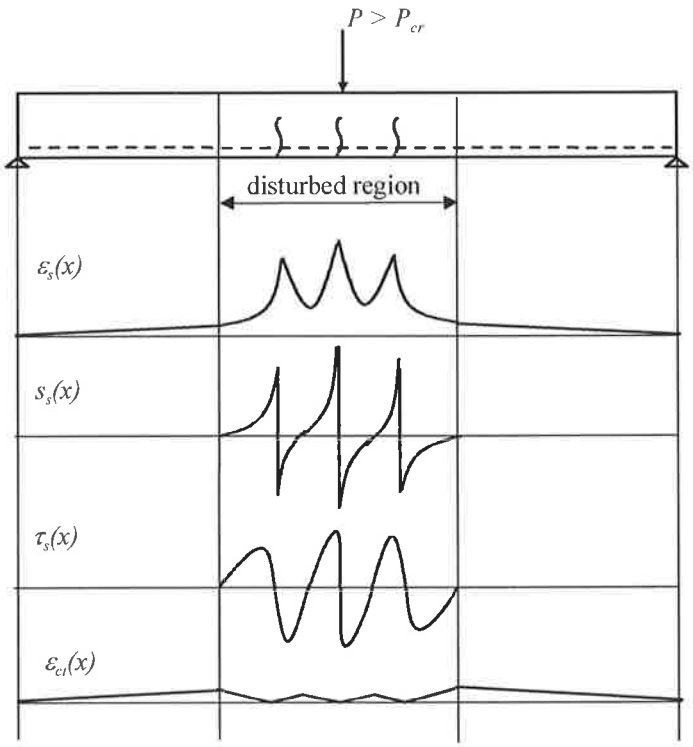

Figure 4.4 Distribution of local deformations at formation of multiple primary cracks

With increasing load, the transfer length, l_{tr}, increases and the next primary crack forms at some distance away from the previously formed primary crack. This primary crack can be expected to occur at, or close to the point of zero slip when the tensile strain in the concrete reaches the tensile strength (Figure 4.4).

At the point of minimum steel strain between the primary cracks, the tensile strain in the concrete is at its maximum. With further increase in load, secondary cracks may also form between primary cracks due to the build up of tensile stress in the concrete.

The variation in the local deformations along the beam, such as the tensile steel strain, slip and bond stress distribution, can be determined from a consideration of the local bond stresses between the steel and the concrete. Before the analysis procedure is fully explained a review of the bond mechanisms is presented.

4.2 BOND BETWEEN STEEL AND CONCRETE

Steel-to-concrete bond allows longitudinal forces to be transferred from the reinforcement to the surrounding concrete. The bond interaction between the concrete and bar is achieved through three mechanisms:

- Chemical adhesion
- Friction
- Mechanical interlock

Bond of plain bars depends primarily on chemical adhesion and friction, although there is some mechanical interlocking due to the roughness of the bar surface. Bond of deformed bars depends mainly on the mechanical interlock between the rib of the bars, the concrete and chemical adhesion and friction are secondary in action (Lutz and Gergely, 1967; Rehm, 1961).

Factors influencing local bond have been well investigated (Tassios, 1979; CEB, Bulletin d'Information N.151, 1981; Rehm, 1961; Eligehausen *et al.*, 1983), and include concrete quality, concrete strength, shrinkage of concrete, confinement, load history, rib geometry of the reinforcing bar, bar corrosion, position of bars during casting, and stress level of reinforcing bar.

The bond characteristics of the bar surrounded by concrete can be best described by a relationship between local bond stress and local slip of the bar (Rehm, 1961). The slip can be divided into two parts, one caused by elastic deformations in the concrete and the other caused by cracking and crushing of the concrete in the vicinity of ribs. For ribbed bars, slip is mostly due to cracking and crushing of the concrete in front of the ribs.

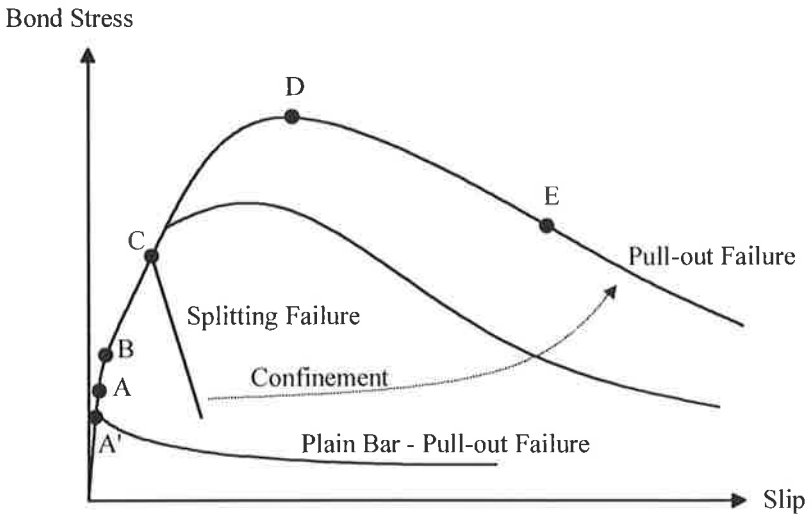

Figure 4.5 Schematic bond-slip relationship

The bond stress versus slip relation in Figure 4.5, based on CEB Bulletin d'Information No.151 (1981) and Eligehausen *et al.* (1983), is used to describe the bond interaction between the steel and the surrounding concrete.

At initial loading the bond resistance depends upon the chemical adhesion up to point A, and the slip is minimal due to concrete deformations close to the interface. For plain bars the low bond shear strength results in loss of chemical adhesion at point A', with only friction remaining. A pull-out failure occurs, and is influenced by the degree of confinement.

For ribbed bars at higher bond stress values, say at point B in Figure 4.5, mechanical interlock between the ribs and the concrete is initiated. The ribs induce large bearing stresses on the adjacent concrete, and produce tensile stresses in the concrete near the rib tip, which, in turn create internal inclined cracks. The inclined cracks are known as bond cracks and have been experimentally demonstrated by Goto (1971). The bond cracks reduce the stiffness of the concrete and larger slip values prevail.

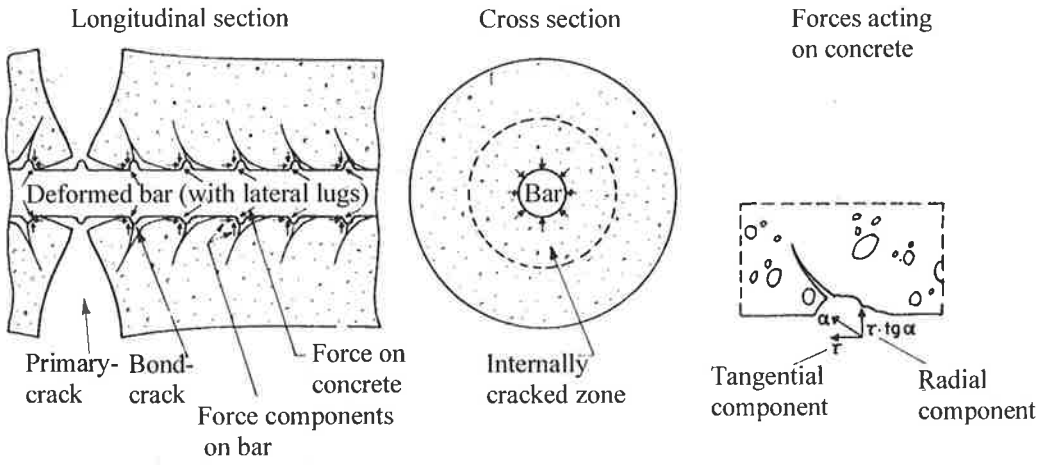

Figure 4.6 Bond cracks according to Goto (1971)

After the occurrence of bond cracks, the stress transfer from the steel to the surrounding concrete is achieved by the inclined compressive forces spreading from the rib tips into the concrete at an angle α. The inclined compressive forces on the concrete can be divided into a tangential and radial component. The tangential component is referred to as the bond stress (Figure 4.6). The radial components of the bond forces are balanced against the tensile rings in the concrete as described by Tepfers (1979), which may cause longitudinal splitting cracks owing to the wedging action of the ribs (Figure 4.7).

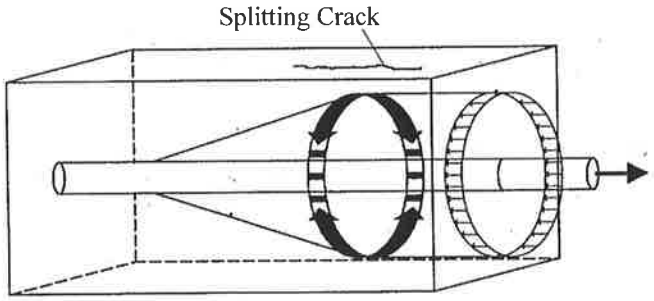

Figure 4.7 Radial components of bond forces, according to Tepfers (1979)

When these cracks reach the surface, say at point C in Figure 4.5, and none or a small amount of confinement is provided, the bond resistance will drop towards zero. This type of failure is referred to as 'splitting failure'.

However, if the concrete is well-confined to prevent splitting of the concrete cover, the load can be further increased and the maximum bond stress is then dependent upon shear cracking between two adjacent ribs (Point D). With increase in slip the bond stress

decreases due to the shear failure in the concrete between the ribs. At point E, the concrete between the ribs is completely sheared off, and the bond mechanism of friction takes over. This type of failure is known as bar 'pull-out failure'.

For moderate confinement, a 'splitting induced pull-out failure' can be defined and the local bond-slip relation lies between the ductile failure of well confined concrete, and the brittle failure associated with a small amount of confinement.

The above description of the bond mechanisms between steel and concrete has evolved from numerous experimental tests (Tassios and Yannopoulos, 1981; Eligehausen *et al.*, 1983; Giuriani, 1981; Gambarova *et al.*, 1989). Analytical bond-slip relations have been developed that are based on the local bond behaviour described above. Of particular interest are the models by Eligehausen *et al.* (1983), CEB-FIP (1993), Engström (1992), Shima *et al.* (1987), and Bigaj (1999).

Eligehausen *et al.* (1983) performed experimental and analytical investigations in the development of their bond-slip relation for ribbed bars in concrete. The non-linear relation for monotonic loading consists of four parts.

The initial non-linear relation is:

$$0 \le s \le s_1 \ : \ \tau = \tau_{\max} \cdot \left(\frac{s}{s_1} \right)^{\alpha} \tag{4.2}$$

followed by a plateau

$$s_1 \le s \le s_2 \ : \ \tau = \tau_{\max} \tag{4.3}$$

then a linear descending branch

$$s_2 \le s \le s_3 \ : \ \tau = \tau_{\max} - \tau_{\max} - \tau_f). \left(\frac{s - s_2}{s_3 - s_2} \right) \tag{4.4}$$

leading to the constant residual bond resistance

$$s \ge s_3 \ : \ \tau = \tau_f \tag{4.5}$$

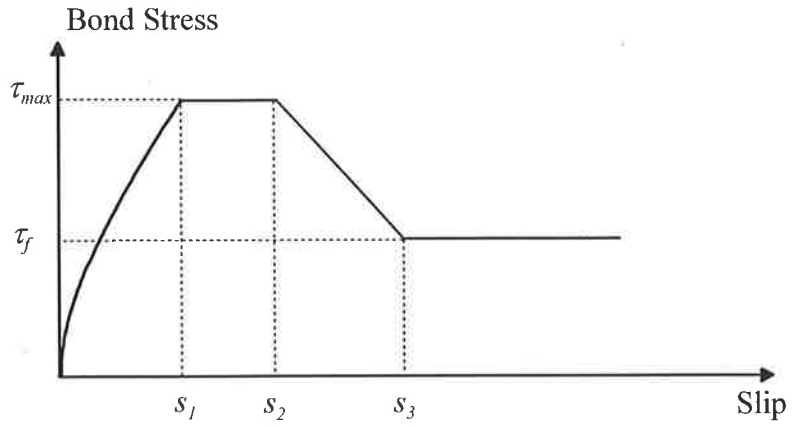

Figure 4.8 Local bond slip relation according to Eligehausen *et al.* (1983)

The bond-slip relation by Eligehausen *et al.* (1983) has formed the basis of the model adopted in the CEB-FIP Model Code (1993). The parameters defining the curves are given in Table 4.1 and are for ribbed bars and depend upon the amount of confinement, bond condition and concrete strength.

Table 4.1 Bond parameters according to CEB-FIP Model Code (1993)

Parameters	Unconfined concrete Cover=1 bar diameter		Confined concrete Cover > 5 bar diameters	
	Good bond conditions	All other bond conditions	Good bond conditions	All other bond conditions
s_1	0.6 mm	0.6 mm	1.0 mm	0.6 mm
s_2	0.6 mm	0.6 mm	3.0 mm	0.6 mm
s_3	1.0 mm	2.5 mm	Clear rib spacing	Clear rib spacing
α	0.4	0.4	0.4	0.4
τ_{max}	$2.0 f_c^{0.5}$ (MPa)	$1.0 f_c^{0.5}$ (MPa)	$2.5 f_c^{0.5}$ (MPa)	$1.25 f_c^{0.5}$ (MPa)
τ_f	0.15 τ_{max} (MPa)	0.15 τ_{max} (MPa)	0.4 τ_{max} (MPa)	0.4 τ_{max} (MPa)

For those parts of the bar which are a distance $\frac{x}{d_b}$ from the next transverse crack the bond capacity is reduced by a factor, λ:

$$\lambda = 0.2\frac{x}{d_b} \leq 1 \tag{4.6}$$

where x represents the distance from the crack and d_b is the bar diameter.

Shima *et al.* (1987), Engström (1992) and Bigaj (1995) found that the bond stress decreases considerably after tensile yielding of the bar. The bond-slip relation by Shima

et al. (1987) takes this into account by implicitly including the steel strain, ε_s in the model formulation.

$$\tau = f_c \frac{0.73[\text{In}(1+5000s/d_b]^3}{1+\varepsilon_s.10^5} \tag{4.7}$$

where $s = 1000S/d_b$ and S is equal to the local slip.

In the model by Engström (1992) the bond model is similar to the CEB-FIP Model Code (1993) but with a decreasing softening branch. The model can be used for well-confined normal and high strength concrete typical to anchorage zones. When the steel yields, a second descending branch II is followed (Figure 4.9).

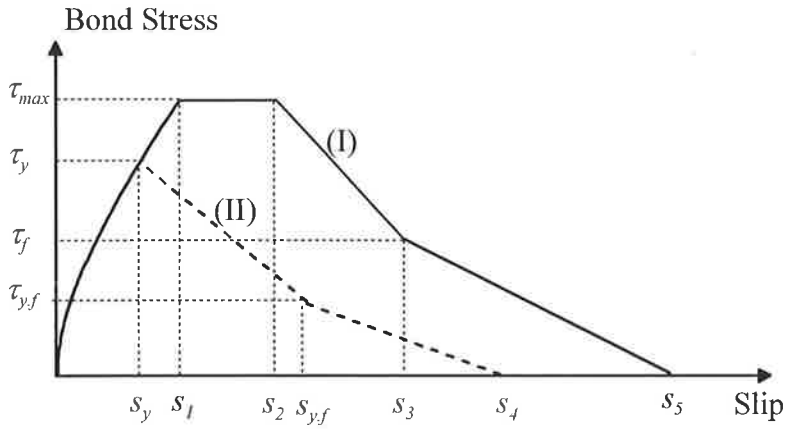

Figure 4.9 Load bond slip relation according to Engström (1992)

In addition to the above type of local bond-slip relations that mainly consider the longitudinal bond stress between the reinforcing bar and the surrounding concrete, the response of the radial stresses have been modelled by assuming a hydraulic pressure analogy of the stresses acting on a thick walled-concrete ring. The concrete ring represents the surrounding concrete. Tepfers (1979) presented a concrete ring model based on this concept for the determination of the cracking resistance of the concrete ring for three stages of behaviour, an elastic stage, a partly cracked elastic stage and a plastic stage.

The bond-slip model developed by Bigaj (1999), see also den Uijl and Bigaj (1996), is based on the partially cracked elastic ring concept of Tepfers (1979). The model considers the confining action of split concrete within a fracture mechanics approach for

normal strength and high strength concrete. The longitudinal bond stress is related to the slip and the radial deformation between the bar and concrete. The effects of plastic steel strains are also accounted for.

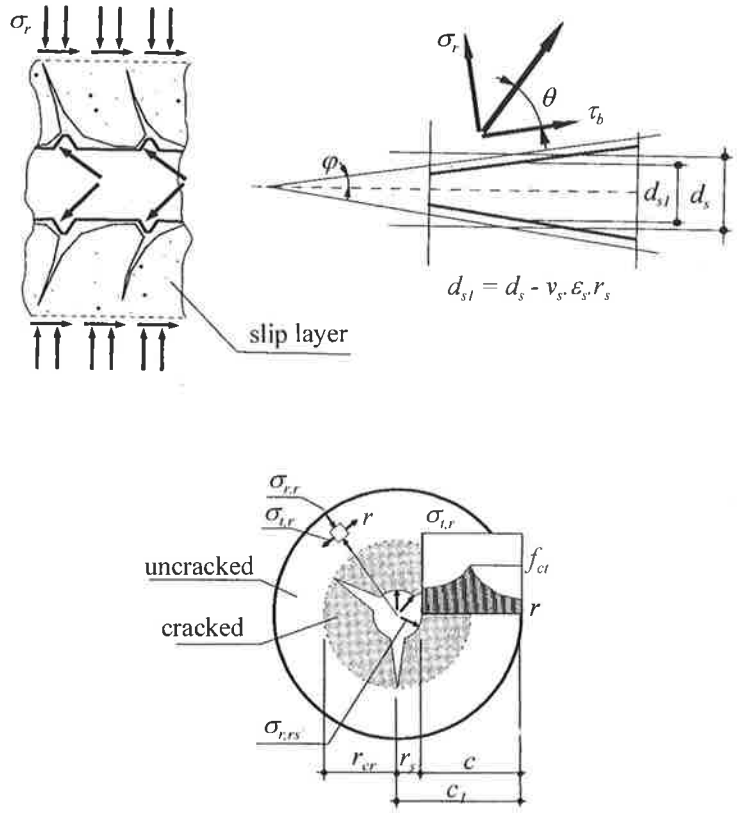

Figure 4.10 Partially cracked thick-walled cylinder, according to Bigaj (1999)

The analysis procedure that will be introduced in the following section of this chapter requires the adoption of a local bond-slip relation. The relation chosen for modelling purposes and used in the remainder of this thesis, is the bond-slip relation by Eligehausen *et al.* (1983) as in the CEB-FIP Model Code (1993). This model has been chosen since it caters for varying degrees of confinement and the reduction of the bond stress near the transverse crack implicitly takes into account the effect of steel yielding. The model by Engström (1992) is attractive, however, in the part of the beam where flexural cracking forms, the member is not necessarily fully confined as in areas such as anchorage zones.

4.3 DESCRIPTION OF ANALYSIS

4.3.1 Simplifying Assumptions and Governing Equations

The analysis procedure is carried out by representing the beam as a succession of discrete blocks (Figure 4.11). The discrete blocks are bounded by flexural cracks in the region of the beam that is in the cracked state. In the region of the beam considered to be uncracked, the blocks are bounded by sections in which perfect bond exists. As explained in Section 4.1 the first primary crack is assumed to form at the section of maximum moment when the cracking moment, M_{cr}, is reached. Subsequent cracks are assumed for simplicity to occur at the positions of zero slip, ie. at distance, l_{tr}, away from the previously formed primary crack, when the moment at this section reaches M_{cr}. Secondary cracking between primary flexural cracks can also occur if the build-up of tensile stress in the concrete between cracks exceeds the tensile strength of concrete.

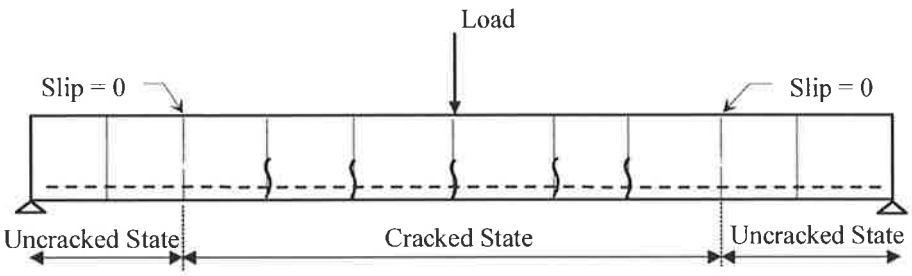

Figure 4.11 Beam representation with discrete blocks

Sectional forces at the boundaries of each discrete block are determined from the moments acting in these sections. Shear is ignored, and as a simplifying approximation it is assumed that strains are linearly distributed at the cracked section as in the uncracked section (Figure 4.12). In the cracked section profile it is assumed that the crack tip is located on the neutral axis and concrete in tension between the crack tip and the neutral axis is ignored. The sectional stresses and strains are then calculated by applying the equations governing the sectional equilibrium, together with the material laws for concrete and steel.

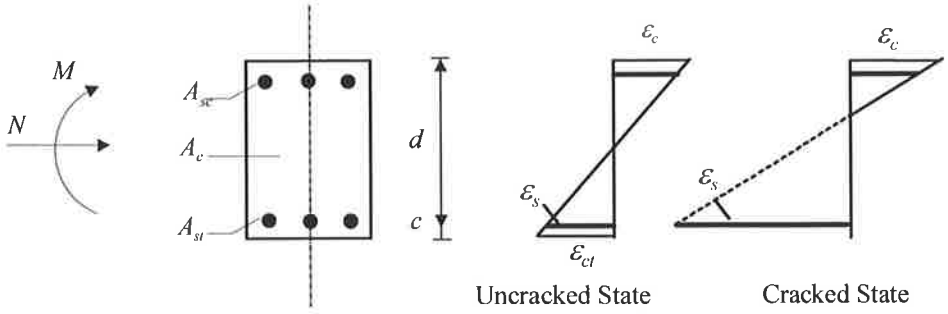

Figure 4.12 Strain profiles

A layered approach is used for the equilibrium calculations at a section where the concrete is divided into a finite number of layers, and the stresses and forces are obtained from the strains. Forces in the steel are also obtained from the section strains.

The equations governing the sectional equilibrium are as follows:

Translational (force) equilibrium of cross section:

$$-\int_{A_c}\sigma_c.dA_c+\int_{A_{ct}}\sigma_{ct}.dA_{ct}-\sigma_{sc}.A_{sc}+\sigma_{st}.A_{st}=N(x) \tag{4.8}$$

Rotational (Moment) equilibrium of cross section:

$$-\int_{A_c}\sigma_c.y_c.dA_c+\int_{A_{ct}}\sigma_{ct}.y_{ct}.dA_{ct}-\sigma_{sc}.y_{sc}.A_{sc}+\sigma_{st}.y_{st}.A_{st}=M(x) \tag{4.9}$$

The material laws for steel and concrete adopted in the analysis may be varied to suit specific materials. But in general the material law for concrete in compression is modelled according to Warner (1969) (Figure 4.13).

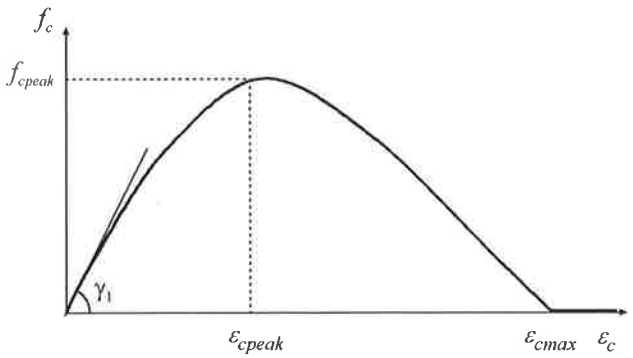

Figure 4.13 Concrete in compression model, according to Warner (1969)

The equations defining the stress-strain relationship are:

$$0.0 \le \bar{\varepsilon}_c < 1.0 \; : \; \bar{f}_c = \gamma_1 \bar{\varepsilon}_c + (3 - 2\gamma_1)\bar{\varepsilon}_c^{\,2} + (\gamma_1 - 2)\bar{\varepsilon}_c^{\,3} \tag{4.10}$$

$$1.0 \le \bar{\varepsilon}_c < \gamma_2 \; : \; \bar{f}_c = 1 - (1 - 2\bar{\varepsilon}_c + \bar{\varepsilon}_c^{\,2})/(1 - 2\gamma_2 + \gamma_2^{\,2}) \tag{4.11}$$

$$\bar{\varepsilon}_c \ge \gamma_2 \; : \; \bar{f}_c = 0.0 \tag{4.12}$$

where

$\bar{\varepsilon}_c$ = normalised strain equal to $\varepsilon_s/\varepsilon_{smax}$

$\bar{f}_c$ = normalised stress equal to f_c/f_{cmax}

γ_1 = $E_c.\varepsilon_{cmax}/f_{cmax}$

E_c = modulus of elasticity of concrete

f_{cmax} = compressive strength of concrete

ε_{smax} = strain corresponding to stress f_{cmax}

The relation for concrete in compression is only applicable for normal strength concrete up to 60MPa. High strength concrete is not considered in this study. Considering the uncracked section profile (Figure 4.12) for concrete in tension, a linear elastic stress-strain relationship is used with modulus E_c.

A bi-linear stress-strain relationship for steel in tension and compression is adopted. The equations defining the relation are:

$$\varepsilon_s \le \varepsilon_{sy} \; : \; \sigma_s = E_s \varepsilon_s \tag{4.13}$$

$$\varepsilon_{sy} < \varepsilon_s \le \varepsilon_{su} \; : \; \sigma_s = \sigma_{sy} + E_{sh}.(\varepsilon_s - \varepsilon_{sy}) \tag{4.14}$$

where

ε_s = steel strain

σ_s = steel stress

ε_{sy} = yield strain

ε_{su} = ultimate steel strain (uniform elongation)

E_s = modulus of elasticity of steel

E_{sh} = strain hardening slope equal to $\dfrac{f_{su} - f_{sy}}{\varepsilon_{su} - \varepsilon_{sy}}$

f_{su} = stress at ultimate strain

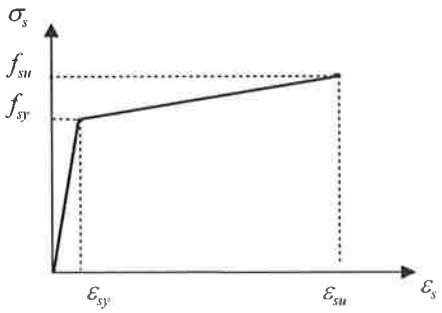

Figure 4.14 Steel model

The descending part of the stress-strain curve for steel is neglected. The maximum steel strain at peak stress is ε_{su}. This relation enables important parameters such as the ratio of ultimate strength to yield strength, f_{su}/f_{sy} and the uniform elongation ε_{su}, to be varied.

Knowing the stresses and strains at the boundaries of the discrete blocks, that is at the flexural cracks, the distribution of strains at intermediate points between the flexural cracks can now be calculated by considering the behaviour of the tensile bar surrounded by the concrete. The longitudinal force equilibrium for the bar is represented by the equation:

$$\frac{dN(x)}{dx} - q(x) = 0 \tag{4.15}$$

where $N = \dfrac{\pi . d_b^{\,2}}{4} \sigma_s$ and $q = \pi . d_b . \tau(x)$

Equation 4.15 can be simplified to:

$$\frac{d\sigma_s(x)}{dx} - \frac{4}{d_b}\tau(x) = 0 \tag{4.16}$$

Equation 4.15 expresses equilibrium of an infinitesimal portion of the bar and connects the axial force in the bar, N, to the resultant per unit length of bond stresses on the perimeter of the bar, q.

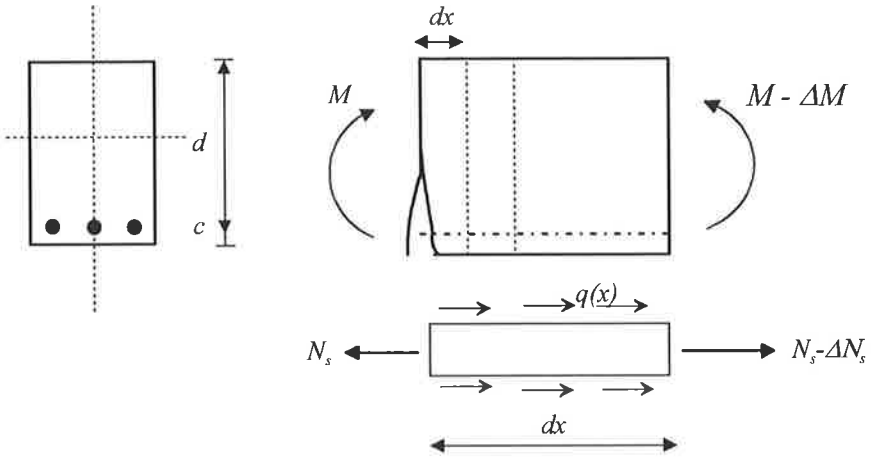

Figure 4.15 Bar equilibrium

For the same portion of the discrete block element the slip between the concrete and the steel can be defined by Equation 4.17.

$$s(x) = s_s(x) - s_{ct}(x) \tag{4.17}$$

Hence by derivation with respect to x:

$$\frac{ds(x)}{dx} = \varepsilon_s(x) - \varepsilon_{ct}(x) \tag{4.18}$$

The tensile strain in the concrete ε_{ct} at the steel level is assumed to be negligible in comparison to the tensile steel strain ε_s.

The Equations 4.15 to 4.18 introduced above, define the local deformations between flexural cracks, and are coupled together with the constitutive law for steel in tension and the local bond-slip relation. The bond-slip relation is given by Equations 4.2 to 4.5 in Section 4.2.

Solution to the problem requires suitable boundary conditions. The principle is to solve the two-point boundary value problem, defined by Equations 4.8, 4.9 and 4.15 to 4.18, coupled with the adopted constitutive material laws for steel and concrete, the local bond-slip relation, and assumed boundary conditions. Different numerical techniques such as finite differences, finite elements, and 'shooting techniques' (Ciampi *et al.*, 1982) can be used to solve the two-point boundary value problem.

At the sections that bound the edges of the block, ie. at the crack positions, Equations 4.8 and 4.9 can be independently evaluated to obtain the strain distribution at the sections. Equations 4.15 to 4.18 then represent the system between the sections that bound the block. The unknown boundary condition is assumed in this case to be the initial slip value at one edge of the block, in order to produce after integration along the length of the block, the strain value in the steel at the other end. The computed boundary condition at the far end has to match the specified value of strain obtained from the sectional boundary condition. A more detailed explanation of the solution procedure is presented in the following section.

The solution provides the deformation distributions relative to the steel bar, along the length of the discrete block. In particular, the distributions of tensile steel strain along the reinforcing bar, the bond stress that is transferred to the concrete surrounding the tensile bar, and the slip between the steel and concrete relative to the tensile bar. The distribution of strains in the concrete compressive zone is assumed to vary linearly between boundaries of the discrete block. The local deformations in the concrete compressive zone have been modelled more accurately by other researchers (Bigaj, 1992; Markeset, 1993), who were interested in simulating local strain deformations not only in tension but also in the compressive damage zone. Since this investigation is mainly interested in steel fracture, a more accurate representation of the concrete compressive zone was not necessary (Figure 4.16).

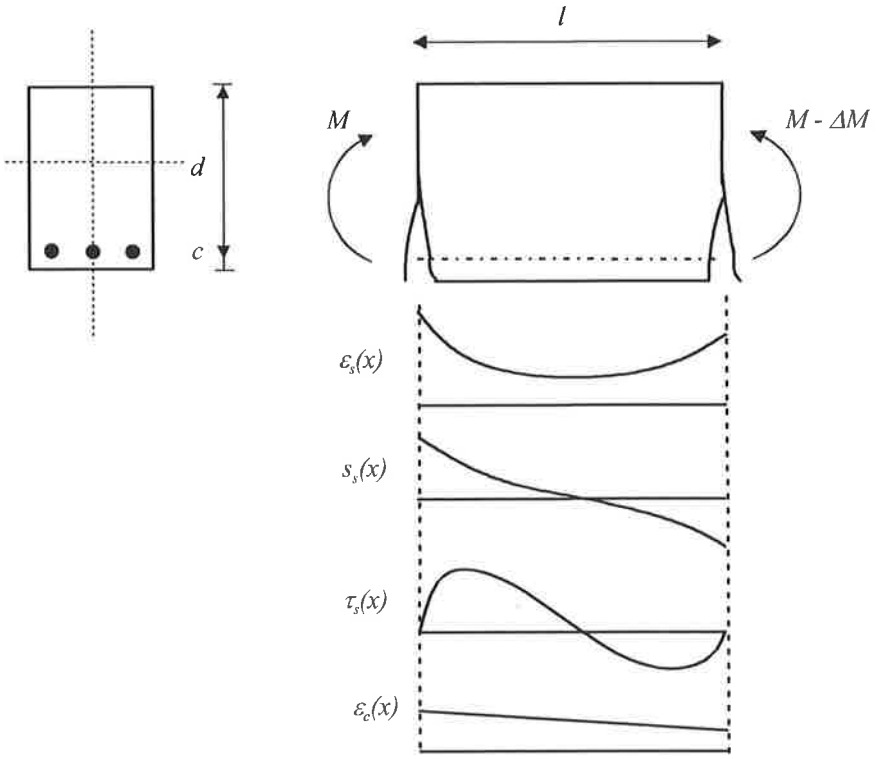

Figure 4.16 Local deformation distribution

Subsequently, the block rotations can be calculated according to the following equation:

$$\theta_{block} = \frac{\int_0^l \varepsilon_s(x).dx + \int_0^l \varepsilon_c(x).dx}{d} \tag{4.19}$$

where l = length of the block, and d is the distance to the tensile steel layer.

4.3.2 Numerical Solution of Block Element

Three block element types exist; a block element bounded by two consecutive cracks, an unbound block element bounded by one crack and the position of zero slip, and an uncracked block element bounded by uncracked sections (Figure 4.11).

For the uncracked block element the local deformation distribution of stresses and strains are assumed to vary linearly since perfect bond exists in this uncracked region.

The solution procedures for the block elements in the cracked region of the beam are now considered.

4.3.2.1 Block bounded by two consecutive cracks

In order to solve the problem of a block element bounded by two consecutive cracks, the block with interval [0,*l*] is discretised by *n* points into *n-1* subintervals. The position along the element is represented by x_i, (i=1,2,....,n: $x_n = l$; $\Delta x_i = x_{i+1} - x_i$) (Figure 4.17). The edges of the block element at $x_1 = 0$ and $x_n = l$ signify the crack locations of two consecutive cracks.

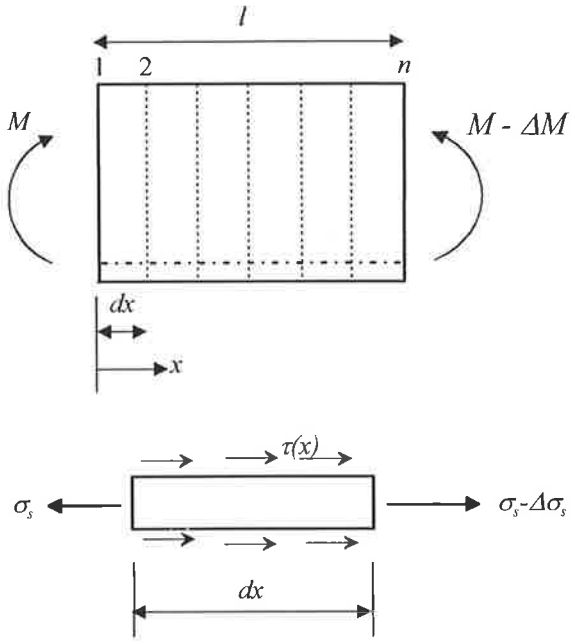

Figure 4.17 Discretisation of block element

At the boundaries, ie. at the cracked sections of the block, the stress and strain in the steel are determined from the equilibrium equations and compatibility conditions introduced in Section 4.3.1. Hence the stress and strain in the tensile steel, $\varepsilon_{s,1}$ and $\varepsilon_{s,n}$, at positions $x_1 = 0$ and $x_n = l$ respectively, are known. While the slip values s_1 and s_n are unknown.

To initiate the solution, a trial value of s_1 is assumed. To advance to the next position along the element the values of σ_{si} and τ_i are thus determined using the material relations, $\sigma_s(x) = \sigma_s(\varepsilon_s(x))$ and $\tau_s(x) = \tau_s(s_s(x))$. Based on the known values of $\varepsilon_{s,i}$, $\sigma_{s,i}$, s_i and τ_i at station i, the solution is advanced to the next station i+1 using the following relations:

$$s_{i+1} = s_i - \frac{\varepsilon_{s,i} + \varepsilon_{s,i+1}}{2}\Delta x_i \tag{4.20}$$

$$\sigma_{s,i} - \sigma_{s,i+1}(\varepsilon_{s,i+1}) - \frac{\tau_i + \tau_{i+1}(s_{i+1})}{2}.\frac{4}{d_s}\Delta x_i = 0 \tag{4.21}$$

Equation 4.20 and Equation 4.21 represent the slip compatibility and bar equilibrium conditions to be satisfied.

The only unknown is $\varepsilon_{s,i+1}$, since Equation 4.20 is substituted into Equation 4.21. The solution is found by employing an iterative procedure until the equilibrium check using Equation 4.21 is satisfied. The steps followed at each iteration are to:

1. Use current guess for $\varepsilon_{s,i+1}$, to compute $s_{s,i+1}$.

2. Use Equation 4.21 to check equilibrium.

3. Repeat (go to step1) with a new value for $\varepsilon_{s,i+1}$ if check is not satisfied.

Once $\varepsilon_{s,i+1}$ has been determined, and $\sigma_{s,i+1}$, s_{i+1} and τ_{i+1} are available, the procedure can be applied to the next subinterval and up to the end point n.

At the end point n the value of tensile steel strain is known, and the convergence of the method can be checked by comparing the computed tensile steel strain in the last section $\varepsilon_{s,n}(s_1)$ to the value obtained from the sectional boundary condition $\varepsilon_{s,n}$ where $x_n = l$.

The convergence method implies the solution of the following equation:

$$f(s_1) = \varepsilon_{s,n}(s_1) - \varepsilon_{s,n} = 0 \tag{4.22}$$

where s_1 is the unknown initial slip value at point 1, $\varepsilon_{s,n}(s_1)$ is the value of tensile steel strain at the end point n, computed based on the guess of the initial slip value s_1, and $\varepsilon_{s,n}$ is the assigned boundary condition at n. If this condition is not satisfied the initial value of s_1 is re-guessed and the analysis between the boundaries of the block is repeated.

The overall procedure for the block element bounded by two consecutive cracks is achieved following these steps:

1. Assume a trial value of initial slip, s_1, at $x_1 = 0$ at the cracked section.

2. Compute $\varepsilon_{s,1}$ at $x_1 = 0$ according to equilibrium Equations 4.8 and 4.9 in Section 4.3.1.

3. For $i = i+1$ and $x_{i+1} = x_i+\Delta x$, integrate Equations 4.20 and 4.21, assuming the tensile strain in the concrete to be negligible, to obtain $\varepsilon_{s,i+1}$, $\sigma_{s,i+1}$, s_{i+1} and τ_{i+1}.

4. Repeat step 3 until $i = n$.

5. At position n, check that $\varepsilon_{s,n}(s_1)-\varepsilon_{s,n} = 0$, where $\varepsilon_{s,n}$ is based on the cracked section conditions. That is, if Equation 4.22 is not satisfied, assume a new trial value for the initial slip, s_1, at $x_1 = 0$ and go to step1.

The first estimate for the unknown initial condition s_1 is evaluated as the multiple of the maximum steel strain at the cracked section, by the distance between two adjacent cracks. From then on, the initial slip guess is taken as a degree of the value of the last converged step.

The secant numerical method seems attractive to solve the iterative problem of Equation 4.22 since it does not require the direct evaluation of derivatives, but requires two initial approximations of the unknown initial condition. A disadvantage of the secant method is that it does not always converge, depending on the initial approximations and on the shape of the function $f(s_1)$ near zero. Therefore, the bisection method has been employed to ensure that the correct solution is obtained even though convergence is slower when compared to the secant method.

4.3.2.2 Secondary cracking

Secondary cracks may also form between primary cracks due to the build up of tensile stress in the steel and hence concrete. At the point of minimum steel strain between the primary cracks, where the tensile strain in the concrete is at its maximum, a check is carried out to determine whether a secondary crack has formed. A calculation is made that determines the amount of bond force that is transferred to the concrete by

integrating from one crack along the length of the steel layer to the position of minimum steel strain (Figure 4.18). An effective area for concrete in tension around the steel bar is assumed. The relationship adopted is that proposed in CEB-FIP Model Code (1993).

According to the CEB-FIP Model Code (1993), the effective concrete area in tension accounts for the non-uniform normal stress distribution by bond forces into the concrete cross-section at the end of the transmission length.

For a beam section the effective concrete area in tension is:

$$A_{ct,eff} = b, \left(2.5(h - d_s) < \frac{(h-x)}{3} \right) \tag{4.23}$$

and for a slab section

$$A_{ct,eff} = b, \left(2.5(c + d_s/2) < \frac{(h-x)}{3} \right) \tag{4.24}$$

where b is the section width, c is the cover, d_s is the centroid of tensile reinforcement, h is height of section and x is the width of slab considered.

Knowing the amount of bond force transferred to the surrounding concrete and the effective tensile concrete area, the tensile stress in the surrounding concrete σ_{ct}, can be determined. This calculation is further explained by the following equations:

The transferred bond force equals:

$$T_c = \int_0^{x(\varepsilon_{s\,min})} \tau_s(x).\rho.dx \tag{4.25}$$

where

τ_s = bond stress relative to the steel bar

ρ = $\pi.d_b$

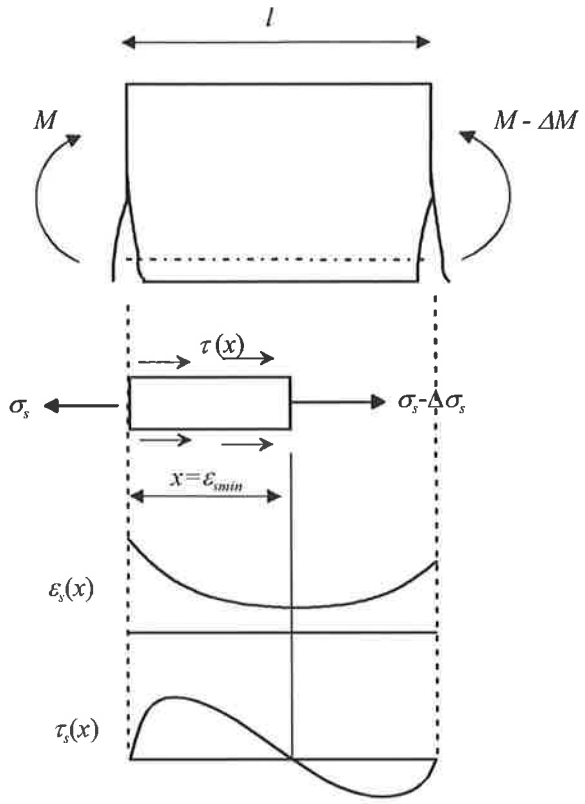

Figure 4.18 Check for secondary crack

4.3.2.3 'Unbound block' element

In order to solve the unbound block element the procedure is applied at Δx increments away from the position of the crack that bounds one end of the 'unbound block' element (Figure 4.19). The Δx increment is applied until the slip equals zero. This position, x_i, at the point of zero slip, represents the transfer length l_{tr}.

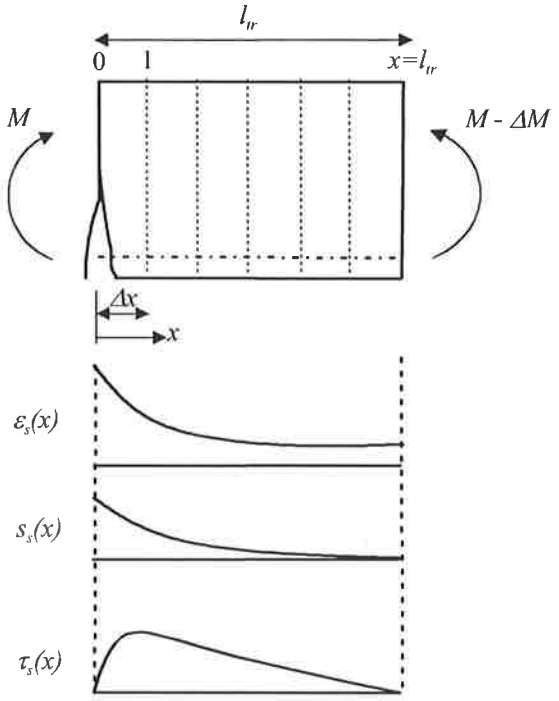

Figure 4.19 Discretisation of 'unbound block' element

At the cracked section where $x_1 = 0$, the tensile steel strain in the reinforcing steel $\varepsilon_s(x_1 = 0)$ can be obtained by applying the section equilibrium and compatibility relations coupled with the material laws introduced in Section 4.3.1. At the position of zero slip where $x_{i+1} = l_{tr}$, the uncracked section profile is assumed and hence $\varepsilon_s(x_{i+1} = 0)$ can be obtained by applying equilibrium and compatibility relations coupled with the material laws as for the cracked section, however, the uncracked strain profile for compatibility is assumed.

The solution procedure for the 'unbound block' element is as follows:

1. Assume a trial value for the maximum slip s_1 ($x_1 = 0$) at the cracked section.

2. Compute $\varepsilon_s(x_1 = 0)$ according to equilibrium Equations 4.8 and 4.9.

3. For $i = i+1$ and $x_{i+1} = x_i + \Delta x$, integrate Equations 4.20 and 4.21, assuming the tensile strain in the concrete to be negligible, to obtain $\varepsilon_{s,i+1}$, $\sigma_{s,i+1}$, s_{i+1} and τ_{i+1}.

4. If $s_{i+1} > 0$ then go to step 3, else go to step 5.

5. By assuming $l_{tr} = x_{i+1}$, and if uncracked conditions are not verified, that is, if $\varepsilon_{s,i+1} \neq \varepsilon_s(x_{i+1} = l_{tr})$, assume a new trial value for maximum slip at crack section and go to step 3.

For the imposed slip value at the crack position, the solution yields the state of deformation distributions along the beam in terms of the tensile stress in the steel and relative bond stress and slip values. As the solution process assumes that the tensile strain in the concrete is negligible compared to the tensile strain in the steel, an assumed distribution for the concrete in tension is adopted (Figure 4.19).

When the bending moment in the cracked section is greater than the cracking moment, M_{cr}, the numerical outcome sometimes can show multiple crack formations at very small spacing within the bond breakdown length l_{tr} (Figure 4.20). Fantilli *et al.* (1999) refer to these cracks as microcracks and have revealed this phenomena in their modelling approach. To overcome the problem they have smeared out the effect by means of an elastic-plastic stress-strain curve for concrete in tension. The smeared concrete in tension relation with no softening slope has also been applied in the presented local deformation analysis. The microcrack affects the development of slips and tensile stresses along the beam, as shown qualitatively in Figure 4.20.

Again it is reminded that the modelling approach presented here differs to the method of Fantilli *et al.* (1999) and Ferretti (1995), since is has extended the analysis past the serviceability range of behaviour and has been applied to continuous beams.

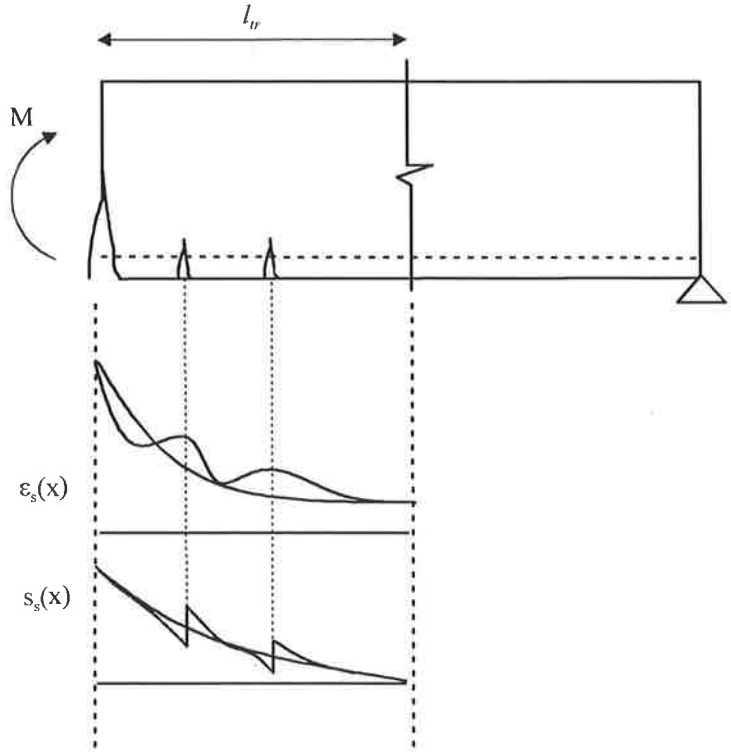

Figure 4.20 Macro and micro cracks

4.3.3 Treatment of Load-pad

An adjustment to the moment diagram is required to account for the influence of the load pad for the beam subjected to a single point load. No adjustment is made to the moment diagram if a uniformly distributed load is applied. The adjustment takes into account the load pad width and the dispersion of the pad pressure into the beam. A 45-degree dispersion to centre of gravity of the element can be assumed. The load pad influences the spread of deformation in the peak moment region, thus the reason for the adjustment to the moment diagram. Similar adjustments have been made by various researchers (Langer, 1987; Cosenza *et al.,* 1991a; and Sigrist, 1995).

Considering the determinate beam in Figure 4.21 subjected to a point load at mid-span, the load pad effect is accounted for by replacing the point load with a uniformly distributed load over the length $2(a+d_{c.g})$. Where a is half the load pad width and $d_{c.g}$ is the distance to the centre of gravity of the element. The hypothetical maximum moment at mid span M^+ is related to the actual maximum moment M_{sp} by the moment reduction factor α.

$$M_{sp}=M^{+}(1-\alpha) \tag{4.26}$$

The moment reduction factor α is statically derived and can be calculated as:

$$\alpha = \frac{a + d_{c.g}}{L} \tag{4.27}$$

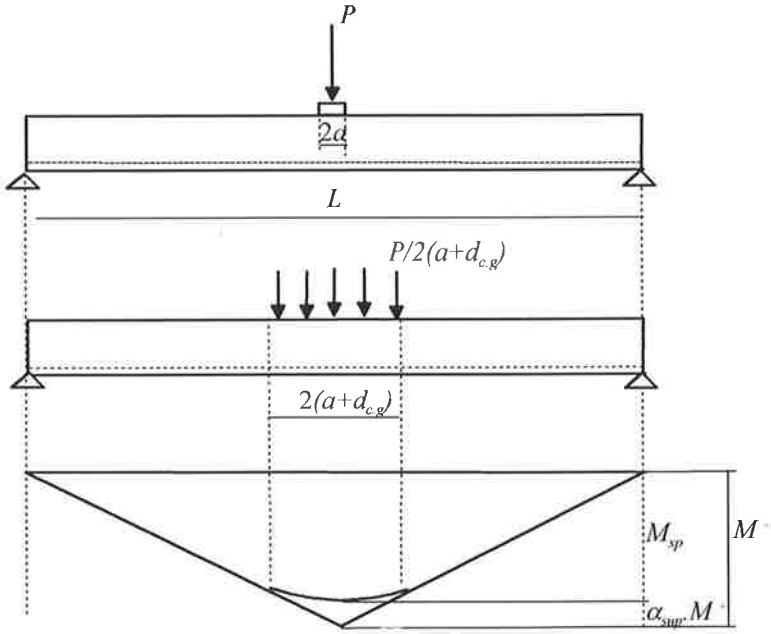

Figure 4.21 Moment diagram including load pad effect

4.3.4 Analytical Procedure

The method predicts the local flexural deformations in a determinate structural beam at all stages of loading, from progressive formation of individual cracks up to failure, induced either by steel fracture or concrete softening. The approach allows the overload behaviour of determinate beams and one-way slabs to be investigated and can determine global deformations such as rotation capacity and deflections.

The analysis proceeds numerically by adopting a deformation control procedure whereby the strain at a driver section chosen to be the section of maximum moment in the span, M_{sp}, is progressively incremented until failure occurs. The extreme concrete local compressive fibre strain or the local tensile steel strain can be incremented in the calculation procedure.

At a particular increment of deformation the moment at the driver section, M_{sp}, is evaluated as in accordance with the equilibrium and compatibility conditions given in

Section 4.3. Since the beam is statically determinate the moment distribution along the length of the beam is fixed by simply statics.

In the analysis due to symmetrical loading only half of the beam is analysed. With the moment distribution known along the beam for a particular increment of deformation, the steps of the analysis are as follows:

1. The beam is divided into a number of cracked and uncracked blocks as explained in Section 4.3. The cracked blocks are pre-determined from the previous load step.

2. The distribution of local deformations over the length of the cracked blocks is carried out considering the bar equilibrium and slip compatibility conditions. An assessment is undertaken to determine whether new cracks have formed at this load stage. That is, a check is made at the minimum steel strain position between two consecutive cracks and at the point of zero slip at the extremity of the cracked region. (Section 4.3). If a new crack has formed the cracked blocks are re-configured to take into account the new crack position.

3. Once it is established that no more new cracks have formed, the remainder of the beam is divided into a number of uncracked blocks. The local deformations between the boundaries of the uncracked blocks are assumed to vary linearly since perfect bond exists, and the moment values are relatively small in comparison to the remainder of the beam region.

4. The block rotations are calculated applying Equation 4.19 and the global deflections and rotations for the structural element are determined by applying the moment-area theorem.

The flow chart in Figure 4.22 summarises the analysis procedure.

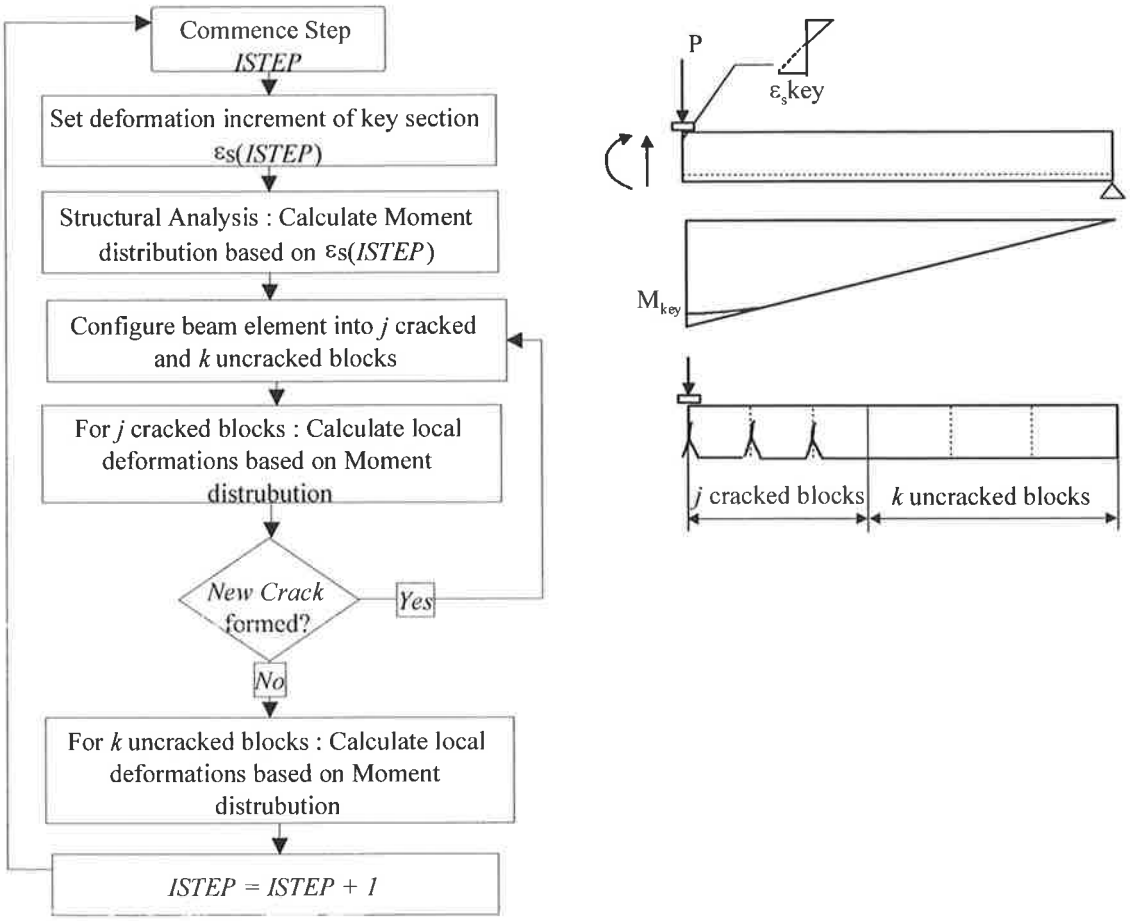

Figure 4.22 Analysis procedure flow chart

4.3.4.1 Post-peak Behaviour

A snap-back phenomenon can occur in the analysis procedure as the load drops off once peak load has been reached. Since the analysis is controlled by local strain deformation not average deformation, the local sections along the structural element length cannot sustain an increase in deformation and must unload, except for the driver section which has an imposed increase in local deformation. All other adjoining sections will unload causing an overall reduction in deformation. In actual fact a finite region along the beam length will continue to increase in deformation. In particular, in the concrete compressive zone the localised strain deformations are affected over a considerable length. This has been demonstrated in many test results (Markeset, 1993; Bigaj, 1999).

To overcome the local deformation drop off in the analysis, so that the post-peak deformations follow the actual behaviour as depicted in experimental curves, the concrete compressive strains are approximated as shown in Figure 4.23.

The post-peak behaviour of the structural element provides an upper limit on the deformation capacity. The deformation capacity of a structural element is related to the peak load, since in the post-peak range of behaviour the material softening parameters for steel in tension are not clearly known. Thus the above approximations to overcome snap back seem reasonable, since accurate representation of deformations post-peak are not entirely necessary within the aims of this investigation.

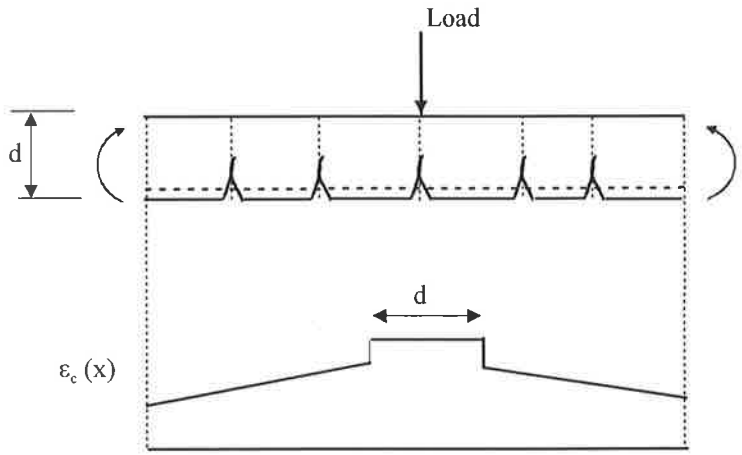

Figure 4.23 Localised concrete strain distribution in compressive zone

4.3.5 Definition of Plastic Rotation

The CEB-FIP Model Code (1993) defines the plastic rotation capacity of the hinge as, *the difference between the total rotation of the hinge at maximum load, and that at the onset of yielding of the reinforcement.*

The plastic rotation of the hinge θ_{pl} is therefore equal to:

$$\theta_{pl} = \theta_{max} - \theta_y \tag{4.28}$$

where θ_{max} and θ_y are the total rotations in the hinge at maximum load and at the onset of yielding of the reinforcement, respectively (Figure 4.24). This definition of plastic rotation is adopted in this thesis.

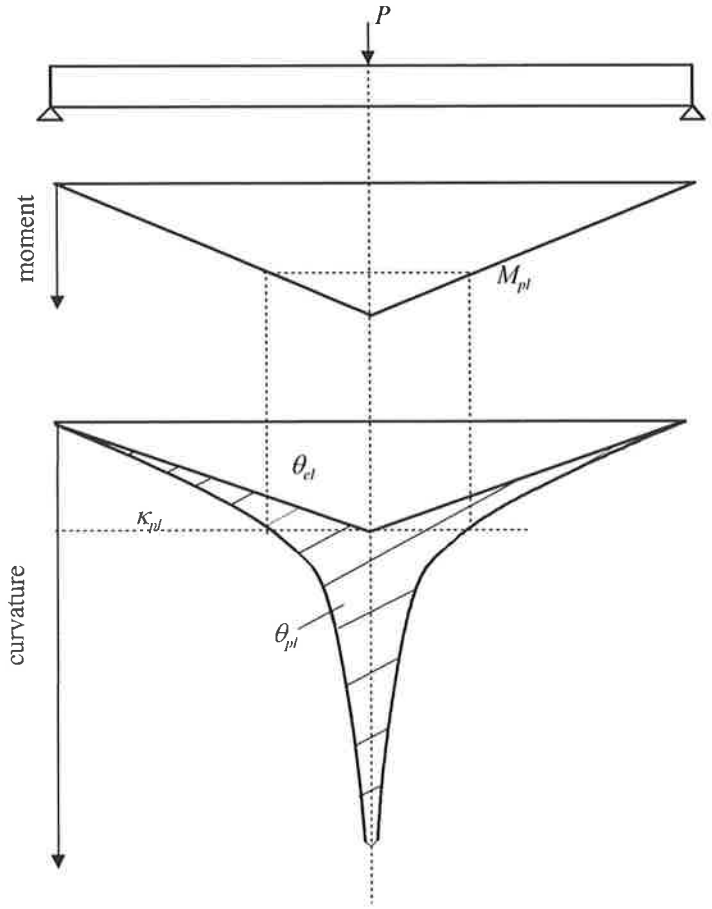

Figure 4.24 Definition of plastic rotation according to CEB-FIP Model Code (1993)

4.3.6 Numerical Example

To demonstrate the use of the computerised analysis procedure, a simply supported beam loaded at mid-span by a single point load with span length equal to 4.8m is chosen. The cross section considered was 300mm in width, 550mm effective depth with a tensile reinforcement percentage of 0.4%. The section was reinforced with ribbed bars 16mm in diameter. The concrete cover was chosen to equal 2 bar diameters. An average concrete strength of 32MPa was used and the steel properties were as follows:

Yield Stress	f_{sy} = 560MPa
Tensile Strength	f_{su} = 640MPa
Uniform elongation	ε_{su} = 4.0%

The analysis is driven by the tensile steel strain at the section of maximum moment at mid-span. At each load step, the moment diagram is known and is calculated based on

simple statics. Iterations are required at each load step to determine stresses and strains at the boundaries of the block elements (ie. at flexural crack positions) and the local deformations between flexural cracks, in accordance with the method explained in Sections 4.3.1 to 4.3.3. The analysis is quite rapid to converge, requiring approximately 5 minutes to analyse a typical determinate beam using a 600MHz processor.

Figure 4.25 shows the distribution of moment along the beam at the four load stages considered: when the first crack forms at mid-span, M_{cr}; at a load stage between the cracking moment and the yield moment, $M_{cr} < M < M_y$; at the onset of yielding, M_y; and at maximum moment, M_{max}. It can be observed that the load pad effect is taken into account by rounding of the moment in the mid-span region.

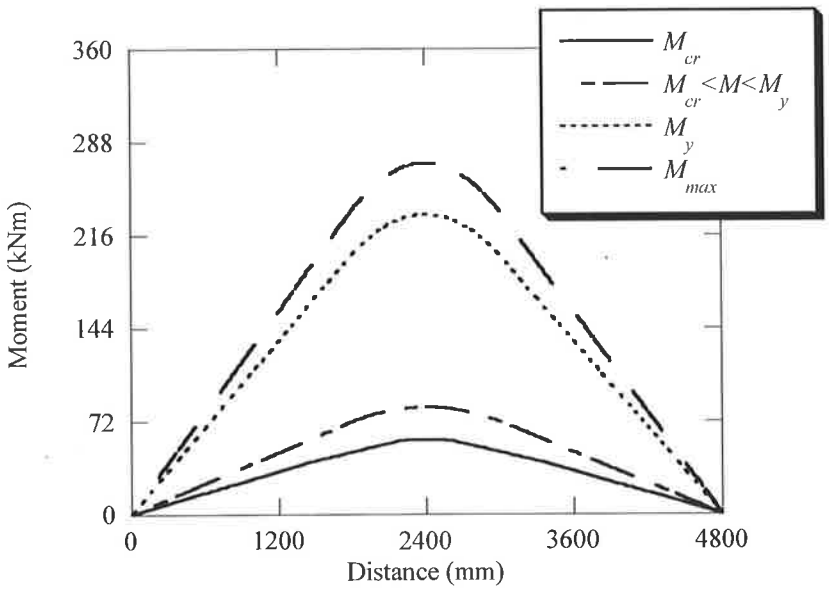

Figure 4.25 Distribution of moment along the beam

For this case, the first crack forms at the mid-span section at a moment value of 57.9kNm. In Figure 4.26 it can been seen that the formation of the crack causes a sudden jump in the tensile steel strain at the mid-span section, from the uncracked to cracked state. The slip and bond stress distributions are also displayed in Figures 4.27 and 4.28.

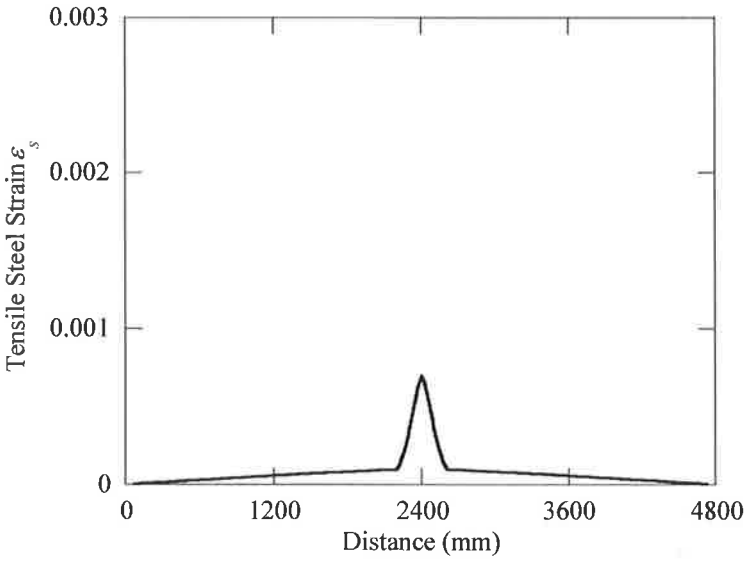

Figure 4.26 Distribution of tensile steel strain at formation of first crack

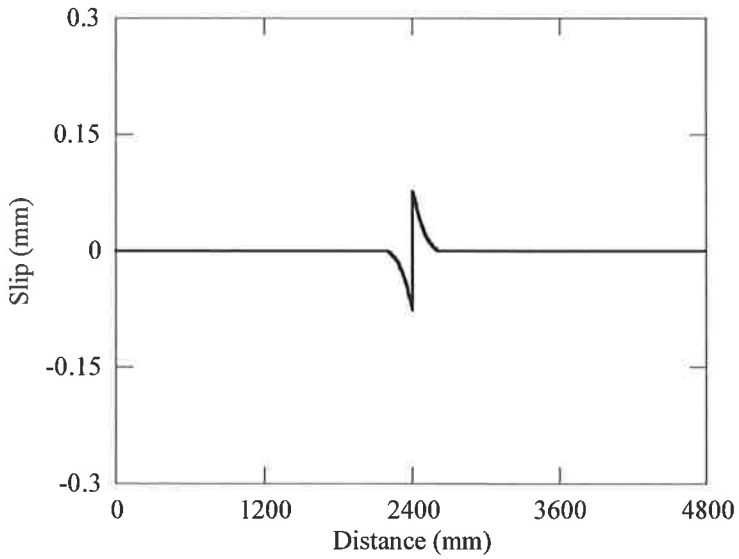

Figure 4.27 Distribution of slip at formation of first crack

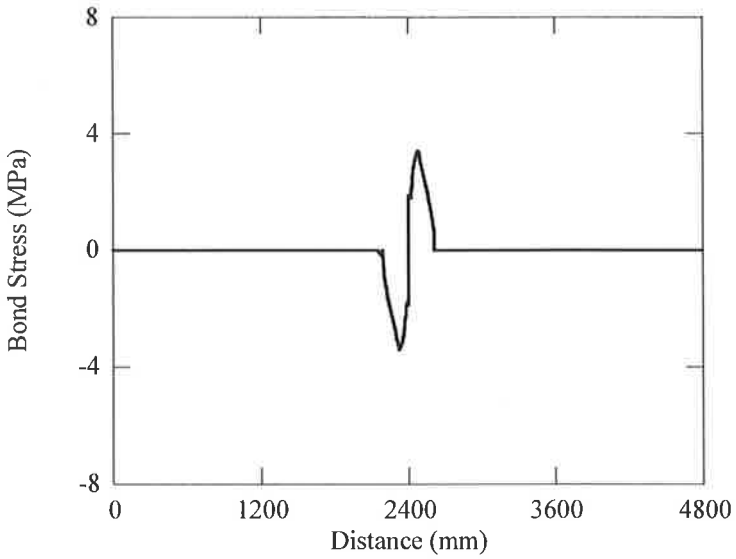

Figure 4.28 Distribution of bond stress at formation of first crack

With further increase in load, additional primary cracks form at a spacing of approximately 220mm (Figure 4.29). Once the yield load has been reached, the cracking pattern has stabilised (Figure 4.30). In addition to further primary cracks forming, secondary cracks have also developed due to the build up of concrete tensile stress between primary cracks. It is interesting to note that the average crack spacing is now approximately 122mm. In Figure 4.30, the uneven dips in the strain distribution are due to the formation of secondary cracks.

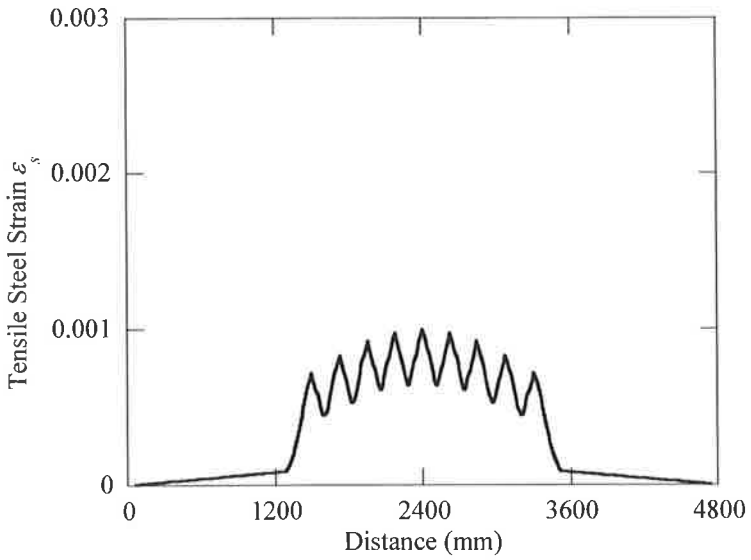

Figure 4.29 Distribution of tensile steel strain at formation of additional primary cracks

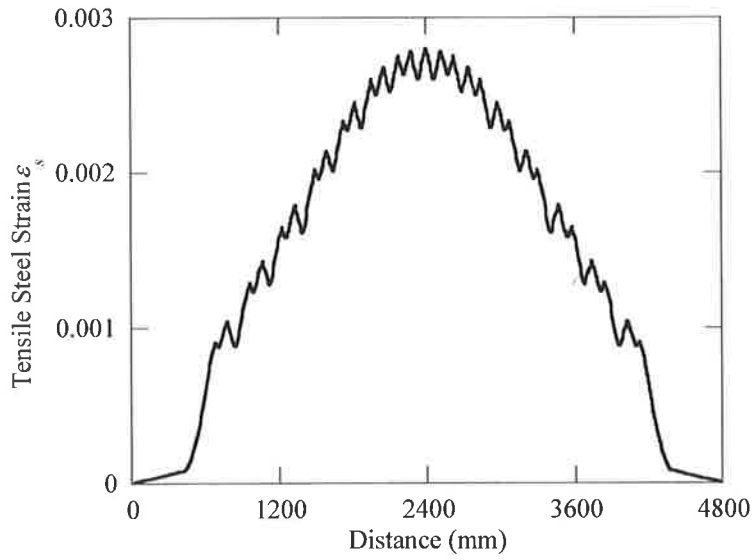

Figure 4.30 Distribution of tensile steel strain at yield load

The failure mode for this example is governed by steel fracture due to the low percentage of tensile reinforcement and low steel ductility adopted. Thus the peak tensile steel strain of 0.04 is reached in the mid-span section at maximum load (Figure 4.30). Figure 4.30 shows the distribution of tensile steel strain along the steel bar at maximum load. The yielded region is defined as the region containing a number of cracks, in which the tensile steel strain exceeds the yield strain of the reinforcing steel.

The plastic hinge length l_p is then equal to the length of this region. For this case the plastic hinge length is equal to 1.16m, approximately two times the section depth.

The maximum crack width at mid-span is calculated from the slip distribution shown in Figure 4.32. At mid-span the maximum slip value on the left side of the crack is -2.3 mm and on the right side is +2.3 mm. The magnitude of the maximum slip values on the left and right side of the crack are equal, due to symmetrical loading. The maximum crack width is calculated as the summation of the absolute maximum slip values on the left and right side of the mid-span crack. The bond stress distribution is shown in Figure 4.33. In Figures 4.32 and 4.33, higher slip and bond stress values exist in the plastic hinge region, as opposed to the non-yielded regions at the extremity of the beam.

The total rotation at the onset of yielding and at maximum load is calculated by integrating the tensile steel strains in Figures 4.30 and 4.31 respectively, together with the concrete compressive strain distributions, assumed to vary linearly between the boundaries of the block elements as described in Section 4.3.1. The plastic rotation is determined in accordance with Equation 4.28. For this case the total rotation at the onset of yield and at maximum load is 0.0168 radians and 0.0663 radians respectively. The plastic rotation capacity is therefore equal to 0.0494 radians.

This section has illustrated the type of results that can be obtained from the analysis program developed for determinate beams incorporating the local deformation model.

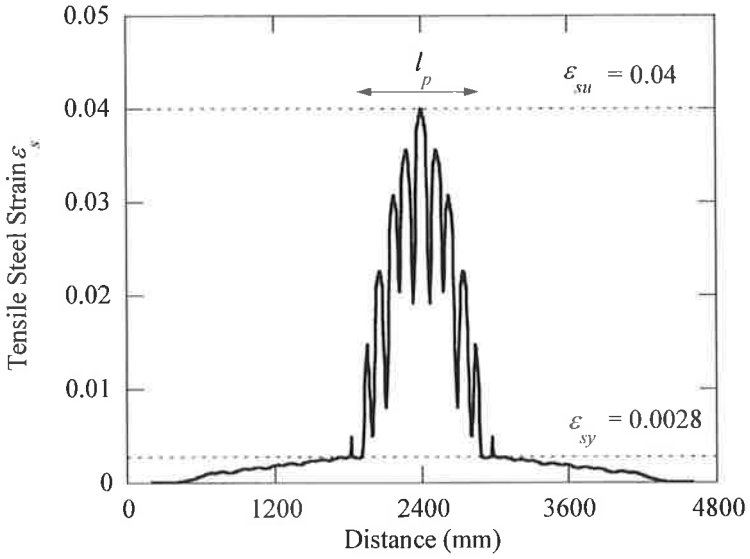

Figure 4.31 Distribution of tensile steel strain at maximum load

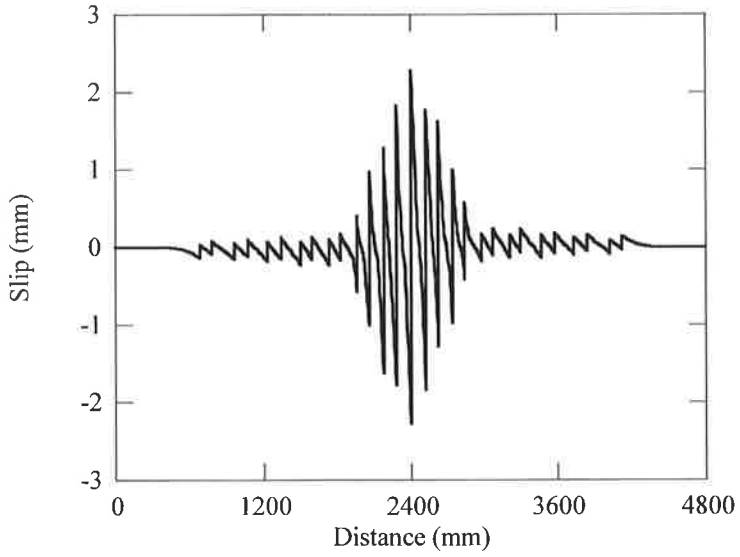

Figure 4.32 Distribution of slip at maximum load

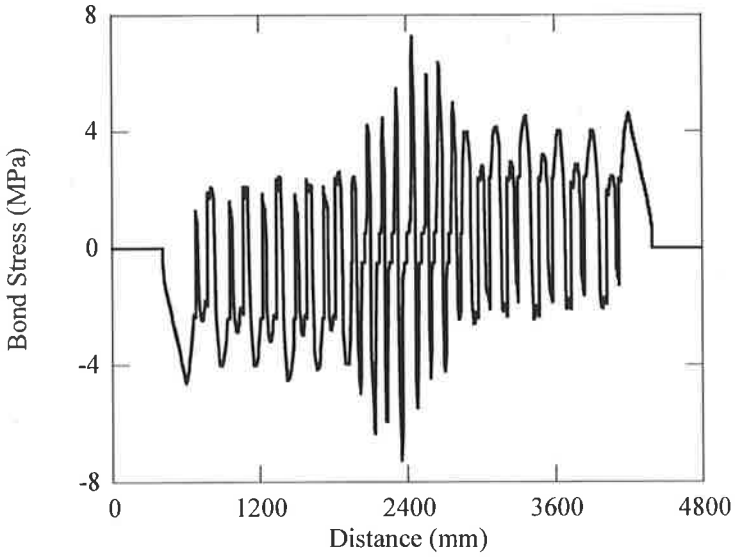

Figure 4.33 Distribution of bond stress at maximum load

4.4 SUMMARY

This chapter introduced a local deformation model that can simulate the distribution of local stresses and strains between flexural cracks. The rotation capacity in plastic hinge regions can thus be determined.

The limitations of the local deformation model are that it is only applied to reinforced concrete beams and one-way slabs subjected predominately to flexure. Therefore flexure crack formations have been assumed. Also the analysis attempts to provide an accurate representation of the behaviour up to the peak load capacity. Post-peak behaviour is approximated. The ability of the local deformation model to predict the flexural behaviour of determinate beams up to peak load capacity will now be discussed in the following chapter.

5

ACCURACY OF LOCAL DEFORMATION MODEL

This chapter utilises previously published beam test data to demonstrate the adequacy of the local deformation model introduced in Chapter 4 to predict rotation capacities, average crack spacing, crack widths, local tensile steel strain distributions, and load deflection curves for determinate beams reinforced with limited ductility steels.

In searching the literature for beam test data, a difficulty was encountered, in that only a few of the reported beam tests gave the necessary data to run the simulation program, such, as the strain-hardening ratio and uniform elongation of the reinforcing steels. Approximately 50 references were surveyed, of which only a few of the published beam tests were adopted for checking the accuracy of the simulation program.

Use has been made of four experimental programs, namely the tests by Eibl and Bühler (1991), Calvi *et al.* (1993), Bigaj and Walraven (1993) and Eifler (1991) in which reinforcing steels with limited ductility, typical of the steels produced in Europe, are used in flexural beam tests. In total 23 beams are used to compare test results with predicted results.

Test results involving Australian reinforcing steels are very limited. However the properties of Australian reinforcing steels are similar to the steels produced in Europe; thus the test programs selected provide useful results of rotation capacity to compare to predicted values. An experimental program was beyond the scope of this investigation. Much work is concentrated on the development of the analytical procedure to simulate local deformations and the extension to indeterminate beams.

5.1 EXPERIMENTAL PROGRAMS

5.1.1 Tests by Eibl and Bühler (1991)

The test program by Eibl and Bühler (1991) investigated the influence of steel properties on the rotational behaviour of reinforced concrete slabs. Six tests were carried out on simply supported, one-way slabs, loaded by a single point load at mid-span with the aim of simulating one-way continuous slab arrangements typically used in house construction in Germany. A load pad width of 100mm was used in the tests. The dimensions of the test specimen were kept constant and were 800mm in width, 180mm thick and span equal to 2m, with a total length of 2.2m. The effective depth of the cross section was 160mm with concrete cover of 20mm. The reinforcement area was chosen to be equal to $A_{st} = 303mm^2$. The diameter of the bars were 8mm.

The test specimens were reinforced with ribbed welded mesh, ribbed unwelded bars and smooth welded mesh. The reinforcement used varied in steel ductility properties and various tests were performed to determine the main steel properties. Table 5.1 summarises the average steel properties of the slabs tested. Only five of the six tests were used in the simulation. Test number RPL3 was eliminated since it was reinforced with smooth wires. This investigation is only interested in the behaviour of ribbed bars and ribbed wire used in fabric reinforcement, since the bond model used is applicable to ribbed bars. The average concrete cylinder strength was equal to 27MPa. The total rotation at first yield, total rotation at maximum load and deflections and crack widths at the mid-span crack were recorded in the tests.

Table 5.1 Mechanical properties of reinforcing steel, in tests by Eibl and Bühler (1991)

Specimen	Steel Type	f_{sy} (MPa)	f_{su} (MPa)	f_{su}/f_{sy}	ε_{su} (%)
RPL1	Ribbed Welded mesh	703	732	1.04	2.0
RPL2	Ribbed unwelded mesh	502	594	1.16	10.4
RPL4	Ribbed welded mesh	590	629	1.08	4.4
RPL5	Ribbed welded mesh	590	629	1.08	4.4
RPL6	Ribbed unwelded	532	612	1.17	4.3

5.1.2 Tests by Calvi *et al.* (1993)

The experimental program by Calvi *et al.* (1993) involved the testing of 36 specimens

simply supported slabs in 12 test series (3 nominally identical beams per series). The main parameters of the test were the type of reinforcing mesh, varying bar diameter (6mm or 10mm) with varying bar spacing (100mm and 200mm), bond properties (smooth or high bond) and the steel quality (heat treated or cold worked). Table 5.2 summarises the test program and material parameters. Ten of the twelve test series involved simply supported slabs loaded at mid-span by a single point load. In test series S09 and S10, the beams were loaded by four point loads.

Only test series S01, S02, S04, S05 and S07 reinforced with ribbed wires were considered in the simulations. The remaining test series were reinforced with smooth wires or the loading arrangement did not involve a single point load. The load pad width was not recorded hence a load pad width of 100mm was assumed. In the tests chosen the span length was equal to 2m. The cross section of the specimens was kept constant to 440mm in width, 160mm in depth. Compression reinforcement consisting of bars 6mm in diameter with a spacing of 200mm was used. The tensile reinforcement percentage varied between 0.64% and 0.23%. The effective depth of the tensile reinforcement was 140mm with concrete cover of 20mm. The concrete strength was kept constant. On average the concrete compressive cylinder strength was 38MPa.

Table 5.2 Test specimens and material parameters, in tests by Calvi *et al.* (1993)

Specimen	Steel Type	Bar surface	f_{sy} (MPa)	f_{su} (MPa)	f_{su}/f_{sy}	ε_{su} (%)	Main reo.	ρ (%)
S01	B	Ribbed	609	667	1.1	3.4	5 d_b 10	0.6
S02	A	Ribbed	584	653	1.12	7.9	5 d_b 10	0.64
S03	B	Smooth	589	633	1.08	4.0	5 d_b 10	0.64
S04	-	Ribbed	619	657	1.06	2.3	3 d_b 6	0.23
S05	A	Ribbed	611	738	1.21	5.6	3 d_b 6	0.23
S06	B	Smooth	581	616	1.06	2.8	3 d_b 6	0.23
S07	B	Ribbed	575	619	1.09	2.9	3 d_b 10	0.38
S08	B	Smooth	589	630	1.07	3.8	3 d_b 10	0.38
S11	-	Smooth	575	619	1.08	2.4	3 d_b 6	0.23
S12	-	Smooth	574	594	1.03	2.8	3 d_b 6	0.23
S092)	-	Ribbed	619	657	1.06	2.3	3 d_b 6	0.23
S102)	B	Smooth	581	616	1.06	2.8	3 d_b 6	0.23

Note: reo. = reinforcement

In the experimental program the rotations were measured by specially designed inclinometers that were positioned symmetrically to the centre line. The distance

between inclinometers was 250mm and 450mm respectively.

5.1.3 Tests by Bigaj and Walraven (1993)

The aim of the test program by Bigaj and Walraven (1993) was to investigate the size effect on the rotation capacity of plastic hinges in reinforced concrete beams and to investigate the localisation process in the hinge region, in particular in the compression zone of the member. The test program was limited to three prime parameters; member size, reinforcement ratio, and concrete mix composition. A total of ten specimens were tested, each having the same span/height/width ratio. The specimens were simply supported beams loaded at mid-span by a single point load. Three different beam sizes (span = 1, 2 and 5 metres) were used. Two reinforcement ratios were used (ρ = 0.28% and 1.12%). The concrete strength was kept constant (average cylinder strength 28MPa). Two concrete mixes were used with varying maximum aggregate size (4 and 16mm). The details of the beams are summarised in Table 5.3. The beams were reinforced with ribbed bars. The steel properties are presented Table 5.4. Rotations at maximum load, and at the onset of yielding were recorded.

Table 5.3 Specimen details, in tests by Bigaj and Walraven (1993)

Specimen	*H* (mm)	*d* *(mm)*	*B* (mm)	*reo.*	ρ *(%)*	*L* (mm)	*L/d*	Max Aggr. Size (mm)	f'_{cm} (MPa)
B.0.1.4	120	90	50	1 d_b 4	0.28	1000	11.1	4	25.4
B.0.2.4	210	180	100	1 d_b 8	0.28	2000	11.1	4	27.5
B.0.3.4	490	450	250	4 d_b 10	0.28	5000	11.1	4	26.8
B.0.2.16	210	180	100	1 d_b 8	0.28	2000	11.1	16	32.5
B.0.3.16	490	450	250	4 d_b 10	0.25	5200	11.5	16	29.8
B.1.1.4	120	90	50	1 d_b 8	1.12	1000	11.1	4	26.5
B.1.2.4	210	180	100	1 d_b 16	1.12	2000	11.1	4	28.2
B.1.3.4	490	450	250	4 d_b 20	1.12	5200	11.5	4	25.8
B.1.2.16	210	180	100	1 d_b 16	1.12	2000	11.1	16	31.8
B.1.3.16	490	450	250	4 d_b 20	1.12	5200	11.5	16	28.3

Note: reo. = reinforcement and Aggr. = aggregate

Table 5.4 Steel properties, in tests by Bigaj and Walraven (1993)

Ribbed bar diameter	f_{sy} (MPa)	f_{su} (MPa)	f_{su}/f_{sy}	ε_{su} (%)	Steel type
4	590	678	1.15	3.7	B
8	562	641	1.14	6.2	A
10	568	641	1.13	6.4	A
16	573	661	1.15	6.9	S
20	550	650	1.18	7.7	S

5.1.4 Tests by Eifler (1991)

The aim of the experimental program by Eifler (1991) was to investigate the influence of the reinforcement percentage, the shape of the beam section, the type of steel and the load application. The experiments involved five reinforced concrete T-beams, and two rectangular beams. The two rectangular beams, 4m in length, simply supported and subjected to a uniformly distributed load have been chosen for the purpose of verification. Table 5.5 summarises the two specimen details. The properties of the reinforcing steel were of normal ductile steel produced by hot-rolling. Table 5.6 presents the properties of the reinforcing steels used in the simulation. An average concrete cylinder strength of 31MPa was adopted for the two tests.

Table 5.5 Specimen details, in tests by Eifler (1991)

Specimen	H (mm)	B (mm)	ρ (%)	D (mm)	d_b (mm)	No. bars
R10	440	160	0.52	387	10	4
R16	440	160	1.32	380	16	4

Table 5.6 Steel properties, in tests by Eifler (1991)

Specimen	f_{sy} (MPa)	f_{su} (MPa)	f_{su}/f_{sy}	ε_{su} (%)
R10	510	670	1.31	11.0
R16	487	619	1.27	11.6

5.2 TENSILE STEEL STRAIN DISTRIBUTION

The distribution of tensile steel strain along the beam is closely related to the amount of tension stiffening between flexural cracks, and can indicate the spread of the yielded region, and thus the plastic hinge length. Since the rotation capacity of critical regions is

a result of the integration of such local strains over a finite length, the analysis procedure is required to predict local tensile steel strains accurately.

The experimental program by Eifler (1991), described in Section 5.1.4, has been used to show how the model can predict the local tensile steel strain distribution. In the testing program the steel elongation values were measured by marking the bar at 30mm intervals before placing the concrete. On completion of the testing, the bars were removed from the specimens and the elongations of the markings on the bar were measured. Thereby the plastic steel strain values were recorded.

For the test specimens R10 and R16, Figures 5.1 and 5.2 show the simulation results of the tensile steel strain distribution at ultimate load, compared to the measured tensile steel strain taken from the tests. The measured tensile steel strains plotted include the yield and plastic steel strains.

Specimens R10 and R16 were reinforced with low and high steel percentages respectively, Figures 5.1 and 5.2 show good agreement between the tensile steel strain values based on the measured and simulated results. The spread of the yielded region is also well predicted. Table 5.7 summarises the maximum tensile steel strain, plastic hinge lengths, yield moment, maximum moment, and the maximum rotation at peak load.

Table 5.7 Comparison of measured results with simulation values for specimens R10 and R16, test by Eifler (1991)

	M_{pl} (kNm)		M_{max} (kNm)		s_{rm} (mm)		$\varepsilon_{s,max,pl}$ (%)		l_p (mm)	
	Model	Test	Model	Test	Model	Test	Model	Test	Model	Test
R10	58.4	62.5	71.6	70.5	126	139	5.1	5.2	1280	1140
R16	132	134	139	140	149	128	2.5	2.1	596	440

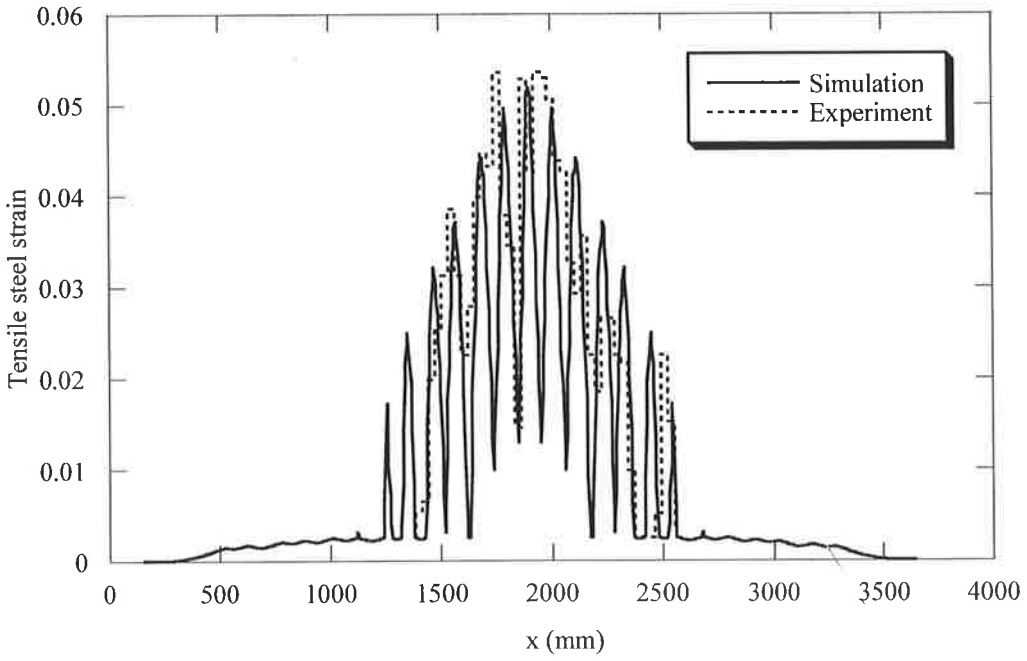

Figure 5.1 **Comparison of measured local tensile steel strain distribution with simulation values, specimen R10, test by Eifler (1991)**

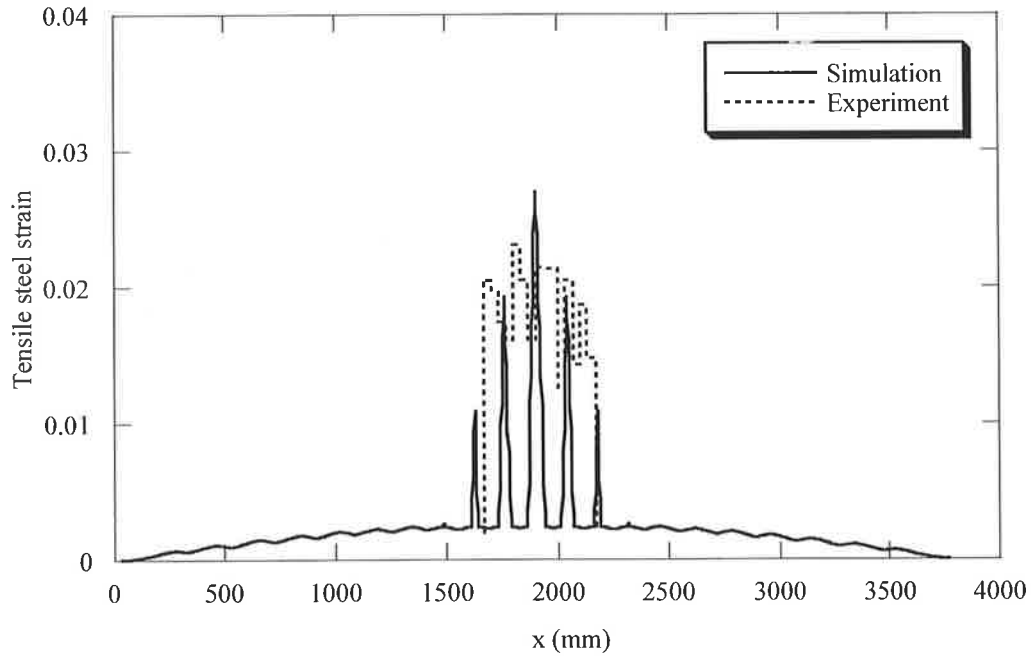

Figure 5.2 **Comparison of measured local tensile steel strain distribution with simulation values, specimen R16, test by Eifler (1991)**

5.3 ROTATION CAPACITY

Here the ability of the local deformation model to predict the rotation capacity of reinforced concrete structural elements is investigated. Tables 5.8 to 5.10 compare simulation results with measured results of the rotation capacities at maximum load, θ_{max}, at the onset of yielding, θ_y, and the plastic rotation, θ_{pl}. The plastic rotation is defined as the difference between the rotation at maximum load and the rotation at first yield. When evaluating the plastic rotation the correct assessment of the yield moment and of the corresponding rotation is important. Tables 5.8 to 5.10 also compare the moments or loads at yield and at the maximum load stage.

Table 5.8 Summary of test and simulation results, tests by Eibl and Bühler (1991)

Rotation Capacities						
Specimen	**Measured Values**			**Simulation Results**		
	θ_y (rad)	θ_{max} (rad)	θ_{pl} (rad)	θ_y (rad)	θ_{max} (rad)	θ_{pl} (rad)
RPL1	0.018	0.029	0.012	0.019	0.029	0.010
RPL2	0.005	0.034	0.023	0.011	0.046	0.035
RPL4	0.008	0.019	0.011	0.016	0.028	0.012
RPL5	0.012	0.028	0.016	0.016	0.030	0.014
RPL6	0.008	0.025	0.017	0.011	0.032	0.021

Moments				
Specimen	**Measured Values**		**Simulation Results**	
	M_y (kNm)	M_{max} (kNm)	M_y (kNm)	M_{max} (kNm)
RPL1	30.5	34.7	31.7	34.0
RPL2	21.9	29.7	22.6	25.9
RPL4	25.7	31.8	26.6	29.2
RPL5	25.7	31.1	26.6	29.3
RPL6	23.2	30.9	24.2	28.8

Table 5.9 Summary of test and simulation results, tests by Calvi *et al.* (1993)

Rotation Capacities						
Specimen	**Measured Values Measurement length = 250mm**			**Simulation Results Measurement Length = 250mm**		
	θ_y (rad)	θ_{max} (rad)	θ_{pl} (rad)	θ_y (rad)	θ_{max} (rad)	θ_{pl} (rad)
S01	0.009	0.027	0.017	0.011	0.025	0.014
S02	0.006	0.089	0.083	0.011	0.030	0.019
S04	0.004	0.011	0.007	0.008	0.013	0.005
S05	0.005	0.033	0.028	0.008	0.030	0.022
S07	0.006	0.024	0.018	0.008	0.018	0.010
Specimen	**Measured Values Measurement length = 450mm**			**Simulation Results Measurement Length = 450mm**		
	θ_y (rad)	θ_{max} (rad)	θ_{pl} (rad)	θ_y (rad)	θ_{max} (rad)	θ_{pl} (rad)
S01	0.144	0.035	0.021	0.017	0.031	0.014
S02	0.013	0.099	0.086	0.012	0.031	0.020
S04	0.009	0.018	0.009	0.012	0.018	0.005
S05	0.010	0.047	0.037	0.010	0.033	0.023
S07	0.014	0.036	0.023	0.012	0.022	0.010
Moments						
Specimen	**Measured Values**			**Simulation Results**		
	M_y (kNm)	M_{max} (kNm)		M_y (kNm)	M_{max} (kNm)	
S01	30.6	34.0		30.5	34.4	
S02	27.9	31.9		29.3	31.9	
S04	11.9	13.2		11.6	13.1	
S05	11.9	15.2		11.4	14.9	
S07	18.8	21.2		17.6	20.0	

Table 5.10 Summary of test and simulation results, tests by Bigaj and Walraven (1993)

Rotation Capacities						
Specimen	**Measured Values**			**Simulation Results**		
	θ_y (rad)	θ_{max} (rad)	θ_{pl} (rad)	θ_y (rad)	θ_{max} (rad)	θ_{pl} (rad)
B.0.1.4	0.001	0.027	0.017	0.012	0.030	0.018
B.0.2.4	0.013	0.077	0.063	0.011	0.040	0.029
B.0.3.4	0.004	0.033	0.029	0.007	0.025	0.018
B.0.2.16	0.012	0.087	0.075	0.009	0.032	0.023
B.0.3.16	0.010	0.047	0.037	0.011	0.029	0.018
B.1.1.4	0.024	0.061	0.038	0.020	0.024	0.040
B.1.2.4	0.019	0.031	0.013	0.017	0.019	0.003
B.1.3.4	0.070	0.016	0.009	0.009	0.010	0.001
B.1.2.16	0.019	0.032	0.012	0.016	0.020	0.004

Loads				
Specimen	**Measured Values**		**Simulation Results**	
	P_y (kN)	P_{max} (kN)	P_y (kN)	P_{max} (kN)
B.0.1.4	2.5	3.3	2.5	2.9
B.0.2.4	10.3	11.3	9.5	11.2
B.0.3.4	50.2	54.9	60.0	69.5
B.0.2.16	10.4	11.4	9.5	11.3
B.0.3.16	50.1	59.2	57.8	67.5
B.1.1.4	9.8	10.6	8.7	9.0
B.1.2.4	35.0	35.7	35.7	37.1
B.1.3.4	210.2	214.8	204.7	212.3
B.1.2.16	38.5	39.8	36.1	37.8

The rotation capacities at yield and maximum load are presented in Figures 5.3 to 5.6. For the experimental program by Eibl and Bühler (1991), only a slight scatter of results between measured and simulated results is present which reflects the favourable comparison between measured and simulated moment values at yield, and maximum load shown in Table 5.8.

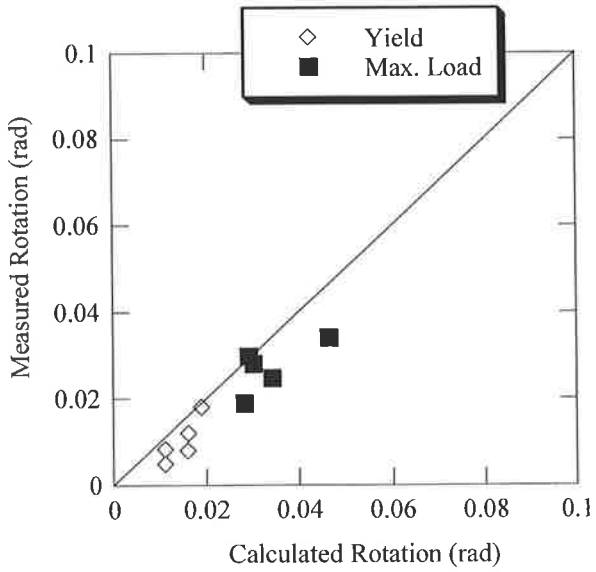

Figure 5.3 Comparison of measured rotations at yield and maximum load with simulation values, tests by Eibl and Bühler (1991)

With regard to the testing program by Calvi *et al.* (1993), the comparison of measured and simulated rotation capacities based on a 250mm and 450mm gauge length are shown. In general the measured rotations are greater than the simulated rotations at maximum load. The influence of the measuring gauge length has been shown to provide slight differences. The large difference in results of test specimen S02 is unaccounted for, but may be attributed to the variability of material behaviour in the testing environment.

The experimental programs by Eibl and Bühler (1991) and Calvi *et al.* (1993) have shown the ability of the local deformation model to predict the rotation capacity of reinforced concrete members with varying steel properties.

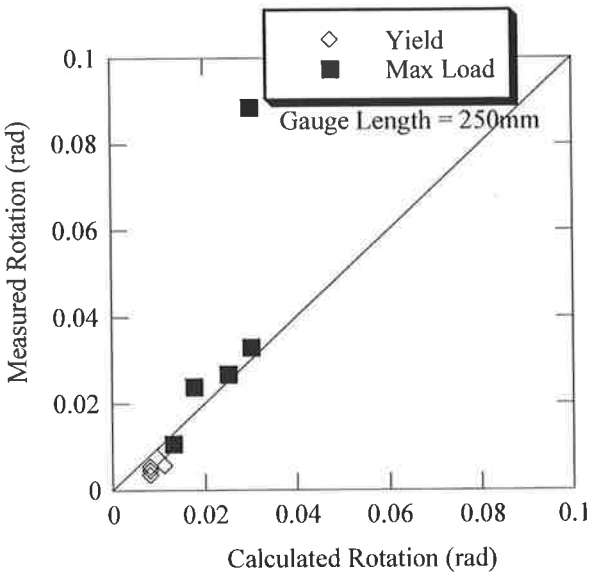

Figure 5.4 Comparison of measured rotations at yield and maximum load with simulation values, tests by Calvi *et al.* (1993), Gauge length 250mm

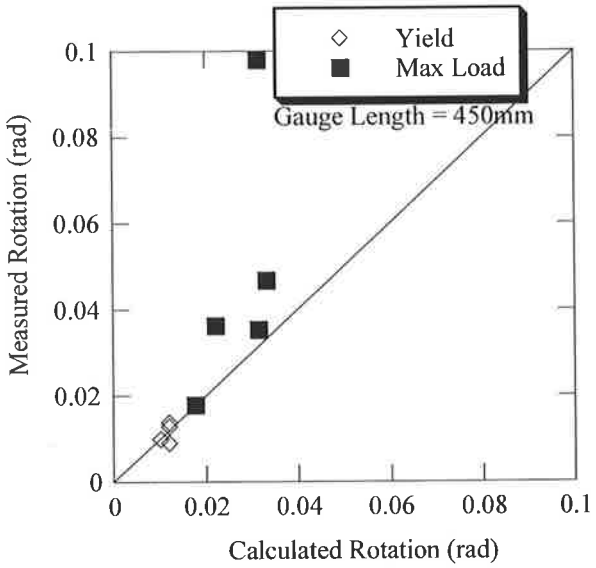

Figure 5.5 Comparison of measured rotations at yield and maximum load with simulation values, tests by Calvi *et al.* (1993), Gauge length 450mm

Further to the above experiments that investigated the influence of varying material properties, the beam designs by Bigaj and Walraven (1993) took into account the size effect, in addition to varying steel properties. Therefore the experimental program by Bigaj and Walraven (1993) can determine the ability of the local deformation model to consider size effect in the evaluation of rotation capacities.

Comparison of measured and simulated rotation capacities from the experimental program by Bigaj and Walraven (1993) agreed sufficiently well. However for test specimens B.0.2.4, B.0.2.16 and B.1.1.4, the measured rotation capacities are about 2.5 times larger than the calculated values (Table 5.10). These tests had a width of 100mm and reinforced with a single bar 8mm in diameter. It is believed that the unusual reinforcement layout influenced the high measured rotation values. Also, in such a specimen there would not be much confinement of concrete and excessive spalling of the concrete would have taken place.

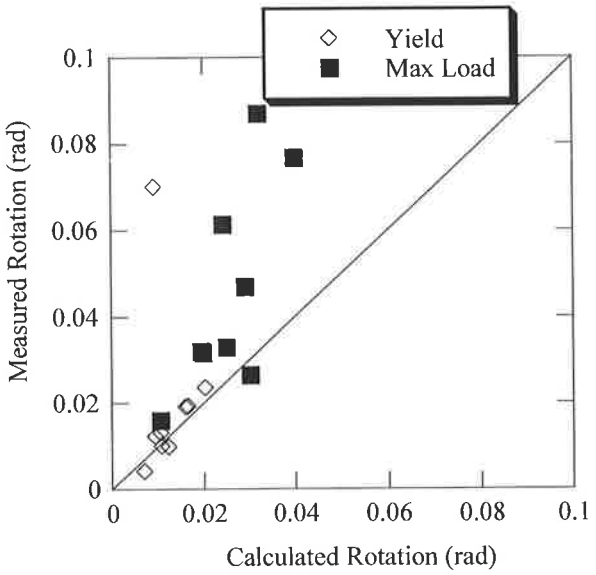

Figure 5.6 Comparison of measured rotations at yield and maximum load with simulation values, tests by Bigaj and Walraven (1993)

The plastic rotations for the beam tests considered are summarised in Figure 5.7. For a few cases, namely S02, B.0.2.4 and B.1.1.4, the model greatly underestimates the plastic rotational capacity. The differences in results have been explained in the preceding paragraphs and were due mainly to unusual reinforcement layouts. It should be noted here that the differences in measured and calculated results can be attributed to the bond parameters used in the simulations. However, generally it can be observed in Figure 5.7 that the simulation program is able to produce safe and conservative results.

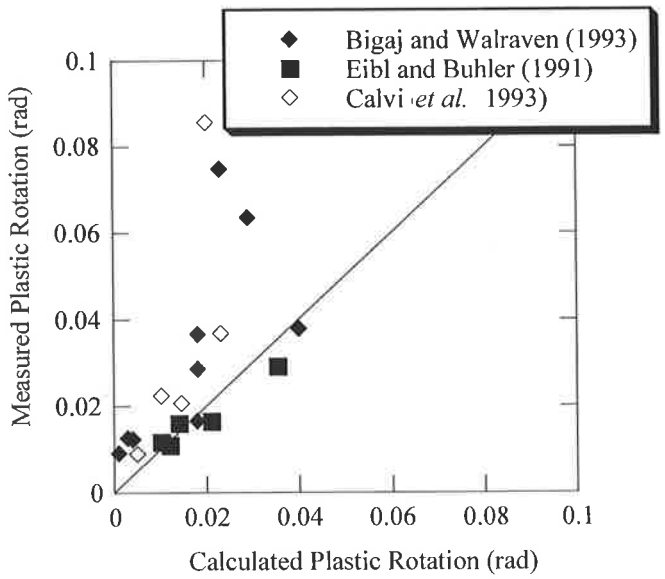

Figure 5.7 Comparison of measured plastic rotations with simulation values, tests by Eibl and Bühler (1991), Calvi *et al.* (1993) and Bigaj and Walraven (1993)

5.4 AVERAGE CRACK SPACING

The simulation program is unique to previously developed models (see Chapter 3) since an average crack spacing is not assumed. Instead the crack spacing is solved as a solution to the problem and considers the member geometry, bond characteristics and material strength, in comparison to the majority of crack spacing formula that are based on the bar diameter, concrete cover and the effective reinforcement ratio (CEB-FIP, 1993; Eurocode No.2, 1990).

In the analysis procedure, the progressive formation of flexural cracks in moment gradient regions is determined and an average crack spacing is calculated at every load stage. For the purpose of comparison, the calculated average crack spacing is taken at maximum load, however, when yielding occurs the cracking pattern has stabilised. The development of crack patterns and consequently crack locations affect the local deformation in plastic hinge regions, therefore successful crack spacing predictions are needed.

The measured average crack spacing from the experimental results of Eibl and Bühler (1991), Calvi *et al.* (1993), Bigaj and Walraven (1993) and Eifler (1991) have been used

to compare calculated average crack spacing (Figure 5.8). Eibl and Bühler (1991) reported that in general, the crack spacing obtained for all 6 specimens was approximately 150mm, which related to the spacing of transverse tensile reinforcement. This explains why only one point relating to the experimental program by Eibl and Bühler (1991) is plotted. In Figure 5.8 good correlation is shown between the measured and calculated average crack spacing. Therefore the modelling procedure is able to take into consideration not only the steel properties, but also the size effect when determining the crack spacing for flexural members.

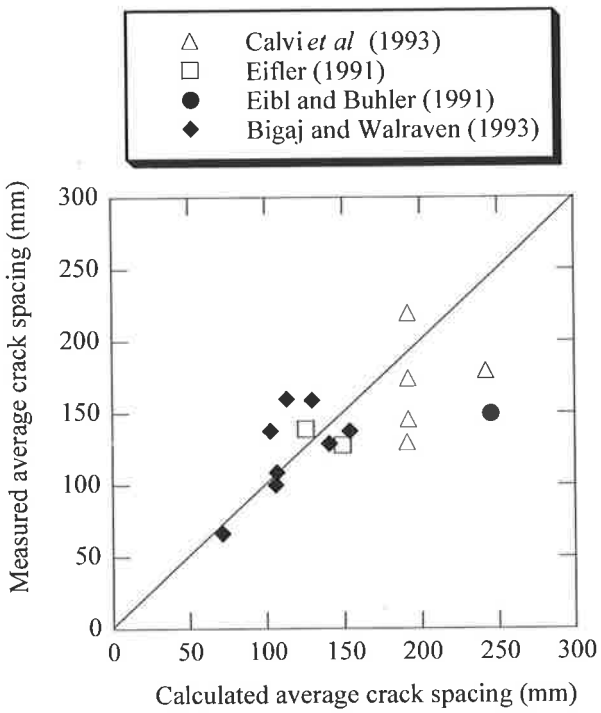

Figure 5.8 Comparison of measured and calculated average crack spacing

5.5 LOAD-CRACK WIDTH CURVE

To further reinforce the ability of the model to simulate local deformations, use has been made of the load versus maximum crack width plots taken from the experimental program by Eibl and Bühler (1991). The ability of the simulation program to predict rotation capacity can also be related to the measurement of crack widths.

The experimental program by Eibl and Bühler (1991) presented results on load versus maximum crack width relating to the mid-span crack. In the analysis it is assumed that

the first crack will form at this position of maximum moment. The experimental programs of Calvi *et al.* (1993) and Bigaj and Walraven (1993) have not presented results of load versus crack width measurements and therefore have not been considered in the comparison of crack widths.

Figures 5.9 to 5.13 displays the comparison between simulated and measured crack widths at all stages of loading. Agreeable findings resulted up to the peak load capacity. The extent of the model to predict crack widths depend upon the local bond-slip model used and the parameters adopted. Post-peak, the crack widths are greatly under-estimated. It should be remembered that the analysis procedure is concerned with the behaviour up to the peak load. The behaviour up to the peak load provides a lower bound and conservative result. Post–peak behaviour predicted by the analysis procedure is not reliable and this is represented in the figures.

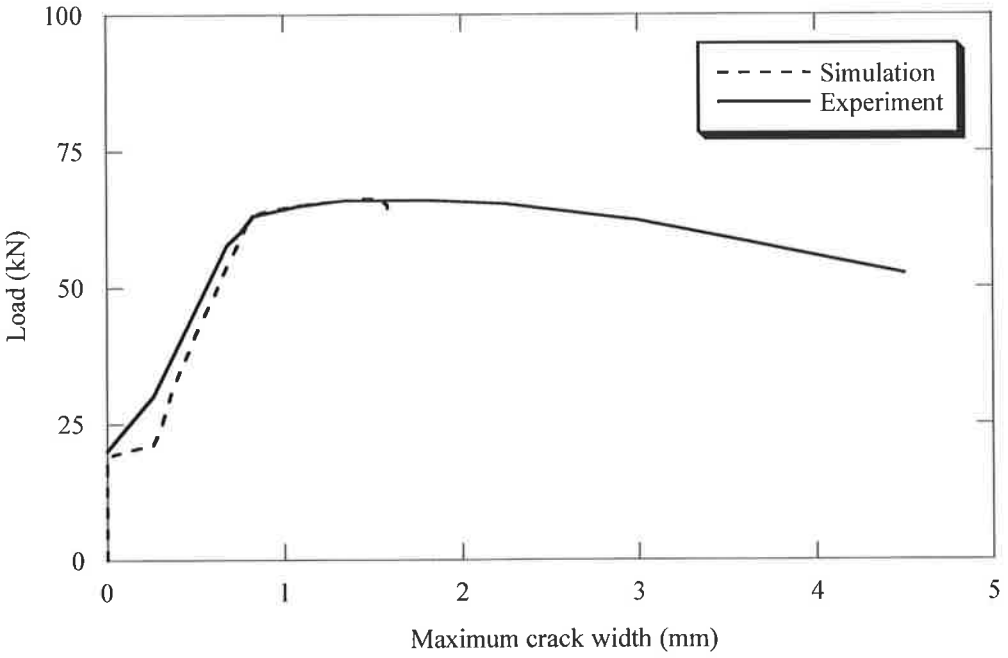

Figure 5.9 Comparison of measured load versus maximum crack width with simulation values, specimen RPL1, test by Eibl and Bühler (1991)

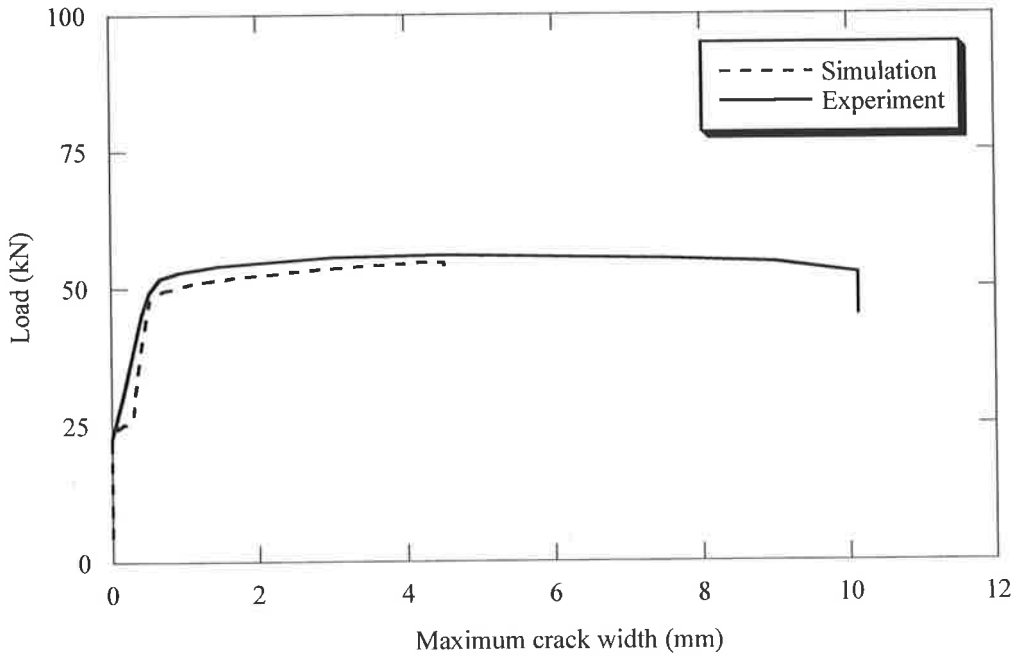

Figure 5.10 Comparison of measured load versus maximum crack width with simulation values, specimen RPL2, test by Eibl and Bühler (1991)

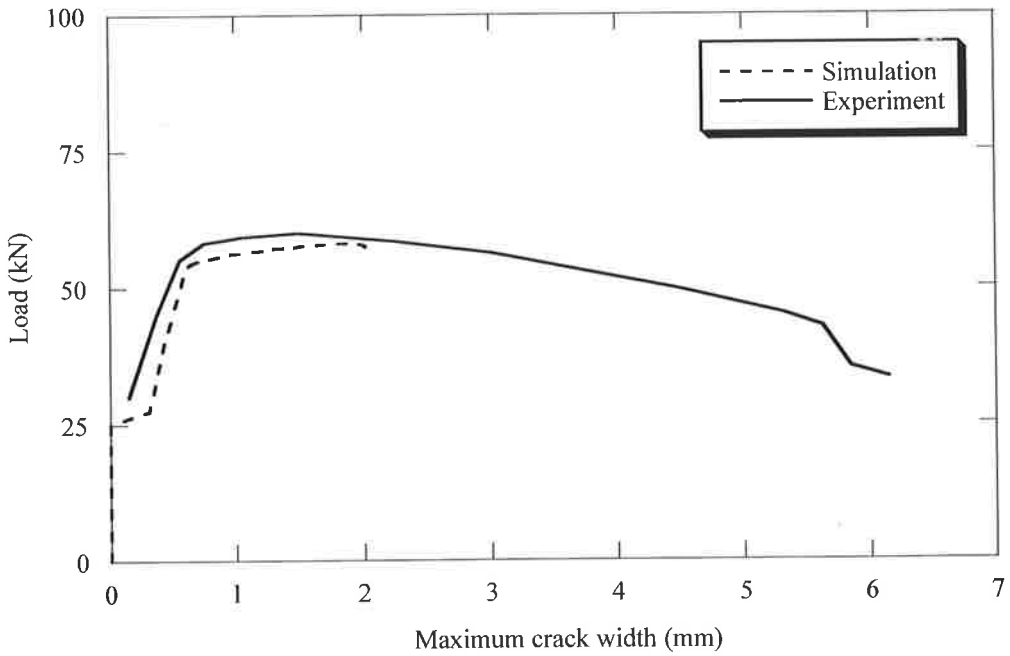

Figure 5.11 Comparison of measured load versus maximum crack width with simulation values, specimen RPL4, test by Eibl and Bühler (1991)

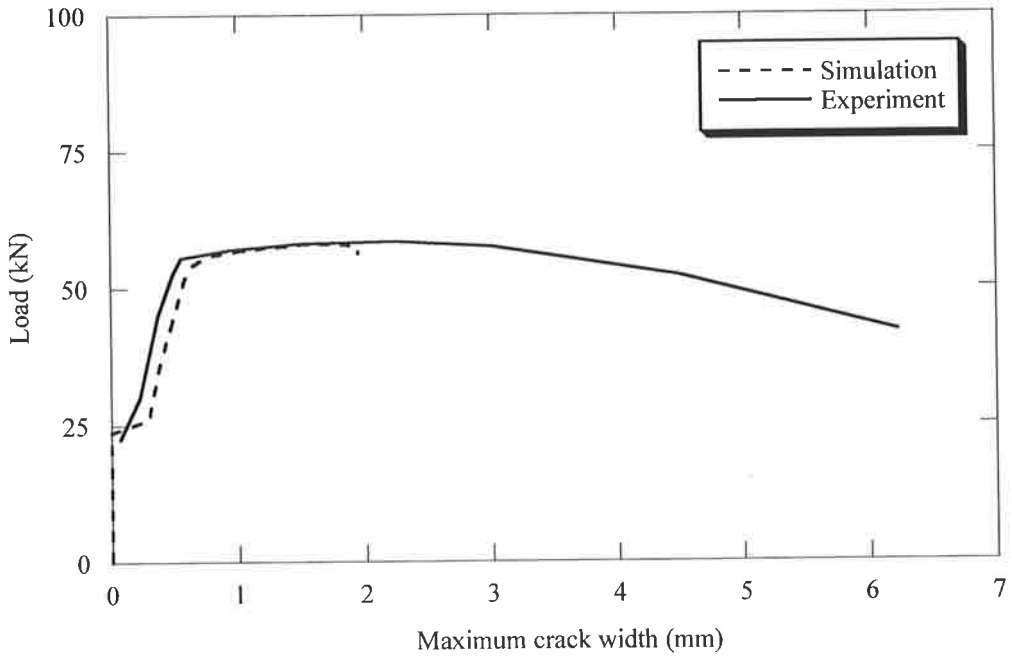

Figure 5.12 Comparison of measured load versus maximum crack width with simulation values, specimen RPL5, test by Eibl and Bühler (1991)

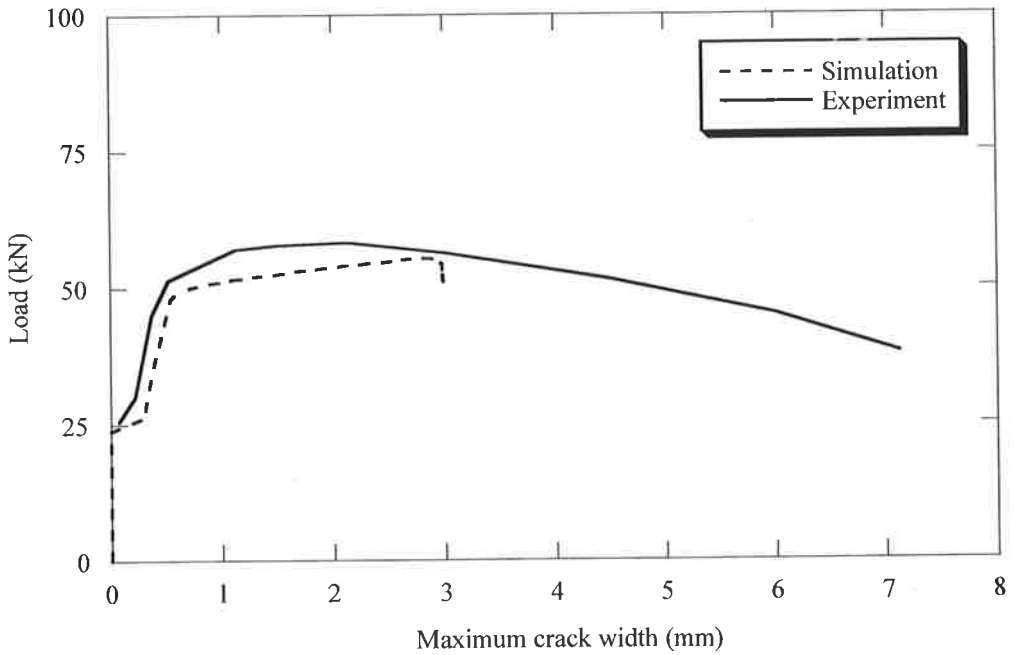

Figure 5.13 Comparison of measured load versus maximum crack width with simulation values, specimen RPL6, test by Eibl and Bühler (1991)

5.6 LOAD-DEFLECTION CURVE

Load deflection curves available from the experimental programs reported in Section 5.1 have been used to examine the ability of the modelling procedure to predict the load deflection response of the reinforced concrete beam specimens from initial cracking, to yielding of the steel, up to peak load and past peak load. (Figures 5.15 to 5.21).

Lets first consider the behaviour from initial cracking to pre-yield of the tensile steel (Figures 5.15 to 5.21). The procedure initially provides a softer stiffness as the analysis requires a sudden jump from the uncracked to cracked stiffness on a sectional level. That is, at the driver section at mid-span, a load control procedure is adopted where a sudden horizontal jump from the uncracked section stiffness under constant moment is analysed, as opposed to a deformation controlled procedure providing a vertical jump in load (Figure 5.14). Hence over a finite region, a reduced stiffness results. Another contributing affect is the procedure adopted for the local deformation analysis between flexural cracks (Chapter 4) that considers the bar equilibrium, and slip compatibility between the steel and surrounding concrete on a local level. The local deformation procedure neglects the tensile concrete contribution between the cracks as it is assumed to be negligible, which is true at the stage when the strain in the tensile steel increases toward the steel yield strain. However, it should be kept in mind that this research is interested in the post-yield plastification behaviour of reinforced concrete elements in the range where stage steel fracture may occur.

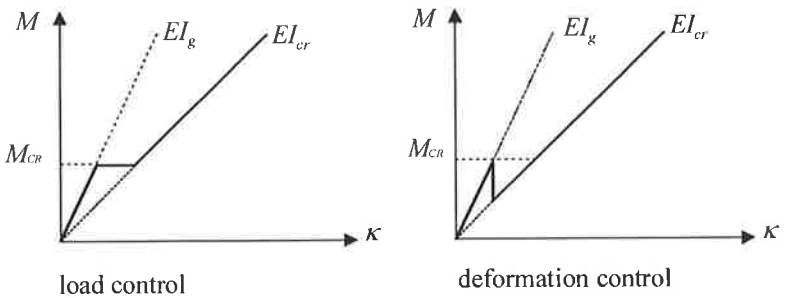

Figure 5.14 Behaviour at cracked section

In the post-yield plastification range of behaviour, the model is able to predict the performance of the structural element and good agreement is found with the yield and maximum moment, and the extent of deflection at these key points.

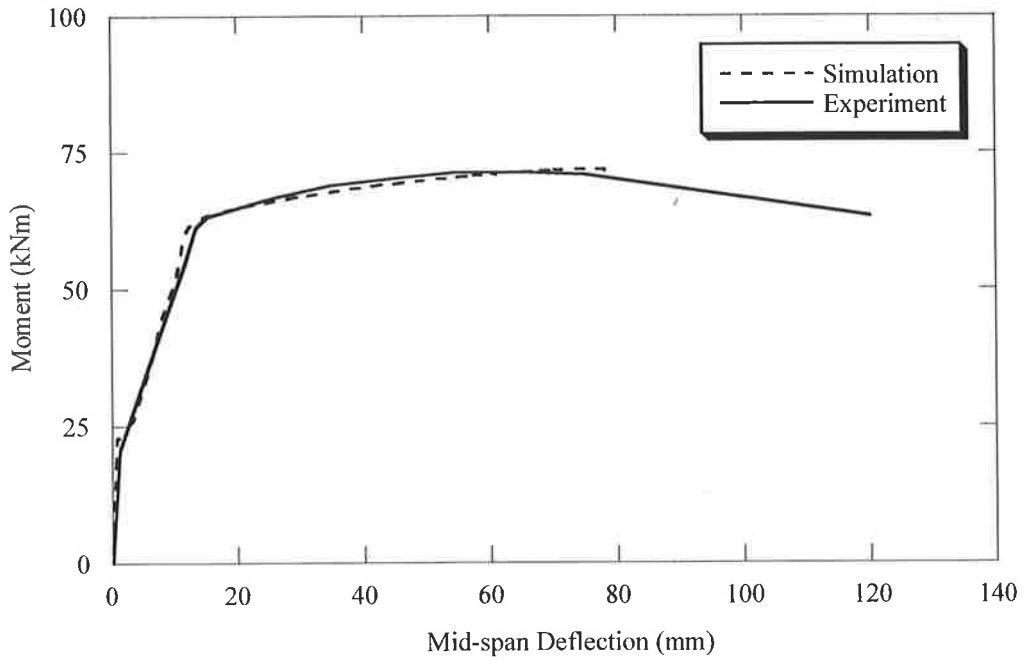

Figure 5.15 Comparison of measured load versus deflection curve with simulation values, specimen R10, test by Eifler (1991)

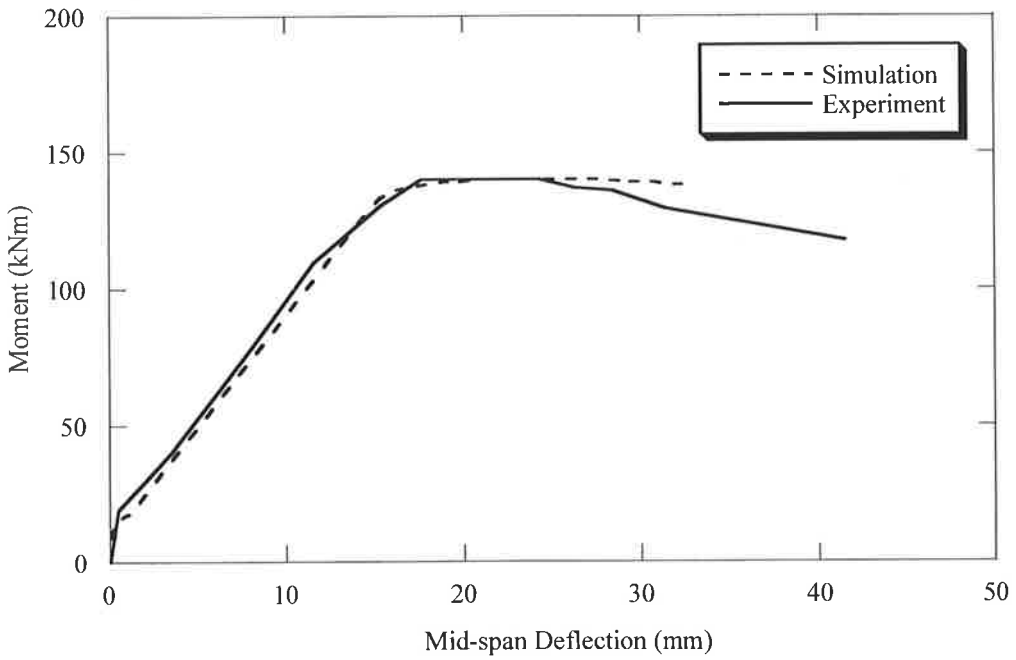

Figure 5.16 Comparison of measured load versus deflection curve with simulation values, specimen R16, test by Eifler (1991)

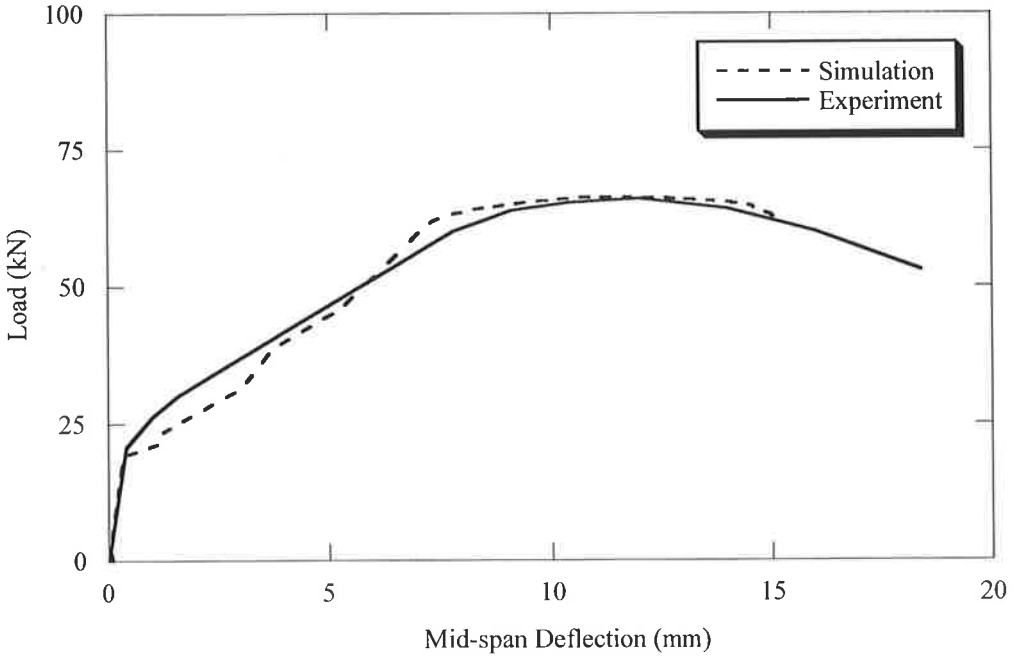

Figure 5.17 Comparison of measured load versus deflection curve with simulation values, specimen RPL1, test by Eibl and Bühler (1991)

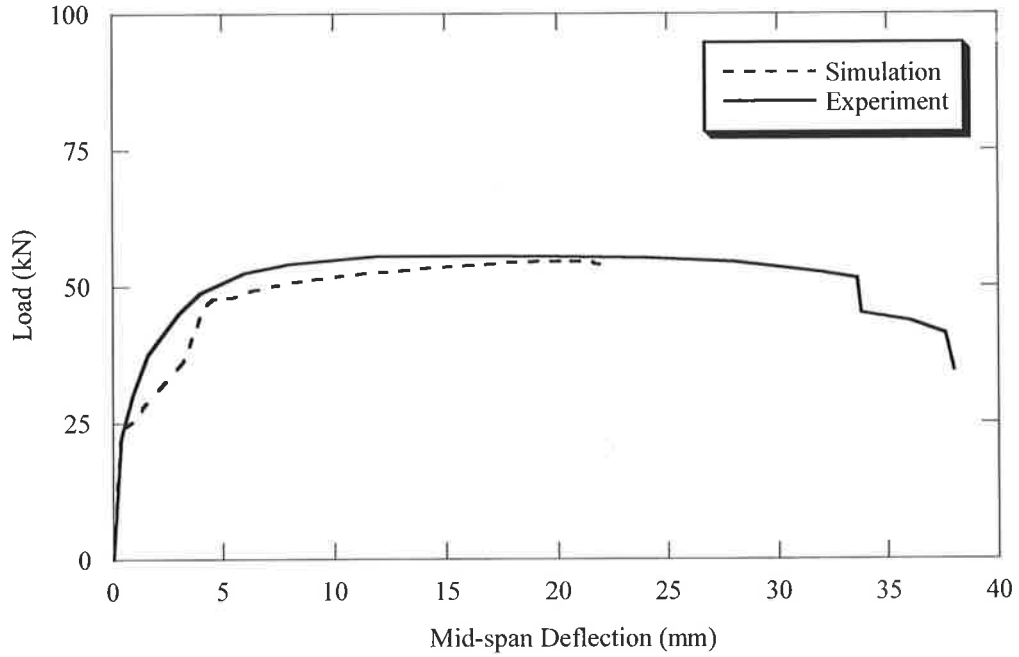

Figure 5.18 Comparison of measured load versus deflection curve with simulation values, specimen RPL2, test by Eibl and Bühler (1991)

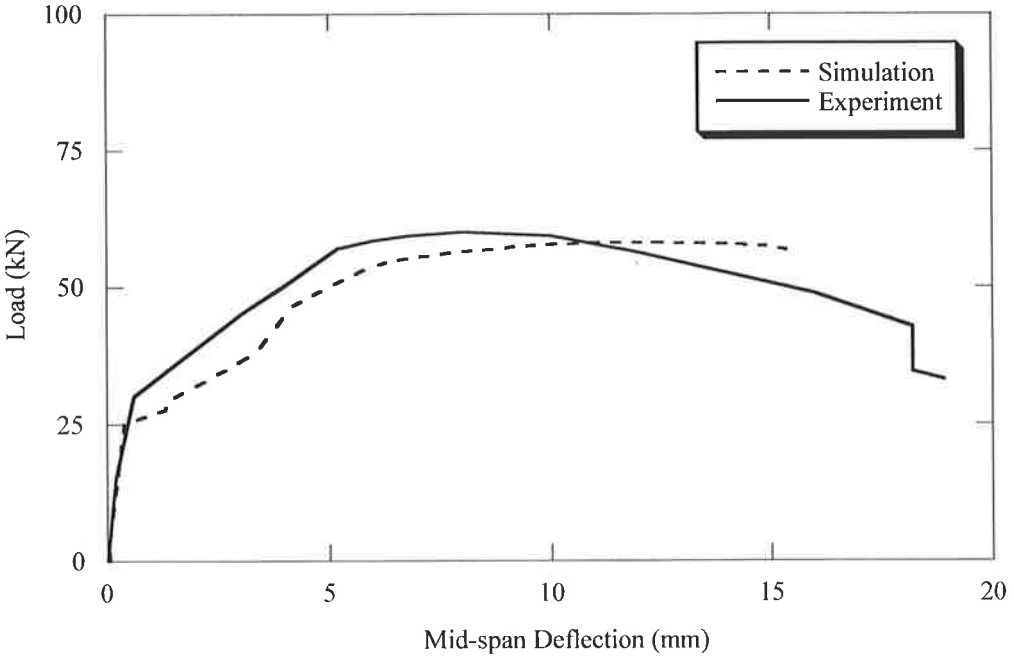

Figure 5.19 Comparison of measured load versus deflection curve with simulation values, specimen RPL4, test by Eibl and Bühler (1991)

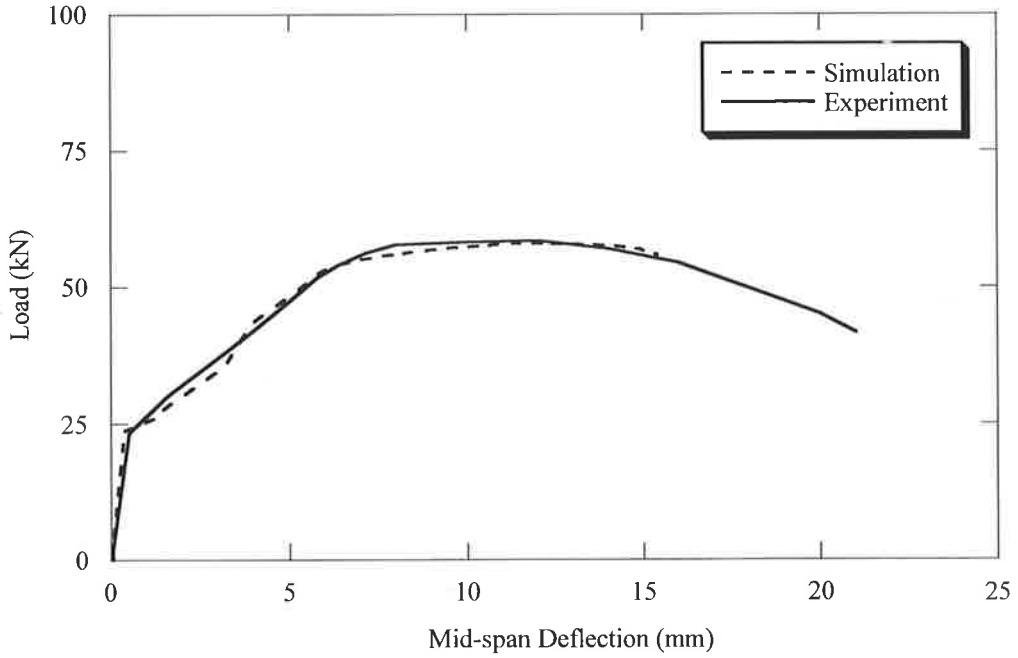

Figure 5.20 Comparison of measured load versus deflection curve with simulation values, specimen RPL5, test by Eibl and Bühler (1991)

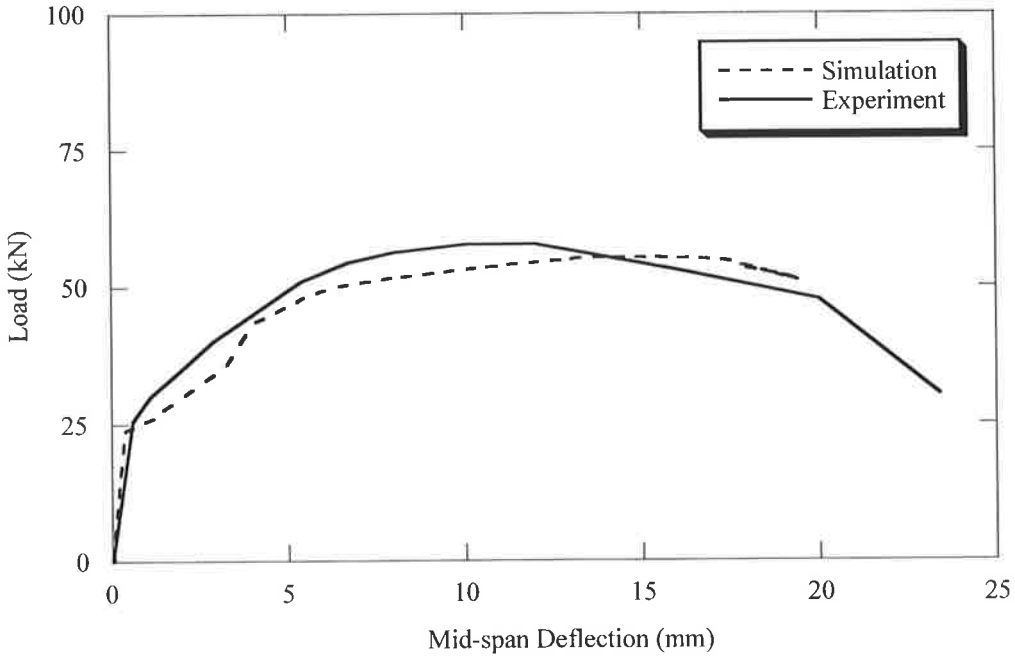

Figure 5.21 Comparison of measured load versus deflection curve with simulation values, specimen RPL6, test by Eibl and Bühler (1991)

5.7 SUMMARY

The comparisons given in this chapter between measured and simulated results show that the local deformation model, presented in Chapter 4, is able to predict rotation capacity, crack spacing, load versus deflection, load versus crack width and local tensile strain distributions with reasonable accuracy.

The next chapter presents the results from the study investigating the available rotation capacity of flexural plastic hinge regions reinforced with 500MPa grade steels of Class L and Class N ductility.

6

ROTATION CAPACITY OF FLEXURAL PLASTIC HINGE REGIONS

In this chapter the results of a parametric study that has been undertaken to investigate the factors influencing rotation capacity in plastic hinge regions of reinforced concrete flexural members are presented. The local deformation model introduced in Chapter 4 has been implemented in these simulations. The main parameters considered were the steel properties, effective depth of the section, slenderness ratio and concrete strength.

6.1 Details of Parametric Study

The study conducted here considers a simply supported beam, rectangular in cross-section, loaded by a single point load at mid-span through a load pad. The simulations are performed for tensile reinforcement ratios of 0.25%, 0.50%, 0.75%, 1.0%, 1.25%, 1.50%, 1.75%, 2.0%, 2.5% and 2.7% to include failure types either by steel fracture or concrete softening. The effect of the steel properties, effective depth, slenderness ratio or concrete strength is studied independently by keeping the other parameters constant.

To investigate the influence of the steel properties on the ductility of reinforced concrete flexural members, the strain-hardening ratio and uniform elongation have been varied. Two steel ductility classes, Class N (normal ductility) and Class L (low ductility) steels are considered. The effective depth, d, slenderness ratio, L/d, and concrete strength, f_{cm}, have been kept constant to 400mm, 20, and 50MPa, respectively.

The effect of the uniform elongation, ε_{su}, is studied by evaluating the results obtained for steel types N1, N5 and N3, N4 of normal ductility and for steel types L1, L2, L3 of

low ductility steel. The influence of the strain-hardening ratio f_{su}/f_{sy} is studied by considering steel types N1, N2, N3 and steels L1, L4, L5 (See Tables 6.1 and 6.2).

The values chosen for the strain-hardening ratio f_{su}/f_{sy} and the uniform elongation ε_{su} are chosen to fit the profile of Australian steels. Mean values are used since the aim is to model the real behaviour. Tables 6.1 and 6.2 display the combinations of the steel characteristics used. The mean yield strength for Class N (f_{sy} = 550MPa) and Class L (f_{sy} = 600MPa) steels is kept constant.

Table 6.1 Steel ductility Class N

		f_{su}/f_{sy}		
		1.05	**1.08**	**1.2**
ε_{su} (%)	**3**		N5	
	5	N2	N1	N3
	10			N4

Table 6.2 Steel ductility Class L

		f_{su}/f_{sy}		
		1.03	**1.04**	**1.05**
ε_{su} (%)	**1.5**	L1	L2	L3
	2.5	L4		
	3.5	L5		

The size effect has been studied by altering the effective depth of the section from 200, 400 to 800mm. The slenderness ratio equal to 20, the concrete strength equal to 50MPa, and steel properties have been kept constant. The steel properties relating to Steel N1 and Steel L1 have been adopted.

Variation in the slenderness ratio is investigated by considering slenderness ratios of 20 and 30 and adopting an effective depth equal to 400mm, concrete strength equal to 50MPa and steel properties relating to Steel N1 and Steel L1.

Investigation into the effect of the concrete compressive strength, f_{cm}, was limited to normal strength concrete and solely the peak compressive stress, f_{cm}, was adjusted. Average concrete strengths of 30MPa and 50MPa were used. An effective depth of 400mm, concrete strength of 50MPa and steel properties relating to Steel N1 and Steel L1, are kept constant.

In total 200 beams were simulated, that is for each shaded box in the Tables 6.3 and 6.4 beams were designed to cover the 10 reinforcement ratios considered. The tables provide a summary of the variation in parametric values.

For the beam designs the concrete cover assumed was equal to 2 times the bar diameter, and the bar diameter was adjusted according to the member size, and required reinforcement ratio. Realistic bar diameters were chosen corresponding to the steel ductility class.

Table 6.3 Beam design for influence of steel properties, effective depth constant, d = 400mm

		Steel Class						
		N1&L1	N2&L2	N3&L3	N4&L4	N5&L5		
f_{cm} (MPa)	50						25	*L/d*

Table 6.4 Beam design for influence of effective depth, slenderness ratio and concrete strength, steel ductility class constant, Steel N1 and Steel L1

		d (mm)				
		200	400	800		
f_{cm} (MPa)	30				20	*L/d*
	50				20	
	50				30	

6.2 EFFECT OF STEEL PROPERTIES

6.2.1 Available Rotation Capacity

The influence of the steel ductility class, using the ductility characteristics of Steel N1 and Steel L1, on the amount of rotation capacity is shown in Figure 6.1 as a function of the neutral axis parameter, k_u. The rotation capacity is calculated as explained in Section 4.3.3 of Chapter 4.

For the cases where concrete failure governs, an increase is found in the available rotation capacity past maximum load. It can also be clearly seen with the higher ductility class of the reinforcing steel, an increase in the amount of plastic rotation capacity can be achieved for Steel N1 of normal ductility class compared to Steel L1 of low ductility class (Figure 6.1).

The transition from steel fracture to concrete failure is represented by the sudden change in the direction of the plastic rotation curve. That is, for Steel N1 of normal ductility class, the transition occurs approximately at a neutral axis depth, k_u, of 0.1 which represents a tensile reinforcement ratio of 0.5%. For Steel L1 of low ductility class, steel fracture governs the majority of beam designs and the transition from steel fracture to concrete failure occurs at a much higher k_u value of 0.35. Therefore, in addition to the steel class influencing the amount of available rotation capacity, the ductility class also affects the failure mode that governs.

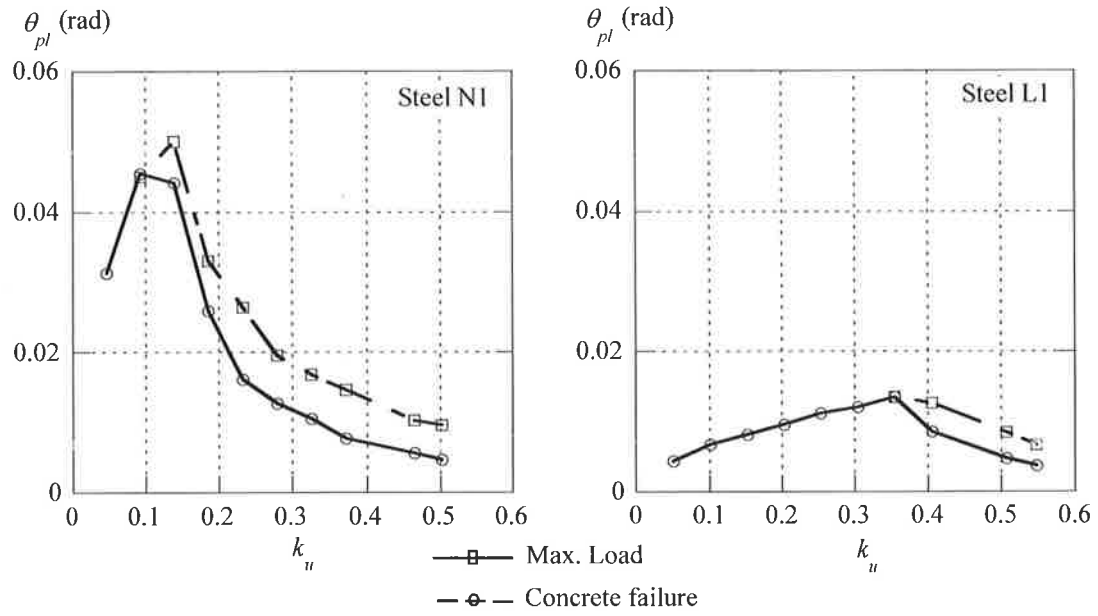

Figure 6.1 Influence of the steel ductility class on available rotation capacity, Steel N1 ε_{su} = 5%, f_{su}/f_{sy} = 1.08 and Steel L1 ε_{su} = 1.5%, f_{su}/f_{sy} = 1.03

Figure 6.2 depicts the effect of the variation of the strain-hardening ratio whilst keeping the uniform elongation constant. An increase in the strain-hardening ratio results in an increase in the rotation capacity, with no obvious shift in the transition point from steel to concrete failure.

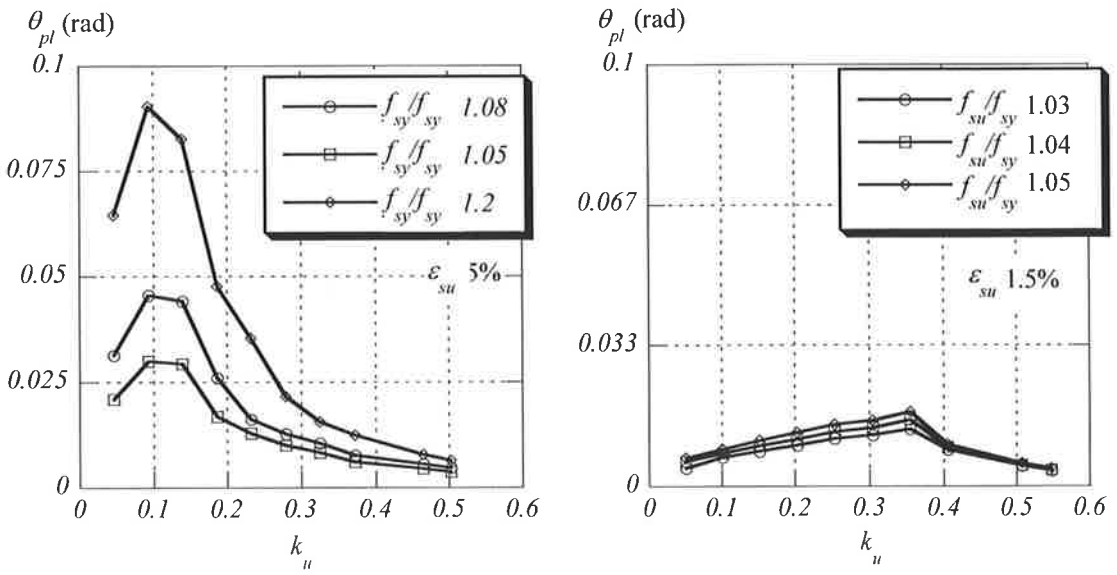

Figure 6.2 Influence of the strain-hardening ratio on available rotation capacity for Class N (LHS) and Class L (RHS) steel, ε_{su} constant

The increase in the uniform elongation (Figures 6.4 and 6.5) has a direct affect on the shift of the transition from steel fracture to concrete failure. As the uniform elongation increases with constant strain-hardening ratio, the transition point shifts towards lower values of the neutral axis depth parameter. In the range where steel fracture governs, the amount of plastic rotation is observed to increase with increase in uniform elongation. On the contrary, in the range where concrete failure governs, the rotation capacity is slightly reduced with increase in the uniform elongation value. This can be explained by considering the stress-strain relation for the steel. With the same strain-hardening ratio an increase in the uniform elongation provides a reduction in the strain-hardening slope, E_{sh}, hence leading to a reduction in the rotation capacity (Figure 6.3).

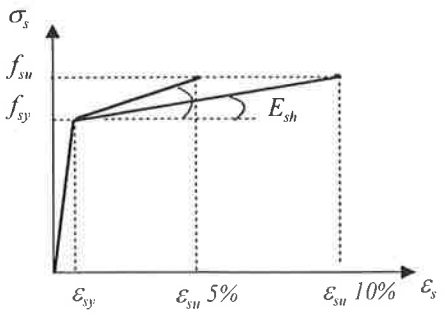

Figure 6.3 Variation in strain-hardening slope, E_{sh}

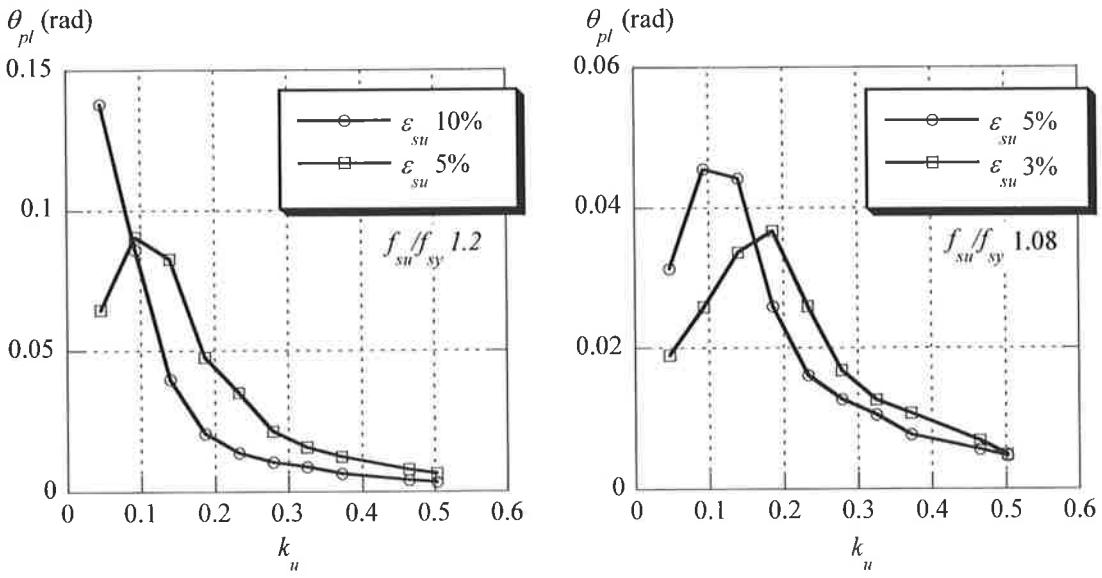

Figure 6.4 Influence of the uniform elongation on available rotation capacity for Class N steel, f_{su}/f_{sy} constant

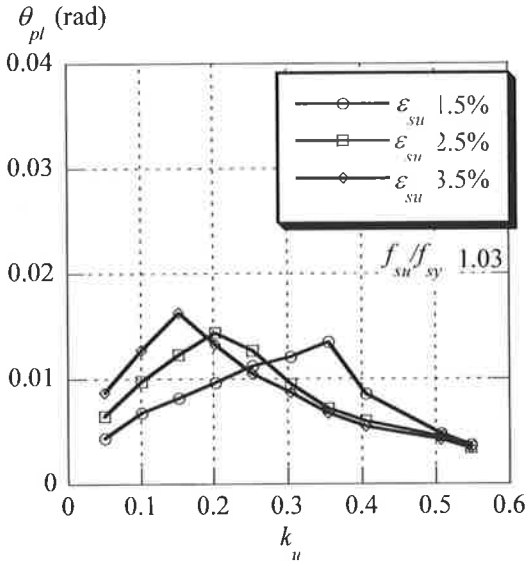

Figure 6.5 Influence of the uniform elongation on available rotation capacity for Class L steel, f_{su}/f_{sy} constant

The tension stiffening effect contributes to the post-yield behaviour and structural ductility of the flexural members. It has been shown that a high contribution of concrete between cracks can reduce the rotation capacity (Eligehausen *et al.*, 1997). The contribution of concrete between cracks can be represented approximately by the ratio between the average steel strain between two consecutive cracks and the peak steel

stress at the cracked section, $\varepsilon_{sm}/\varepsilon_{sr}$. The $\varepsilon_{sm}/\varepsilon_{sr}$ ratio, which may be used as a measure of the tension stiffening effect, further explains how the strain-hardening ratio and uniform elongation influence the available rotation capacity of plastic hinge regions.

Figure 6.6 considers a beam designed with a tensile reinforcement percentage of 5%, however, reinforced with steel of varying ductility, that is Steel N1 or Steel L1. The failure mode for the beam reinforced with Steel N1 or Steel L1 is by steel fracture. For steel N1, fracture occurs at the maximum steel strain, ε_{sr}, of 5% and for Steel L1 at the maximum steel strain, ε_{sr}, of 1.5%.

A high value of the $\varepsilon_{sm}/\varepsilon_{sr}$ ratio corresponds to less contribution of the tension stiffening effect, thus providing higher steel strains between the crack positions and an increase in the rotation capacity of the region. Recalling Class N steel typically achieves more rotation capacity than Class L steels.

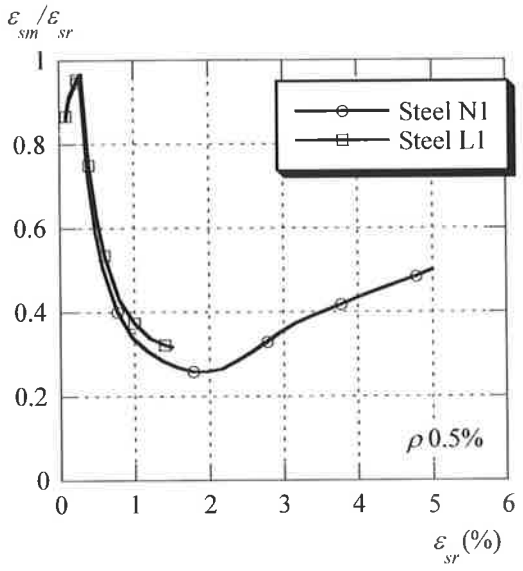

Figure 6.6 Influence of the steel ductility class on the ratio between the mean steel strain and steel strain at the crack, $\varepsilon_{sm}/\varepsilon_{sr}$, as a function of the strain at the crack, ε_{sr}

In Figure 6.7 the influence of the variation of the strain-hardening ratio on the $\varepsilon_{sm}/\varepsilon_{sr}$ ratio is shown. The figure illustrates that with increase in the strain-hardening ratio, f_{su}/f_{sy}, whilst maintaining constant ε_{su}, less contribution of concrete between cracks

prevails, providing more rotation capacity. This is the case whether steel fracture (ρ 0.5%) or concrete softening (ρ 1.75%) governs the failure.

Figures 6.8 and 6.9 show that with an increase in the uniform elongation and constant strain-hardening ratio, if failure is governed by steel fracture (ρ 0.5%), the $\varepsilon_{sm}/\varepsilon_{sr}$ ratio increases providing more rotation capacity. If failure is governed by concrete, the $\varepsilon_{sm}/\varepsilon_{sr}$ ratio decreases, revealing less rotation capacity since the strain-hardening slope, E_{sh}, is reduced with increase in the ε_{su} with constant f_{su}/f_{sy}.

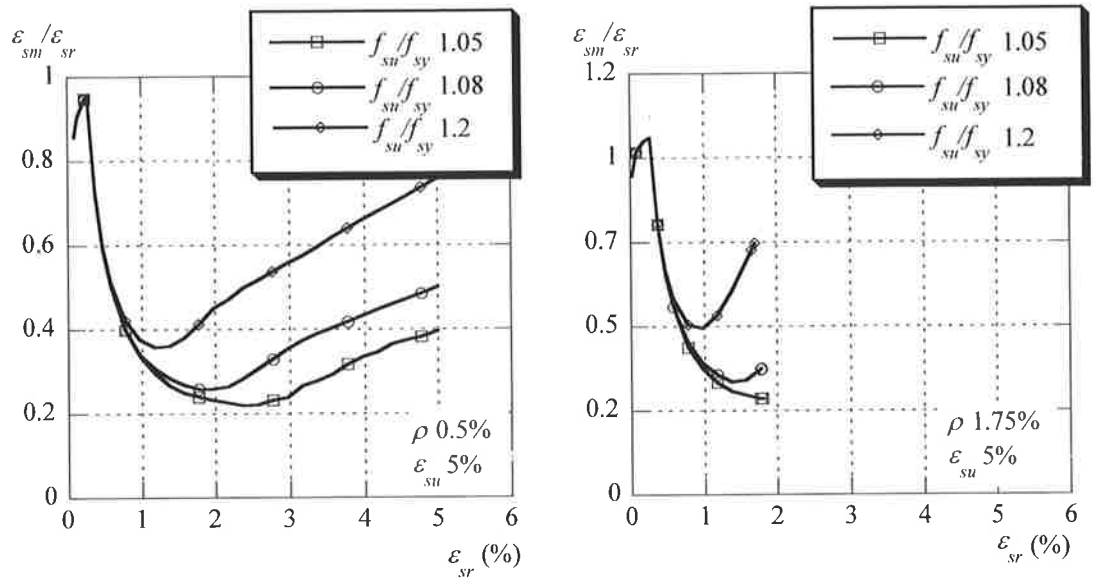

Figure 6.7 **Influence of the strain-hardening ratio, f_{su}/f_{sy}, on the ratio between the mean steel strain and steel strain at the crack, $\varepsilon_{sm}/\varepsilon_{sr}$, as a function of the strain at the crack ε_{sr}, ε_{su} = 5%**

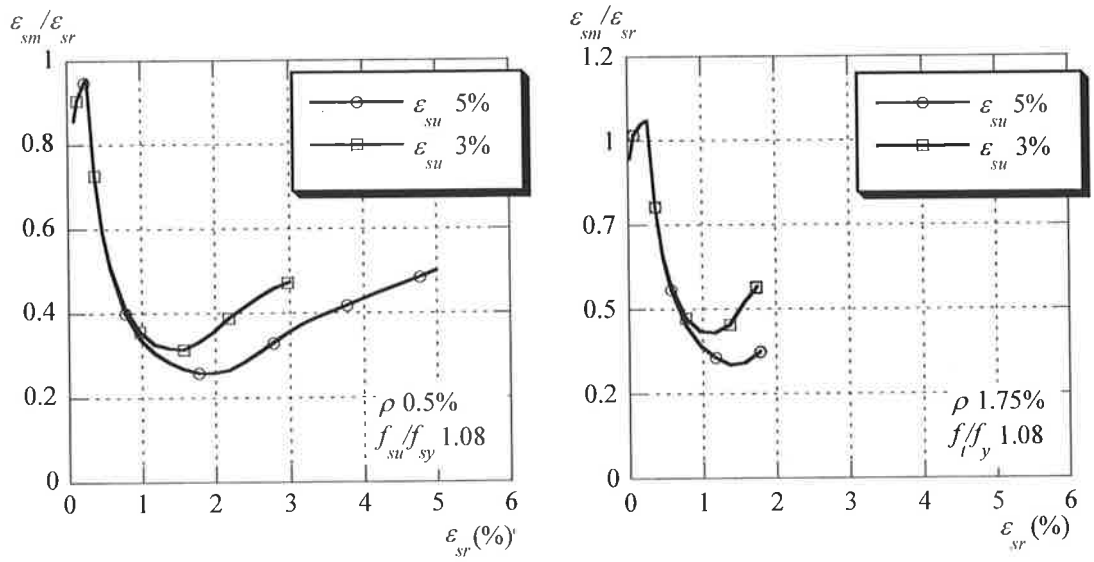

Figure 6.8 **Influence of the uniform elongation, ε_{su}, on the ratio between the mean steel strain and steel strain at the crack, $\varepsilon_{sm}/\varepsilon_{sr}$, as a function of the strain at the crack ε_{sr}, $f_{su}/f_{sy} = 1.08$.**

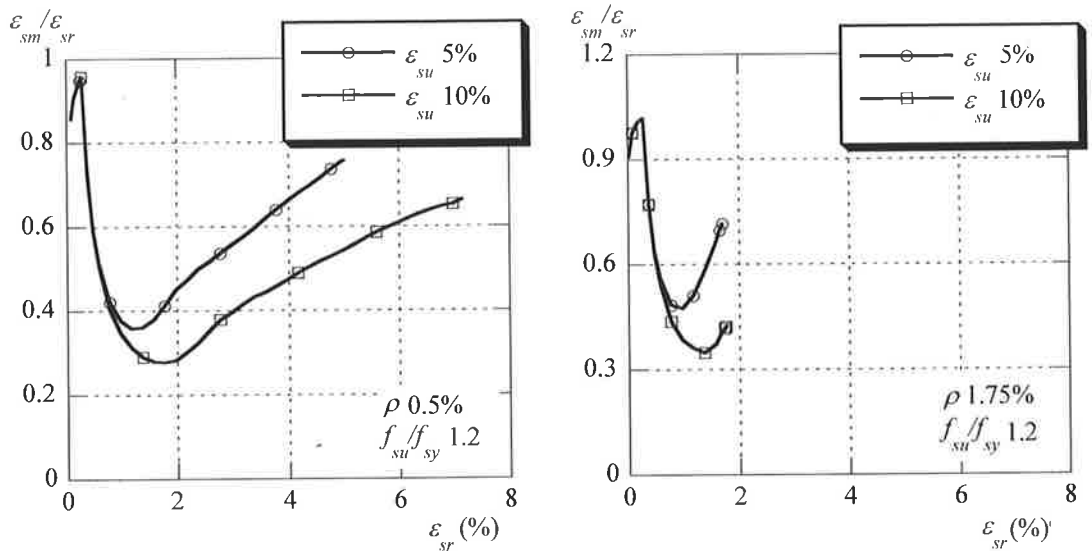

Figure 6.9 **Influence of the uniform elongation, ε_{su}, on the ratio between the mean steel strain and steel strain at the crack, $\varepsilon_{sm}/\varepsilon_{sr}$, as a function of the strain at the crack ε_{sr}, $f_{su}/f_{sy} = 1.2$.**

6.2.2 Plastification Length, Average Crack Spacing and Maximum Crack Width

Consideration of the plastic hinge length, l_p, average crack spacing, s_{rm}, and maximum crack width, w_{cr} can further explain the influence of the strain-hardening ratio and uniform elongation on the available rotation capacity in plastic hinge regions.

Tables 6.5 to 6.8 summarise the influences the variation of strain-hardening ratio and uniform elongation have on the values of l_p, s_{rm} and w_{cr} for low and high percentages of tensile reinforcement, 0.5% and 1.75%, respectively. Steel N1 and Steel L1 have been considered. From the tables the following observations can be made:

- The crack spacing in not influenced by any variation in the strain–hardening ratio, or uniform elongation for low and high tensile reinforcement percentages.

- For low tensile reinforcement percentages where steel fracture governs the overload behaviour, an increase in the strain-hardening ratio produces an increase in the plastic hinge length and maximum crack width at mid-span.

- For high tensile reinforcement percentages where concrete failure governs, an increase in the strain-hardening ratio provides no increase in the plastic hinge length, however the maximum crack width rises.

- With increase in the uniform elongation whilst maintaining a constant strain-hardening ratio, the plastic hinge length remains constant except for the low tensile reinforcement percentage when the failure mode changes from steel fracture to concrete.

- The crack width was found to enlarge with increase in the uniform elongation for low tensile reinforcement percentages and decreased with increases in the uniform elongation for high reinforcement percentages.

From these observation is can be stated that the rotation capacity increases with increase in the strain-hardening ratio for both high and low tensile reinforcement percentages since the maximum crack width intensifies, thus corresponding to less tension-stiffening. This provides higher tensile steel strains between cracks. Also, the increase in the rotation capacity with increase in the strain-hardening ratio corresponds to the higher plastic hinge lengths for cases governed by steel fracture. That is, with increase

in the strain-hardening ratio the spread of the region over which the tensile steel strain has yielded expands (Figure 6.10).

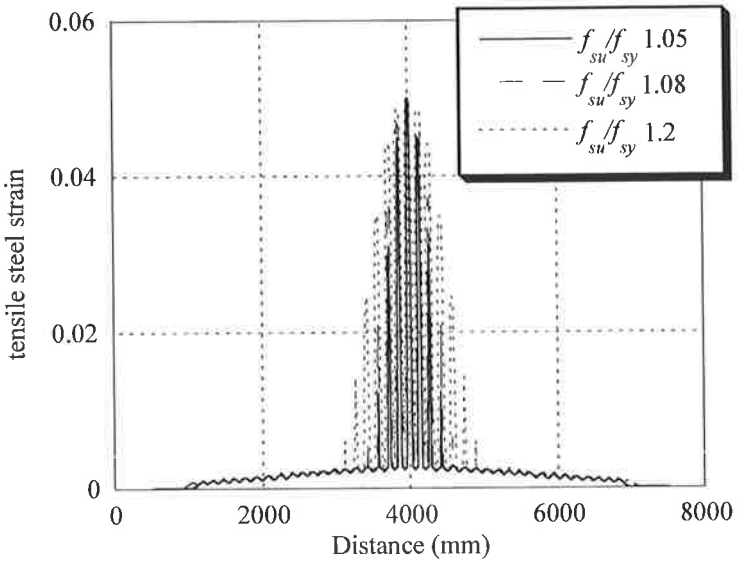

Figure 6.10 Influence of the strain-hardening ratio on plastification length, ρ = 0.5%, Steel N1

The effect of the uniform elongation whilst maintaining constant strain-hardening ratio depends upon the failure mode that governs. If failure is governed by steel fracture, an increase in the uniform elongation results in an increase of the rotation capacity since the crack widths enlarge and higher steel strain between cracks exist. However if failure is governed by concrete, the increase in the uniform elongation reduces the available rotation capacity as the crack widths are reduced due to an increased tension stiffening effect. The plastic hinge length varies only slightly for low and high tensile reinforcement ratio with increase in the uniform elongation.

Table 6.5 Influence of the strain-hardening ratio, Steel N1

ε_{su} (%)	5					
ρ (%)	0.5			1.75		
f_{su}/f_{sy}	l_p (mm)	s_{rm} (mm)	w_{cr} (mm)	l_p (mm)	s_{rm} (mm)	w_{cr} (mm)
1.05	850	148	2.6	750	149	0.46
1.08	1160	148	3.57	750	149	0.61
1.2	1770	148	4.5	750	149	1.24

Table 6.6 Influence of the strain-hardening ratio, Steel L1

ε_{su} (%)	1.5					
ρ (%)	0.5			2.5		
f_{su}/f_{sy}	l_p (mm)	s_{rm} (mm)	w_{cr} (mm)	l_p (mm)	s_{rm} (mm)	w_{cr} (mm)
1.03	900	98	0.41	520	61	0.17
1.04	900	98	0.45	520	61	0.18
1.05	1060	98	0.50	520	61	0.19

Table 6.7 Influence of the uniform elongation, Steel N1

f_{su}/f_{sy}	1.08					
ρ (%)	0.5			1.75		
ε_{su} (%)	l_p (mm)	s_{rm} (mm)	w_{cr} (mm)	l_p (mm)	s_{rm} (mm)	w_{cr} (mm)
3	1160	148	1.99	750	149	0.91
5	1160	148	3.57	750	149	0.61
f_{su}/f_{sy}	1.2					
ρ (%)	0.5			1.7		
ε_{su} (%)	l_p (mm)	s_{rm} (mm)	w_{cr} (mm)	l_p (mm)	s_{rm} (mm)	w_{cr} (mm)
5	1170	148	4.50	750	149	1.24
10	1470 (conc.)	148	6.58	750	149	0.68

(conc.) - refers to concrete failure as opposed to steel fracture at $\rho = 0.5\%$

Table 6.8 Influence of the uniform elongation, Steel L1

f_{su}/f_{sy}	1.03					
ρ (%)	0.5			2.5		
ε_{su} (%)	l_p (mm)	s_{rm} (mm)	w_{cr} (mm)	l_p (mm)	s_{rm} (mm)	w_{cr} (mm)
1.5	900	98	0.41	520	61	0.175
2.5	900	98	0.54	520	61	0.17
3.5	1060 (conc.)	98	0.69	520	61	0.16

(conc.) - refers to concrete failure as opposed to steel fracture at $\rho = 0.5\%$

6.3 SIZE EFFECT

6.3.1 Available Rotation Capacity

The influence of the effective depth on the available rotation capacity is shown in Figure 6.11. For a constant slenderness ratio, an increase in the effective depth reduces

the available rotation capacity in the plastic hinge region. This is the case for both Steel N1 and Steel L1 reinforcing steel including failure by steel fracture or concrete failure.

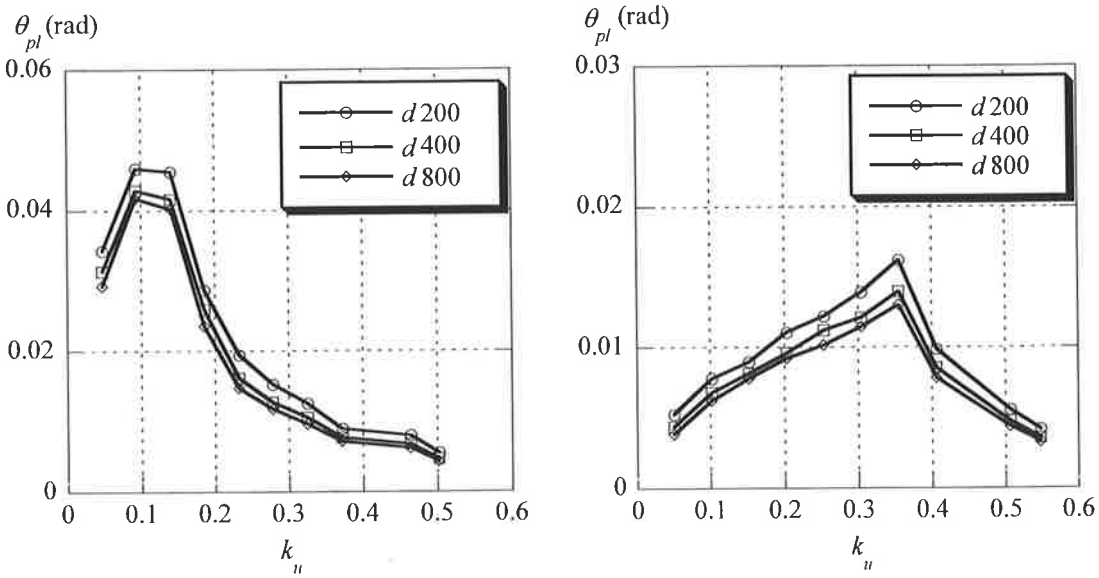

Figure 6.11 Influence of the effective depth, d, on available rotation capacity, Steel N1 (LHS) ε_{su} = 5%, f_{su}/f_{sy} = 1.08 and Steel L1 (RHS) ε_{su} = 1.5%, f_{su}/f_{sy} = 1.03

6.3.2 Plastification Length, Average Crack Spacing and Maximum Crack Width

Tables 6.9 and 6.10 summarise the influence of the effective depth on the values of l_p, s_{rm} and w_{cr} for low and high percentages of tensile reinforcement, 0.5% and 1.75% for Steel N1 and 0.5% and 2.5% for Steel L1. From the tables the following observation can be made:

- For both low and high percentages of tensile reinforcement the plastic hinge length increases with increase in the effective depth, however the average crack spacing and maximum crack width decreases.

- Although the plastification length increase with increase in the effective depth, the length is still relative to the span length, thus a reduction in rotation capacity prevails.

The observations show that a size influence on the average crack spacing is prevalent. The increase in the average crack spacing with decrease in the effective depth

contributes to higher rotation capacity since larger crack widths exist, thus relating to less contribution of concrete between cracks.

Table 6.9 Influence of the effective depth, Steel N1

ρ (%)	0.5			1.75		
d (mm)	l_p (mm)	s_{rm} (mm)	w_{cr} (mm)	l_p (mm)	s_{rm} (mm)	w_{cr} (mm)
200	630	164	3.60	300	179	0.71
400	1160	148	3.57	750	149	0.61
800	2390	139	3.51	1610	132	0.58

Table 6.10 Influence of the effective depth, Steel L1

ρ (%)	0.5			2.5		
d (mm)	l_p (mm)	s_{rm} (mm)	w_{cr} (mm)	l_p (mm)	s_{rm} (mm)	w_{cr} (mm)
200	380	106	0.43	220	70	0.19
400	900	97	0.41	520	61	0.18
800	1790	96	0.40	950	58	0.17

6.4 EFFECT OF SLENDERNESS RATIO

6.4.1 Available Rotation Capacity

The effect of the slenderness on the available rotation capacity is shown Figure 6.12. For a constant effective depth, and steel and concrete properties, an increase in the slenderness ratio produces more rotation capacity in the plastic hinge region since the span length is increased. This is the case for both Steel N1 and Steel L1 reinforcing steel including failure by steel fracture or concrete failure.

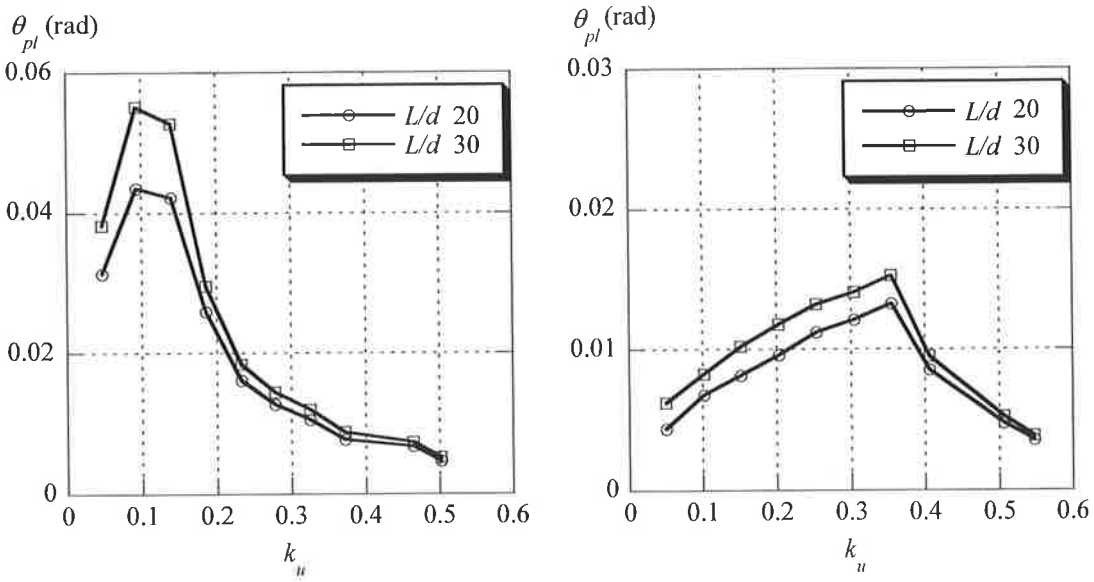

Figure 6.12 Influence of the slenderness ratio, *L/d*, on the available rotation capacity, Steel N1 (LHS) ε_{su} = 5%, f_{su}/f_{sy} = 1.08 and Steel L1 (RHS) ε_{su} = 1.5%, f_{su}/f_{sy} = 1.03

6.4.2 Plastification Length, Average Crack Spacing and Maximum Crack Width

The increase in the available rotation capacity, with increase in the slenderness ratio can be further explained by considering the plastic hinge length, average crack spacing and maximum crack width.

Tables 6.11 and 6.12 summarise the influence of the slenderness ratio on the values of l_p, s_{rm} and w_{cr} for low and high percentages of tensile reinforcement, 0.5% and 1.75% for Steel N1 and 0.5% and 2.5% for Steel L1. From the tables the following observation can be made:

- For both low and high percentages of tensile reinforcement, the plastic hinge length increases with increase in the slenderness ratio, however the average crack spacing and maximum crack width remain almost constant.

The increase in the plastic hinge length thus contributes to more available rotation capacity with increase in the slenderness ratio.

Table 6.11 Influence of the slenderness ratio, Steel N1

ρ (%)	0.5			1.75		
L/d	l_p (mm)	s_{rm} (mm)	w_{cr} (mm)	l_p (mm)	s_{rm} (mm)	w_{cr} (mm)
20	1160	148	3.57	750	149	0.61
30	1720	145	3.57	1000	146	0.61

Table 6.12 Influence of the slenderness ratio, Steel L1

ρ (%)	0.5			2.5		
L/d	l_p (mm)	s_{rm} (mm)	w_{cr} (mm)	l_p (mm)	s_{rm} (mm)	w_{cr} (mm)
20	900	97	0.41	520	61	0.18
30	1080	97	0.41	620	60	0.17

6.5 Effect of Concrete Strength

6.5.1 Available Rotation Capacity

The influence of the concrete compressive strength on the amount of rotation capacity is shown in Figure 6.13 as a function of the percentage of tensile reinforcement in the section, ρ. With increase in the concrete strength the failure mode differs. That is, the transition from steel fracture to concrete failure occurs at a higher reinforcement ratio with increase in the concrete strength. Also, if failure is governed by steel fracture an increase in the concrete strength results in a decrease of the rotation capacity. However if failure is governed by concrete, a higher concrete strength results in more rotation capacity. This can be explained by referring to the maximum steel strain at the mid-span crack at peak load. The generally higher steel strains lead to increased rotation capacity in case of the higher compressive strength (Figure 6.14).

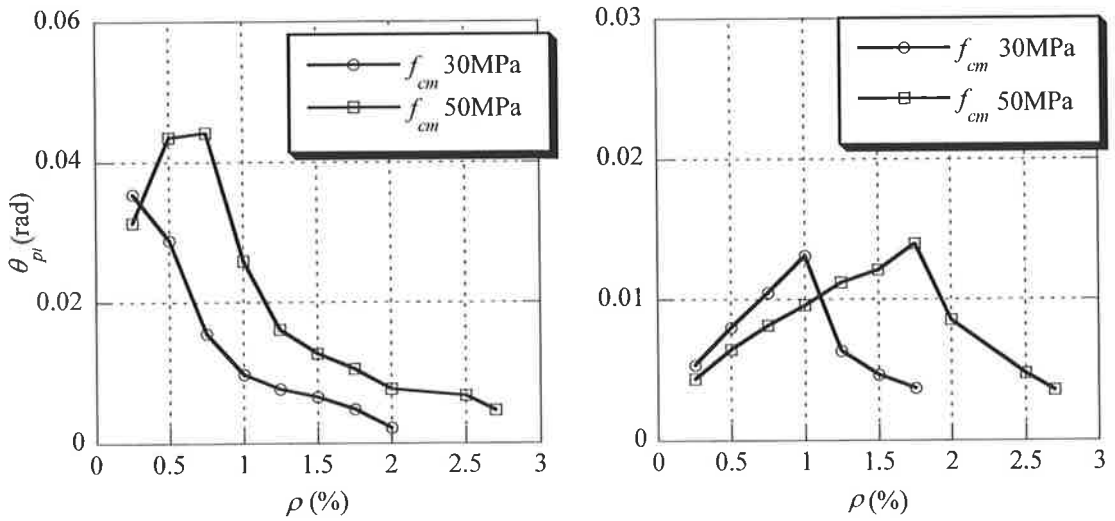

Figure 6.13 Influence of the concrete compressive strength, f_{cm}, on the available rotation capacity, Steel N1 (LHS) ε_{su} = 5%, f_{su}/f_{sy} = 1.08 and Steel L1 (RHS) ε_{su} = 1.5%, f_{su}/f_{sy} = 1.03

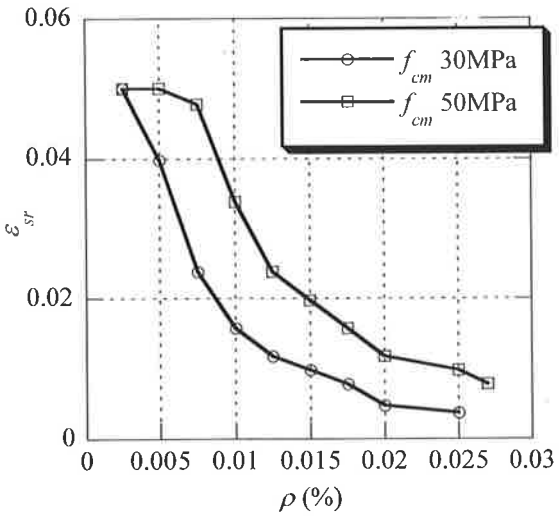

Figure 6.14 Influence of the concrete strength, f_{cm}, on the maximum strain at the mid-span crack ε_{sr}, Steel N1 (LHS) ε_{su} = 5%, f_{su}/f_{sy} = 1.08

When failure is governed by steel fracture, the higher concrete strength provides an increase in bond strength between the steel and surrounding concrete. This results in a stronger reduction of the steel strains in the vicinity of the crack. Therefore the contribution of concrete between cracks, $\varepsilon_{sm}/\varepsilon_{sr}$, is reduced as shown in Figure 6.15 for

a tensile reinforcement ratio, ρ, of 0.5%. Recalling that a high value of $\varepsilon_{sm}/\varepsilon_{sr}$ ratio corresponds to less contribution of concrete between cracks. Since the $\varepsilon_{sm}/\varepsilon_{sr}$ ratio is less for the concrete strength, reduced rotation capacity is available.

For failure by concrete, although the bond strength is increased with increase in the concrete strength, higher maximum steel strain prevails, providing a higher $\varepsilon_{sm}/\varepsilon_{sr}$ ratio and increased rotation capacity for a reinforcement ratio of 1.75% (Figure 6.15).

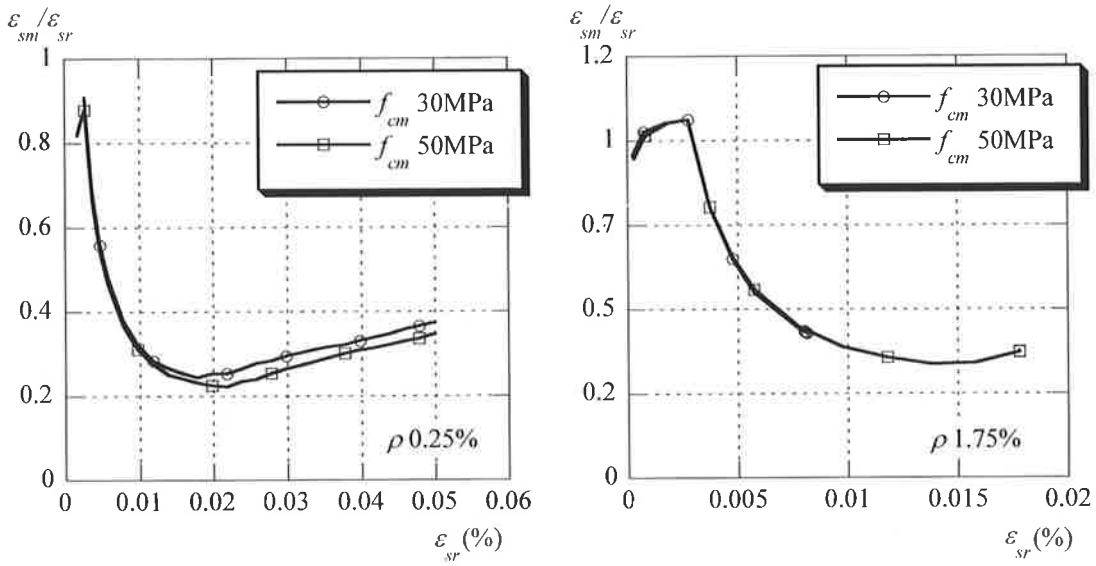

Figure 6.15 Influence of the concrete strength on the ratio between the mean steel strain and steel strain at the crack, $\varepsilon_{sm}/\varepsilon_{sr}$, as a function of the strain at the crack ε_{sr}

6.5.2 Plastification Length, Average Crack Spacing and Maximum Crack Width

Tables 6.13 and 6.14 summarise the influence of the concrete strength on the values of l_p, s_{rm} and w_{cr} for low and high percentages of tensile reinforcement, 0.25% and 1.75% for Steel N1, and 0.5% and 1.75% for Steel L1. From the tables the following observations can be made:

- The plastic hinge length increases with increase in the concrete strength for both low and high tensile reinforcement percentages.

- For low tensile reinforcement percentages in the range where steel fracture governs the overload behaviour, the crack spacing and crack width reduce with increase in the concrete strength.

- For high tensile reinforcement percentages where concrete failure prevails, the crack spacing remains almost constant, however the maximum crack width increases with increase in concrete strength.

From these observations it can be noted that the influence of concrete strength on the available rotation capacity depends upon the failure mode that governs. If failure is governed by steel fracture, an increase in the concrete compressive strength causes a decrease in the available rotation capacity since the average crack spacing and maximum crack width reduce. Also the higher concrete strength provides an increase in bond strength between the steel and surrounding concrete. This results in a stronger reduction of the steel strains in the vicinity of the crack.

If failure is governed by concrete, an increase in the concrete compressive strength provides more rotation capacity in the plastic hinge region since the crack widths enlarge due to the higher steel strains at the cracked section. Thus providing less tension stiffening between cracks even though the bond strength is increased.

Table 6.13 Influence of the concrete strength, Steel N1

ρ (%)	0.25			1.75		
f_{cm} (MPa)	l_p (mm)	s_{rm} (mm)	w_{cr} (mm)	l_p (mm)	s_{rm} (mm)	w_{cr} (mm)
30	1100	190	3.52	260	150	0.40
50	1160	177	3.17	750	149	0.61

Table 6.14 Influence of the concrete strength, Steel L1

ρ (%)	0.5			1.75		
f_{cm} (MPa)	l_p (mm)	s_{rm} (mm)	w_{cr} (mm)	l_p (mm)	s_{rm} (mm)	w_{cr} (mm)
30	800	103	0.43	250	75	0.22
50	900	97	0.41	910	74	0.43

6.6 Effect of Bar Diameter

In the simulation results presented above, the bar diameter has been kept constant for the same reinforcement ratio to reduce the number of dependent variables. However it is

known that the bar diameter affects the amount of bond stress that is transferred from the steel to the surrounding concrete. In Table 6.15 the following observations have been made for two beam designs with reinforcement ratios of 0.5% and 1.75 % respectively. A slenderness ratio of 20, concrete strength of 50MPa and an effective depth of 400mm has been adopted.

- For both low and high percentages of tensile reinforcement an increase in the bar diameter produces an increase in the rotation capacity, average crack spacing and maximum crack width.

- For low and high percentages of tensile reinforcement the plastic hinge length decreases with increase in bar diameter.

Table 6.15 Influence of the bar diameter, Steel N1

ρ (%)	0.5					1.75			
d_b (mm)	θ_{pl} (rad)	l_p (mm)	s_{rm} (mm)	w_{cr} (mm)	d_b (mm)	θ_{pl} (rad)	l_p (mm)	s_{rm} (mm)	w_{cr} (mm)
10	0.041	1250	125	2.82	20	0.0104	630	124	0.505
12	0.046	1160	148	3.57	24	0.0105	750	149	0.617
16	0.049	1100	192	5.04	28	0.0107	600	175	0.785

6.7 DISCUSSION

In Chapter 3 previous parametric studies on the factors influencing the rotation capacity of plastic hinge regions have been reviewed. In comparison to previous studies the parametric study presented in this chapter has observed similar results.

For example, a distinct size effect has also been found in the present study. In addition this study has further illustrated that the higher ductility steels provide more rotation capacity in plastic hinge regions than low ductility steels. Also the contribution of concrete between flexural cracks has been shown to reduce the available rotation capacity of plastic hinges; a similar conclusion has been found in previous studies.

However the influence of the concrete strength on the available rotation capacity has not been well investigated in past studies. The present investigation has attempted to investigate the effect of the concrete strength for normal strength concrete. High strength concrete requires more investigation.

Further, the present study has utilised an analytical procedure whereby the crack spacing is not assumed. Thus the parametric study carried out in this chapter has been able to provide an investigation into the variation of the average crack spacing, maximum crack width and plastic hinge length. It has been illustrated how the variations in these measurements affect the available rotation capacity in plastic hinges.

The ductility properties of Australian reinforcing steels are considered. Australian reinforcing steels are similar to steels produced in Europe, however the ductility classifications that steel producers comply to vary. For example, high-strength low elongation steel is referred to as Class L steel in Australia and has a lower characteristic uniform elongation of 1.5%, compared to similar European steels which adopt a minimum value of 2.5%. The limit on the strain-hardening ratio for Class L steel also differs from 1.03 in Australia to 1.05 in Europe. Therefore the present study provides valuable information on the behaviour of reinforcing steels with ductility characteristics complying with Australian requirements.

6.8 SUMMARY

This chapter has investigated the influence the steel properties, effective depth, slenderness ratio and concrete compressive strength have on the available rotation capacity in the plastic hinge region of reinforced concrete flexural members. From these observations the following conclusions can be drawn:

- The rotation capacity increases with increase in the strain-hardening ratio regardless of the failure type. This is because an increase in the strain-hardening ratio results in higher plastic hinge lengths and crack widths, together with less tension stiffening between cracks.

- The effect of the uniform elongation whilst maintaining constant strain-hardening ratio depends upon the failure mode that governs.

  - If failure is governed by steel fracture, an increase in the uniform elongation results in more available rotation capacity since the crack widths enlarge and higher steel strain between cracks exist.

  - If failure is governed by concrete, the increase in the uniform elongation whilst maintaining a constant strain hardening ratio, reduces the available rotation capacity as the crack widths are shortened due to an increased tension stiffening effect. The increased tension stiffening effect results from lower steel strains between cracks due to the reduction of the strain-hardening slope.

- The rotation capacity increases with decrease in the effective depth. This is due to the fall in crack spacing with decrease in effective depth that imparts higher crack widths and less contribution of concrete between cracks.

- The increase in the plastic hinge length with increasing slenderness ratio results in more available rotation capacity.

- The influence of concrete strength on the available rotation capacity depends upon the failure mode that governs.

  - If failure is governed by steel fracture, an increase in the concrete compressive strength causes a decrease in the available rotation capacity since the average crack spacing and maximum crack width reduce. Also the higher concrete strength provides an increase in bond strength between the steel and surrounding concrete. This results in a stronger reduction of the steel strains in the vicinity of the crack.

  - If failure is governed by concrete, an increase in the concrete compressive strength provides more rotation capacity in the plastic hinge region since the crack widths enlarge due to the higher steel strains at the cracked section. Thus providing less tension stiffening between cracks even though the bond strength is increased.

7

EXTENSION OF ANALYSIS PROCEDURE TO INDETERMINATE BEAMS

In this chapter the local deformation model developed in Chapter 4 is applied simultaneously to negative and positive moment regions in a continuous beam. A force method of analysis is used to deal with the indeterminate beam at each load increment. The full range behaviour of the structure can be predicted, starting with progressive cracking in the peak moment regions, with continuing moment redistribution as the load increases up to failure. The final failure mode may be either by steel fracture or concrete softening. At each load step an iterative analysis is used to determine the internal moments in the indeterminate structure. A computer program has been developed for two beam cases, a fixed end beam, and a propped cantilever. These cases are similar to the interior and exterior spans of continuous beams. Specific cases have been chosen in order to reduce the complexity of the computer programming.

In Section 7.4, the accuracy of the method of analysis is evaluated using available test data. The analysis is used in a parametric study of moment redistribution and collapse behaviour in Chapter 8.

7.1 BEAM CONFIGURATIONS

Two load cases are considered for the fixed end beam; a central point load and a uniformly distributed load. For the propped cantilever a single load case is considered with two point loads. These configurations are shown in Figures 7.1 to 7.3. These figures also indicate the direction of crack propagation, which is assumed to be away from the maximum moment sections.

Adjustments are made to the moment diagram to account for the influence of the support and load pads, similar to the determinate beam case (Chapter 4). In general, the adjustment takes into account the support or load pad width and the dispersion of the pad pressure into the beam. A 45-degree dispersion to the depth of the tensile steel in the support region is assumed. In the span region the dispersion around a point load is taken to the centre of gravity of the element. The method to allow for the support and load pad effect is now presented.

Considering the fixed end beam in Figure 7.1 loaded by a single point load, the hypothetical maximum moments at the support, M^-, and at mid-span, M^+, are related to the static moment M_0, where $M_0 = M^- + M^+ = \frac{PL}{4}$.

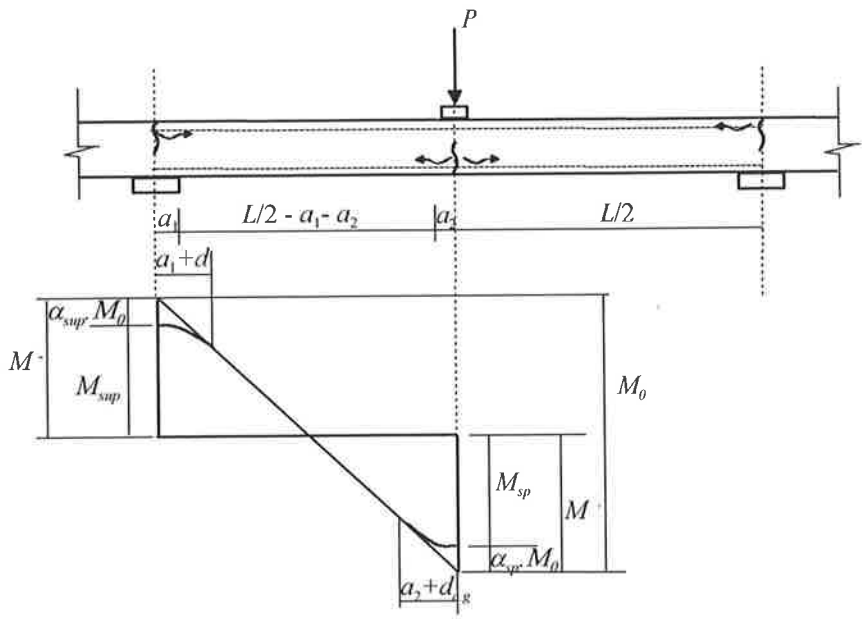

Figure 7.1 Fixed end beam with point load

Due to the support and load pad effect, the rounding of the moment in these regions is taken into account by relating the actual maximum moment in the support, M_{sup}, and span region, M_{sp}, to reduction factors α as follows.

$$M_{sup} = M^- - \alpha_{sup}.M_0 \tag{7.1}$$

$$M_{sp} = M^+ - \alpha_{sp}.M_0 \tag{7.2}$$

The moment reduction factors, α_{sup} and α_{sp} are statically derived (see Appendix A) and can be calculated using the following relations.

$$\alpha_{sup} = \left(\frac{a_1 + d}{L}\right) \tag{7.3}$$

$$\alpha_{sp} = \left(\frac{a_2 + d_{c.g}}{L}\right) \tag{7.4}$$

The terms a_1+d and $a_2+d_{c.g}$ are the distances over which support or load pad effect are considered.

Similar equations relating the hypothetical maximum moment in the support, or span region, to the actual maximum moment have also been derived for the fixed end beam subjected to a uniformly distributed load (Figure 7.2), and the propped cantilever with two points load applied (Figure 7.3).

In the case of a beam with a uniformly distributed load (Figure 7.2), the rounding moment is taken into account at the support.

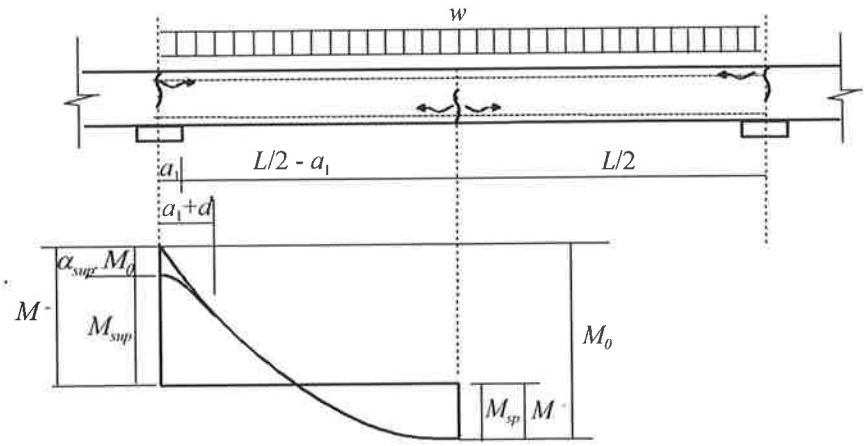

Figure 7.2 Fixed end beam with uniformly distributed load

In this case $M_0 = M^- + M^+ = \frac{wL^2}{8}$, with the actual moment at mid-span M_{sp} equal to the maximum moment M^+, and the moment at the support, M_{sup}, determined according to Equation 7.1. However, for this case the moment reduction factor, α_{sup}, is:

$$\alpha_{sup} = \left(\frac{2(a_1 + d)}{L}\right) \tag{7.5}$$

For the propped cantilever considered in Figure 7.3 the point loads are of equal magnitude.

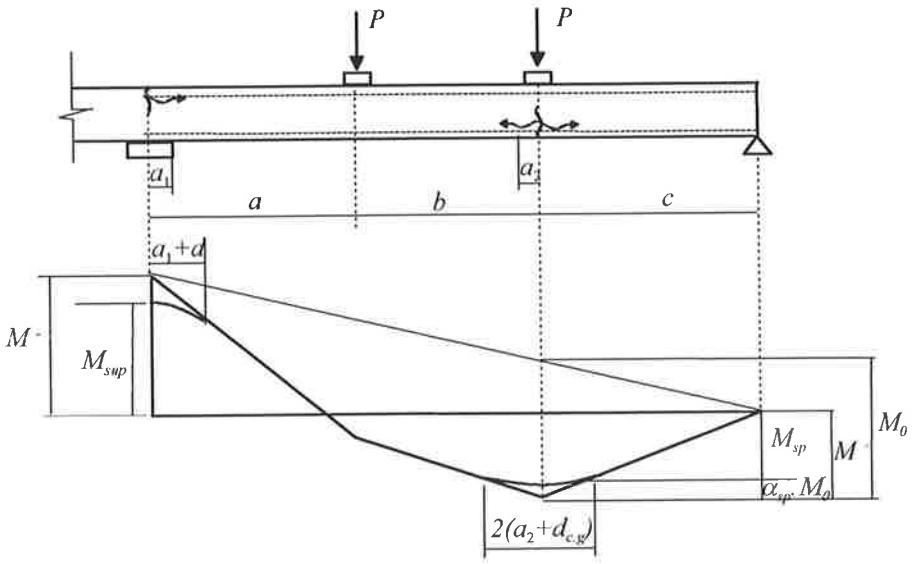

Figure 7.3 Propped cantilever with two point loads

Where the static moment is $M_0 = M^- \frac{c}{L} + M^+ = \frac{Pc(2a+b)}{L}$. The actual moments in the support and span region, M_{sup} and M_{sp}, are calculated using the following equations.

$$M_{sup} = M^- - \left[\alpha_{sup}.M_0 - \frac{a_1 + d}{2L}.M^-\right] \tag{7.6}$$

$$M_{sp} = M^+ - \alpha_{sp}.M_0 \tag{7.7}$$

The following moment reduction factors apply:

$$\alpha_{sup} = \left(\frac{2c+b}{c(2a+b)}\right)\left(\frac{a_1 + d}{2}\right) \tag{7.8}$$

$$\alpha_{sp} = \left(\frac{L}{c(2a+b)}\right)\left(\frac{a_2 + d_{c.g}}{4}\right) \tag{7.9}$$

7.2 DESCRIPTION OF ANALYSIS

The step-by-step numerical analysis is based on a deformation control procedure whereby the strain at a driver section, chosen to be the section of maximum moment in the support region, M_{sup}, is progressively incremented until failure occurs. Either the extreme concrete compressive fibre strain, ε_o, or the tensile steel strain, ε_s, can be used. Steel fracture is assumed to occur when the local tensile steel strain in the driver section reaches the uniform elongation at peak stress, ε_{su}. If concrete softening governs, failure is assumed arbitrarily to occur when the top compressive fibre strain reaches the concrete compressive strain at zero compressive stress, ε_{omax}, approximately equal to 0.008.

To apply the analysis procedure of chapter 4, the negative and positive moment regions are treated separately (Figure 7.4), bound by the point of zero moment, which is variable and dependent upon the load stage.

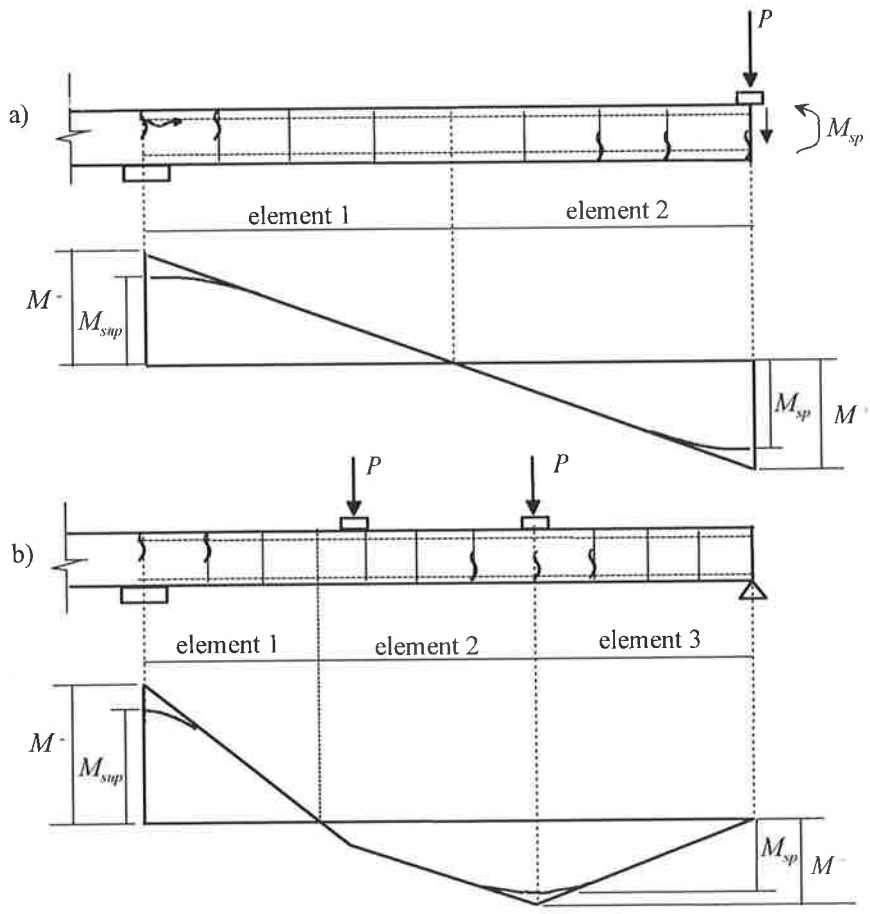

Figure 7.4 Negative and positive moment regions

A force method of analysis is used to deal with each load increment. The maximum moments at the support and span regions, M^- and M^+, are related to the static moment M_0 and the actual maximum support moment M_{sup} and span moment M_{sp} as follows:

$$M_{sup} = \delta M_0 \tag{7.10}$$

$$M^- = \delta M_0 + \alpha_{sup}.M_0 \tag{7.11}$$

$$M^+ = (1-\delta) M_0 + \alpha_{sup}.M_0 \tag{7.12}$$

$$M_{sp} = M^+ - \alpha_{sp}.M_0 \tag{7.13}$$

The static moment, M_0, depends on the beam type and loading arrangement. The moment reduction factors α_{sup} and α_{sp} are applied to calculate hypothetical maximum moments M^+ and M^-, and the actual maximum span moment, M_{sp} (See Section 7.1).

At each strain increment, the corresponding value of M_{sup} is determined from a section analysis. For the chosen strain increment, the iterative cycle adopted to satisfy the equilibrium, compatibility and boundary conditions for the beam, and to determine the local deformations and global deformations is as follows:

1. Calculate M_{sup} from a section analysis. A layered approach is used for the equilibrium calculations at a section, where the concrete is divided into finite numbers of layers and the stresses and forces are obtained from the strains. Forces in the steel are also obtained from the section strains. The forces are then summed across the section and the axial force and moment equilibrium is satisfied.

2. Choose a trial value of the static moment multiplying factor, δ, and hence determine the trial static moment, M_0, and trial moments, M^-, M^+ and M_{sp}, taking into account the moment reduction factors at the support and span regions, α_{sup} and α_{sp}.

3. Check for the formation of new cracks within the elements of the structure considered, both between existing cracks and in the uncracked region in the direction of decreasing moment.

4. Carry out the local deformation analysis for all blocks in the elements that define the indeterminate beam, and thus obtain rotations in all the blocks (Chapter 4).

5. Using the block rotations calculate the global deformations such as deflections and rotations at the key points of the beam. In particular, calculate the slope at mid-span for the fixed end beam and the deflection at the pin support for the propped cantilever. The moment area-theorem is used to calculate the deflections and rotations.

6. Adjust the trial value of δ and repeat the steps 2, 3, 4, and 5 until the calculated slope at mid-span is zero (or within an accepted tolerance value) for the fixed end beam, or the calculated deflection is zero (or within an accepted tolerance value) at the pin support for the propped cantilever case.

In step 4, the local deformation analysis for a block is carried out using the trial moment distribution and the locations of previously formed cracks and tentative new cracks. The local deformation procedure allows the local tensile steel strains to be determined at intermediate points between the flexural cracks. The bond-slip behaviour of the tensile bars surrounded by the concrete is analysed using the bar equilibrium equation and a slip compatibility condition, together with the stress-strain relation for steel and the local bond-versus slip relation. Integration of the local tensile steel strain and the top-fibre concrete strains along the block allows the block rotations to be calculated. The total rotations in the support and span regions are calculated by summing the block rotations.

7.3 NUMERICAL EXAMPLE

To demonstrate the use of the computerised analysis procedure, two numerical examples are used: a fixed end beam subjected to a uniformly distributed load, and a propped cantilever with two point loads. Identical geometrical and material properties are used for the two beams. The cross-sections at the support and mid-span regions are 500mm in width, 200mm in effective depth and both regions are reinforced with a tensile reinforcement percentage of 0.5%. A span to depth ratio of 35 is adopted and the concrete cover is equal to 2 bar diameters. The average concrete strength is 50MPa, and the steel properties are as follows:

Yield Stress	f_{sy} = 550MPa
Tensile Strength	f_{su} = 594MPa
Uniform elongation	ε_{su} = 5.0%

Due to the loading arrangement and the cross-sectional details chosen, the support region governs the overload behaviour for the two cases. The analysis is driven by the tensile steel strain at the section of maximum moment in the support region for both the fixed end beam and propped cantilever. The two beam cases performed in a similar manner in terms of convergence at each load step.

In the uncracked load stage, the procedure converges rapidly, with less iteration required to satisfy equilibrium and compatibility. However, once the first crack has formed at the section of maximum moment in the support region, small increments in the tensile steel strain are required to allow for the formation of successive individual cracks in both the support and span regions. At least double the iteration within each load step is required compared to the uncracked load stage, since the crack pattern is unstable and is continually changing within each load step until the converged solution is reached within an acceptable tolerance.

For the fixed end beam, the iterations at each load step are performed until the calculated slope at mid-span is zero, with the tolerance on convergence set to plus or minus 0.0001 radians. For the propped cantilever, to satisfy the condition that the deflection at the right pin support is zero, a tolerance of plus or minus 0.001mm is set. It is difficult to find a solution with tighter tolerances since the formation position of each crack is variable and dependent upon the trial moment diagram within each load step.

Once the tensile yield strain had been reached, the crack pattern of the member stabilised and the convergence of each load step became more rapid. The analysis was then continued until the maximum steel strain, ε_{su}, was obtained at the driver section.

The indeterminate analysis requires a substantial amount of computing power since convergence is required on a section level at the boundaries of each block element (ie. the crack position), at a local level between flexural cracks, and a global level to satisfy the boundary conditions of the structural member. Typically the analysis of an indeterminate beam takes forty minutes to run using a 600MHz processor. This can be regarded as a limitation to the program, however the program has been successful in

carrying out a parametric study of more than 500 indeterminate beams, the results of which are presented in Chapter 8. Further work could be undertaken to optimise the structure of the program.

From the results of the analysis, first yielding of the tensile reinforcing steel occurred in the support region in both beam cases. The load at which first yield was reached for the fixed end beam was 14.0kN/m. For the propped cantilever, first yield in the support region was attained at a load of 24.0 kN.

The final failure mode for both beams was governed by steel fracture. The tensile steel strain in the support region reached ε_{su}, at a maximum load of 17.7kN/m for the fixed end beam (Figures 7.5 to 7.6), and for the propped cantilever, at a maximum load of 32.9kN (Figures 7.11 and 7.12).

Figures 7.7 to 7.10 at the end of this section, show the distribution of local tensile steel strain and slip between the steel bar and surrounding concrete in the support and span regions of the fixed end beam, and Figures 7.13 to 7.16 for the propped cantilever. The strain distributions are utilised in the calculation of rotation in the support and span regions and to determine the extent of the plastic hinge region. The slip distribution is used to predict the crack widths.

The calculation values for the rotation capacity at first yield in the support region, θ_y, at maximum load, θ_{max}, the plastic rotation capacity in the support region, θ_{pl}, the average crack spacing, s_{rm}, and the plastic hinge length in the support and span regions, l_p, for both beams are summarised in Table 7.1. It can be observed that more rotation in the span region of the propped cantilever is available in comparison to the fixed end beam. This is due to the difference in span length. However, the rotation in the support region for both cases varies slightly in comparison, since the identical geometric details are used for the fixed end beam and propped cantilever and the point of contraflexure is similar.

Table 7.1 Calculation values of rotation capacity, average crack spacing and plastic hinge length for the fixed end beam (F.E.) and the propped cantilever (P.C.)

	Support region					Span region			
	θ_{max} (rad)	θ_y (rad)	θ_{pl} (rad)	s_{rm} (mm)	L_p (mm)	θ_{max} (rad)	θ_y (rad)	s_{rm} (mm)	l_p (mm)
F.E.B.	0.056	0.02	0.036	174	400	0.052	0.02	203	440
P.C.	0.067	0.026	0.41	229	400	0.08	0.03	216	625

Table 7.2 shows the redistribution of moment at the elastic load stage, at working load, at first yield in the support region, and at maximum load for both the fixed end beam and propped cantilever. The redistribution of moment is calculated as the ratio between the maximum moment in the support region and the moment in the span region, M_{sup}/M_{sp}.

Table 7.2 Redistribution of moment for the fixed end beam (F.E.) and the propped cantilever (P.C.)

	$M_{sup,el}/M_{sp,el}$	$M_{sup,serv}/M_{sp,serv}$	$M_{sup,y}/M_{sp,y}$	$M_{sup,max}/M_{sp,max}$
F.E.B.	1.77	1.86	1.87	1.37
P.C.	1.41	1.32	1.43	1.08

The distribution of moment between the support and span region for these cases alters only slightly from the elastic cracked load stage up to first yield, since the geometric details in the support and span region are identical, and cracking in the two regions occur at similar load stages.

In the post–yield stage of behaviour, Table 7.2 shows a considerable amount of moment redistribution in comparison to the cracked pre-yield stage. This increase in the redistribution of moment was necessary to satisfy equilibrium and compatibility conditions in the member since the support region was deforming plastically at a more rapid rate than the span region.

This section has illustrated the type of results that can be obtained from the analysis program developed for indeterminate beams incorporating the local deformation model introduced in Chapter 4.

Fixed end beam

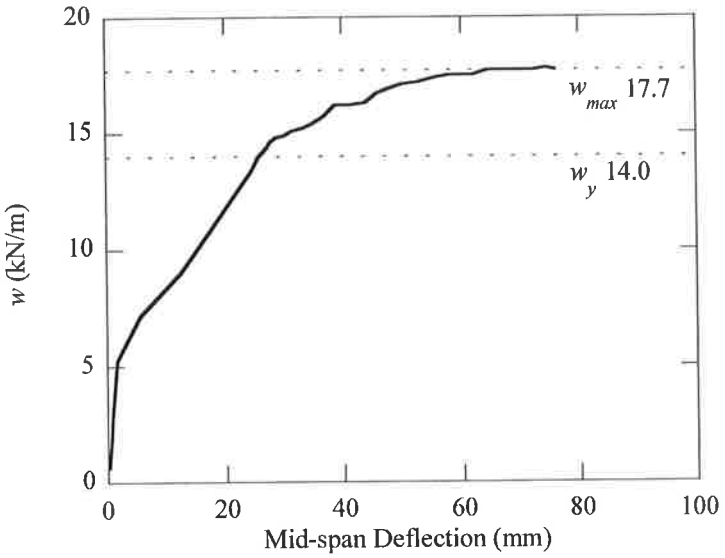

Figure 7.5 Load versus mid-span deflection, fixed end beam

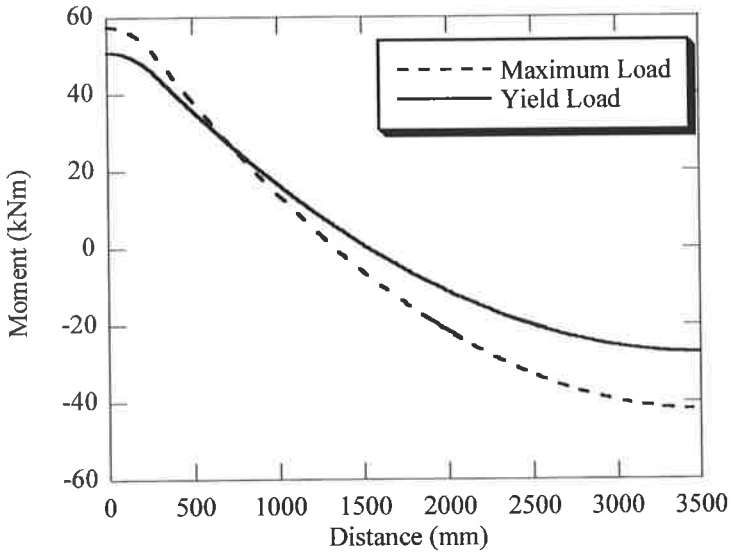

Figure 7.6 Moment distribution at yield and maximum load, fixed end beam

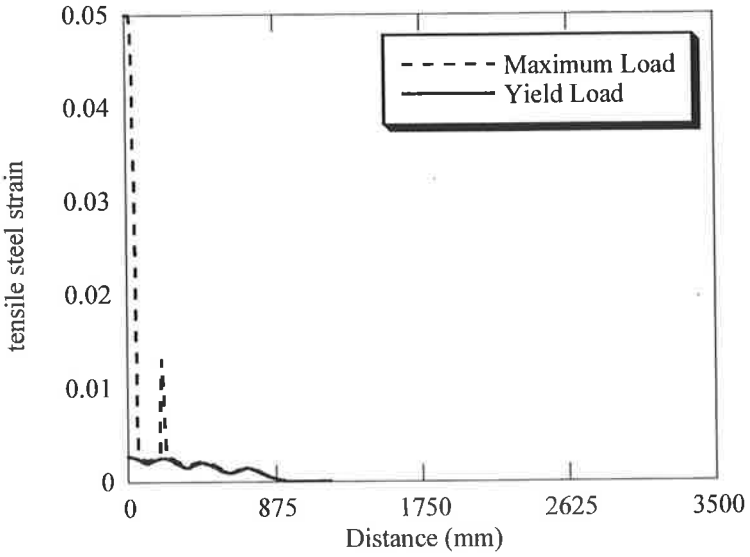

Figure 7.7 **Tensile steel strain distribution in support region at yield and maximum load, fixed end beam**

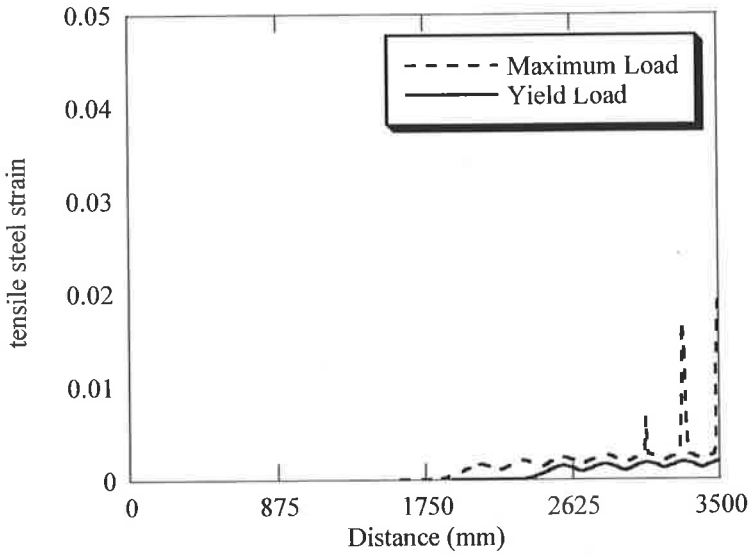

Figure 7.8 **Tensile steel strain distribution in span region at yield and maximum load, fixed end beam**

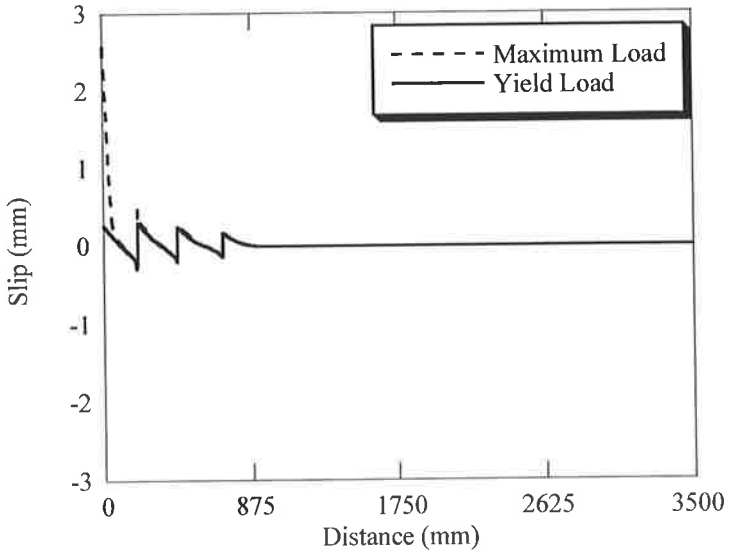

Figure 7.9 Slip distribution in support region at yield and maximum load, fixed end beam

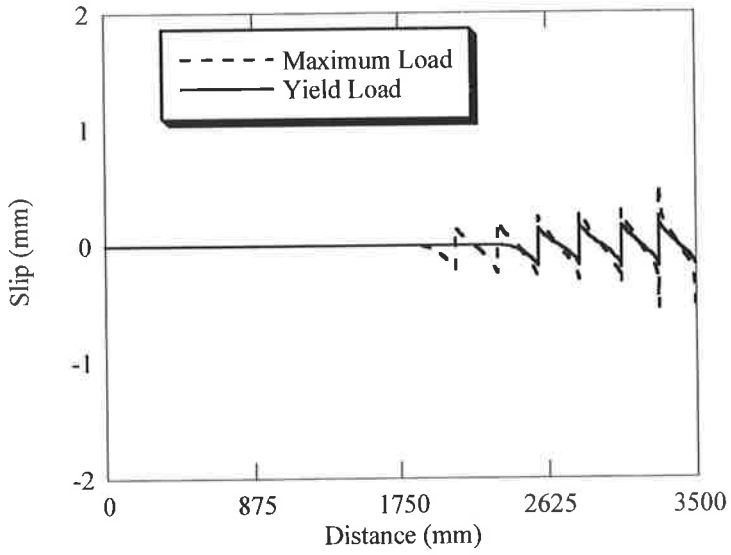

Figure 7.10 Slip distribution in span region at yield and maximum load, fixed end beam

Propped Cantilever

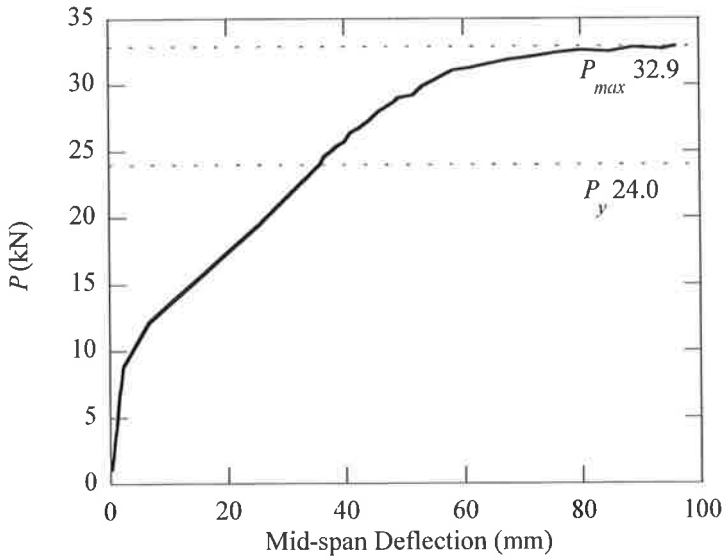

Figure 7.11 Load versus mid-span deflection, propped cantilever

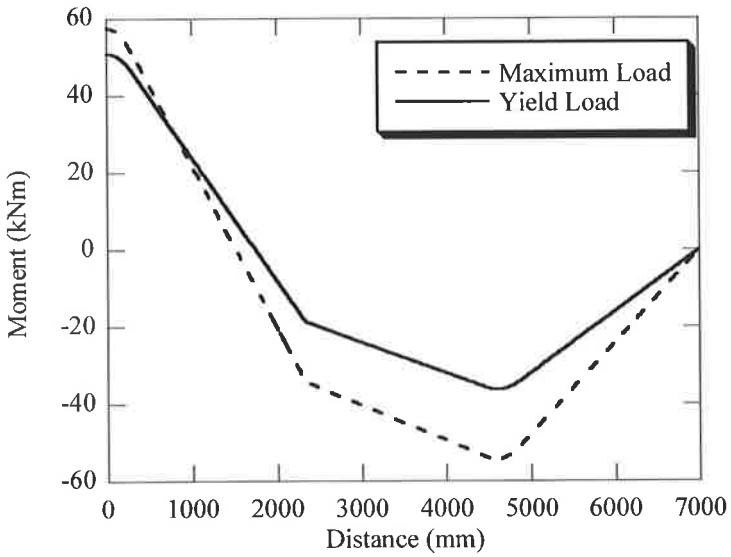

Figure 7.12 Moment distribution at yield and maximum load, propped cantilever

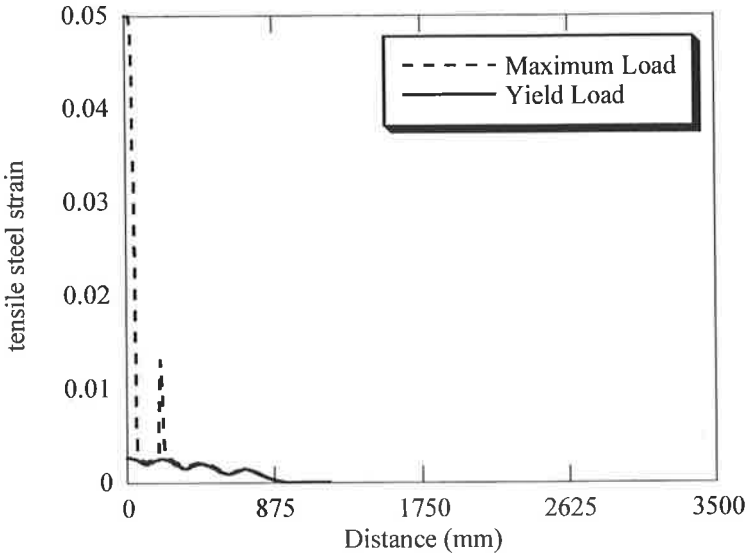

Figure 7.13 Tensile steel strain distribution in support region at yield and maximum load, propped cantilever

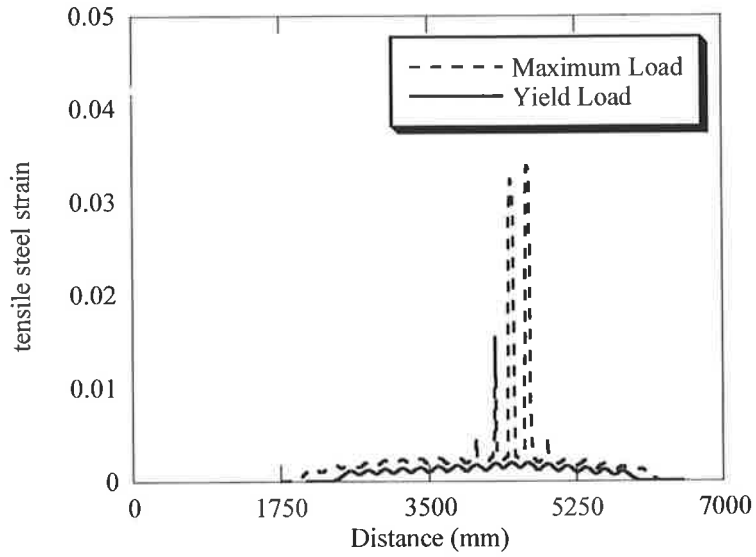

Figure 7.14 Tensile steel strain distribution in span region at yield and maximum load, propped cantilever

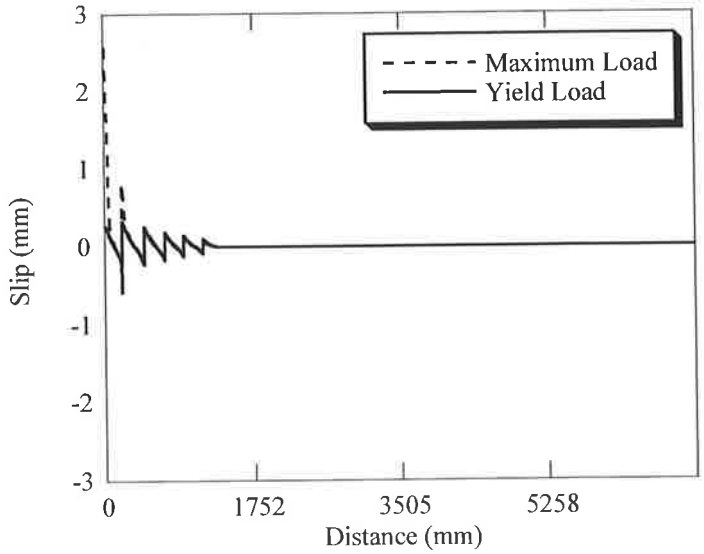

Figure 7.15 Slip distribution in support region at yield and maximum load, propped cantilever

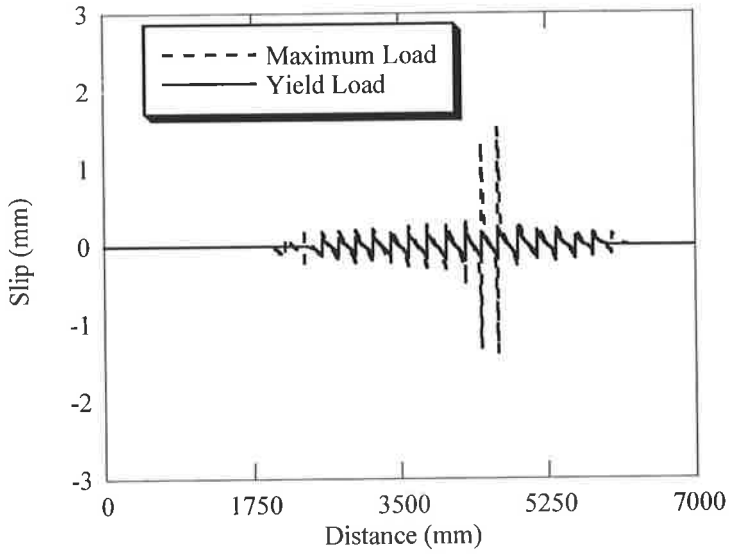

Figure 7.16 Slip distribution in span region at yield and maximum load, propped cantilever

7.4 ACCURACY OF STRUCTURAL ANALYSIS PROCEDURE

In order to check the accuracy of the analysis procedure for continuous beams, three experimental programs from previous studies have been used to compare measured load versus deflection and moment redistribution versus deflection plots, to simulation

results (Patrick *et al.*, 1997; Eligehausen *et al.*, 1995; and Bachmann and Thürlimann, 1965). From the experimental programs a selection of tests have been chosen for the comparisons.

The experiments by Patrick *et al.* (1997) are particularly relevant since two-span continuous beams reinforced with high strength, low ductile reinforcing steel typical of the reinforcing mesh currently produced in Australia were used.

The tests by Eligehausen *et al.* (1995) also consider similar high strength low elongation steel and in addition varied the statical system. Hence the ability of the local deformation model to simulate the behaviour of a fixed end and a two-span continuous beam is demonstrated.

Although brittle steel fracture did not occur in the tests carried out by Bachmann and Thürlimann (1965), the tests have been utilised to show the ability of the model to predict the structural response of two-span continuous beams with high and low percentages of reinforcement where failure is governed by concrete.

7.4.1 Tests by Patrick *et al.* (1997)

Patrick *et al.* (1997) carried out tests on three full-scale continuous reinforced concrete beams. The tests were used to demonstrate that non-ductile behaviour could occur in reinforced concrete beams when a small amount of high-strength low ductility steel is present.

The beams varied in overall depth and the amount of moment redistribution assumed in their design. Specimens ADF.B02 and ADF.B03 were chosen to be relatively deep so that they would simulate the behaviour of deep beams, while ADF.B01 was intended to represent a deep slab. For the purpose of verification, beams ADF.B01 and ADF.B02 have been used in this comparison.

The longitudinal reinforcement utilised in the beams consisted of cold-reduced ribbed wire with an average diameter of 10.65mm. The average tensile properties of the steel were as follows:

Yield Stress	f_{sy} = 648MPa
Tensile Strength	f_{su} = 685MPa
Uniform elongation	ε_{su} = 1.6%

The continuous beam was supported on three supports, forming a continuous member with equal spans of 6 metres and loaded by two point loads of equal magnitude in the spans. The test-set-up used is shown in Figure 7.17. The propped cantilever case of the simulation program, (Section 6.1), was used to represent the experimental beam set-up.

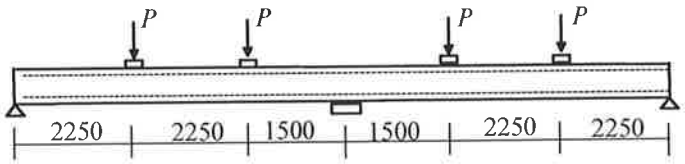

Figure 7.17 Test set-up by Patrick *et al.* (1997)

The cross section details of the beams ADF.B01 and ADF.B02 are given in Table 7.3. The beams were reinforced with longitudinal reinforcement that continued along the length of the members. Closely spaced stirrups were used to prevent shear failure and also to hold the longitudinal wires in position. For the simulation, the confining effect of the stirrups was taken into account when applying the local bond-slip model. However for the concrete compression model the concrete confinement has been neglected, since the failure mode that governs the behaviour in these tests is steel fracture.

Table 7.3 Cross section details, in tests by Patrick *et al.* (1997)

			Top reinforcement		Bottom reinforcement		
Specimen	***H*** **(mm)**	***B*** **(mm)**	***d*** **(mm)**	ρ **(%)**	***d*** **(mm)**	ρ **(%)**	f'_{cm} **(MPa)**
ADF.B01	259	296	211	0.6	56	0.6	45.5
ADF.B02	509	301	449	0.4	67	0.4	41.2

7.4.2 Tests by Eligehausen *et al.* (1995)

Eligehausen *et al.* (1995) undertook an experimental program that investigated the rotation capacity and moment redistribution in two static beam systems.

The first system was a continuous one-way slab over two spans, with a cross section of 550mm in width and 180mm in section height, and an effective depth equal to 161mm. Two tests numbered DMR1 and DMR2 were tested. The results from test DMR1 are

used in the comparison, since in test DMR2 the load was kept constant once the peak value predetermined from test DMR1 was reached.

The second system was a slab with fixed ends at both sides of which the cross-section is the same as the continuous system. To test this arrangement the beam was constructed with a cantilever at each end and a point load was applied at the end to calculate the support reactions (Figure 7.18). The test was numbered DMR3.

In the continuous case the percentage of reinforcement was 0.3% both in the spans and over the support. For the fixed end case the reinforcement percentage was 0.3% over the supports and 0.55% in the span

Figure 7.18 shows the loading arrangement for the two systems. Note the top longitudinal reinforcement was not continuous over the length of the member.

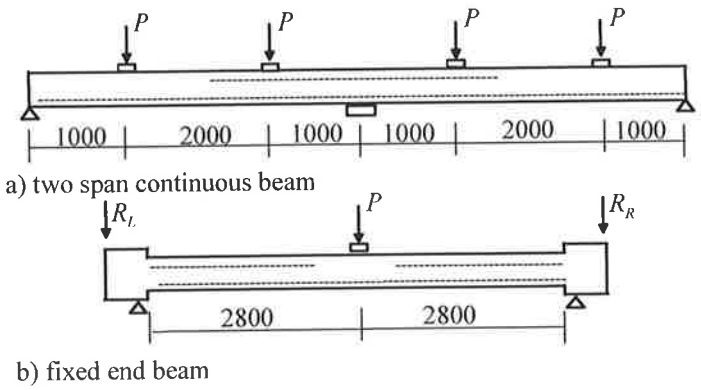

Figure 7.18 Test set-up by Eligehausen *et al.* (1995)

Table 7.4 summarises the steel and concrete material properties for test DMR1 and DMR3. The average steel properties were used in the simulation for the support and span regions. The slabs were reinforced with welded deformed wire mesh of low ductility. In both cases the diameter of the main reinforcing bars was 7.5mm.

Table 7.4 Steel and concrete properties in tests by Eligehausen *et al.* (1995)

Specimen	f_{sy} (MPa)	f_{su} (MPa)	ε_{su} (%)	f'_{cm} (MPa)
DMR1	607	624	2.1	59.5
DMR2	606	626	2.64	62.6

7.4.3 Tests by Bachmann and Thürlimann (1965)

Bachmann and Thürlimann (1965) carried out tests on the plastic behaviour of two-span continuous reinforced concrete beams. The experimental program consisted of six rectangular beam tests. The beams were identical in section size but varied in the amount of tensile steel in the support and span regions and anchorage details. For this reason only beams A2 and A5 have been used in the simulation. The anchorage details have not been considered here.

Figure 7.19 shows the test set-up and the reinforcement layout for beams A2 and A5. The beams were reinforced with steel of much higher ductility than currently produced and used in Australia and Europe. Thus the problem of steel fracture was not encountered in the tests. The test results have been used here to show that the simulation program is able to predict the behaviour of RC indeterminate beams regardless of the failure type.

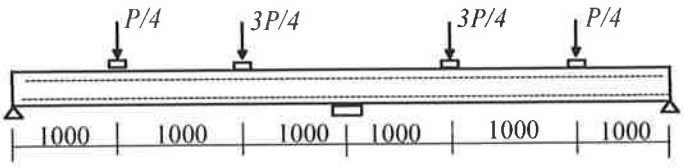

Figure 7.19 Test set-up by Bachmann and Thürlimann (1965)

The cross section details of the beams A2 and A5 for the span and support regions are given in Table 7.5. The beams were reinforced with longitudinal reinforcement that continued along the length of the members. Closely–spaced stirrups were used to prevent shear failure. For the simulation, the confining effect of the stirrups was taken into account when applying the local bond-slip model. The overall section height and width for both specimens was 380mm and 180mm, respectively. The tensile reinforcement in the support region for beam A2 and A5 was 1.17%. In the span region the tensile reinforcement percentage for beams A2 and A5 was 0.34% and 1.17% respectively. Both regions contained 0.34% of compressive reinforcement. The material properties used in the specimens are given in Table 7.6.

Table 7.5 Cross section details of specimens, in tests by Bachmann and Thürlimann (1965)

Specimen	Support region						Span region					
	Tensile reo.			Compression reo.			Tensile reo.			Compression reo.		
	d_{st}	d_b	A_{st}	d_{st}	d_b	A_{st}	d_{st}	d_b	A_{st}	d_{st}	d_b	A_{st}
A2	26	$3d_b18$	741	351	$2d_b12$	218	351	$2d_b12$	218	26	$2d_b12$	218
A5	26	$3d_b18$	741	351	$2d_b12$	218	351	$3d_b18$	741	26	$2d_b12$	218

Note: d_{st} (mm), d_b(mm), A_{st} (mm^2)

Table 7.6 Material properties, in tests by Bachmann and Thürlimann (1965)

Specimen	f_{sy} (MPa)	f_{su} (MPa)	ε_{su} (%)	f'_{cm} (MPa)
A2	373	504	0.088	46.5
A5	380	569	0.078	46.5

7.4.4 Comparison of Experimental and Analytic Results

Applied loads, deflections and the moment distribution in the support and span regions, have been recorded throughout the duration of the experimental tests introduced above. The comparison between the experimental and simulation results are now presented.

Figures 7.20 to 7.25 display the comparison between the experiment and simulation results of the applied load versus mid-span deflection. The comparisons show good correlation between the peak load and the extent of mid-span deflection. It can be noticed again, as in the determinate beam cases (see Chapter 5) that at initial stages of loading, that is from post-cracking to pre-yield behaviour, the global stiffness of the structure is over estimated. However, in general the post-yield behaviour is simulated well, which is the main area of investigation in this thesis.

Beams A2 and A5 taken from the test program of Bachmann and Thürlimann (1965) are simulated with a slightly stiffer structural response in the post-yield range (Figures 7.24 and 7.25). This can be attributed to the bond parameters used. The bond-slip model used in the simulation has been developed for steel produced recently, therefore the bond characteristics of the steel used in the tests dating back to 1965 may be different. Also from observing the cracking patterns, shear cracks in the support region can be seen. Shear cracks are not considered in the modelling approach. The effect of shear cracks provides an increase in local deformation, hence rotation capacity (Bachmann, 1967).

The failure modes for the beams tested by Patrick *et al.* (1997) and Eligehausen *et al.* (1995), involved fracture of the longitudinal reinforcing steel to initially occur at the support regions which was also observed in the simulations. The beams tested by Bachmann and Thürlimann (1965) were reinforced with steel of good ductility, that is, uniform elongation values of 8%, hence failure was governed by concrete softening which was also predicted by the analysis. Table 7.7 compares the average crack spacing in the support and span regions. Adequate agreement can be found between experimental and simulated average crack spacing in the support and span regions. For the tests by Patrick *et al.* (1997) average crack spacings were not available.

Table 7.7 Comparison of measured average crack spacings in support and span regions with simulation values

Specimen	Support region		Span region	
	s_{rm} exp. (mm)	s_{rm} sim. (mm)	s_{rm} exp. (mm)	s_{rm} sim. (mm)
Dmr1	153	203	148	186
Dmr3	141	180	134	138
A2	158	210	183	221
A5	150	200	135	152

Note: exp.= experiment values. sim.= simulation values

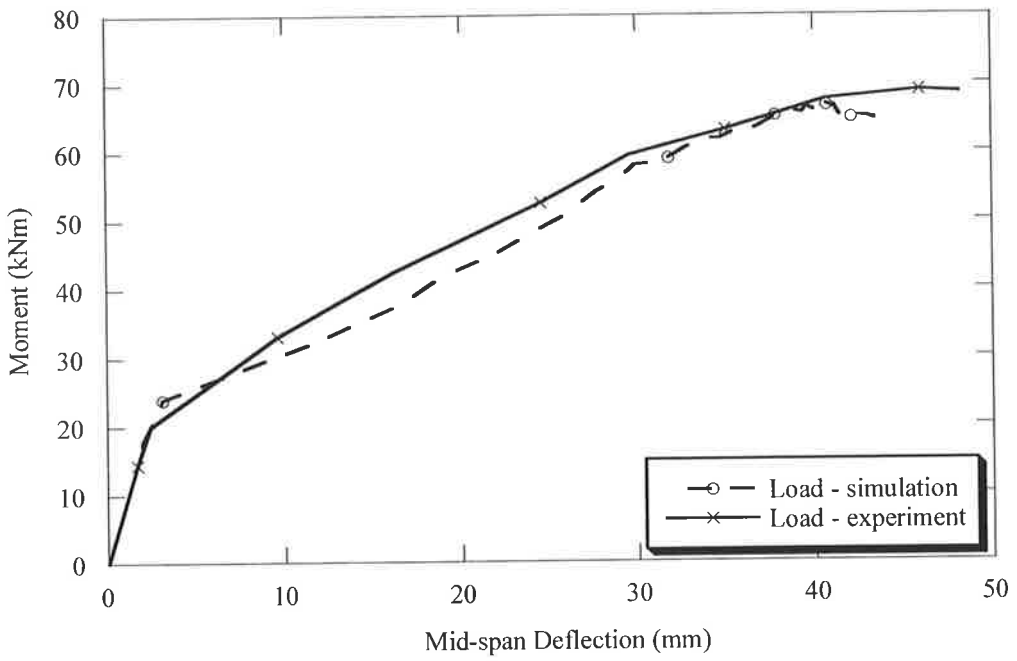

Figure 7.20 Comparison of measured load versus deflection curve with simulation values, test by Patrick *et al.* (1997) beam ADF.B01

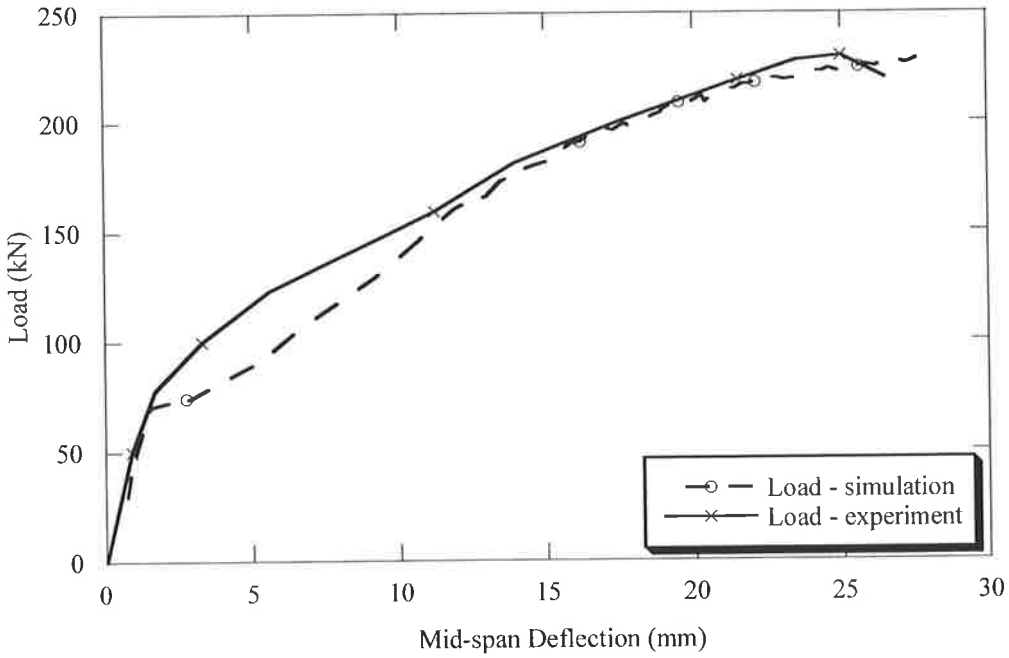

Figure 7.21 Comparison of measured load versus deflection curve with simulation values, test by Patrick *et al.* (1997) beam ADF.B02

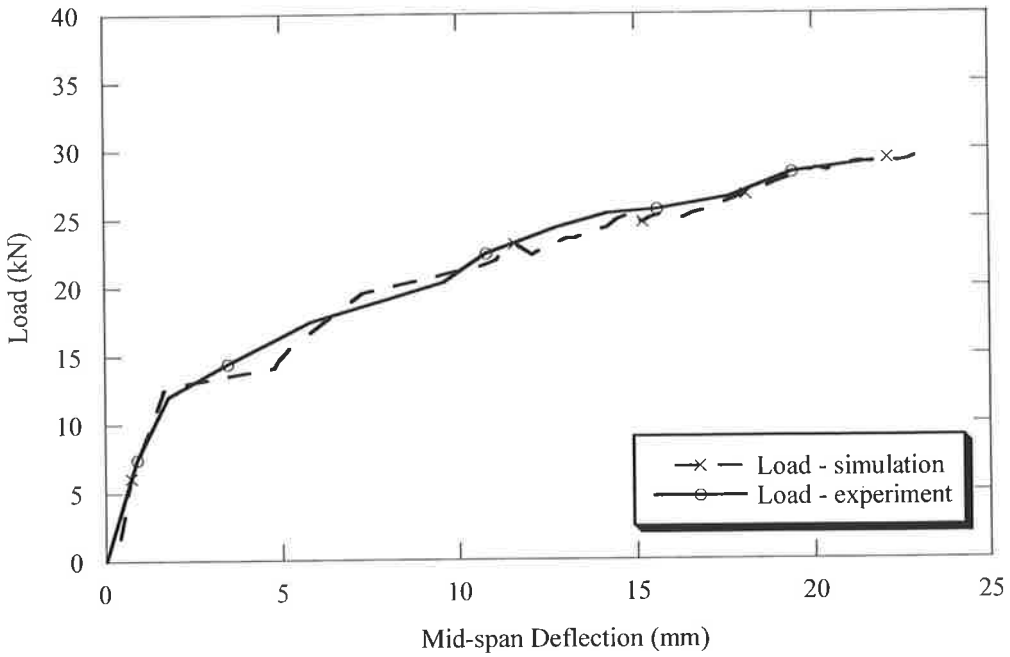

Figure 7.22 Comparison of measured load versus deflection curve with simulation values, test by Eligehausen *et al.* (1995) beam DMR1

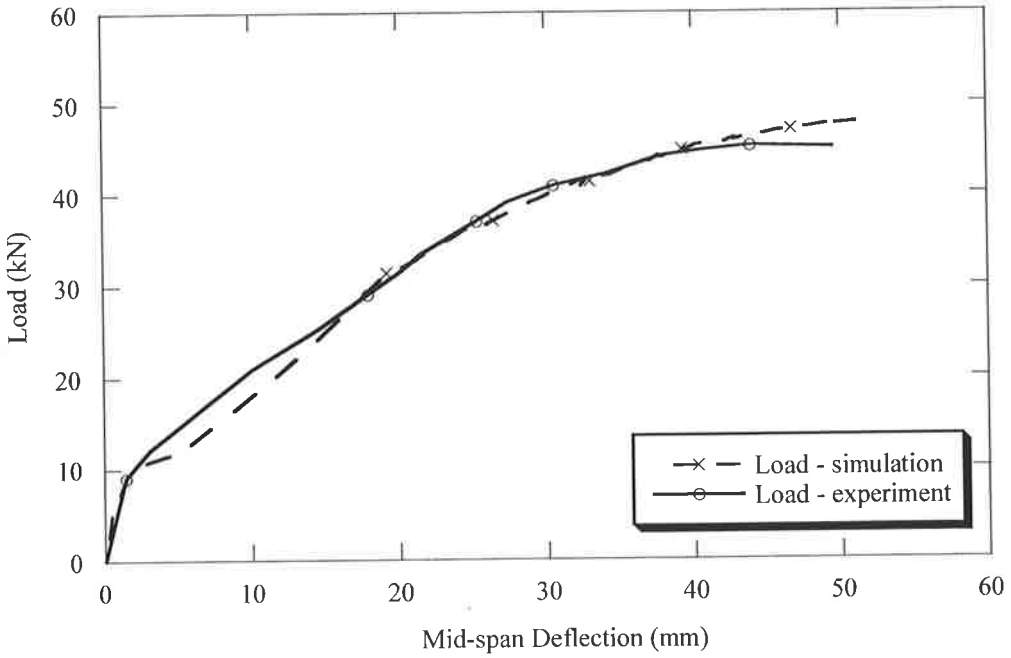

Figure 7.23 Comparison of measured load versus deflection curve with simulation values, test by Eligehausen *et al.* (1995) beam DMR3

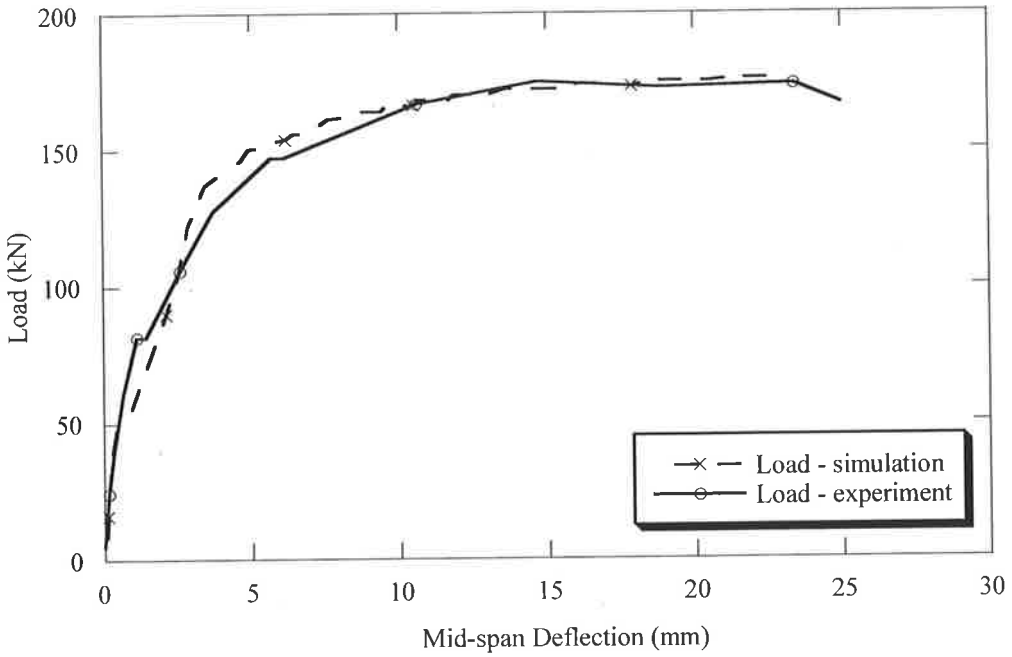

Figure 7.24 Comparison of measured load versus deflection curve with simulation values, test by Bachmann and Thürlimann (1965) beam A2

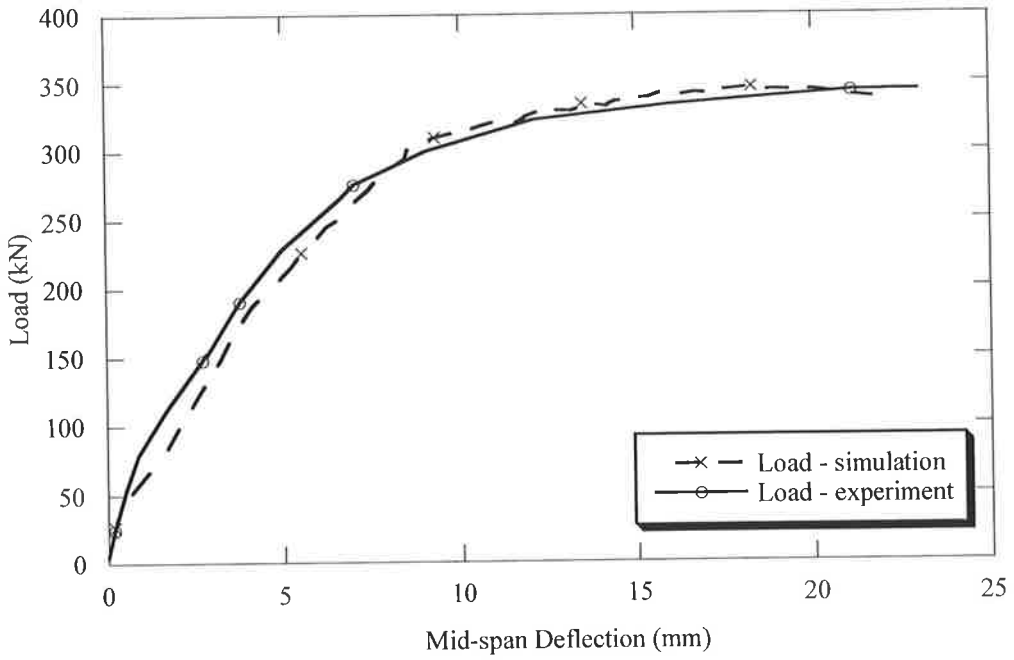

Figure 7.25 Comparison of measured load versus deflection curve with simulation values, test by Bachmann and Thürlimann (1965) beam A5

Tables 7.8 and 7.9 summarise the comparison between experiment and simulations results of the moment in the support and span regions, and the load and deflection, at the onset of yielding in the support region and at maximum load. For beams ADF.B01 and ADF.B02 yielding of the reinforcement in the span region did not occur.

Table 7.8 Comparison of measured moment values in support and span region at yield and maximum load stage with simulation values

	Support region				Span region			
	M_y (kNm)		M_{max} (kNm)		M_y (kNm)		M_{max} (kNm)	
Specimen	**Exp.**	**sim.**	**exp.**	**sim.**	**exp.**	**sim.**	**Exp.**	**sim.**
ADF.B01	40	41.5	47.1	46.8	--	--	43.4	40
ADF.B02	124	136	151.5	153	--	--	152.3	157
Dmr1	25.6	21.3	26.8	27	--	23.4	24.9	25
Dmr3	23.5	24.8	25.2	25	45.9	43.7	49.2	49.8
A2	73.3	84	116	113	27.1	25.4	32.1	33.7
A5	97.5	98	139	133	90	86.5	108	114

Table 7.9 Comparison of measured load and deflections at yield and maximum load stage with simulation values

	P_y (kN)		Δ_y (mm)		P_{max} (kN)		Δ_{max} (mm)	
Specimen	**Exp.**	**sim.**	**exp.**	**sim.**	**exp.**	**sim.**	**Exp.**	**sim.**
ADF.B01	52.5	54.4	25.2	27.7	68	65	48.2	43.4
ADF.B02	155	160	11.3	11.9	225	227	25	27.6
Dmr1	22.4	19.5	11	7.28	29.1	29.7	21.6	23.4
Dmr3	35	31	22	19	45	48	51	49.5
A2	123	137	3.75	3.47	173	176	23.4	23.2
A5	196	187	3.77	4.11	361	343	21.1	19

Note: exp.= experiment values. sim.= simulation values

The modelling approach is able to simulate the moment redistribution due to cracking and yielding of the reinforcement as can be seen in Figures 7.26 to 7.37. These figures show the ratio between the moment at the support and the moment at the span M_{sup}/M_{sp} versus the mid-span deflection. The good agreement between load versus mid-span deflection is dependent upon the ability of the analysis procedure to model the formation of cracking, and the subsequent redistribution of moments not only at cracking, but also during post-yield behaviour. Different statical systems have also been tested, that is a fixed end beam and a propped cantilever, and the model has been proven to simulate the structural response of the statical systems adequately.

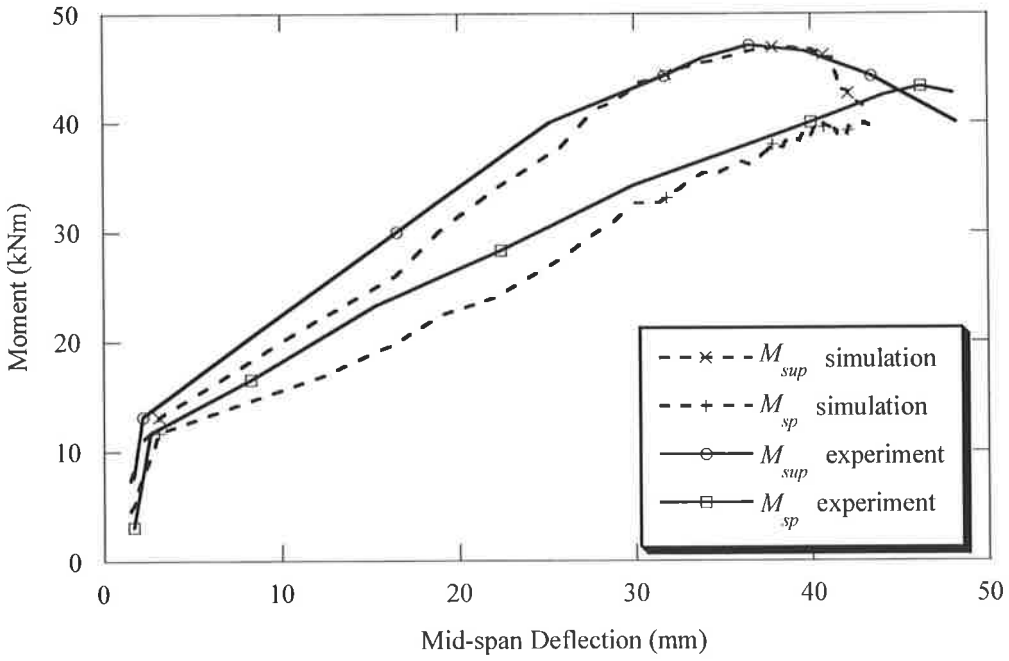

Figure 7.26 Comparison of measured moment versus mid-span deflection with simulation values, test by Patrick *et al.* (1997) beam ADF.B01

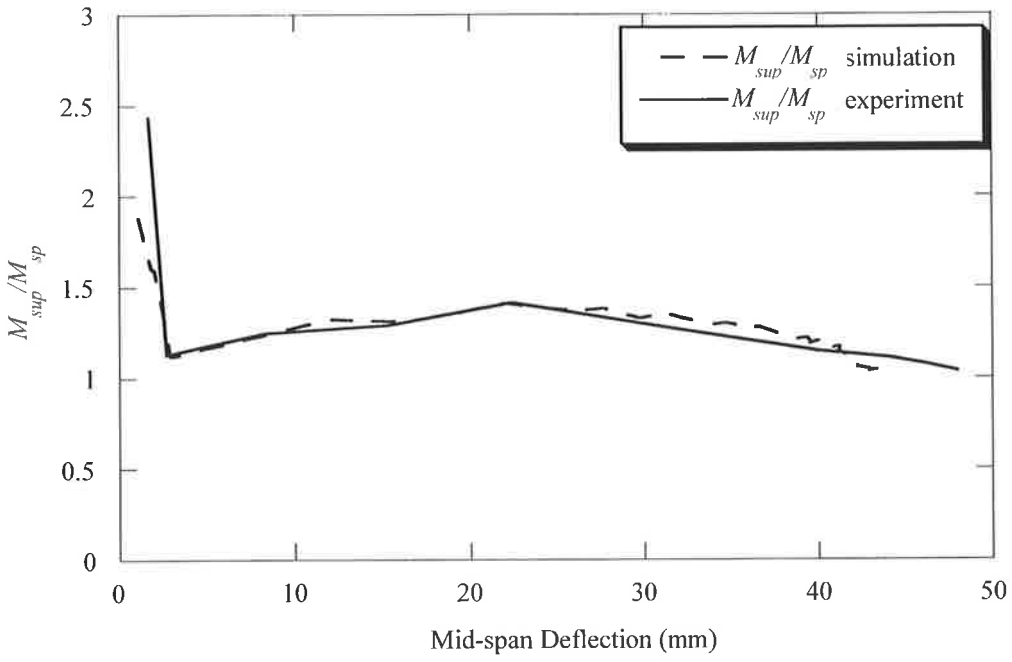

Figure 7.27 Comparison of measured moment redistribution versus mid-span deflection with simulation values, test by Patrick *et al.* (1997) beam ADF.B01

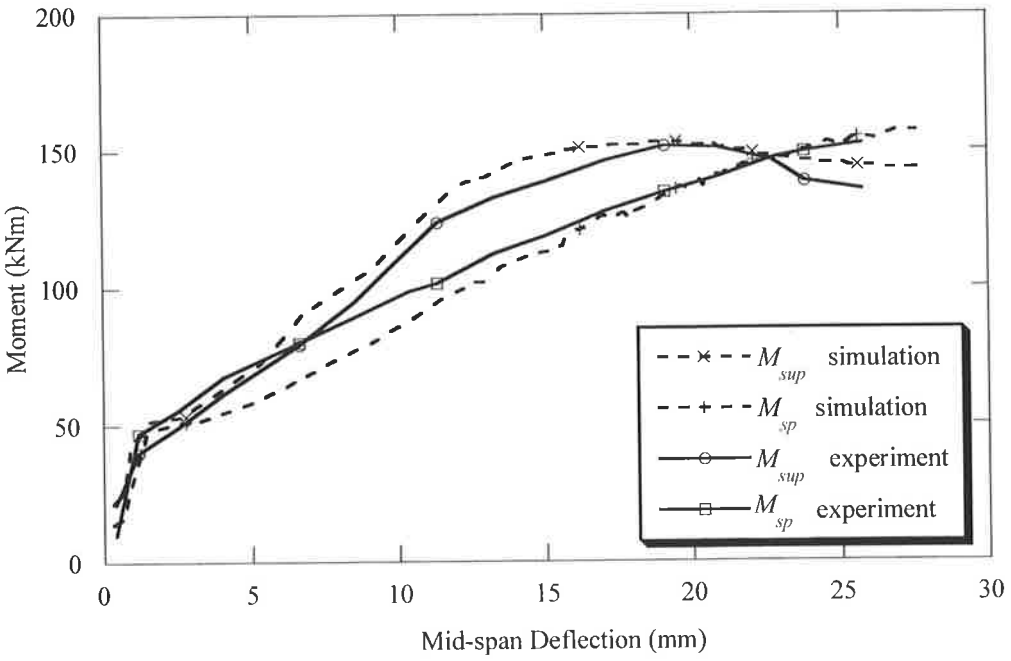

Figure 7.28 Comparison of measured moment versus mid-span deflection with simulation values, test by Patrick *et al.* (1997) beam ADF.B02

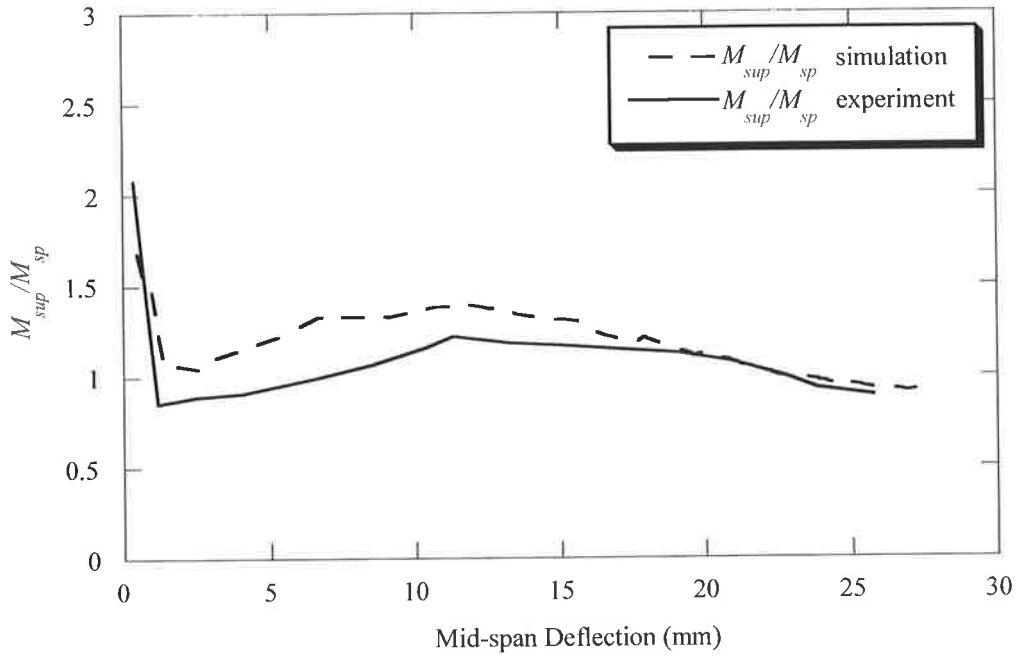

Figure 7.29 Comparison of measured moment redistribution versus mid-span deflection with simulation values, test by Patrick *et al.* (1997) beam ADF.B02

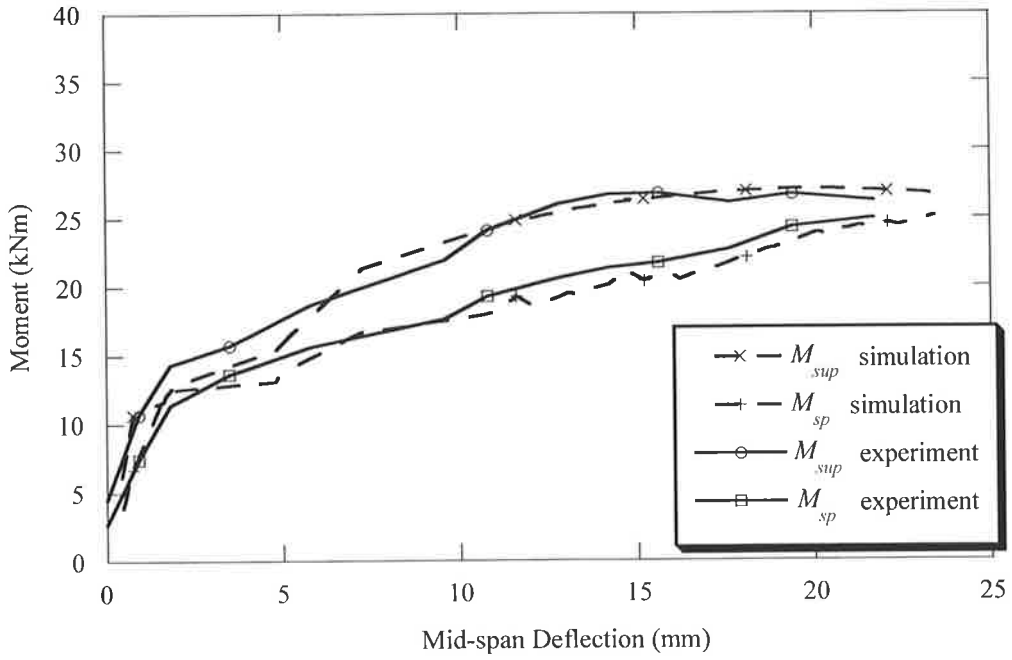

Figure 7.30 Comparison of measured moment versus mid-span deflection with simulation values, test by Eligehausen *et al.* (1995) beam DMR1

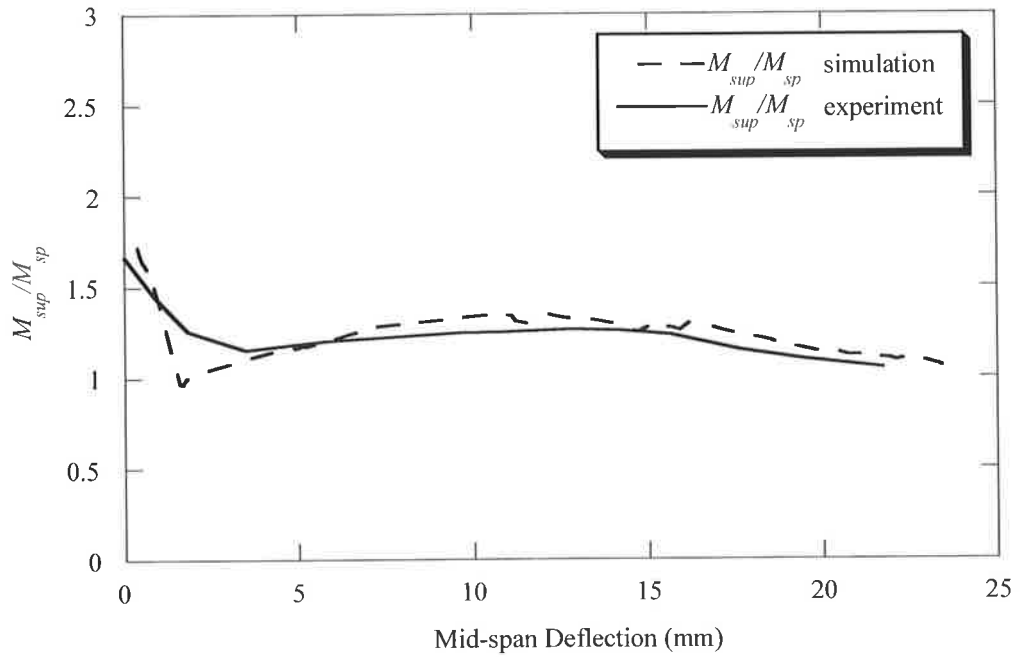

Figure 7.31 Comparison of measured moment redistribution versus mid-span deflection with simulation values, test by Eligehausen *et al.* (1995) beam DMR1

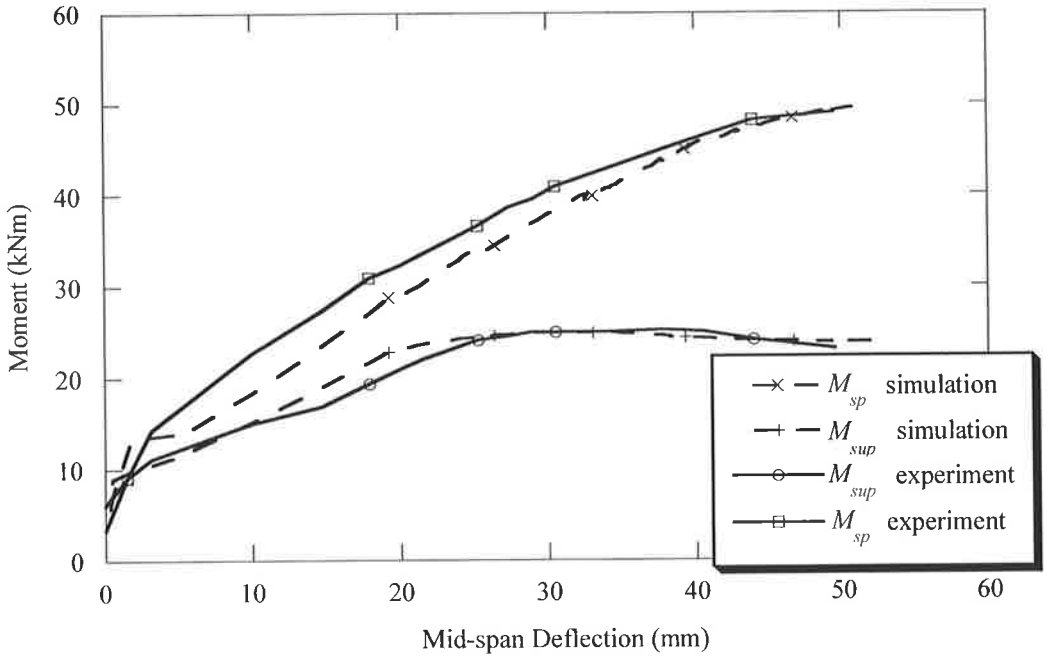

Figure 7.32 Comparison of measured moment versus mid-span deflection with simulation values, test by Eligehausen *et al.* (1995) beam DMR3

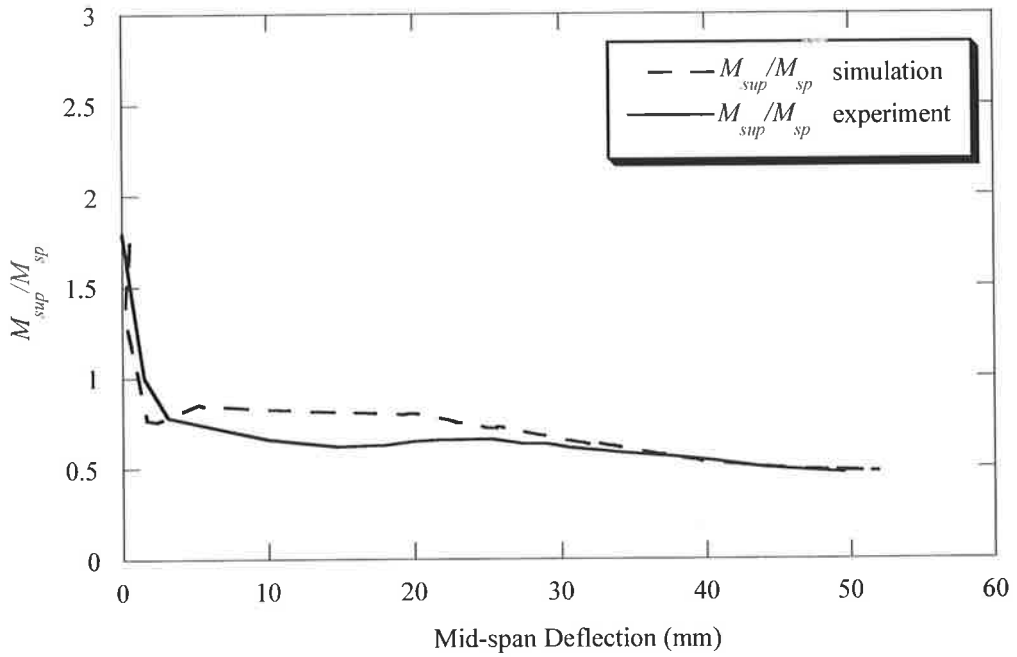

Figure 7.33 Comparison of measured moment redistribution versus mid-span deflection with simulation values, test by Eligehausen *et al.* (1995) beam DMR3

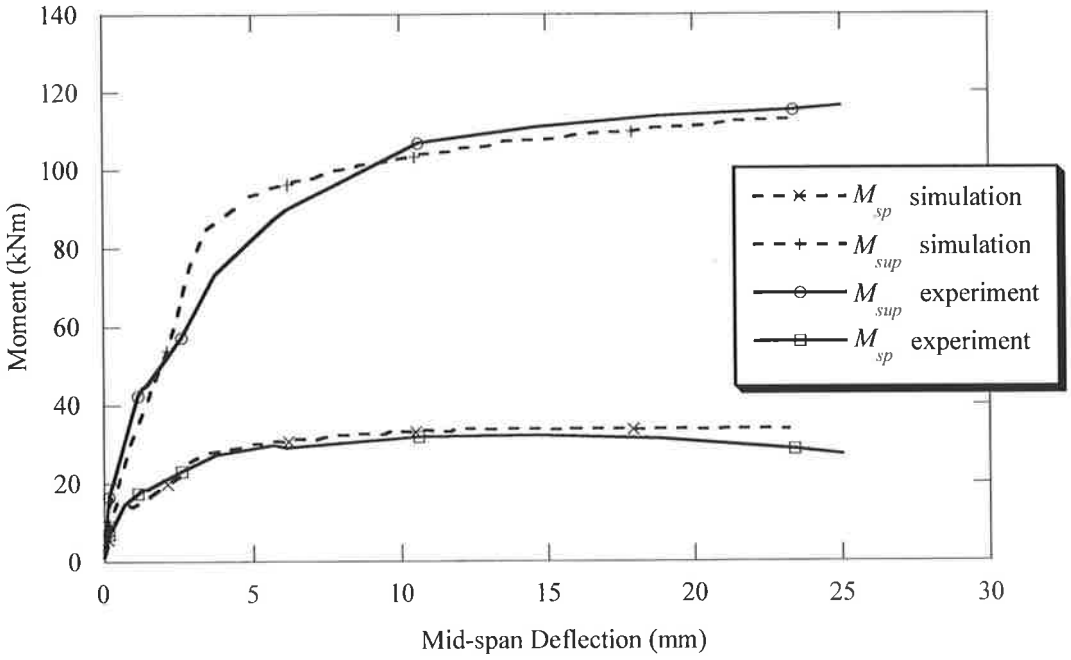

Figure 7.34 Comparison of measured moment versus mid-span deflection with simulation values, test by Bachmann and Thürlimann (1965) beam A2

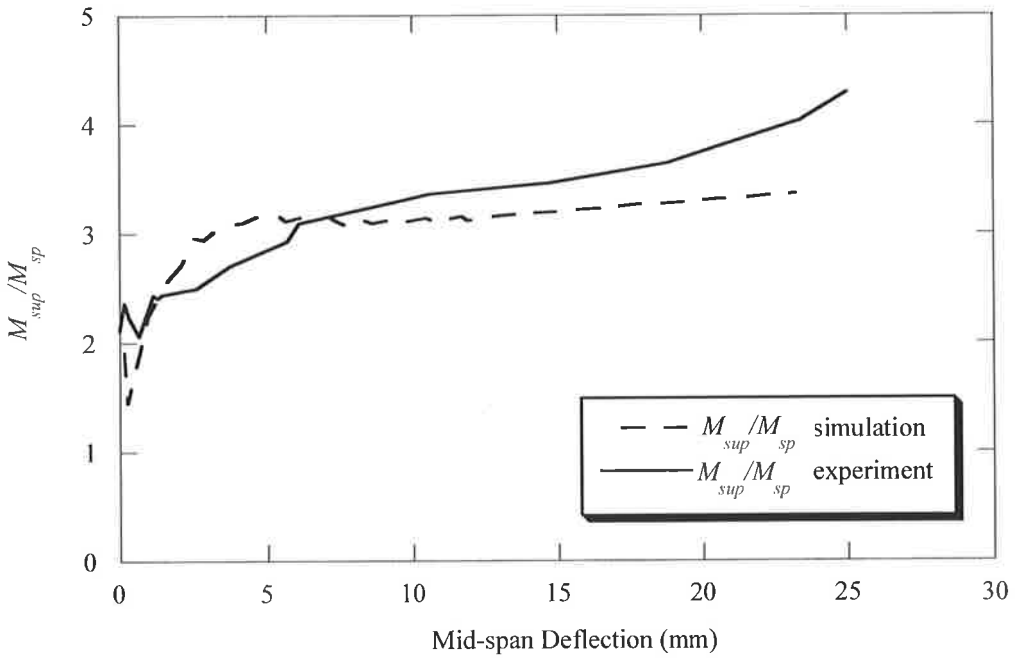

Figure 7.35 Comparison of measured moment redistribution versus mid-span deflection with simulation values, test by Bachmann and Thürlimann (1965) beam A2

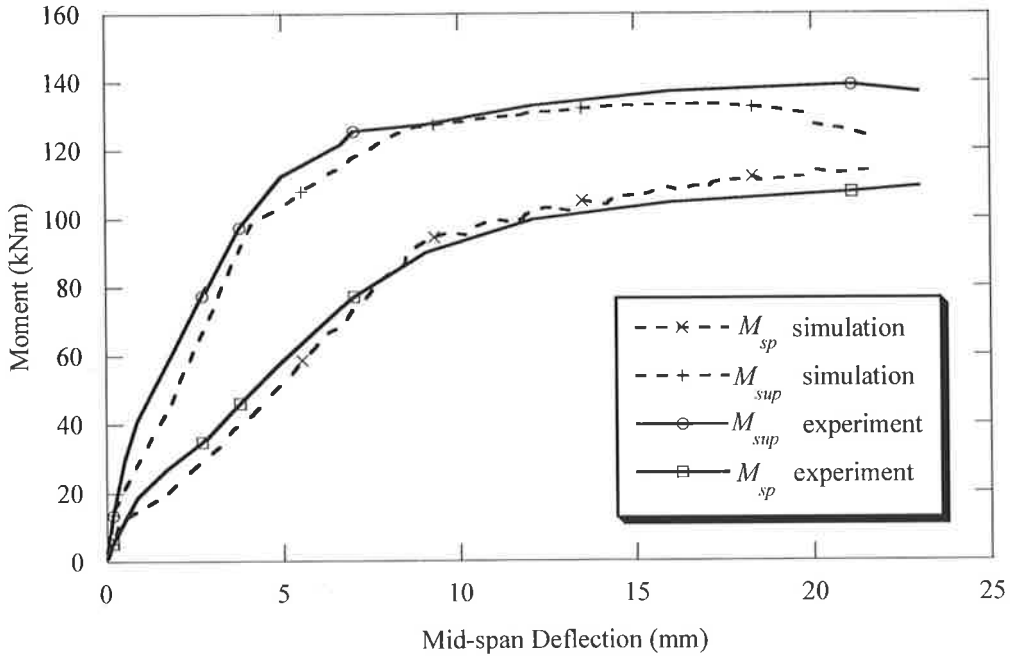

Figure 7.36 Comparison of measured moment versus mid-span deflection with simulation values, test by Bachmann and Thürlimann (1965) beam A5

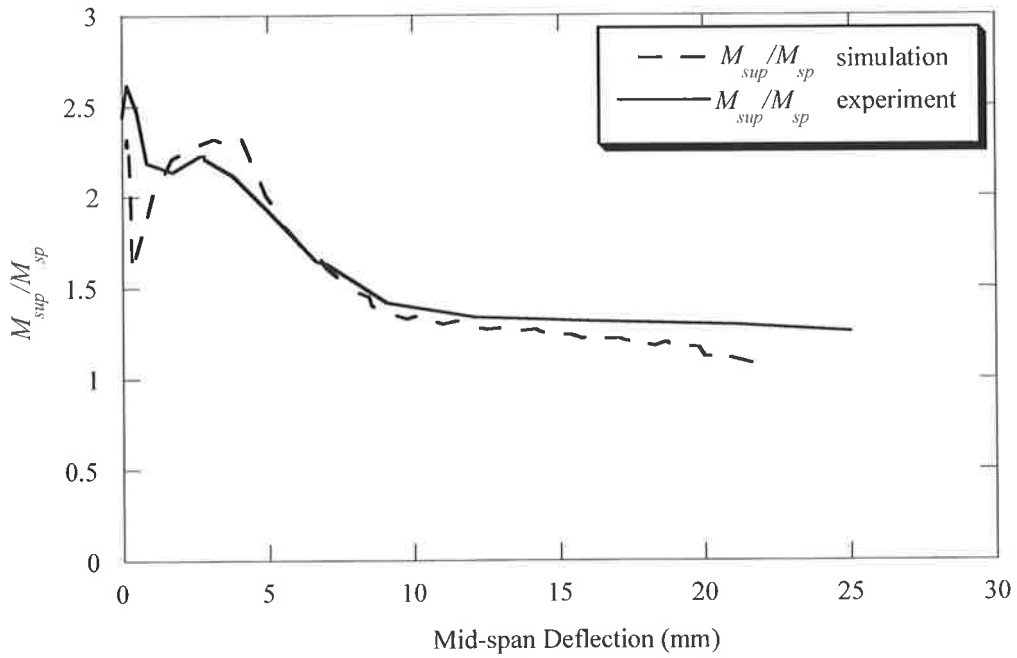

Figure 7.37 Comparison of measured moment redistribution versus mid-span deflection with simulation values, test by Bachmann and Thürlimann (1965) beam A5

7.5 SUMMARY

This chapter has presented an analysis procedure for indeterminate beams incorporating the local deformation model. Comparisons between experiment and simulation results show that the analysis can predict the non-linear overload behaviour of reinforced concrete indeterminate structural elements with reliable accuracy. In particular the redistribution of moments during progressive loading was well predicted, as well as the failure mode, whether by steel fracture or concrete softening.

The next chapter utilises the structural analysis procedure to investigate the parameters that influence the rotation capacity, and degree of moment redistribution in continuous beams.

8

MOMENT REDISTRIBUTION IN INDETERMINATE BEAMS

In this chapter the method of analysis developed in Chapter 7 is used to investigate moment redistribution in continuous reinforced concrete beams at high overload. A parametric study is used to investigate both factors affecting the degree of moment redistribution that can occur, as well as the moment redistribution that can be adopted in design. In Section 8.3 the current structural design clauses in AS 3600 for linear elastic analysis with moment redistribution are evaluated. Recommendations for modification to the design clauses are proposed in Section 8.4.

Previous studies (Eligehausen and Langer, 1987; Langer, 1987; and Bigaj, 1999) have investigated the allowable degree of moment redistribution in indeterminate structures by approximating the support region of a continuous beam with a statically determinate beam cut-out from the real system. The approach used here is an advancement since it is based on a realistic model of indeterminate system behaviour. In addition to evaluating the deformation capacity, strength implications are also evaluated.

8.1 Calculation of Degree of Moment Redistribution

The allowable degree of moment redistribution can be calculated by comparing the required and available rotation capacity of plastic hinges necessary to develop a plastic hinge mechanism in statically indeterminate reinforced concrete members.

The available rotation capacity in a given region depends upon various sectional properties, such as the section size and shape, the amount and distribution of the steel reinforcement, the deformational properties of the steel and concrete, the bond-slip

properties of the steel-concrete interface, and the extent of the plastification region. Conversely, the required rotation capacity depends on the design loads (distributions and combinations), the support details, and the amount of moment redistribution chosen by the designer. Other factors, more difficult to quantify, include the magnitude of imposed external and internal deformations during the life of the structure.

Only moment redistribution from the support to span region of a continuous beam is considered in this investigation. Negative moment redistribution is used most commonly in design practice.

8.1.1 Required Rotation Capacity

Determination of the required plastic rotation capacity in the support region of the fixed end beam in Figure 8.1, is achieved by applying a simplified procedure which considers the deformations in a beam just prior to collapse. The method takes into account influential parameters such as the assumed degree of redistribution, the slenderness ratio of the member and the percentage of reinforcement in the section.

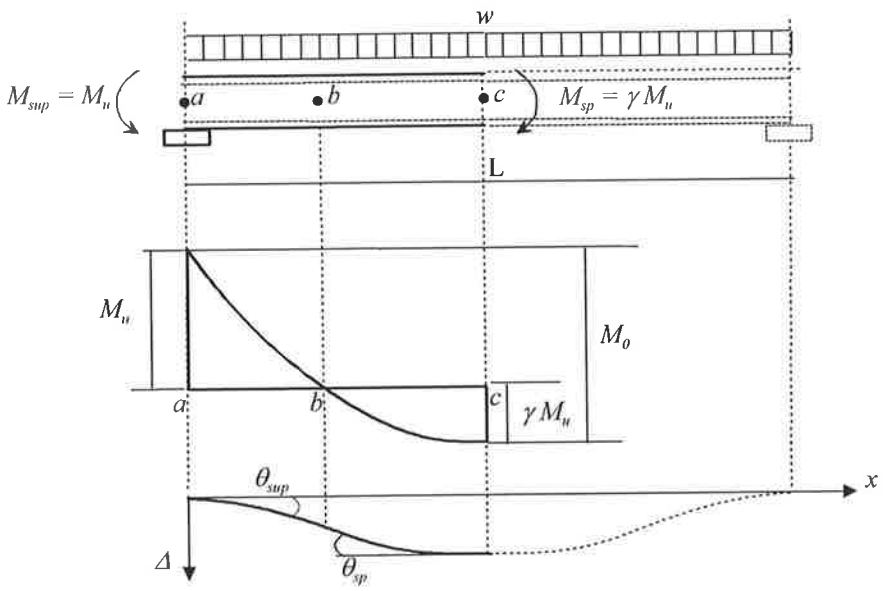

Figure 8.1 Schematic of fixed end beam for calculation of required rotation capacity

Considering the fixed end beam (Figure 8.1) subjected to a uniformly distributed load, symmetry requires that the deflection curve at mid-span has zero slope, so the total

rotation in the negative moment region must be equal to the total rotation in the positive moment region.

For a simplified calculation of the required plastic rotation in the negative moment region, θ_{req}, we can assume that total rotation in the support region, θ_{sup} is made up of a plastic component:

$$\theta_{sup} = \theta_{req} + \theta_{sup,el} \tag{8.1}$$

and that just prior to plastification in the mid-span region the rotation in the mid-span region is purely elastic, ie. $\theta_{sp,el}$. We thus have:

$$\theta_{req} = \theta_{sp,el} - \theta_{sup,el} \tag{8.2}$$

The bending moment at the support and at mid-span at the ultimate load w, are related with the assumed degree of redistribution, β, (eg; 0%, 10%, 20%, 30%) and this relation is given in the following equation:

$$\frac{wl^2}{8} = M_0 = M_u + \gamma M_u \tag{8.3}$$

Here, M_u is the moment capacity over the support, and γ is the ratio of the positive moment capacity to the negative moment capacity:

$$\gamma = \left(\frac{\frac{1}{3} + \beta\frac{2}{3}}{\frac{2}{3} - \beta\frac{2}{3}} \right) \tag{8.4}$$

For the derivation of this expression for γ, refer to Appendix B.1.

The underlying assumption here is that the behaviour in the positive and negative moment regions is elastic, except where the moment capacity is approached, so that the individual block rotations in non-peak regions can be evaluated using an effective cracked section stiffness, EI_{eff}.

In Equation 8.2, the elastic rotations in the span and support region are calculated by integrating the curvature along the beam in the following way.

$$\theta_{sup} = \int_a^b \frac{M}{EI_{eff}} . dx, \text{ and } \theta_{sp} = \int_c^b \frac{M}{EI_{eff}} . dx \tag{8.5}$$

The distribution of moment along the beam element is calculated taking into account the load pad effect in the support region and the ultimate moment capacity at the support and span section (see Chapter 7). The stiffness along the beam is calculated using Branson's effective cracked section stiffness (Branson, 1963).

$$I_{eff} = I_{cr} + (I_g - I_{cr})\left(\frac{M_{cr}}{M}\right)^3 \tag{8.6}$$

Figure 8.2a shows values for the required plastic rotation as calculated for a number of different beam designs (neutral axis parameter, k_u, ranging from 0.05 to 0.5). The values are plotted against k_u and the degree of moment redistribution assumed in the beam design. The required rotation capacity clearly increases with degree of moment redistribution, if the material and geometrical characteristics are kept constant. With decrease in the slenderness ratio the required rotation capacity also reduces (Figure 8.2b). This method for calculating required rotation capacity is comparable to methods used by other researchers (Cosenza *et al.*, 1991b; Bigaj, 1999; Macchi 1976).

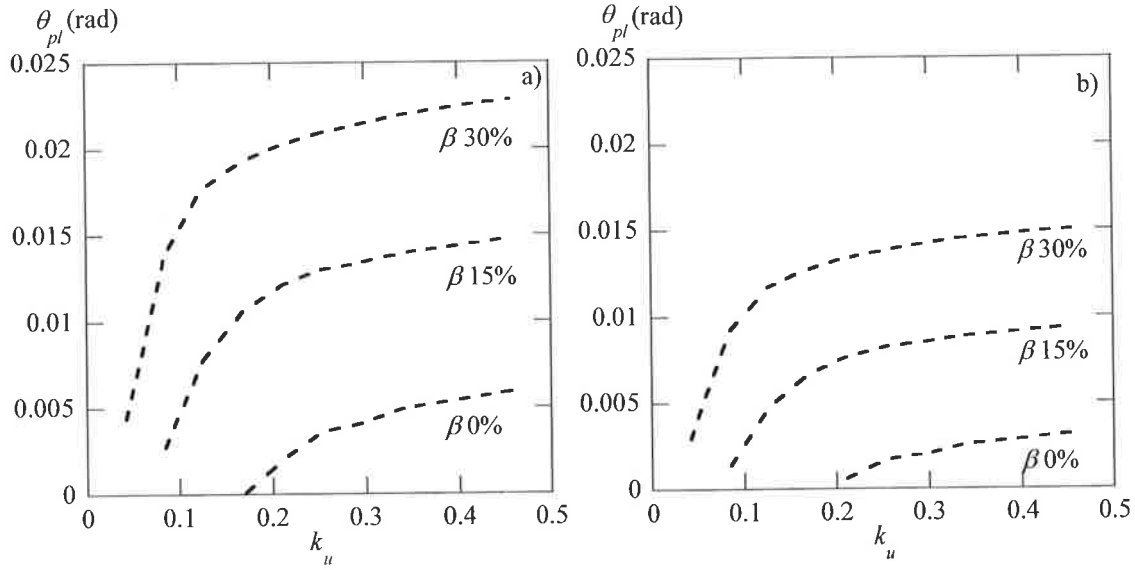

Figure 8.2 Required rotation capacity, f_{cm} = 50MPa, a) L/d = 35, b) L/d = 25

8.1.2 Available Rotation Capacity

Calculation of the available rotation capacity in the support region of the fixed end beam is carried out applying the analysis method for indeterminate beams incorporating the local deformation model as introduced in Chapter 7.

The available rotation capacity in the hinge region of the support is calculated as the difference between the total rotation at ultimate (maximum) load, and the total rotation at the onset of yielding. The rotation in the support region is calculated out to the point of contraflexure. In Figure 8.3 it can be seen that with increase in the degree of redistribution the available rotation capacity in the support region reduces.

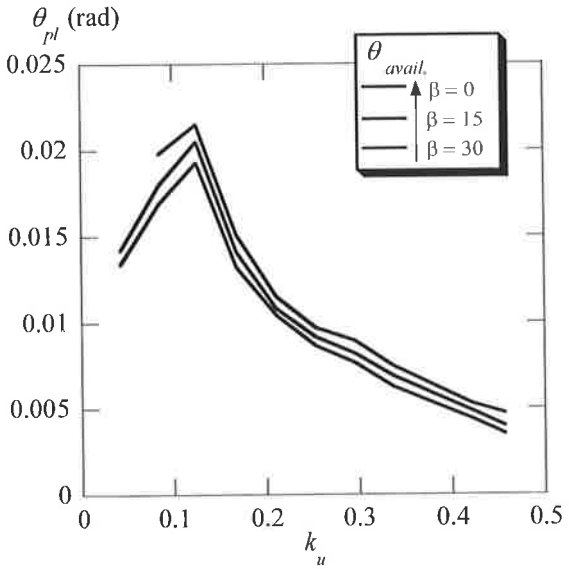

Figure 8.3 Available rotation capacity, f_{cm} = 50MPa, L/d = 35

8.1.3 Degree of Moment Redistribution

The intersection between the curves of available and required plastic rotations provides the limiting value of k_u that will allow the chosen degree of moment redistribution to occur. The intersection points are used to plot the β-k_u relation.

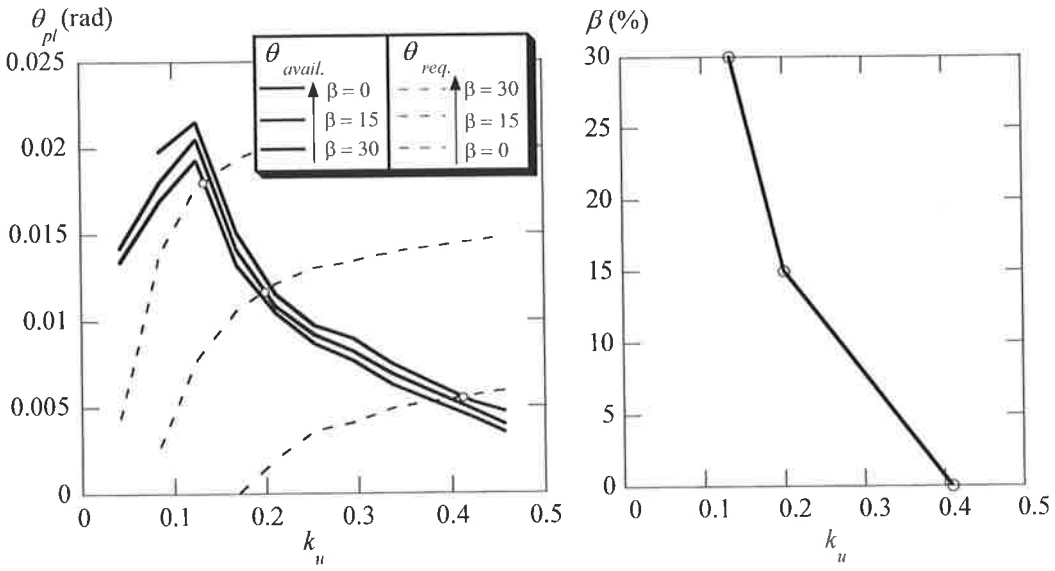

Figure 8.4 Available degree of redistribution, f_{cm} = 50MPa, L/d = 35

Results of a study involving a wide range of beam and one-way slab designs are given in the following section to evaluate whether limits for the simplified approach to design of linear elastic analysis with moment redistribution given in AS 3600, deliver safe and conservative results.

8.2 PARAMETRIC STUDY

The study considers a fixed end beam subjected to a uniformly distributed load, which is a conservative approach to modelling an interior span of a continuous beam. Two section geometry types have been chosen; a one-way slab section and a rectangular beam section. The study investigates the influence of the following parameters:

For the rectangular beam designs:

- Three effective beam depths: 200mm, 500mm and 800mm
- Two average concrete strengths: 30MPa and 50MPa
- Two slenderness ratios: 20 and 30.

For the one-way slab designs:

- Two ductility steel classes: Class N (normal) and Class L (low) ductility steel
- Two average concrete strengths: 30MPa and 50MPa
- Two slenderness ratios: 25 and 35.

In a further study (Section 8.2.5), the influence of the statical system on the degree of moment redistribution is investigated by considering a propped cantilever loaded at third points.

To investigate the influence of the steel properties on the degree of moment redistribution, the one-way slab section is chosen as it represents real situations where Class L (low ductility mesh) and Class N (normal ductility bar) steels are used in practice in Australia.

The rectangular beam design was selected to study the size effect. To achieve this, the span to depth ratio, L/d, is kept constant and the effective depth, d, is varied. The steel characteristics have been kept constant to represent reinforcing steel of Class N ductility. Typically, Class L mesh is not used as the main longitudinal reinforcement in the construction of suspended beams.

In addition to investigating the influence of the steel properties and the size effect on the degree of moment redistribution, the span to depth ratio, L/d, and concrete strength, f'_{cm}, have also been varied in the designs for the one-way slab and rectangular beam section types.

The beams and one-way slabs were designed for a range of tensile steel percentages, ρ, to cover both failure modes of steel fracture and concrete softening (0.25%, 0.38%, 0.5%, 0.63%, 0.75%, 1.0%, 1.5%, 1.75%, 2.0%, 2.5%, 2.75%). The range of ρ values provides theoretical k_u values between 0.04 to 0.5. Subsequent to altering the percentage of steel in the designs, the degree of moment redistribution from the support to span region was varied, 0%, 15% and 30%.

To limit the number of influencing parameters, the concrete cover assumed was equal to 2 times the bar diameter, and the bar diameter was adjusted according to the member size and required reinforcement ratio. Realistic bar diameters were chosen corresponding to the steel class.

Tables 8.1 and 8.2 summarise the properties varied in the simulation runs. In total 627 beams were simulated, that is for each shaded box, 33 beams were designed to cover the range of tensile reinforcement ratios, and the assumed degree of moment redistribution (11 reinforcement ratios by 3 degrees of moment redistribution).

The strain-hardening ratio and uniform elongation have been varied for both steel types of Class N and Class L, hence relating to the steels defined as Steel N1 to N5 and Steel L1 to L5 (see Table 8.3 and in Section 8.2.1).

Table 8.1 One-way slab design, effective depth constant, d = 200mm, B = 500mm

		Steel Class						
		N1/L1	N2/L2	N3/L3	N4/L4	N5/L5		
f'_{cm} (MPa)	30						35	*L/d*
	50						35	
	50						25	

Table 8.2 Rectangular beam design, steel ductility class constant, Steel N1, B = 400mm

		d (mm)				
		200	500	800		
f'_{cm} (MPa)	30				20	*L/d*
	50				20	
	50				30	

Since the real behaviour is to be modelled, average values are used for the material properties. Therefore, the values of degree of moment redistribution to be given in this section are not to be interpreted as design values. Section 8.4 will deal with design recommendations.

8.2.1 Effect of Steel Properties

The influence of the steel properties is studied by keeping the concrete strength equal to 50MPa and slenderness ratio equal to 35 and adopting the one-way slab section. The steel properties varied in the simulation were the strain-hardening ratio f_{su}/f_{sy} and the uniform elongation ε_{su}. Steels N1-N5 represent steels of normal ductility and L1-L5 low ductility steel. Tables 8.3 and 8.4, taken from Chapter 6 display the values varied for the steel classes.

Table 8.3 Normal ductility steel

		f_{su}/f_{sy}		
		1.05	**1.08**	**1.2**
ε_{su} (%)	**3**		N5	
	5	N2	N1	N3
	10			N4

Table 8.4 Low ductility steel

		f_{su}/f_{sy}		
		1.03	**1.04**	**1.05**
ε_{su} (%)	1.5	L1	L2	L3
	2.5	L4		
	3.5	L5		

Figures 8.5 and show the influence of the steel ductility class on the degree of moment redistribution calculated as explained in Section 8.1. Typically, for Class N steel the available rotation capacity is higher than for Class L steels, and the transition from steel fracture to concrete failure occurs at a lower ratio of tensile reinforcement in the section. This in turn results in a higher degree of allowable moment redistribution for Steel N1 compared to Steel L1. Figures C.1 to C.8 in Appendix C show the results of the degree of moment redistribution for the beam designs reinforced with steel of varying ductility properties, in accordance with Tables 8.3 and 8.4.

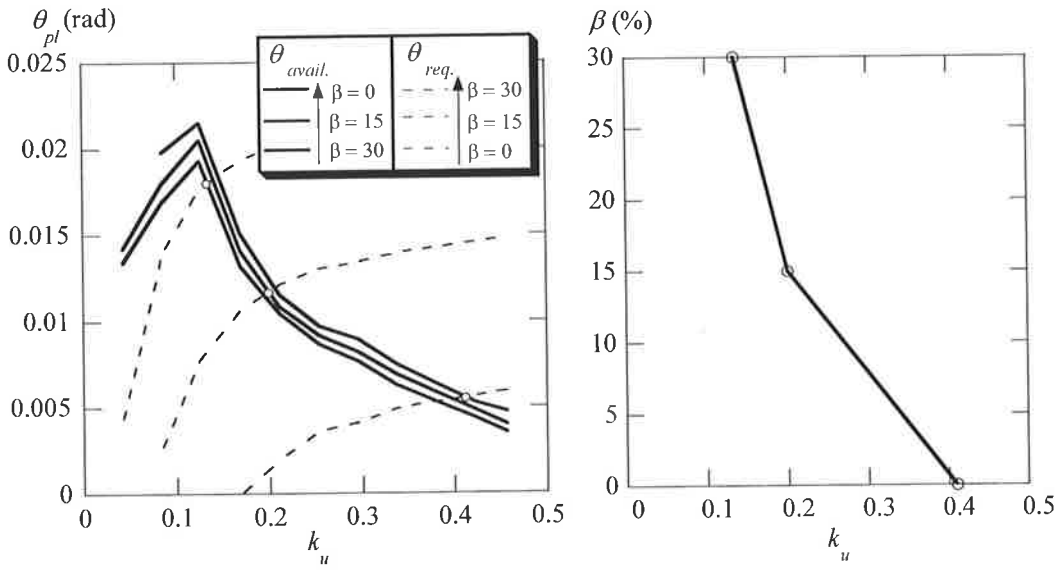

Figure 8.5 Available degree of redistribution for Steel N1 $\varepsilon_{su} = 5\%, f_{su}/f_{sy} = 1.08$

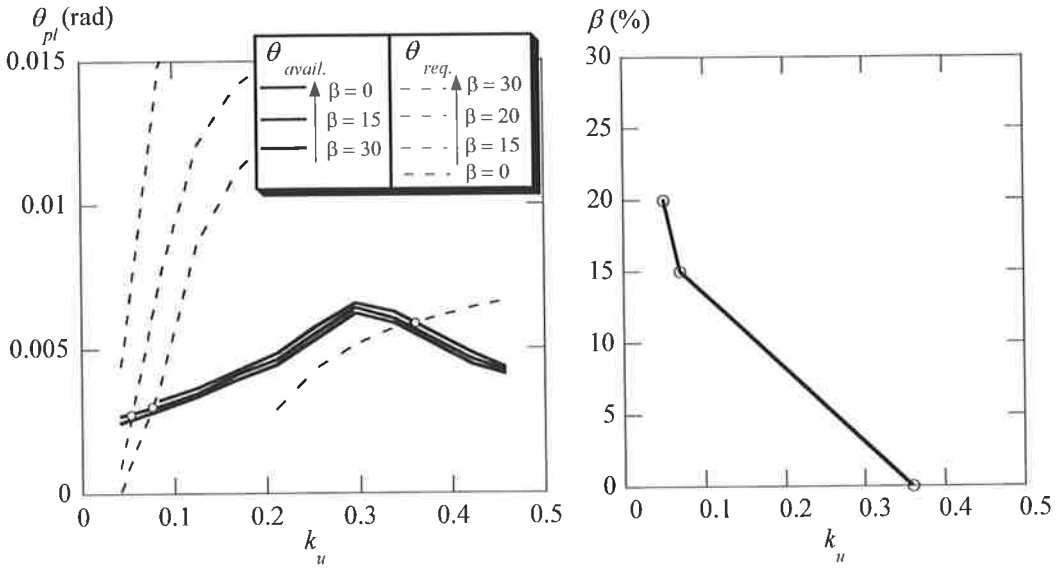

Figure 8.6 Available degree of redistribution for Steel L1 ε_{su} = 1.5%, f_{su}/f_{sy} = 1.03

To summarise the findings, the effect of the variation of the strain-hardening ratio and the uniform elongation on the degree of moment redistribution is displayed in Figures 8.7 to 8.11.

It can be seen that with a constant value of the uniform elongation, an increase in the strain-hardening ratio, f_{su}/f_{sy}, provides a higher degree of moment redistribution for the same designs. This is true for both Steel N1 and Steel L1. An increase in the strain-hardening ratio imparts higher plastic hinge lengths and crack widths together with less tension stiffening between cracks. The outcome results in a higher rotation capacity in the critical post-yield regions.

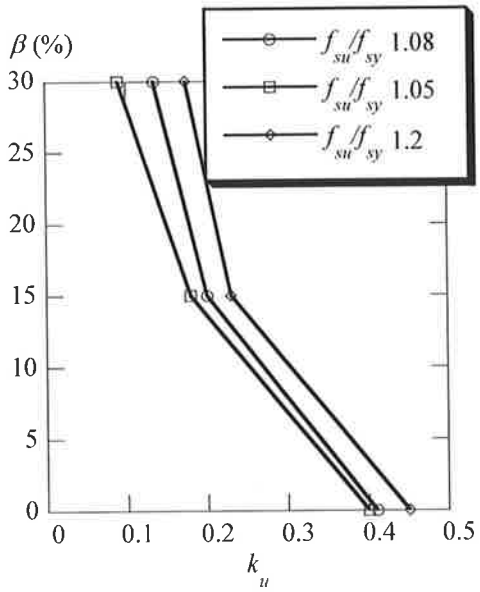

Figure 8.7 **Influence of the variation strain-hardening ratio, f_{su}/f_{sy}, on degree of moment redistribution for Class N steels, $\varepsilon_{su} = 5\%$**

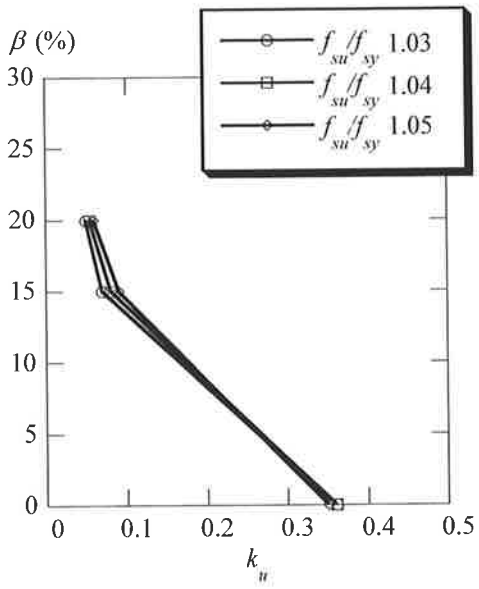

Figure 8.8 **Influence of the variation strain-hardening ratio, f_{su}/f_{sy}, on degree of moment redistribution for Class L steels, $\varepsilon_{su} = 1.5\%$**

Considering the influence of the uniform elongation whilst maintaining a constant strain-hardening ratio, if failure is governed by steel fracture, an increase in the uniform elongation provides a higher degree of moment redistribution. However if failure is governed by concrete, an increase in the uniform elongation causes a reduction in the

degree of moment redistribution since the strain hardening slope, E_{sh}, is reduced providing less rotation capacity.

It is clearly evident in Figure 8.9 for Steel L1, with increase in the uniform elongation for the cases governed by steel fracture, that is at the assumed degrees of moment redistribution of 15% to 30%, an increase in the allowable degree of re-distribution can be achieved. This can also be observed Figure 8.10 at 30% degree of moment re-distribution where failure is governed by steel fracture.

In Figure 8.11 it is shown that with increase in the uniform elongation for the same strain-hardening ratio, since failure is governed by concrete at the points where the available and required rotation capacities meet, a reduction in the allowable degree of moment redistribution results.

Hence for low tensile reinforcement ratios represented by low k_u values in the range where steel fracture governs, an increase in the strain-hardening ratio will produce more rotation capacity. In this range of behaviour an increase in the uniform elongation with constant f_{su}/f_{sy} ratio will also provide a positive effect on the allowable degree of moment redistribution. However a negative effect on the degree of moment re-distribution is found for high tensile reinforcement ratios where concrete failure governs, since an increase in the uniform elongation with constant f_{su}/f_{sy} ratio will provide a reduced rotation capacity. Therefore if the steel ductility parameters are to be improved to provide safer and more conservative designs, an increase in the uniform elongation ε_{su} value should be followed by an increase in the strain-hardening ratio f_{su}/f_{sy}.

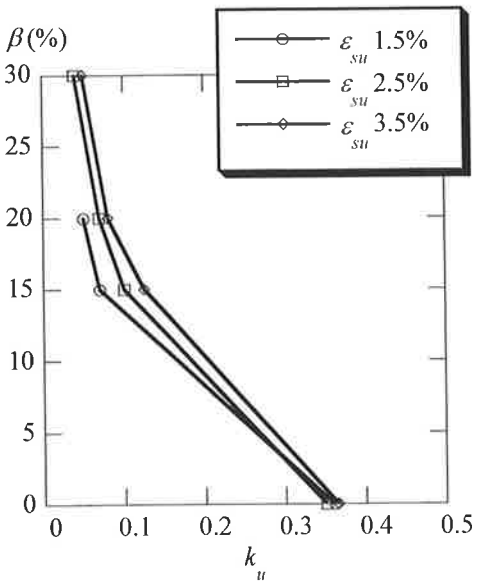

Figure 8.9 **Influence of the uniform elongation, ε_{su}, on degree of moment redistribution for Class L steels, f_{su}/f_{sy} = 1.03**

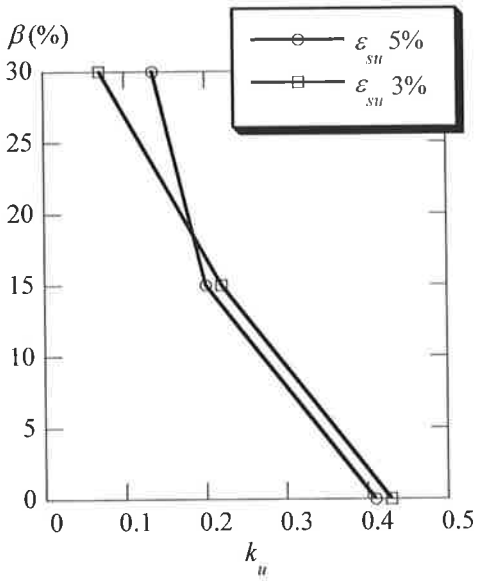

Figure 8.10 **Influence of the uniform elongation, ε_{su}, on degree of moment redistribution for Class N steels, f_{su}/f_{sy} = 1.08**

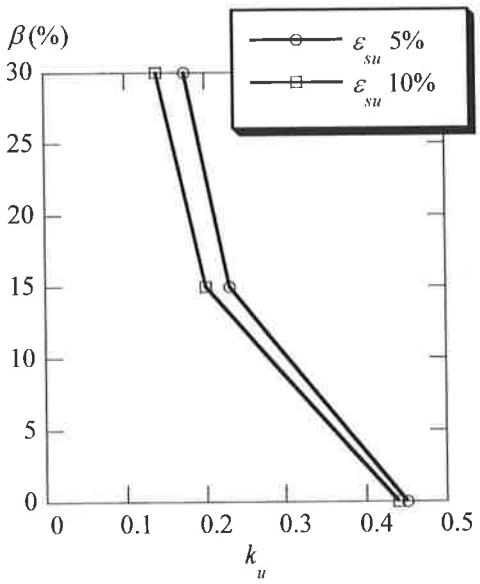

Figure 8.11 Influence of the uniform elongation, ε_{su}, on degree of moment redistribution for Class N steels, $f_{su}/f_{sy} = 1.2$

8.2.2 Size Effect

The size effect has been investigated using the rectangular beam section and varying the effective depth of the section, where d equals 200, 500 or 800mm. The slenderness ratio and concrete strength have been kept constant to 20 and 50MPa respectively. The simulations were carried out for Steel N1.

Figures 8.12 to 8.15 show, with increase in the section size whilst maintaining a constant slenderness ratio the available rotation capacity reduces, therefore corresponding to a decrease in the allowable degree of moment redistribution for the design. Recalling from Chapter 6, that with increase in the section depth, the plastic hinge length increases, however the crack spacing and maximum crack width are reduced, thus leading to a reduction in rotation capacity with increase in section depth for the same slenderness ratio.

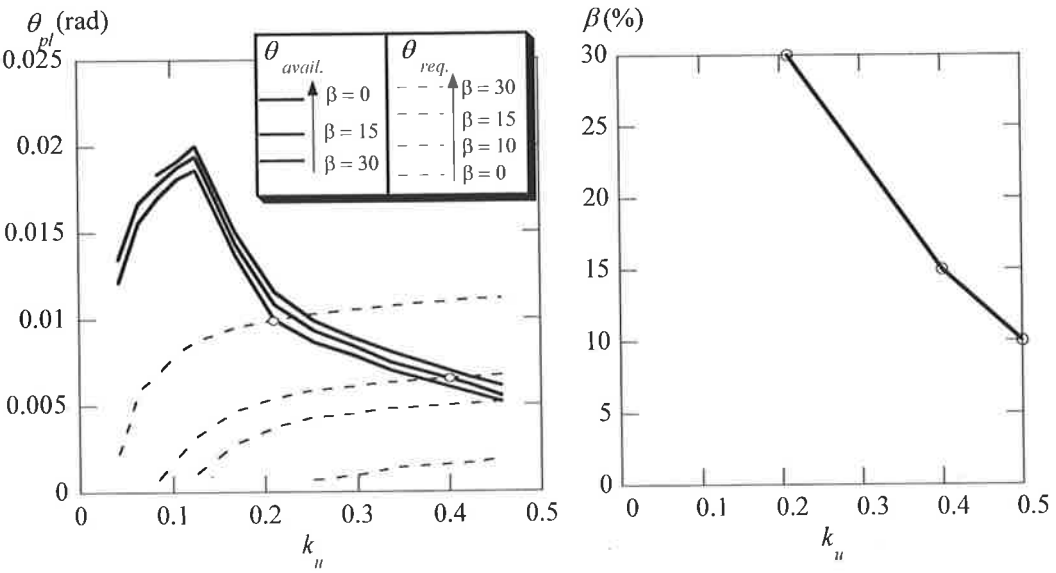

Figure 8.12 Available degree of redistribution for Steel N1, d = 200mm, f_{cm} = 50MPa, L/d = 20

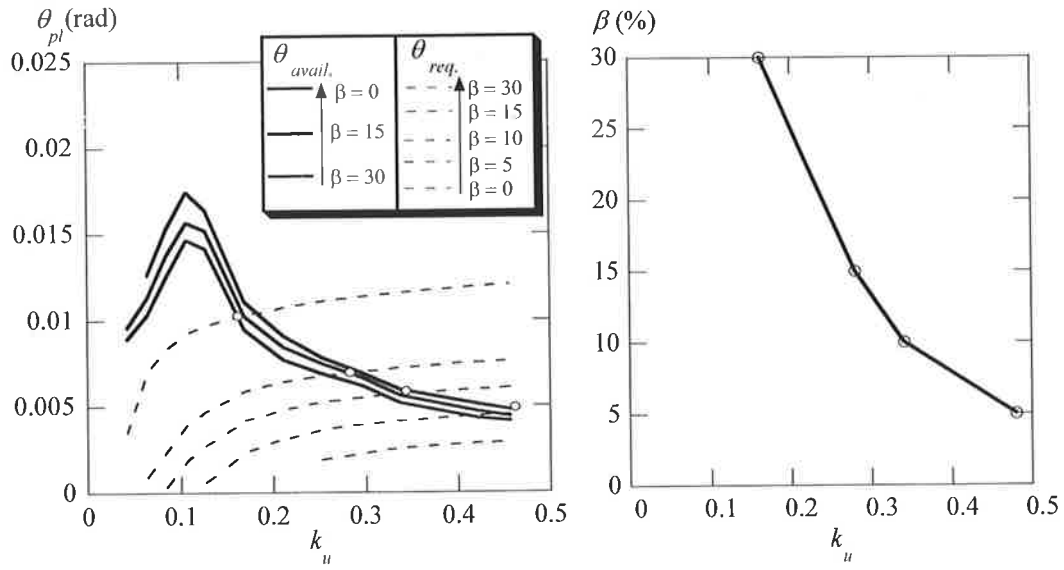

Figure 8.13 Available degree of redistribution for Steel N1, d = 500mm, f_{cm} = 50MPa, L/d = 20

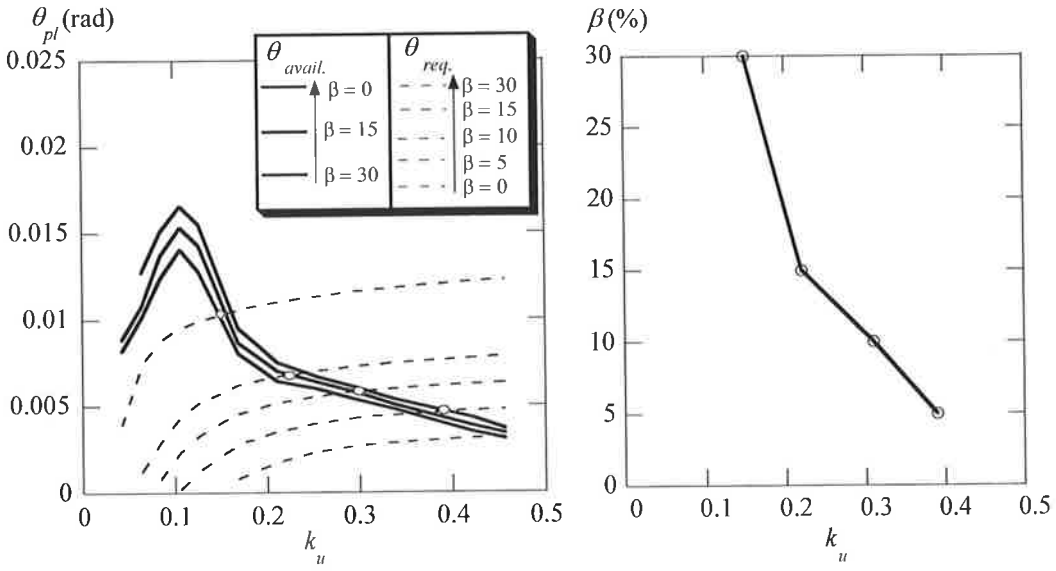

Figure 8.14 Available degree of redistribution for Steel N1, d = 800mm, f_{cm} = 50MPa, L/d = 20

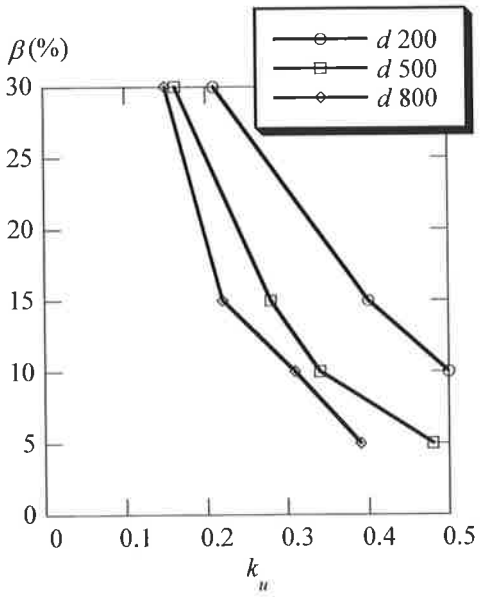

Figure 8.15 Influence of the effective depth on degree of moment redistribution, Steel N1, f_{cm} = 50MPa, L/d = 20

8.2.3 Effect of Slenderness Ratio

The influence of the slenderness ratio on the degree of moment redistribution is studied utilising the rectangular beam section, in which case the effective depth d = 500mm, and the one-way slab section, d = 200mm. In the simulations the concrete strength, f_{cm} = 50MPa, and steel characteristics have been kept constant.

With increase in the slenderness ratio, the available rotation capacity in the support region increases marginally relative to the increase in the required rotation capacity (refer to Figures 8.16 to 8.18). The marginal increase in available rotation capacity can be attributed to the increase in plastic hinge length with higher slenderness ratios as shown in Chapter 6. Overall, this effect provides a higher degree of allowable moment redistribution for lower slenderness ratios since less rotation capacity is required for the design. The same effect is observed for Class L steels (Figure 8.19) and for the varying cross section details (Also see Appendix C and refer to Figures C.9 to C.12).

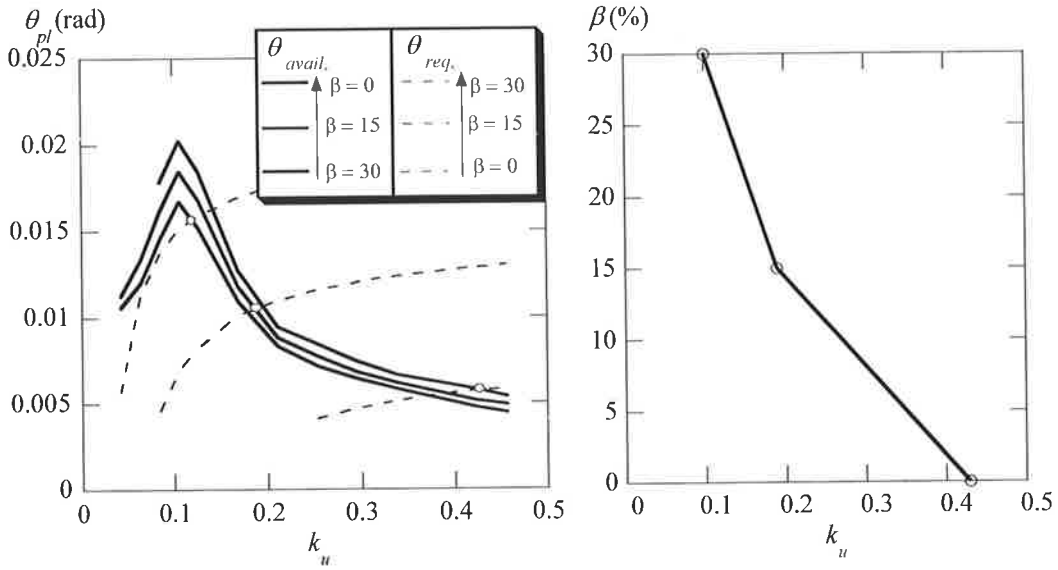

Figure 8.16 Available degree of redistribution for Steel N1, rectangular beam design, d = 500mm, f_{cm} = 50MPa, L/d = 30

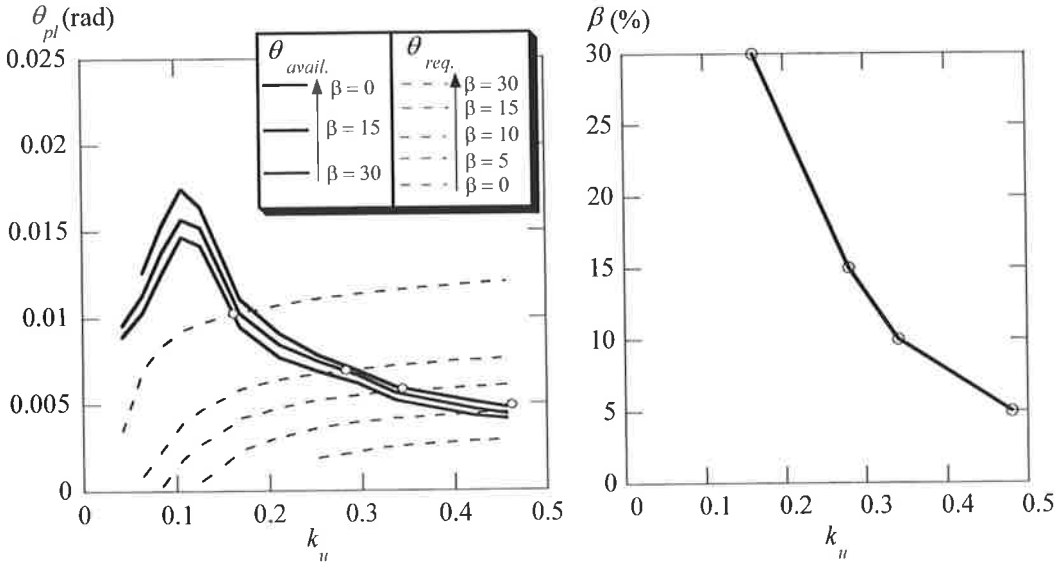

Figure 8.17 Available degree of redistribution for Steel N1, rectangular beam design, d = 500mm, f_{cm} = 50MPa, L/d = 20

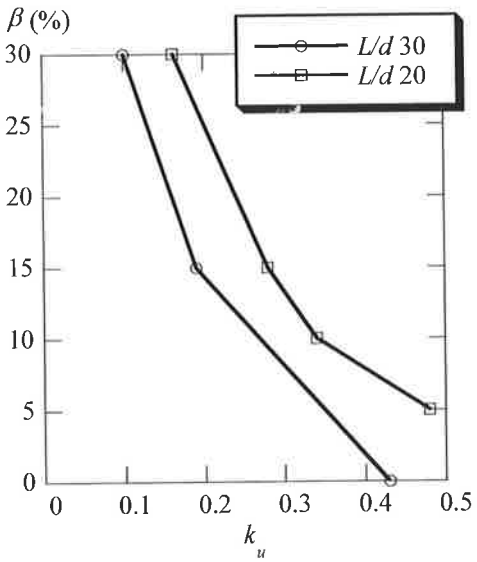

Figure 8.18 Influence of the slenderness ratio on degree of moment redistribution, rectangular beam design, Steel N1, d = 500mm, f_{cm} = 50MPa

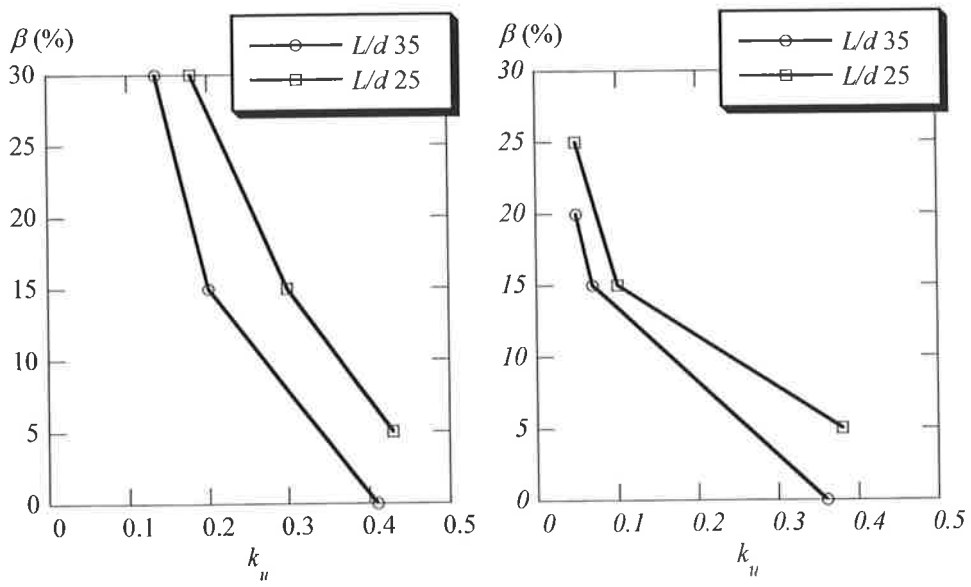

Figure 8.19 Influence of the slenderness ratio on degree of moment redistribution, one-way slab design, a) Steel N1, b) Steel L1, d = 200mm, f_{cm} = 50MPa,

8.2.4 Effect of Concrete Strength

Investigation into the effect of the concrete strength on the degree of moment redistribution was limited to normal strength concrete and consequently, the peak compressive stress, f_{cm}, was adjusted. Again the rectangular beam section and the one-way slab were used in the simulations. The slenderness ratio, steel properties and effective depth were kept constant. Concrete strengths of 30MPa and 50MPa were used which relate to average concrete strengths that can be achieved for specified 24MPa and 32MPa concrete.

It is acknowledged that with high strength concrete the strain at peak stress is an important variable but in this case normal strength concrete is considered. An increase in the concrete compressive stress only is investigated.

For normal strength concrete, Figures 8.20 and 8.21 show, with increase in the concrete strength the available rotation capacity increases and the transition from steel fracture to concrete failure occurs at a higher percentage of tensile steel reinforcement. Recalling from Chapter 6, when failure is governed by concrete, for a higher concrete compressive strength and unchanged tensile reinforcement ratio, an increase in the steel strains and the bond strength between cracks, results in increased crack widths and

overall rotation capacity. So the increase in the concrete strength together with the higher bond strength between cracks is actually an advantage when it comes to the deformability of the reinforced concrete member. Thus for normal strength concrete an increase in the compressive strength a higher degree of moment redistribution can be achieved. This trend is also observed for Class L and Class N steels and for both the rectangular and one-way slab designs (Figures 8.22 and 8.23). (Also see Appendix C and refer to Figures C.13 to C.16).

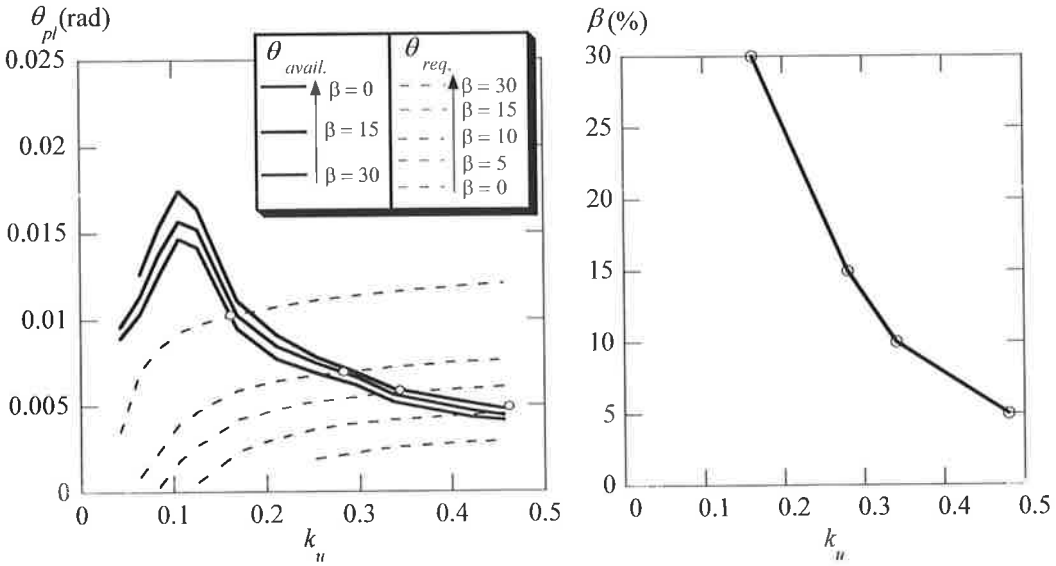

Figure 8.20 Available degree of redistribution for Steel N1, rectangular beam design, d = 500mm, L/d = 20, f_{cm} = 50MPa

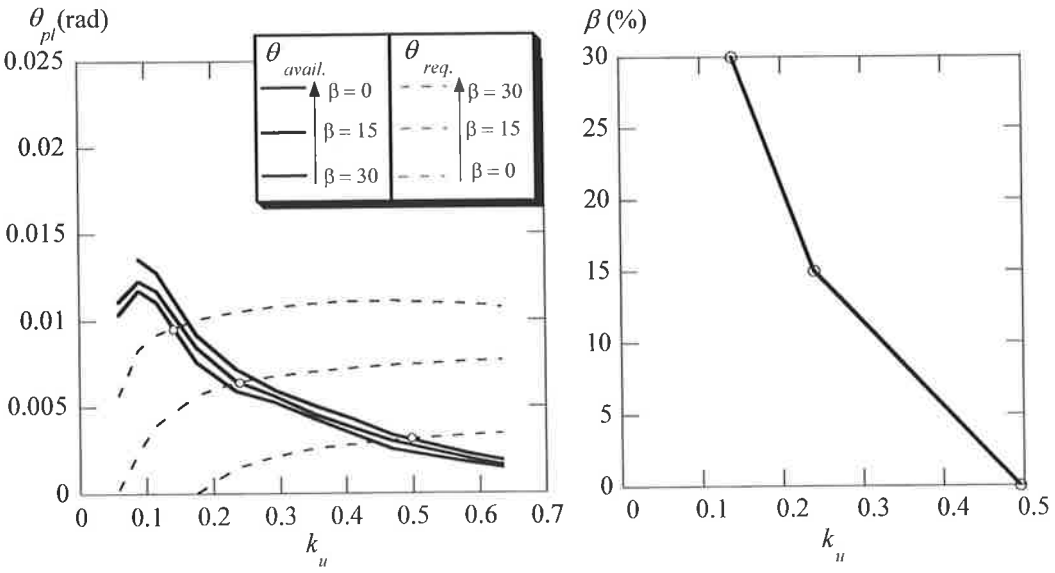

Figure 8.21 **Available degree of redistribution for Steel N1, rectangular beam design, d = 500mm, L/d = 20, f_{cm} = 30MPa**

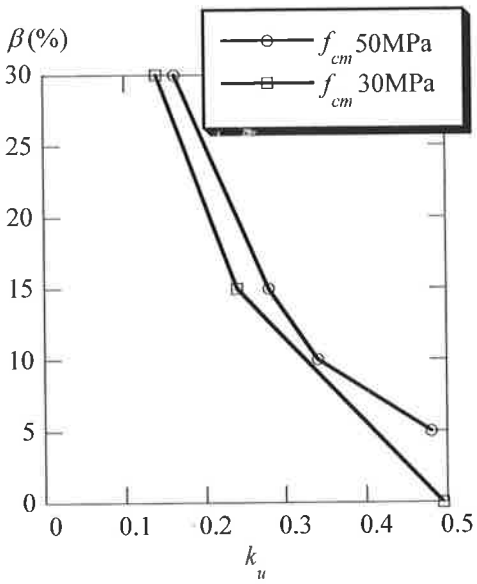

Figure 8.22 **Influence of the concrete strength on degree of moment redistribution, rectangular beam design, Steel N1, d = 500mm, L/d = 20**

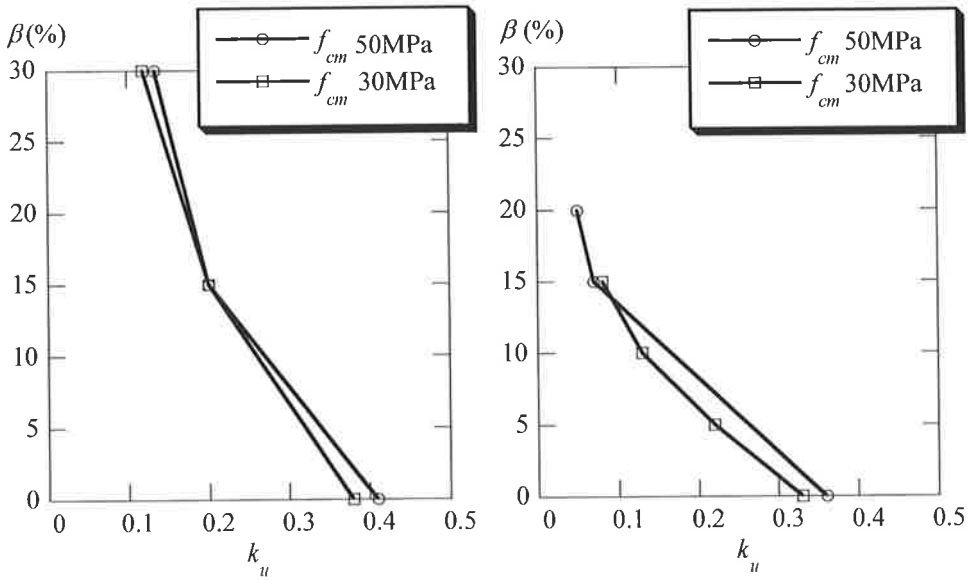

Figure 8.23 Influence of the concrete strength on degree of moment redistribution, one-way slab design, a) Steel N1, b) Steel L1, d = 200mm, L/d = 35

8.2.5 Effect of Statical System

The influence of the statical system on the degree of moment redistribution is investigated by considering a propped cantilever loaded at third points, and a fixed end beam subjected to a uniformly distributed load. The steel properties, effective depth, slenderness ratio and concrete strength have been kept constant to Steel N1, d = 200, L/d = 35 and f_{cm} = 50MPa, respectively. Investigation into the effect of the statical system is undertaken to demonstrate that the fixed end beam is a more critical case compared to the propped cantilever case for studying the allowable degree of moment redistribution.

Similar to the case of the fixed end beam, steps are taken to develop a procedure to calculate the required rotation capacity in the support region of the propped cantilever (Figure 8.24). The method for the propped cantilever is now introduced.

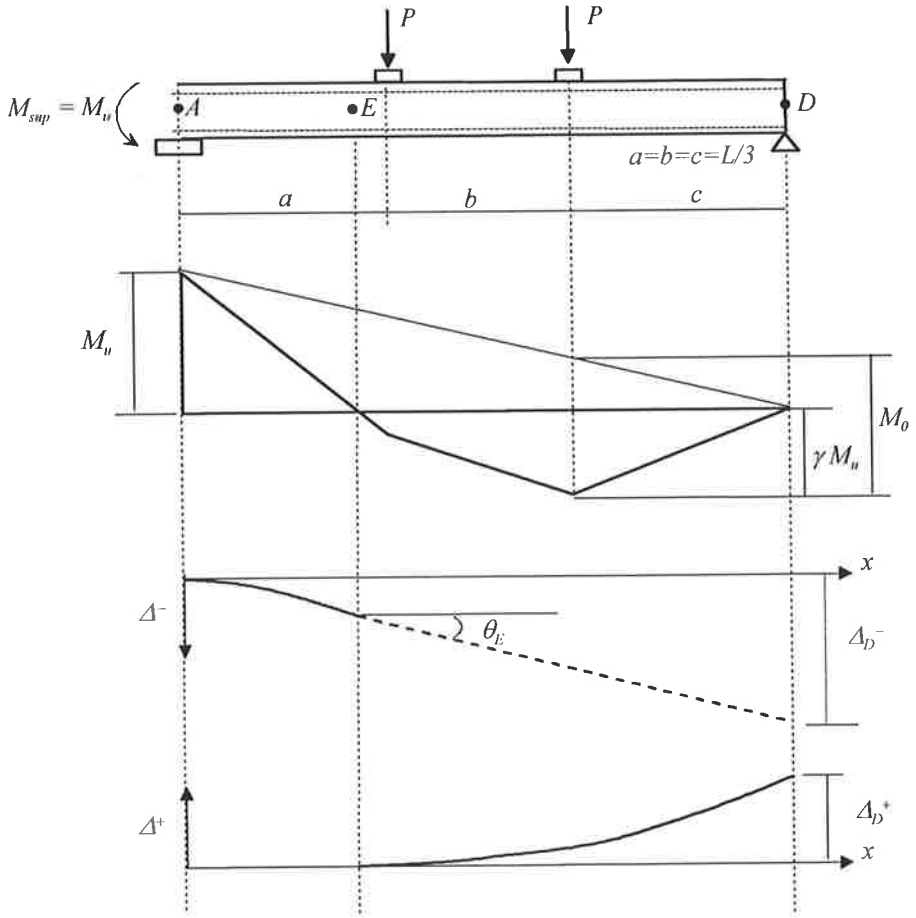

Figure 8.24 Schematic of propped cantilever for calculation of required rotation capacity

For a simplified calculation of the required plastic rotation in the negative moment region, we can assume that the total rotation in the negative moment region, θ_E, is made up of an elastic component and a plastic component (Figure 8.24):

$$\theta_E = \theta_{E,el} + \theta_{E,pl} \tag{8.7}$$

and the deformations in the negative moment region AE due to the negative curvature, Δ_D^-, are also made up of an elastic and plastic component:

$$\Delta_D^- = \Delta_{D,el}^- + \Delta_{D,pl}^- \tag{8.8}$$

also just prior to collapse it is assumed that the deformations due to the positive curvature, Δ_D^+, are purely elastic:

$$\Delta_D^{+} = \Delta_{D,el}^{+} \tag{8.9}$$

To satisfy the boundary condition of the system the deformations due to the negative curvature and positive curvature need to be equal:

$$\Delta_D^{-} = \Delta_D^{+} \tag{8.10}$$

$$\Delta_{D,pl}^{-} = \Delta_{D,el}^{+} - \Delta_{D,el}^{-} \tag{8.11}$$

The derivation of the procedure to calculate the required plastic rotation capacity in the support region, $\theta_{E,pl}$, to satisfy compatibility can be found in Appendix D, and is calculated according to the following equation:

$$\theta_{E,pl} = \frac{\Delta_{D,el}^{+} - \Delta_{D,el}^{-}}{(L - \frac{d}{2})} \tag{8.12}$$

where d is equal to the effective depth and is the assumed distance that the required plastic rotation is concentrated over in the support region. The deformation due to the positive curvature and negative curvature, Δ_D^{+} and Δ_D, respectively, is calculated applying the Second Moment of Area Theorem (See Appendix D).

The bending moment at the support and span at ultimate load P, are related by the assumed degree of redistribution, β, according to the following equation:

$$\frac{PL}{3} = M_0 = \frac{1}{3} M_u + \gamma M_u \tag{8.13}$$

Here, M_u is the moment capacity over the support, and g is the ratio of the positive moment capacity to the negative moment capacity:

$$\gamma = \frac{1}{3} \cdot \left(\frac{\frac{2}{3} + \beta \frac{1}{3}}{\frac{1}{3} - \beta \frac{1}{3}} \right) \tag{8.14}$$

For the derivation of this expression for γ, refer to Appendix B.2.

As in the case for the fixed end beam, the distribution of moment along the beam element is calculated taking into account the load pad effect and the ultimate moment capacity in the support and span region (see Chapter 6).

In Figures 8.25 to 8.26, it can be seen that less rotation capacity in the support region of the propped cantilever is required in comparison to the fixed end beam. This is due to the difference in the compatibility requirements of the two statical systems considered. The fixed end beam demands more rotation capacity in the support region to satisfy the compatibility condition that the total rotation in the support region must be equal to the total rotation in the span region. However, the available rotation capacity determined from the simulation program is only slightly increased in comparison to the fixed end beam, since the structural properties have been kept constant and the area of negative moment alters only slightly.

Therefore, an increase in the degree of moment redistribution in the propped cantilever compared to the fixed end beam can be achieved (Figure 8.27). This confirms the assumption that the fixed end beam is a more critical case to consider when investigating the allowable degree of moment redistribution in continuous beams.

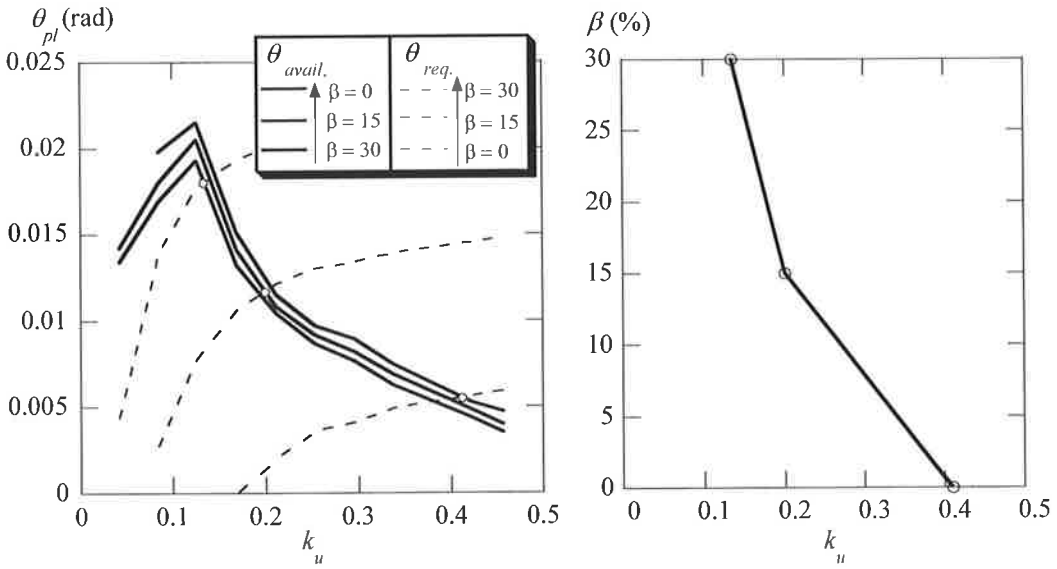

Figure 8.25 Available degree of redistribution for Steel N1, fixed end beam, d = 200mm, f_{cm} = 50MPa, L/d = 35

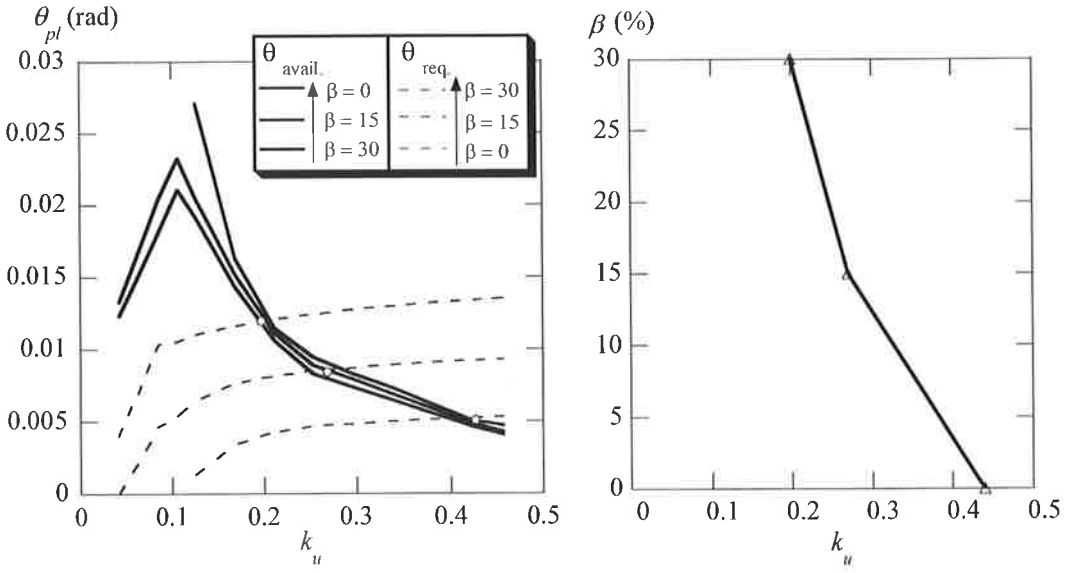

Figure 8.26 Available degree of redistribution for Steel N1, propped cantilever, d = 200mm, f_{cm} = 50MPa, L/d = 35

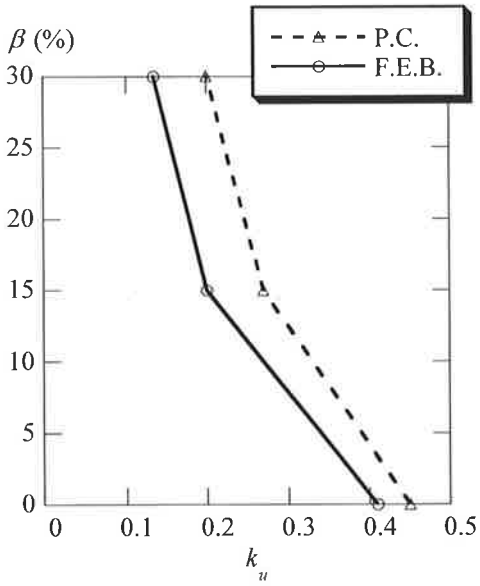

Figure 8.27 Influence of the statical system on degree of moment redistribution, one-way slab design, propped cantilever (P.C.) and fixed end beam (F.E.B.)

8.2.6 Summary

This section has investigated the influence the steel properties, effective depth, slenderness ratio, concrete strength and statical system have on the allowable degree of moment redistribution. The following observations have been made:

- An increase in the strain-hardening ratio whilst maintaining a constant uniform elongation provides a higher degree of moment redistribution.

- For tensile reinforcement ratios in which steel fracture governs, an increase in the uniform elongation whilst maintaining a constant strain-hardening ratio provides an increase in the allowable degree of moment redistribution. However if failure is governed by concrete, an increase in the uniform elongation whilst maintaining a constant strain-hardening ratio causes a reduction in the allowable degree of moment redistribution.

- To improve the allowable degree of moment redistribution, an increase in the uniform elongation should be followed by an increase in the strain-hardening ratio.

- With increase in the effective depth of the section whilst maintaining a constant slenderness ratio the available rotation capacity reduces, thus corresponding to a decrease in the allowable degree of moment redistribution for the design.

- A higher allowable degree of moment redistribution is achieved with lower slenderness ratios since less rotation capacity is required by the design.

- For normal strength concrete an increase in the compressive strength provides an increase in the allowable degree of moment redistribution.

- The allowable degree of moment redistribution is greater for the propped cantilever compared to the fixed end beam case.

8.3 Evaluation of Current Ductility Requirements for Design Clauses in AS 3600

This section evaluates the ductility requirements for design according to AS 3600 specific to the structural analysis method of linear elastic analysis with moment redistribution.

Ductility requirements for structural design procedures according to AS 3600 have been reviewed in Chapter 2. For ductility, the design procedure of linear elastic analysis with moment redistribution sets limits on the neutral axis parameter, k_u, and the assumed

degree of moment redistribution, β, for both Class N and Class L reinforcing steels. Figure 8.28 depicts the allowable degree of redistribution that can be adopted in design. At present no moment redistribution is allowed for the design of reinforced concrete beams constructed with Class L steels.

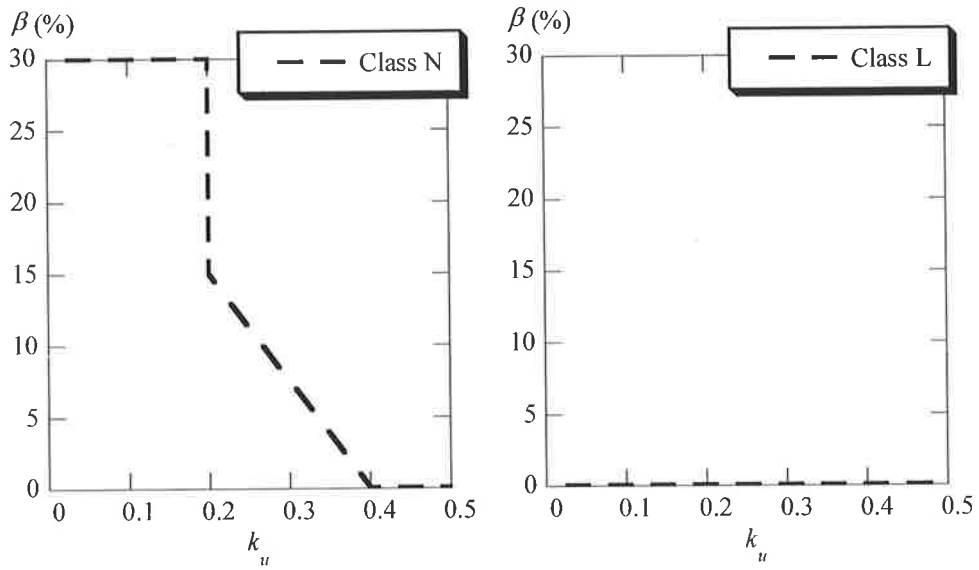

Figure 8.28 Allowable degree of moment redistribution according to AS 3600

To evaluate the current ductility requirements for linear elastic analysis with moment redistribution, the results from the numerical study presented in Section 8.2 have been utilised.

Further to comparing the simulation results with the degree of moment redistribution according to AS 3600, the evaluation also considers the strength implications. That is, the strength capacity reserve is measured as the ratio between the maximum available load, P_{avail}, and the maximum required load, P_{req}, for the beam designs. If the P_{avail}/P_{req} ratio is less than one, this signifies that the required maximum load is less than the available maximum load. Therefore the assumed degree of moment redistribution is not necessarily attained with relation to strength.

The procedure presented to evaluate the allowable degrees of moment redistribution for design is thus able to assess whether the deformation and strength capacities satisfy the following conditions:

$$\theta_{req} \leq \theta_{avail} \tag{8.15}$$

$$P_{req} \leq P_{avail} \tag{8.16}$$

Previous studies on the allowable degree of moment redistribution have not necessarily considered the strength implication in addition to the deformation capacities, since realistic indeterminate beams have not been considered.

8.3.1 Class N Steel

Figures 8.29 to 8.36 show the influence the steel properties, effective depth, slenderness ratio and concrete strength have on the allowable degree of moment redistribution. The simulations have been carried out for the fixed end beam case considering a rectangular beam section or a one-way slab section.

The plots on the left-hand side are compared to the allowable degree of moment redistribution according to AS 3600. The figures on the right-hand side consider the strength implication by plotting the ratio of P_{avail}/P_{req} versus the neutral axis parameter, k_u, for the case on the left-hand side that lies well below the AS 3600 limit.

In general, it can be seen that at the assumed degree of moment redistribution of 0% and 15%, the simulation results either lie at or above the limiting value according to AS 3600. However at an assumed degree of moment redistribution of 30%, the simulation results lie well below the maximum allowable value according to AS 3600.

Considering the strength implications at an assumed degree of moment redistribution of 30% the figures generally show that limited strength is available as the value of k_u approaches 0.2. In some cases at a k_u value of 0.2, the required load is less than the available load, the percentage difference can be up to 10%. For k_u values greater than 0.2, the required maximum load outweighs the available maximum load.

This suggests that the allowable degree of moment redistribution according to AS 3600 of up to 30% moment redistribution for k_u values less than, or equal to 0.2 may not provide a safe design.

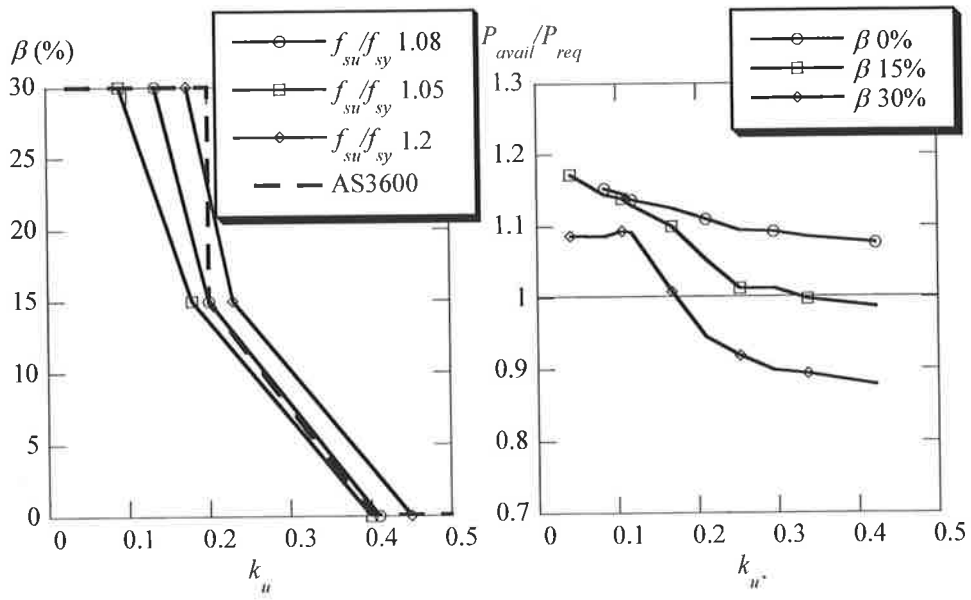

Figure 8.29 **Comparison of simulation results with AS 3600 limits on degree of moment redistribution for Class N steel (LHS) and strength capacity (RHS). Influence of the variation strain-hardening ratio, f_{su}/f_{sy}, ε_{su} = 5%, f_{cm} = 50MPa, L/d = 35**

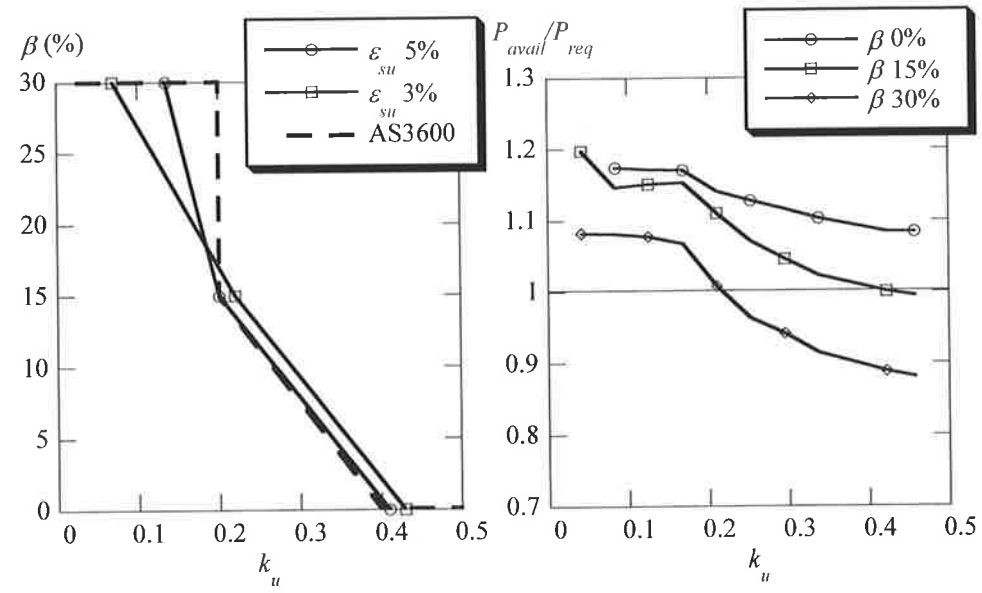

Figure 8.30 **Comparison of simulation results with AS 3600 limits on degree of moment redistribution for Class N steel (LHS) and strength capacity (RHS). Influence of the uniform elongation, ε_{su}, f_{su}/f_{sy} = 1.08, f_{cm} = 50MPa, L/d = 35**

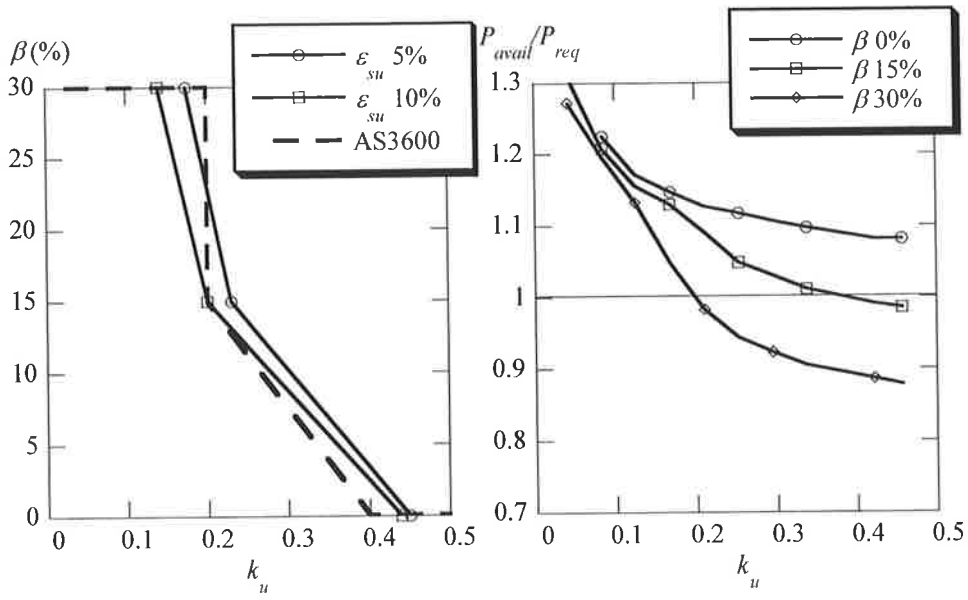

Figure 8.31 **Comparison of simulation results with AS 3600 limits on degree of moment redistribution for Class N steel (LHS) and strength capacity (RHS). Influence of the uniform elongation, ε_{su}, f_{su}/f_{sy} = 1.2, f_{cm} = 50MPa, L/d = 35**

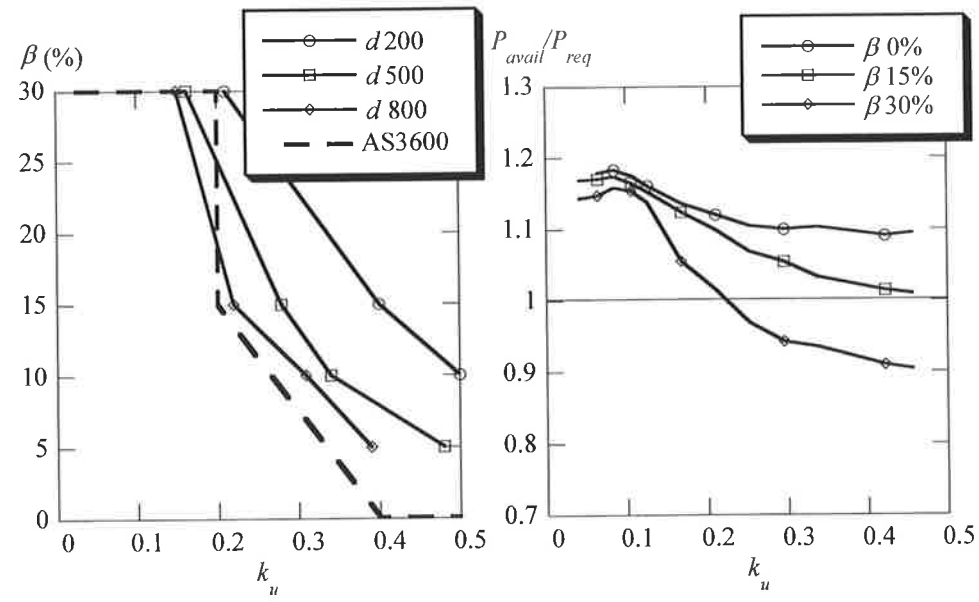

Figure 8.32 **Comparison of simulation results with AS 3600 limits on degree of moment redistribution for (LHS) and strength capacity (RHS). Influence of the effective depth, rectangular beam design, Steel N1, f_{cm} = 50MPa, L/d = 20**

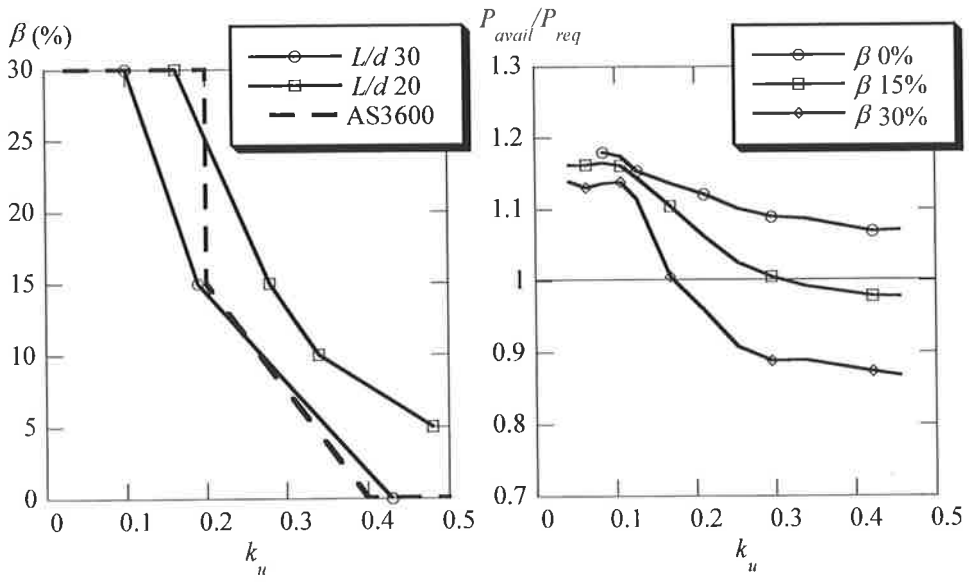

Figure 8.33 **Comparison of simulation results with AS 3600 limits on degree of moment redistribution (LHS) and strength capacity (RHS). Influence of the slenderness ratio, rectangular beam design, Steel N1, f_{cm} = 50MPa**

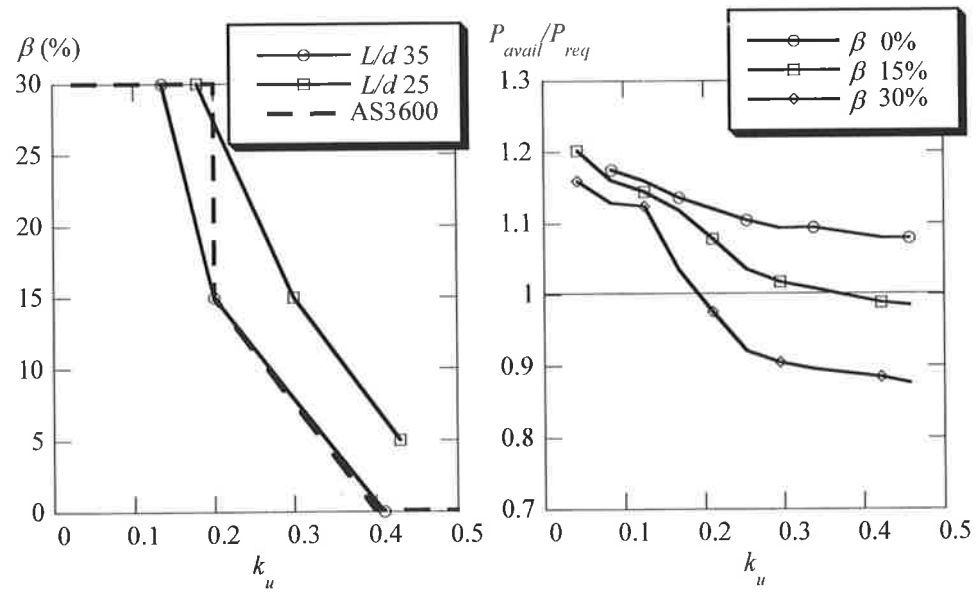

Figure 8.34 **Comparison of simulation results with AS 3600 limits on degree of moment redistribution (LHS) and strength capacity (RHS). Influence of the slenderness ratio, one-way slab design, Steel N1, f_{cm} = 50MPa**

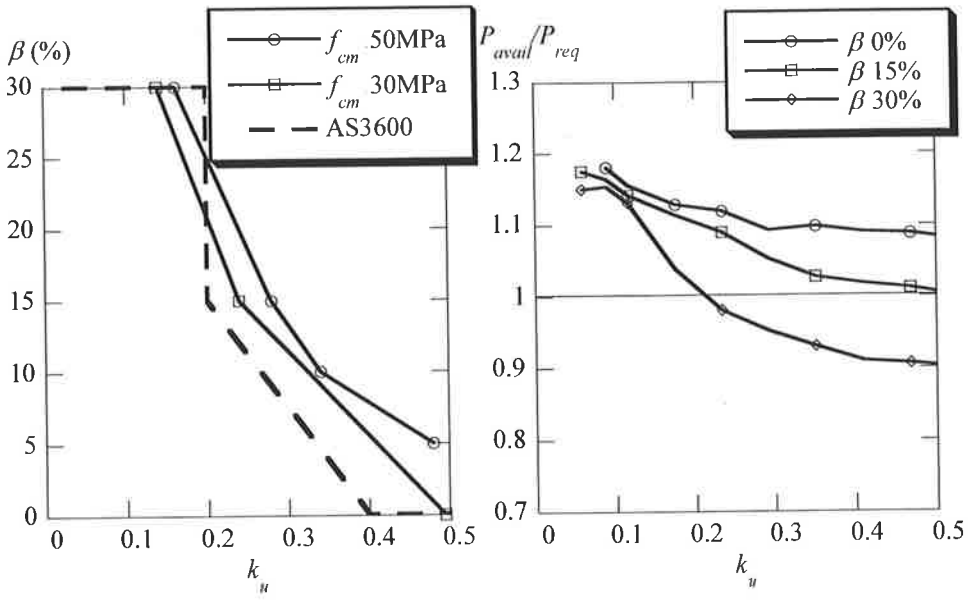

Figure 8.35 **Comparison of simulation results with AS 3600 limits on degree of moment redistribution (LHS) and strength capacity (RHS). Influence of the concrete strength, rectangular beam design, Steel N1, $L/d = 20$**

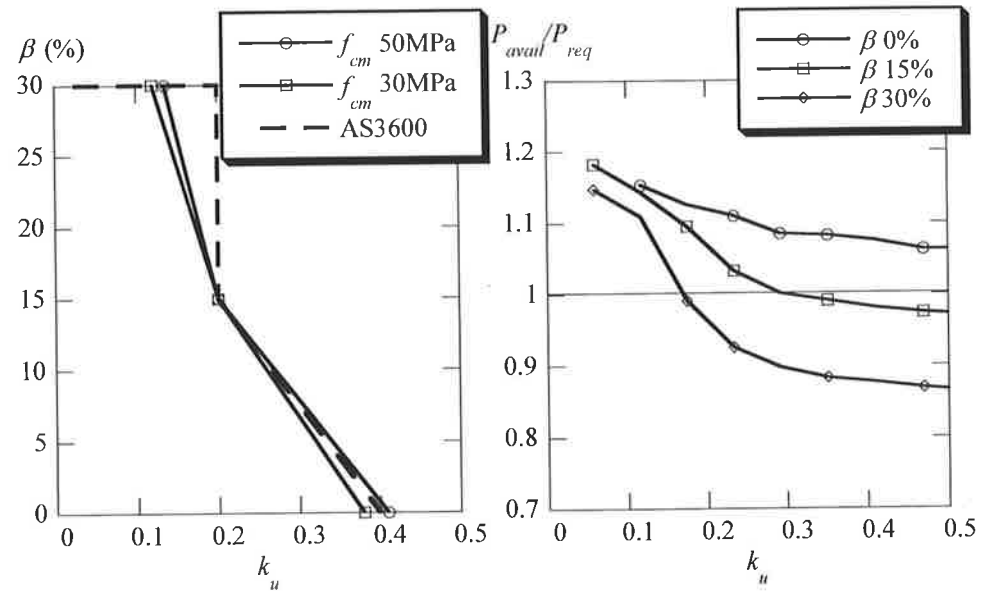

Figure 8.36 **Comparison of simulation results with AS 3600 limits on degree of moment redistribution (LHS) and strength capacity (RHS). Influence of the concrete strength, one-way slab design, Steel N1, f_{cm} = 50MPa, $L/d = 35$**

8.3.2 Class L Steel

Figures 8.37 to 8.40 show the influence the steel properties, slenderness ratio and concrete strength have on the allowable degree of moment redistribution for Class L steels. The fixed end beam case considering a one-way slab section has been used.

Currently, AS 3600 (Standards Australia, 2001) does not allow any moment redistribution to be adopted in the design of continuous reinforced concrete beams constructed with Class L steel. However, it can be seen in Figures 8.37 to 8.40 that a considerable degree of moment redistribution can be achieved in the design. Also at the assumed degree of moment redistribution of 0, 15 or 20% a substantial amount of strength capacity is available. This suggests that in AS 3600 the ductility requirement not allowing any degree of moment redistribution to be adopted in design for Class L steel may be too conservative.

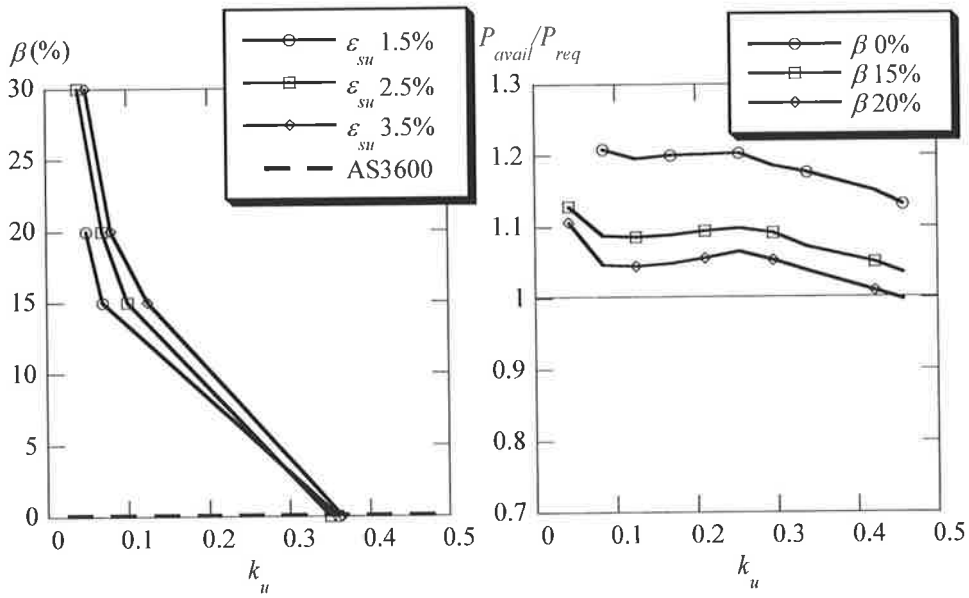

Figure 8.37 Comparison of simulation results with AS 3600 limits on degree of moment redistribution (LHS) and strength capacity (RHS). Influence of the uniform elongation, ε_{su}, for Class L steels, f_{su}/f_{sy} = 1.03, f_{cm} = 50MPa, L/d = 35

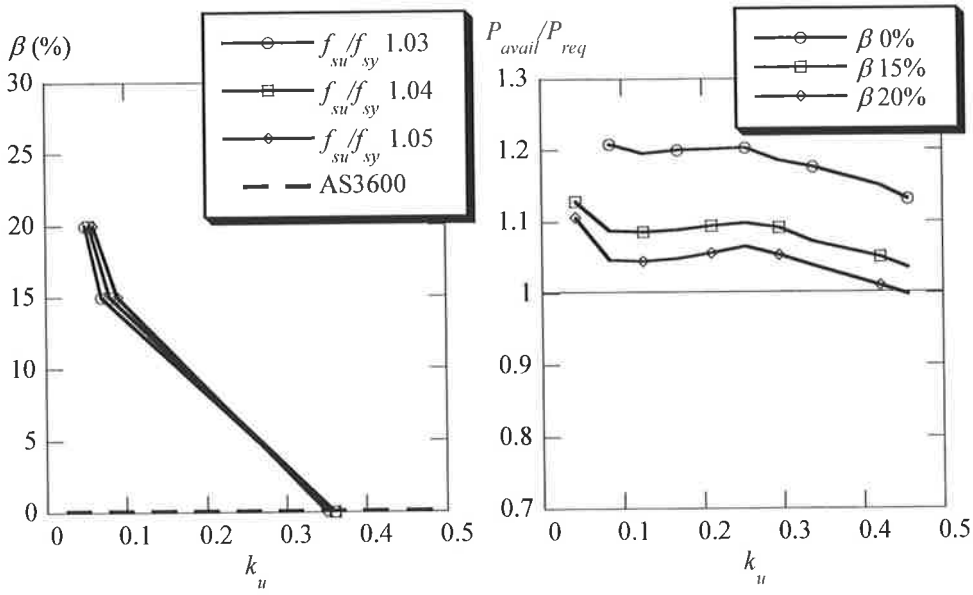

Figure 8.38 **Comparison of simulation results with AS 3600 limits on degree of moment redistribution (LHS) and strength capacity (RHS). Influence of the strain-hardening ratio, f_{su}/f_{sy}, for Class L steels, ε_{su} = 1.5%, f_{cm} = 50MPa, L/d = 35**

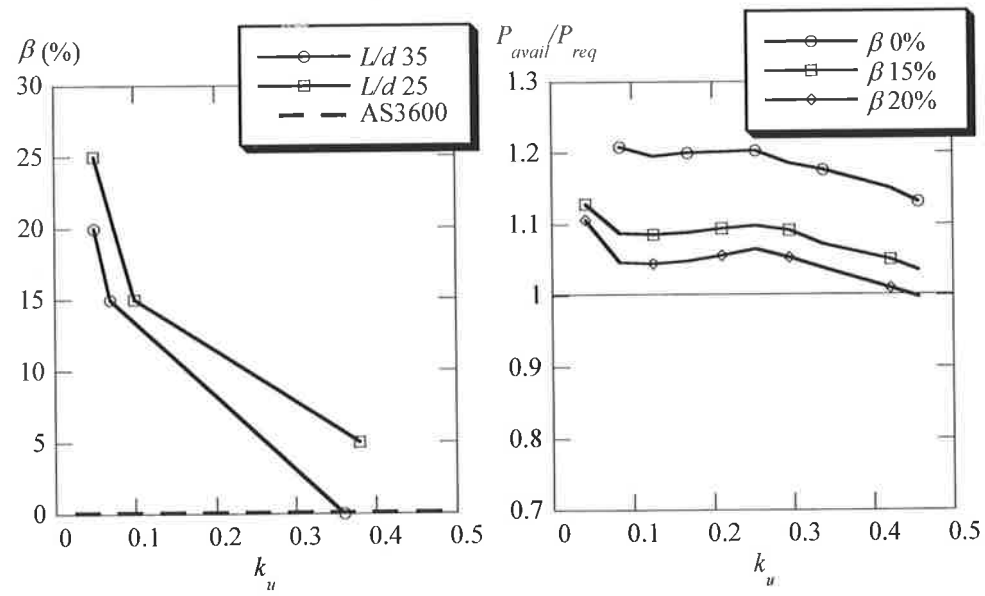

Figure 8.39 **Comparison of simulation results with AS 3600 limits on degree of moment redistribution (LHS) and strength capacity (RHS). Influence of the slenderness ratio, one-way slab design, Steel L1, f_{cm} = 50MPa**

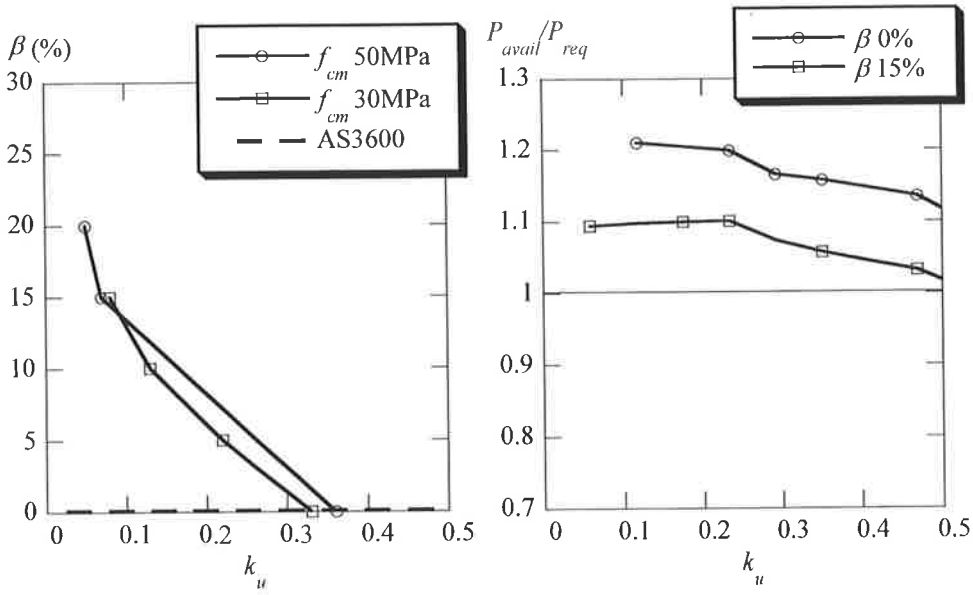

Figure 8.40 Comparison of simulation results with AS 3600 limits on degree of moment redistribution (LHS) and strength capacity (RHS). Influence of the concrete strength, one-way slab design, Steel L1, *L/d* = 35

8.4 Recommendations for Ductility Requirements for Design According to AS 3600

The ductility requirements for the simplified method of linear elastic analysis with moment redistribution have been evaluated in the Section 8.3. From this evaluation the following recommendations for design according to AS 3600 are made:

- In Clause 7.6.8.2, for Class N steel, the maximum allowable degree of moment redistribution of 30% for k_u values up to 0.2, should be reduced to 20% to ensure not only adequate deformational capacity, but also sufficient strength capacity. For k_u values between 0.2 and 0.4, the allowable degree of moment redistribution remains unchanged to ensure that the redistribution does not exceed 75 (0.4-k_u)%. If k_u exceeds 0.4, no redistribution is permitted.

- In Clause 7.6.8.3, for Class L steel, a maximum allowable degree of moment redistribution of 10% should be allowed for k_u values up to 0.15. For k_u values between 0.15 to 0.3, the allowable degree of redistribution should not exceed

$66\frac{2}{3}$(0.3-ku)%. If k_u exceeds 0.3, no redistribution is permitted. An additional requirement for this clause would be, the clause is valid provided no significant support settlement occurs.

The proposal for the allowable degree of moment redistribution for Class N and Class L steel is shown Figure 8.41.

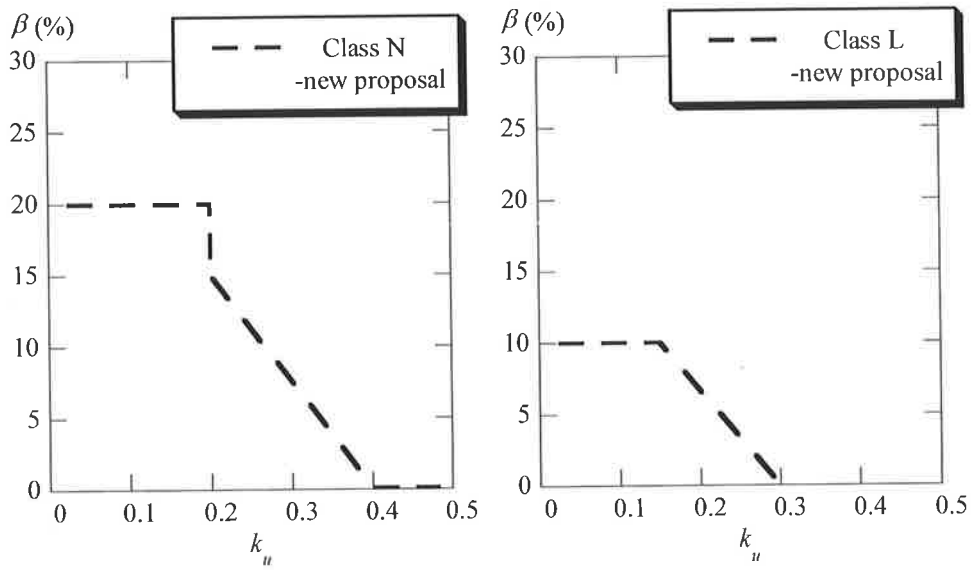

Figure 8.41 Proposal for allowable degree of moment

As an alternative to design according to the simplified method of linear elastic analysis with moment redistribution, Clause 7.6.8.1 in AS 3600 (Standards Australia, 2001) states:

"The elastically determined bending moments at any interior support may be reduced or increased by redistribution, provided an analysis is undertaken to show that there is adequate rotation capacity in the critical moment regions to allow the assumed distribution of bending moment to be achieved"

The method presented in this chapter, whereby the available rotation capacity is compared to the required rotation capacity in critical high moment regions of indeterminate structural members, can be used as an alternative design approach to ensure adequate rotation capacity and sufficient ductility.

The available rotation capacity is calculated based on the stress-strain characteristics of the reinforcing steel and concrete, the bond properties between the steel and surrounding concrete, and the static equilibrium of the structural member. To calculate the required rotation capacity, a simplified procedure is introduced and is based on the assumed degree of redistribution, the slenderness ratio of the member and the percentage of reinforcement in the section.

The limitation of this method is that a computer program is required to run the analysis for the available rotation capacity. Therefore, a simplified procedure to calculate the available rotation capacity should be further investigated. Examples of simplified calculations for available rotation capacity adopted in other codes of practice have been reviewed in Chapter 2.

A new Clause C7.6.8.1, could be added to the Commentary of AS 3600 giving details of a first principles approach to design for moment redistribution. The approach requires the calculation of the available rotation capacity and the required rotation capacity in critical regions, to ensure that the former is larger than the latter. The methods for calculating the available and required rotation capacities could be similar to those described in this thesis.

9

CONCLUSIONS AND RECOMMENDATIONS

In this thesis a theoretical study is made of the non-linear overload behaviour of reinforced concrete flexural members. The study concentrates on the rotation capacity and ductility of local high-moment regions and on moment redistribution in continuous beams. A prime aim of the study was to examine the adequacy of the current design clauses in the Australian reinforced concrete design standard in relation to ductility and moment redistribution.

The investigation has led to the following conclusions and recommendations.

9.1 CONCLUSIONS

(a) The local deformation model presented in this thesis can predict the flexural behaviour of reinforced concrete beams under increasing load, including the progressive formation of flexural cracks, crack spacing, crack widths, local deformations, bond-slip behaviour between the steel and surrounding concrete, and the final plastic deformations at failure. The model also predicts the mode of flexural failure, whether by steel fracture or concrete softening, and allows the rotation capacity and ductility of critical regions to be investigated.

(b) The local deformation model has been applied simultaneously to the positive and negative moment regions in continuous beams, thereby providing a means for analysing the full-range behaviour of the indeterminate system, and thus allowing non-linear system effects such as moment redistribution to be studied.

(c) Comparisons made with published beam test data and analytic predictions show that both the local deformation model and the continuous beam analysis are

reasonably accurate, and can be used to determine local deformations at high overload, as well as overall system behaviour.

(d) The local deformation model was used to undertake a parametric study of the factors influencing the rotation capacity of high moment regions in reinforced concrete beams. The main parameters investigated were: uniform elongation and the strain-hardening ratio of the reinforcing steel; percentage of tensile reinforcement; the effective depth of the section; slenderness ratio of the beam; and the concrete strength.

(e) The parametric study of rotation capacity led to the following conclusions:

- Beams constructed with Class N steels exhibit more rotation capacity than those constructed with Class L steels. Also the transition from steel fracture to concrete failure for beams with Class N steel occurs at much lower k_u values, than those with Class L steel. That is, many more beam designs are governed by steel fracture when reinforced with Class L steel, as compared to Class N steel.

- An increase in the strain-hardening ratio results in an increase in the rotation capacity with no obvious shift in the transition point from steel fracture to concrete failure.

- With an increase in the uniform elongation whilst maintaining a constant strain-hardening ratio, the transition from steel fracture to concrete failure shifts towards lower k_u values.

- In the range where steel fracture governs, an increase in the uniform elongation, whilst maintaining a constant strain-hardening ratio, leads to an increase in rotation capacity. However if failure is governed by concrete, an increase in the uniform elongation results in lower rotation capacity.

- A definite size effect was observed as the rotation capacity decreased with increase in the effective depth of the flexural member. This was due to the average crack spacing increasing with decrease in the effective depth that imparts larger crack widths.

- With increase in the slenderness ratio the rotation capacity increases since the plastic hinge length increases accordingly.

- The influence of the concrete compressive strength on the available rotation capacity, in the range of normal strength concrete, depends upon the failure mode that governs. If failure if governed by steel fracture, an increase in the concrete compressive strength provides a decrease in the available rotation capacity, since the average crack spacing and maximum crack width reduce due to the higher bond strength between the steel and surrounding concrete. If failure is governed by concrete, an increase in the concrete compressive strength provides more rotation capacity in the plastic hinge region since the crack widths enlarge due to the higher steel strains that are achieved at the cracked section.

(f) The indeterminate beam analysis was used in a numerical study of moment redistribution in a range of fixed end beams and propped cantilevers. The main parameters considered in this study were the following: uniform elongation and the strain-hardening ratio of the reinforcing steel; the effective depth of the section; the percentage of tensile reinforcement; the slenderness ratio; and the concrete strength.

(g) The numerical study of continuous beams confirmed the results of the parametric study summarised under item (e).

(h) The numerical study of continuous beams led to the following conclusions regarding moment redistribution:

- The degree of moment redistribution that can occur in an indeterminate beam increases, as the strain-hardening ratio of the steel increases while the uniform elongation remains constant.

- For beams with steel reinforcement ratios such that failure is by steel fracture, the degree of moment redistribution that can occur increases as the steel uniform elongation increases, while the strain-hardening ratio remains constant.

- For beams with steel reinforcement ratios such that failure is by concrete softening, a decrease in the uniform elongation at constant strain-hardening ratio causes a reduction in the degree of moment redistribution that can occur.

- In dealing with moment redistribution, designers need to be aware that a size effect exists. The degree of moment redistribution available effectively decreases as the effective depth of the member increases, at constant slenderness ratio. On the other hand, a higher degree of moment redistribution is achieved at lower slenderness ratios with constant effective depth.

- For normal strength concrete, an increase in compressive strength leads to an increase in the allowable degree of moment redistribution.

- The degree of moment redistribution that can be allowed in a propped cantilever has been shown to be greater than for a comparable fixed end beam.

(i) Following from (h), if changes are made to steel manufacturing techniques, in order to increase the uniform elongation of the reinforcing steel, then it is important also to simultaneously increase the strain-hardening ratio.

(g) The numerical study has revealed several in adequacies in the current design clauses in AS 3600 for ductility and moment redistribution.

- In relation to continuous beams constructed with Class N steel, unsafe designs are likely to result if 30 per cent design moment redistribution is used together with a neutral axis parameter less than or equal to 0.2. Specifically, premature failure is likely to occur, with a loss of strength of as much as 10 per cent.

- In relation to continuous beams constructed with Class L steel, the present AS 3600 clauses can lead to over conservative results as no moment redistribution is allowed. Numerical calculations in fact show that moment redistribution of up to 10 per cent can be achieved in certain circumstances without premature failure and loss of strength.

(k) Details are given in this thesis of a method of analysis for evaluating the required rotation capacity in the negative moment region of a continuous beam in order to achieve any assumed design moment redistribution. This allows beam design with moment redistribution to be undertaken from first principles, hence avoiding the simplified design clauses in AS 3600 regarding ductility and moment redistribution. In the first principles approach, the available rotation capacity in critical regions is simply compared with the rotation capacity required by the assumed design moment redistribution.

9.2 RECOMMENDATIONS FOR DESIGN

The results of this investigation suggest the need for modifications to several current design clauses in AS 3600 relating to moment redistribution and minimum ductility requirements. Specific recommendations are as follows:

(a) In Clause 7.6.8.2, which presents a simplified approach for Class N steels, the maximum moment redistribution allowed for k_u values up to 0.2 should be reduced from the present values of 30 per cent to 20 per cent. For values of k_u larger that 0.2, the present requirements do not need to be changed.

(b) In Clause 7.6.8.3, which stipulates no redistribution of moments for beams which contain any Class L steel, could well be relaxed. The rewording of the Clause could be very similar to the present clause 7.6.8.2, however with a maximum degree of moment redistribution of 10 per cent allowed for k_u values up to 0.15. For k_u values between 0.15 to 0.3, the allowable redistribution should not exceed $66\frac{2}{3}$(0.3-ku), with no redistribution allowed when k_u exceeds 0.3. The desirable additional requirement for this clause would be, the clause is applicable provided no significant support settlement occurs.

(c) A new Clause C7.6.8.1, could be added to the Commentary of AS 3600 giving details of a first principles approach to design for moment redistribution. The approach requires the calculation of the available rotation capacity and the required rotation capacity in critical regions, to ensure the former is larger than

the latter. The methods for calculating the available and required rotation capacities could be similar to those described in this thesis.

9.3 RECOMMENDATIONS FOR FURTHER RESEARCH

Further research into the following areas is recommended:

(a) Improvement to the present modelling procedure to more accurately consider local deformations in the concrete compressive damage zone and shear deformations.

(b) Additional experimental testing of reinforced concrete beams and slabs constructed with high-strength reinforcement are required whereby local deformation measurements such as local tensile steel strains, crack widths and bond stresses are recorded, thus providing results to further validate the modelling procedure.

(c) Further numerical studies investigating the influence of high-strength concrete on the available rotation capacity and allowable degree of moment redistribution in continuous beams.

(d) Extension of the model to prestressed concrete structures where ductility may also be a concern and consideration of non-plane strain profiles at cracked sections.

(e) Development of a simplified procedure designers can incorporate into practice to calculate the available rotation capacity in plastic hinge regions of continuous beams, considering the ductility level of the reinforcing steel.

10

REFERENCES

ACI Committee 318 (1999), *Building Code Requirements for Structural Concrete (ACI 318-99) and Commentary (ACI 318R-99)*, American Concrete Institute, Farmington Hills, p369.

Bachmann, H. (1967), *Zur plastizitätstheoretischen Berechnung statish unbestimmter Stahlbetonbalken*, PhD Thesis, ETH Zurich, Switzerland.

Bachmann, H. (1970), Influence of Shear and Bond on Rotational Capacity of Reinforced Concrete Beams, *IABSE Reports*, Vol. 30, No.2, p11-28

Bachmann, H. and Thürlimann, B. (1965), *Versuche über das Plastiche Verhalten von Zweifeldrigen Stahlbetonbalken*, Report No. 6203-2, Institut für Baustatik Eidgenössiche Technische Hochschule, December, p130.

Baker, A. L. L. and Amarakone, A. M. M. (1965), Inelastic Hyperstatic Frame Analysis, *Proceedings, International Symposium, Flexural Mechanics of Reinforced Concrete, ASCE-ACI*, Miami, ACI SP-12, p85-142.

Bazant, Z. P. and Oh, B. H. (1984), Deformation of Progressively Cracking Reinforced Concrete Beams, *ACI Journal*, Vol. 81, No.3, p268-278.

Beeby, A. W. (1968), *Short-term Deformations of Reinforced Concrete Members*, Technical report, TRA 408, Cement and Concrete Association, London.

Beeby, A. W. (1996), *Ductility of Reinforced Concrete*, University of Leeds.

Beeby, A. W. (1997), Ductility in Reinforced Concrete, *The Structural Engineer*, Vol. 75, No.18, p311-318.

Beeby, A. W. (1998), Tests to Investigate the Influence of Reinforcement Parameters on Rotation Capacity, *CEB Bulletin d'Information No.242*, fib (CEB-FIP) fédération international du bèton, Lausanne.

Bigaj, A. (1992), *Size Effect on Rotational Capacity of Plastic Hinges in Reinforced Concrete Beams*, Vol. 3, Delft University of Technology.

Bigaj, A. (1995), *Bond Behaviour of Deformed Bars in NSC and HSC- Experimental Study*, 25.5-95-II, September, Delft University of Technology , Department of Civil Engineering.

Bigaj, A. J. (1999), *Structural Dependence of Rotation Capacity of Plastic Hinges in RC Beams and Slabs*, Delft University of Technology.

Bigaj, A. and Walraven, J. C. (1993), Size Effect on Rotational Capacity of Plastic Hinges in Reinforced Concrete Beams, *CEB Bulletin d'Information No.218*, Comitè Euro International du Bèton, Lausanne, p7-24.

Birkenmaier, M. (1983), Über Nachweise im Gebrauchszustand, *Schweizer Ingenieur und Architekt*, Vol. 6, p120-125.

Branson, D. E. (1963), *Instantaneous and Time-dependent Deflections of Simple and Continuous Reinforced Concrete Beams*, Report No.7, Alabama Highway Research Report, Bureau of Public Roads.

Bridge, R. Q. and Smith, R. G. (1982), Tension Stiffening Model for Reinforced Concrete Members, *8th Australasian Conference on the Mechanics of Structures and Materials*, Newcastle, p4.1-4.6.

Calvi, G. M., Cantu, E., Macchi, G. and Magenes, G. (1993), Rotation Capacity of R.C. Slabs as a Function of Steel Properties, *CEB Bulletin d'Information No.218*, Comitè Euro International du Bèton, Lausanne, p45-64.

CEB (1981), *Bond Action and Bond Behaviour of Reinforcement- State of the Art Report*, CEB Bulletin d'Information No.151, Comitè Euro International du Bèton, Lausanne, p153.

CEB (1993), *Ductility Requirements for Structural Concrete-Reinforcement Progress report of Task Group 2.2*, CEB Bulletin d'Information No.218, Comitè Euro International du Bèton, Lausanne, p273.

CEB-FIP (1993), *Model Code 1990 for Concrete Structures*, CEB Bulletin d'Information No.213/214, Comitè Euro International du Bèton, Lausanne, p460.

CEB-FIP (1998), *Ductility of Reinforced Concrete Structures - Synthesis Report of CEB Task Group 2.2*, CEB Bulletin d'Information No.242, Comitè Euro International du Bèton, Lausanne, p332.

Ciampi, V., Eligehausen, R., Bertero, V. and Popov, E. (1982), *Analytical Model for Concrete Anchorages of Reinforcing Bars under Generalised Excitations*, Report No. UCB/EERC-82/23, University of California, November, p111.

Cohn, R. and Riva, P. (1987), A Comprehensive Study of the Flexural Behaviour of Structural Concrete Elements, *Studi e Ricerche*, Corso di Perfezionamento per le Costruzioni in Cemento Armato F.lli Pesenti. Politecnico di Milano, Italy, Vol.9, p365-413.

Corley, W. G. (1966), Rotational Capacity of Reinforced Concrete Beams, *Journal of the Structural Division, ASCE*, Vol. 92, No.5, p121-146.

Cosenza, E., Greco, C. and Manfredi, G. (1991a), *La Valutazione Teorica di Spostamenti e Rotazioni in Fase Anelastica negli Elementi Monodimensionali in Cemento Armato*, Serie IX, Volume II - Fascicolo 3, Atti Della Accademia Nazionale Dei Lincei.

Cosenza, E., Greco, C. and Pecce, M. (1991b), Nonlinear Design of Reinforced Concrete Continuous Beams, *Structural Engineering International*, Vol. 1, No.1, p19-27.

Creazza, G. and Di Marco, R. (1993), Bending Moment-Mean Curvature Relationship with Constant Axial Load in Presense of Tension Stiffening, *Materials and Structures*, Vol. 26, p196-206.

den Uijl, J. A. and Bigaj, A. J. (1996), A Bond Model for Ribbed Bars based on Concrete Confinement, *Heron*, Vol. 41, No.3, p201-225.

Dilger, W. (1966), *Veränderlichkeit der Beige-und Schubtragfähigkeit bei Stahlbetontragwerken und ihr Einfluß auf Schnittkraftverteilung und Traglast bei statisch unbestimmter Lagerung*, Deutscher Ausschuss für Stahlbeton, Heft 179, p101.

Eibl, J. and Bühler, A. (1991), *Untersuchung des Einflusses verschiedener Stahlparameter auf die mögliche plastiche Rotation bei Stahlbetonplatten*, Institut für Massivbau und Baustofftechnologie, Abteilung Massivbau, Universität Karlsruhe, Germany, p19.

Eifler, H. (1991), *Die Drehfähigkeit plastischer Gelenke in Stahlbeton-Plattenbalken, bewehrt mit naturharten Betonstahl BSt 500 S, im Bereich negativer Biegemonte*, Report No.179, Bundesabstalt für Materialforschung und -prüfung (BAM), p80.

Eligehausen, R., Bertero, V. and Popov, E. (1983), *Local Bond Stress-slip Relationships of Deformed Bars under Generalised Excitations*, Report No.UCB/EERC-83/23, University of California, October, p162.

Eligehausen, R., Ciampi, V., Bertero, V. and Popov, E. (1981), Analytical Model for Deformed Bar Bond under Generalised Excitations, *IABSE Report*, Vol 33-34, p53-67.

Eligehausen, R. and Langer, P. (1987), Rotation Capacity of Plastic Hinges and Allowable Degree of Moment Re-distribution, *CEB Bulletin d'Information No.175*, Comitè Euro-International du Bèton, Lausanne, pI.7.9-I.7.41.

Eligehausen, R. and Li, L. (1992), Rotation Capacity of Prestressed Concrete Members, *Proceedings of the International Conference in Concrete, CEB*, Riga, Latvia, p2.58-2.67.

Eligehausen, R., Ozbolt, J. and Mayer, U. (1997), Contribution of Concrete Between Cracks at Inelastic Steel Strains and Conclusions for the Optimisation of Bond, *ACI Special publications, Seminar on Bond*, ACI Spring Convention, Seattle.

Eligehausen, R., Zhao, R. and Fabritius, E. (1995), *Test Report on Continuous Slabs Reinforced with Welded Wire Mesh*, Report No.652/1-95/1, Institut für Werkstoffe im Bauswessen, Universität Stuttgart, April, p77.

Engström, B. (1992), Anchorage of Ribbed Bars in the Post-yield Stage, *Proceedings of the International Conference in Concrete, CEB*, Riga, Latvia, p1.110-1.199.

Engström, B. (1992), *Ductility of Tie Connections in Precast Structures*, PhD Thesis, Chalmers University of Technology, Goteborg, Sweden.

Eurocode No.2 (1990), *Design of Concrete Structures*, European Committee for Standardisation, Brussels, p173.

Fantilli, A., Ferretti, D., Iori, I. and Vallini, P. (1999), Minimum Reinforcement in Concrete Members, *Elsevier*, ESIS Publication 24, p99-125.

Ferretti, D. (1995), *Sul Comportamento a Breve Termine di Elementi Inflessi in Conglomerato Cementizio Armato*, PhD Thesis, Politecnico di Torino, Turin, Italy.

Gambarova, P. G., Rosati, G. P. and Zasso, B. (1989), Steel-concrete Bond after Concrete Splitting: (I) Test Results; (II) Constitutive Laws and Interface Deterioration, *Material and Structures*, Vol. 22, No.35-47, p347-356.

Gilbert, I. and Warner, R. F. (1978), Tension Stiffening in Reinforced Concrete Slabs, *Journal of the Structural Division, ASCE*, Vol. 104, No.12, p1885-1900.

Giuriani, E. (1979), L'influenza del Softening dell'Aderenza e deglo Effetti Diffusivi nella Fessurazione di una Trave in Cemento Armato, *Studi e Ricerche*, Corso di Perfezionamento per le Costruzioni in Cemento Armato F.lli Pesenti. Politecnico di Milano, Italy, Vol. 1, p71-101.

Giuriani, E. (1981), Experimental Investigation on the Bond-slip Law of Deformed Bars in Concrete, *IABSE Colloquium on advanced mechanics of reinforced concrete*, Delft, The Netherlands, p121-142.

Giuriani, E. and Plizzari, G. (1989), Propagation and Distance of Cracks in R.C. Beams with a Bending Moment Gradient, *Studi e Ricerche*, Corso di Perfezionamento per le

Costruzioni in Cemento Armato F.lli Pesenti. Politecnico di Milano, Italy, Vol.11, p61-106.

Goto, Y. (1971), Cracks Formed in Concrete Around Tension Bars, *ACI Journal*, Vol. 68, No.4, p241-251.

Graubner, C.-A. (1987), *Schnittgrössenvertleilung in Statisch unbestimmten Stahlbetonbalken unter Berücksichtigung Wirklichkeitsnaher Stoffgestetze*, PhD Thesis.

Gupta, A. K. and Maestrini, S. R. (1990), Tension-stiffness Model for Reinforced Concrete Bars, *Journal of the Structural Division, ASCE*, Vol. 116, No.3, p769-791.

Hillerborg, A. (1983), Analysis of One Single Crack, *Fracture Mechanics of Concrete*, p223-249.

Kreller, H. (1989), *Zum nichtlinearen Trag-und Verformungsverhalten von Stahlbetontragwerken unter Last- und Zwangseinwirkung*, PhD Thesis, University of Stuttgart.

Langer, P. (1987), *Verdrehfähigkeit plastizier Tragwerksbereiche im Stahlbetonbau*, PhD Thesis, University of Stuttgart.

Li, L. (1995), *Rotationsfähigkeit von plastischen Gelenken im Stahl- und Spannbetonbau*, PhD Thesis, University of Stuttgart.

Lin, C. S. and Scordelis, A. C. (1975), Nonlienar Analysis of RC Shells of General Form, *Journal of the Structural Division, ASCE*, Vol. 103, No.3, p523-538.

Lutz, L. A. and Gergely, P. (1967), Mechanics of Bond and Slip of Deformed Bars in Concrete, *Journal of the American Concrete Institute*, Vol. 64, No.11, p711-721.

Maldague, M. (1965), Établissement des Lois Moments-courbures, *Annales de l'Institut technique du Bâtiment et des Travaux Publics*, No.213, p1170-1218.

Mander, J. B., Priestley, M. J. N. and Park, R. (1988), Theoretical Stress-strain Model for Confined Concrete, *Journal of the Structural Division, ASCE*, Vol. 114, No.8, p1804-1825.

Markeset, G. (1993), Size Effect on Stress-strain Relationship of Concrete in Compression, *3rd Symposium on Utilization of High-strength Concrete*, Lillehammer, p1146-1153.

Mattock, A. H. (1965), Rotational Capacity of Hinging Regions in Reinforced Concrete Beams, *Proceedings, International Symposium, Flexural Mechanics of Reinforced Concrete, ASCE-ACI*, Miami, ACI SP-12, p143-181.

Patrick, M., Akbarshahi, E. and Warner, R. F. (1997), Ductility Limits for the Design of Concrete Structures Containing High-strength, Low-elongation Steel Reinforcement, *Concrete Institute of Australia - Concrete 97*, Adelaide, p65-71.

Priestly, M. J. N., Park, R. and Lu, F. P. S. (1971), Moment-curvature Relationships for Prestressed Concrete in Constant-moment Zones, *Magazine of Concrete Research*, Vol. 23, No.75, p69-78.

Rehm, G. (1961), Ueber die Grundlagen des Verbundes zwischen Stahl und Beton (On the Basic Behaviour of Bond between Steel and Concrete), *Schriftenreihe des Deutschen Ausschusses fuer Stahlbeton,* Heft 138, Berlin.

Sato, R., Ujike, I., Minato, H. and Dilger, W. (1992), Basic Bond Equations in a Reinforced Concrete Flexural Element, *Proceedings of the International Conference in Concrete, CEB*, Riga, Latvia, p2.89-2.98.

Shima, H., Chou, L.-L. and Okamura, H. (1987), Bond Characteristics in Post-yield Range of Deformed Bars, *Translation from Proceedings of JSCE*, Vol.6, No.378, p113-124.

Sigrist, V. (1995), *Zum Verformungsvermögen von Stahlbetonträgem*, PhD Thesis, Institut für Baustatik und Konstruktion, ETH.

Sigrist, V., Alvarez, M. and Kaufmann, W. (1995), *Shear and Flexure in Structural Concrete Beams*, No.0009, IBK Sonderdruck, December.

Standards Australia (1994), *Concrete Structures*, AS 3600, North Sydney, Australia.

Standards Australia (2001), *Concrete Structures*, AS 3600, North Sydney, Australia.

Standards Australia (1991a), *Steel Reinforcing Bars for Concrete*, AS 1302, North Sydney, Australia.

Standards Australia (1991b), *Steel Reinforcing Wire for Concrete,* AS 1303, North Sydney, Australia.

Standards Australia (1991c), *Welded Wire Reinforcing Fabric for Concrete*, AS 1304, North Sydney, Australia.

Tassios, T. P. (1979), Properties of Bond between Concrete and Steel under Load Cycles Idealising Seismic Actions, *Proceedings AICAP-CEB Symposium*, Rome, p67-122.

Tassios, T. P. and Yannopoulos, P. J. (1981), Analytical Studies on Reinforced Concrete Members under Cyclic Loading Based on Bond Stress-slip Relationship, *ACI Journal*, Vol. 78, No.3, p206-216.

Tepfers, R. (1979), Cracking of Concrete Cover along Anchored Deformed Reinforcing Bars, *Magazine of Concrete Research*, Vol. 31, No.106, p3-12.

Vasiliev, P. I. and Belov, V. V. (1993), A Study of the Flexural Behaviour of R/C Cracked Beams, by Means of a 3D Block Model, *Studi e Ricerche*, Corso di Perfezionamento per le Costruzioni in Cemento Armato F.lli Pesenti. Politecnico di Milano, Italy, Vol. 14, p435-452.

Warner, R. F., Rangan, B. V. and Hall, A. S. (1998), *Reinforced Concrete*, Longman Australia, Melbourne, p974.

Westergaard, H. M. (1933), Stresses at a Crack, Size of Crack and the Bending of Reinforced Concrete, *ACI Proceedings*, Vol. 5, No.6, p93-102.

APPENDIX A

DERIVATION OF MOMENT REDUCTION FACTORS TO CONSIDER THE LOAD AND SUPPORT PAD EFFECT

A.1 FIXED END BEAM WITH SINGLE POINT LOAD

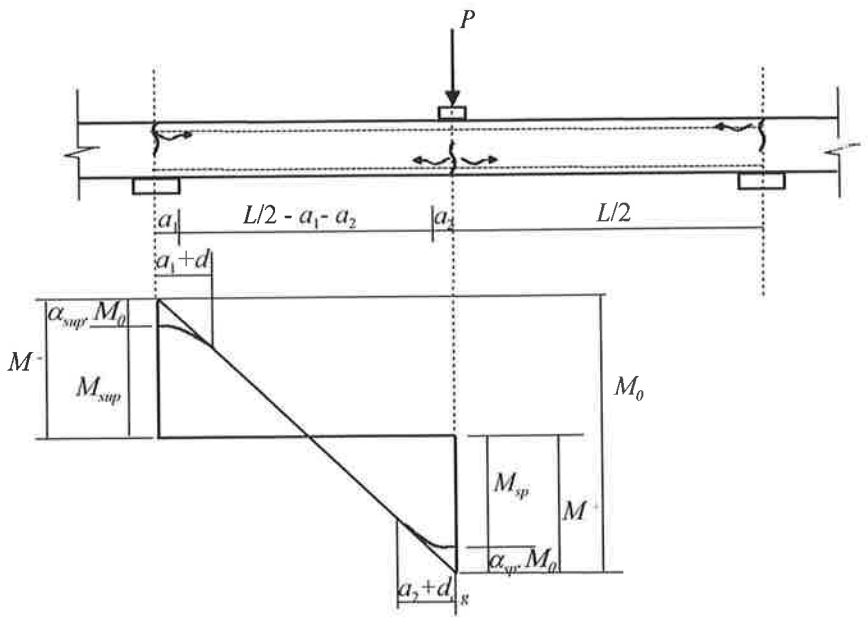

Figure A.1 Fixed end beam with point load

The static moment for this case is $M_0 = \frac{PL}{4} = M^- + M^+$. The maximum moment experienced at the support, M_{sup}, and mid-span section, M_{sp}, is less than the hypothetical maximum moments M^- and M^+ and is determined as follows.

Support Region

First consider the concentrated load at the support and determine M_e.

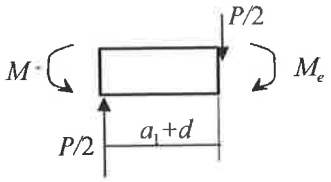

Figure A.2 Concentrated load at support

therefore:

$$M_e = M^- - \frac{2M_0}{L}(a_1 + d) \tag{A.1}$$

Now consider the distributed load due to support pad.

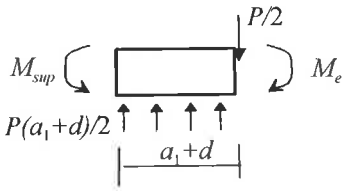

Figure A.3 Distributed load at support

where:

$$M_{sup} = M_e + \frac{M_0}{L}(a_1 + d) \tag{A.2}$$

Substituting Equation A.1 into Equation A.2 thus gives:

$$M_{sup} = M^- - M_0 \frac{(a_1 + d)}{L} \tag{A.3}$$

Therefore the moment reduction factor for the support region, α_{sup} is:

$$\alpha_{sup} = \left(\frac{a_1 + d}{L}\right) \tag{A.4}$$

Span Region

To determine the moment reduction factor in the span region, α_{sp}, consider the distributed load at the load pad.

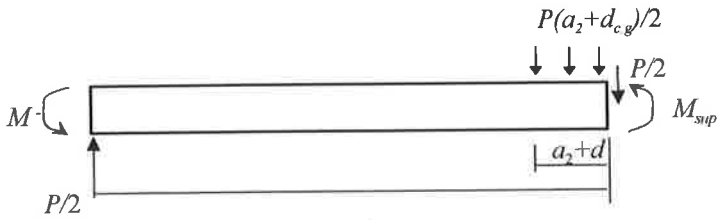

Figure A.4 Distributed load at span due to load pad

where:

$$M_{sp} = M_o - M^- - M_0\left(\frac{a_2 + d_{c.g}}{L}\right) \tag{A.5}$$

since $M^+ = M_0 - M^-$ then:

$$M_{sp} = M^+ - M_0\left(\frac{a_2 + d_{c.g}}{L}\right) \tag{A.6}$$

Therefore the moment reduction factor in the span region is determined from the following equation:

$$\alpha_{sp} = \left(\frac{a_2 + d_{c.g}}{L}\right) \tag{A.7}$$

A.2 FIXED END BEAM WITH UNIFORMLY DISTRIBUTED LOAD

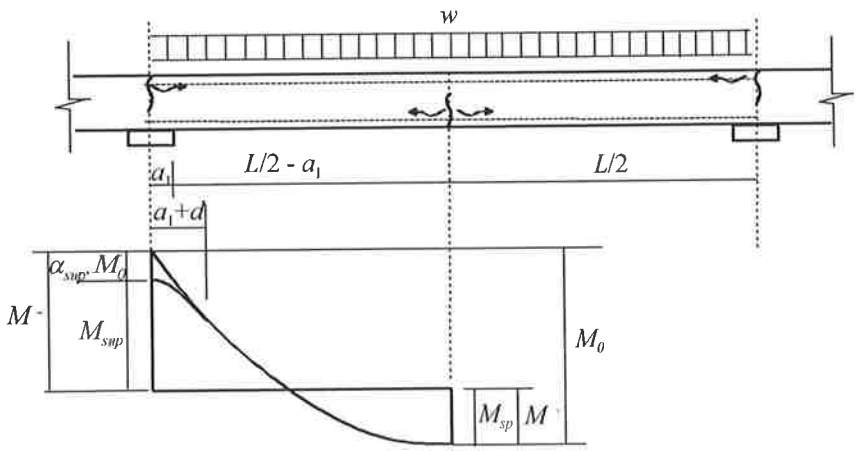

Figure A.5 Fixed end beam with uniformly distributed load

The static moment for this case is $M_0 = \frac{wL^2}{8} = M^- + M^+$.

Support Region

To determine α_{sup} first consider the concentrated load at the support pad.

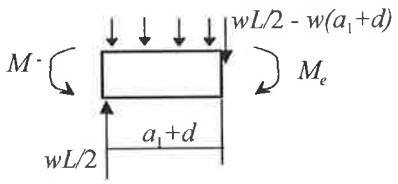

Figure A.6 Concentrated load at support

where:

$$M_e = M^- + M_0\left[4\frac{(a_1+d)}{L} - 4\frac{(a_1+d)^2}{L}\right] \qquad \text{(A.8)}$$

Now consider distributed load at support pad.

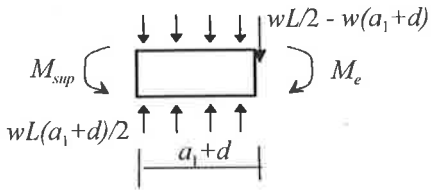

Figure A.7 Distributed load at support

$$M_{sup} = M_e + M_0\left[2(a_1+d)\text{-}4(a_1+d)^2\right] \quad \text{(A.9)}$$

Substituting Equation A.7 into Equation A.8 thus gives:

$$M_{sup} = M^- - M_0\frac{2(a_1+d)}{L} \quad \text{(A.10)}$$

Therefore the moment reduction factor for the support region, α_{sup} is:

$$\alpha_{sup} = \left(\frac{2(a_1+d)}{L}\right) \quad \text{(A.11)}$$

A.3 PROPPED CANTILEVER WITH TWO POINT LOADS

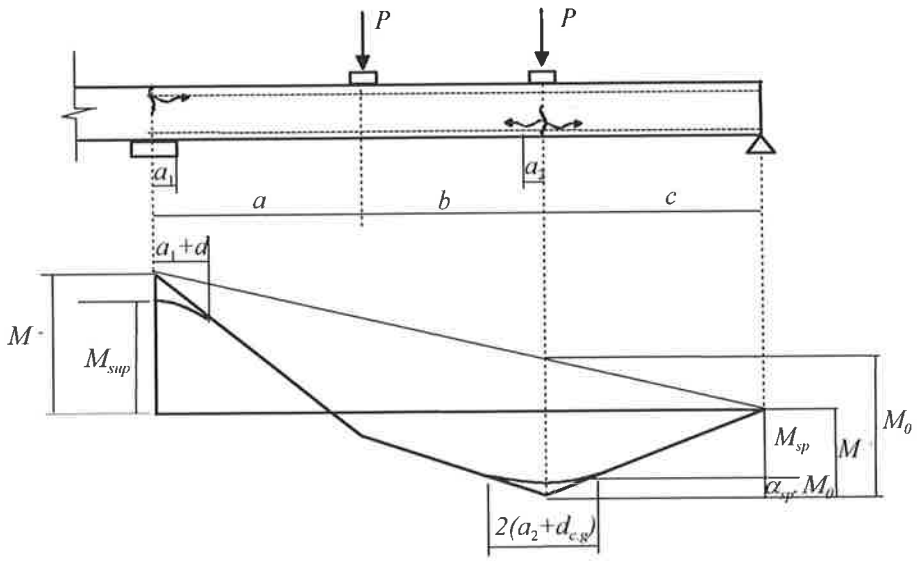

Figure A.8 Propped cantilever with two point loads

The static moment for this case is $M_0 = M^-\frac{c}{L} + M^+ = \frac{Pc(2a+b)}{L}$

Support Region

To determine α_{sup} first consider the concentrated load at the support pad.

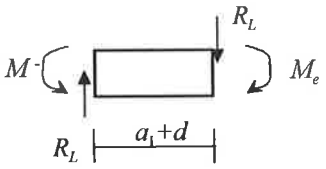

Figure A.9 Concentrated load at support

where:

$$M_e = M^- - R_L(a_1 + d) \tag{A.12}$$

and:

$$R_L = \frac{P(2c+b)}{L} + \frac{M^-}{L} \tag{A.13}$$

Now consider distributed load at support pad.

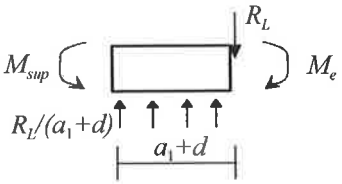

Figure A.10 Distributed load at support

$$M_{sup} = M_e + R_L \frac{(a_1 + d)}{2} \tag{A.14}$$

Substituting Equation A.11 and Equation A.12 into Equation A.13 thus gives:

$$M_{sup} = M^- - \left[\left(\frac{2b+d}{c(2a+b)}\right)\left(\frac{a_1+d}{2}\right).M_0 - \frac{a_1+d}{2L}.M^-\right] \tag{A.15}$$

Therefore the moment reduction factor for the support region, α_{sup} is:

$$\alpha_{sup} = \left(\frac{2c+b}{c(2a+b)}\right)\left(\frac{a_1+d}{2}\right) \tag{A.16}$$

Span Region

To determine the moment reduction factor in the span region, α_{sp}, consider the distributed load at the load pad.

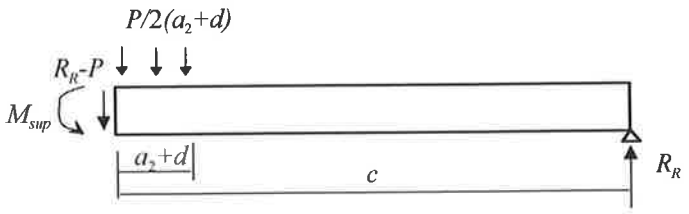

Figure A.11 Distributed load at span due to load pad

where:

$$M_{sup} = R_R - \frac{P(a_2 + d_{c.g})}{4} \tag{A.17}$$

and:

$$R_R = \frac{P(2a+b)}{L} - \frac{M^-}{L} \tag{A.18}$$

Substituting Equation A.17 into Equation A.16 thus gives:

$$M_{sp} = M^+ - M_0\left(\frac{L}{c(2a+b)}\right)\left(\frac{a_2 + d_{c.g}}{4}\right) \tag{A.19}$$

Therefore the moment reduction factor in the span region is determined from the following equation:

$$\alpha_{sp} = \left(\frac{L}{c(2a+b)}\right)\left(\frac{a_2 + d_{c.g}}{4}\right) \tag{A.20}$$

APPENDIX B

DERIVATION OF RATIO BETWEEN MOMENT RESISTANCE AT THE SUPPORT AND SPAN

B.1 FIXED END BEAM

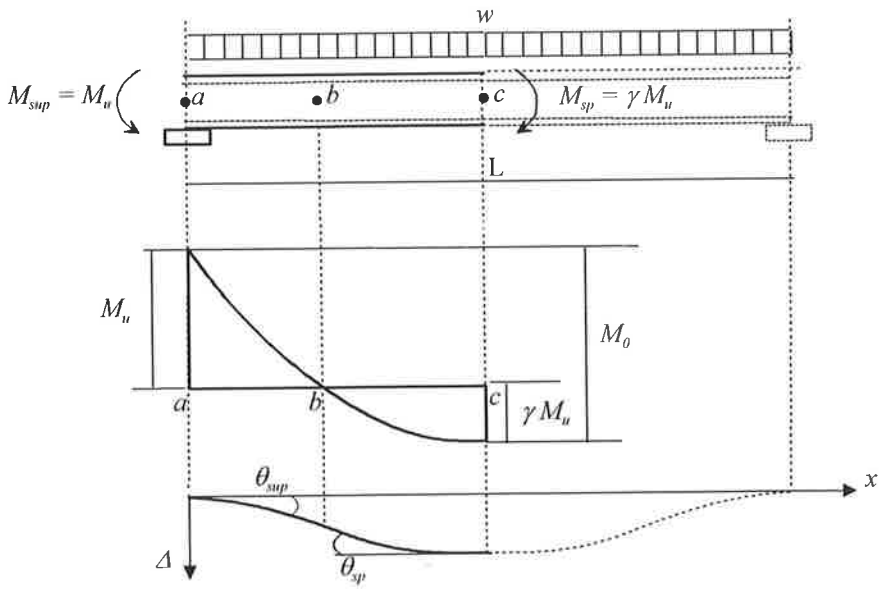

Figure B.1 Fixed end beam

For the fixed end beam case in Figure B.1 the ratio between the moment resistance at the support and at the span, γ, for the assumed degree of redistribution, β, is determined from the following equations.

The static moment for the beam case is given by:

$$\frac{wl^2}{8} = M_0 = M_{\sup} + M_{sp} \qquad \text{(B.1)}$$

and is also equal to:

$$\frac{wl^2}{8} = M_0 = \frac{2}{3} M_0 + \frac{1}{3} M_0 \tag{B.2}$$

The reduction of moment in the support is followed by the same increase of moment in the span by a factor, $\beta\frac{2}{3}$, to maintain equilibrium:

$$\frac{wl^2}{8} = M_0 = \left(\frac{2}{3} - \beta\frac{2}{3}\right) M_0 + \left(\frac{1}{3} + \beta\frac{2}{3}\right) M_0 \tag{B.3}$$

Now let $M_u = M_{sup}$:

$$M_u = \left(\frac{2}{3} - \beta\frac{2}{3}\right) M_0 \tag{B.4}$$

Therefore the static moment is related to the ultimate moment capacity, M_u, by the following equation:

$$M_0 = \frac{M_u}{\left(\frac{2}{3} - \beta\frac{2}{3}\right)} \tag{B.5}$$

By substituting Equation B.5 into Equation B.3 the following expression is found:

$$\frac{wl^2}{8} = M_u + \left(\frac{\frac{1}{3} + \beta\frac{2}{3}}{\frac{2}{3} - \beta\frac{2}{3}}\right) M_u \tag{B.6}$$

Thus the ratio between the moment in the support and in the span, γ, can be found using Equation B.7 based on the assumed degree of moment redistribution, β.

$$\gamma = \left(\frac{\frac{1}{3} + \beta\frac{2}{3}}{\frac{2}{3} - \beta\frac{2}{3}}\right) \tag{B.7}$$

B.2 PROPPED CANTILEVER

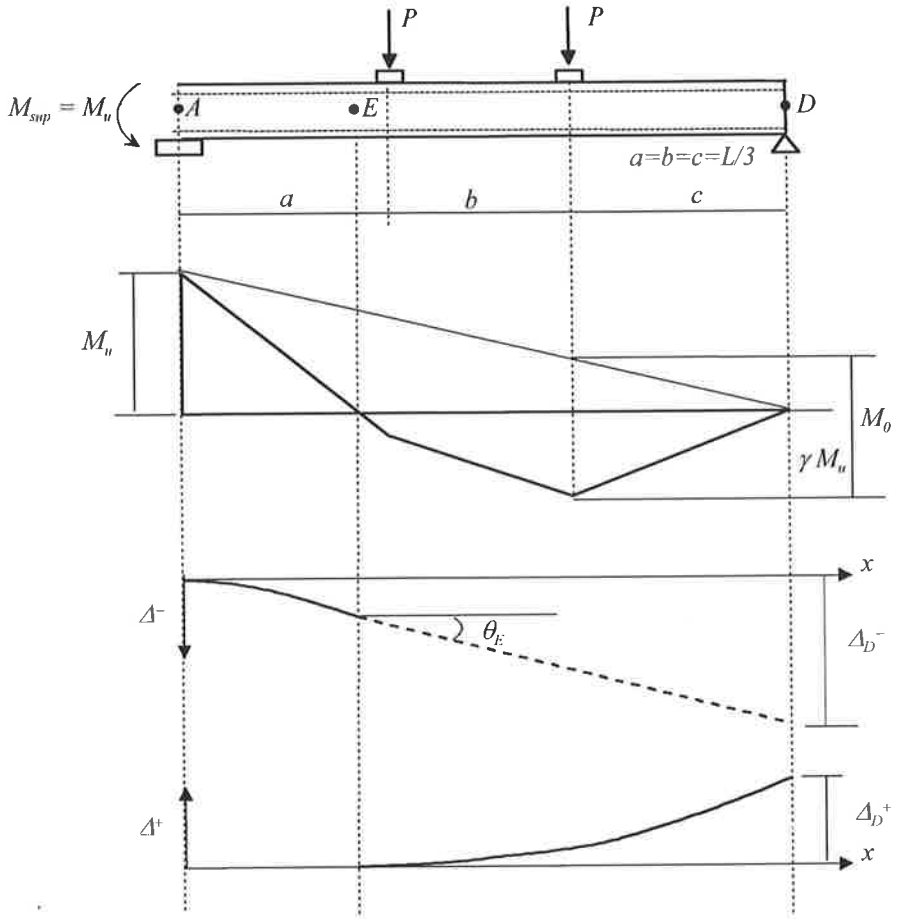

Figure B.2 Propped cantilever

For the propped cantilever case in Figure B.2, the ratio between the moment at the support and at the span, γ, for the assumed degree of redistribution, β, is determined from the following equations.

The static moment for the beam case is given by:

$$\frac{PL}{3} = M_0 = \frac{1}{3} M_{sup} + M_{sp} \tag{B.8}$$

and is also equal to:

$$\frac{PL}{3} = M_0 = \frac{1}{3} M_0 + \frac{2}{3} M_0 \tag{B.9}$$

The reduction of moment in the support results in the same increase of moment in the span by a factor $\beta\frac{1}{3}$.

$$\frac{PL}{3} = M_0 = \left(\frac{1}{3} - \beta\frac{1}{3}\right)M_0 + \left(\frac{2}{3} - \beta\frac{1}{3}\right)M_0 \tag{B.10}$$

Now let $M_u = M_{sup}$:

$$\frac{1}{3}M_u = \left(\frac{1}{3} - \beta\frac{1}{3}\right)M_0 \tag{B.11}$$

Therefore the static moment is related to the ultimate moment capacity, M_u, by the following equation:

$$M_0 = \frac{1}{3}\cdot\frac{M_u}{\left(\frac{1}{3} - \beta\frac{1}{3}\right)} \tag{B.12}$$

By substituting Equation B.12 into Equation B.10 the following expression is found:

$$\frac{PL}{3} = \frac{1}{3}M_u + \frac{1}{3}\cdot\left(\frac{\frac{2}{3} + \beta\frac{1}{3}}{\frac{1}{3} - \beta\frac{1}{3}}\right)M_u \tag{B.13}$$

Thus the ratio between the moment in the support and in the span, γ, can be found using Equation B.14 based on the assumed degree of moment redistribution, β.

$$\gamma = \frac{1}{3}\cdot\left(\frac{\frac{2}{3} + \beta\frac{1}{3}}{\frac{1}{3} - \beta\frac{1}{3}}\right) \tag{B.14}$$

APPENDIX C

NUMERICAL RESULTS FOR AVAILABLE DEGREE OF MOMENT REDISTRIBUTION

C.1 INFLUENCE OF STEEL PROPERTIES

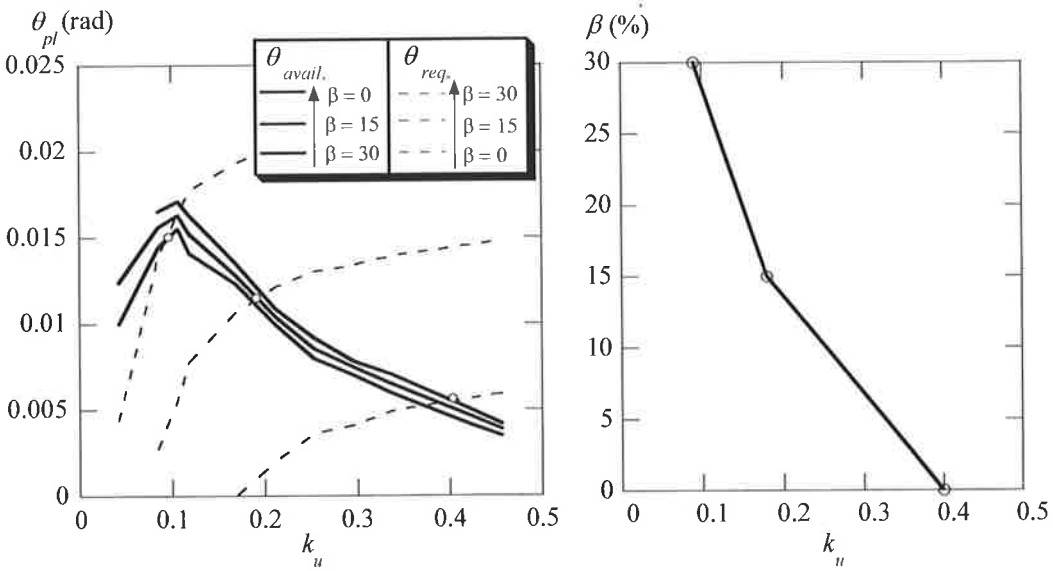

Figure C.1 **Available degree of redistribution for Steel N2, ε_{su} = 5.0%, f_{su}/f_{sy} = 1.05**

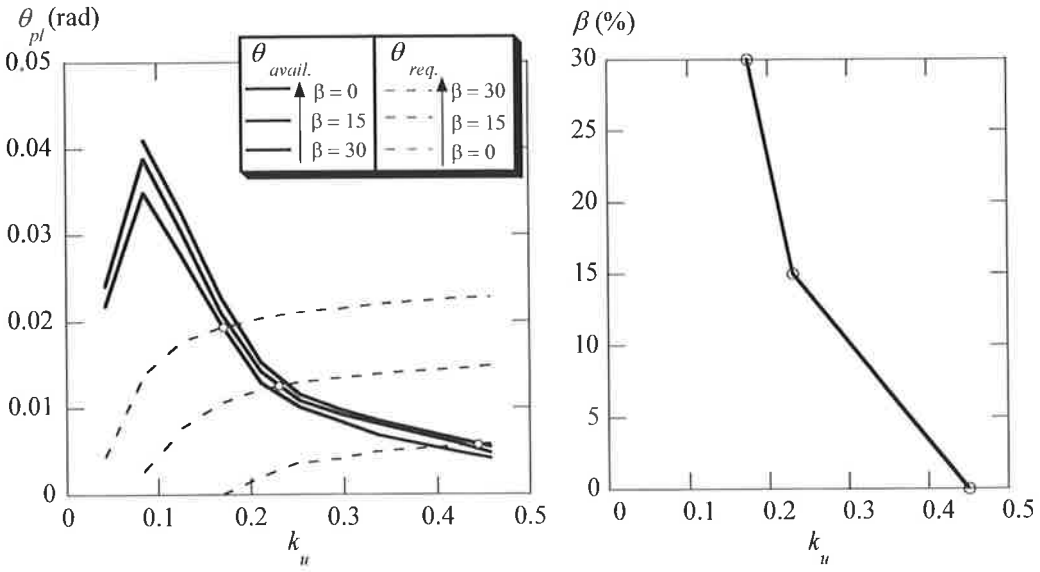

Figure C.2 Available degree of redistribution for Steel N3, ε_{su} = 5.0%, f_{su}/f_{sy} = 1.2

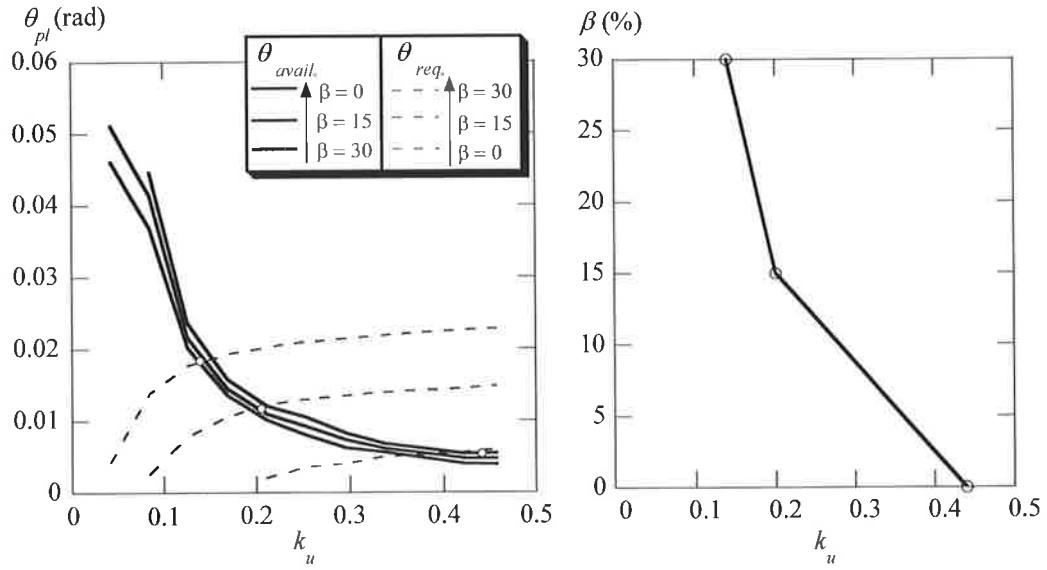

Figure C.3 Available degree of redistribution for Steel N4, ε_{su} = 10.0%, f_{su}/f_{sy} = 1.2

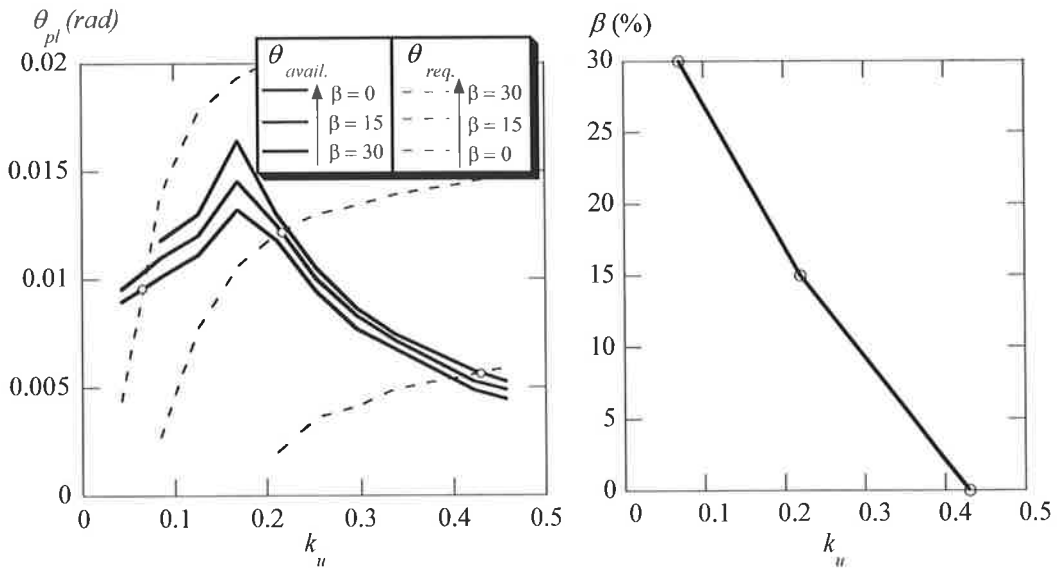

Figure C.4 Available degree of redistribution for Steel N5, ε_{su} = 3.0%, f_{su}/f_{sy} = 1.08

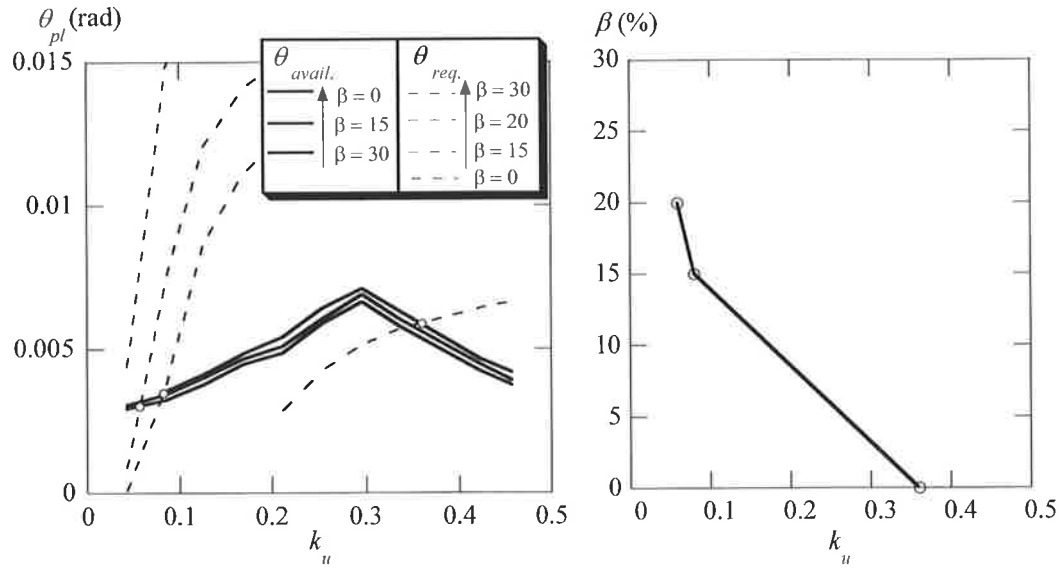

Figure C.5 Available degree of redistribution for Steel L2, ε_{su} = 1.5%, f_{su}/f_{sy} = 1.04

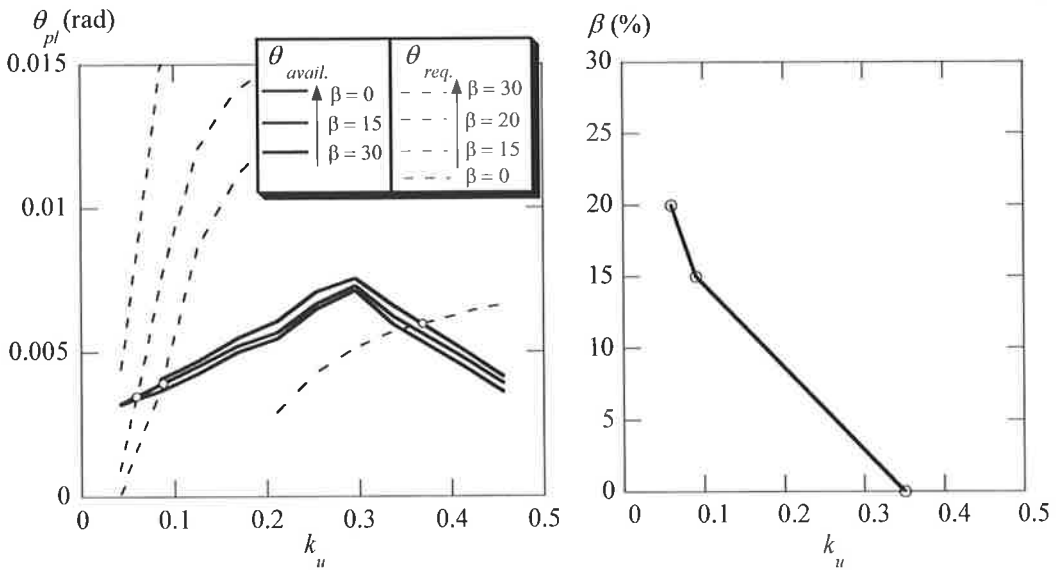

Figure C.6 Available degree of redistribution for Steel L3, ε_{su} = 1.5%, f_{su}/f_{sy} = 1.05

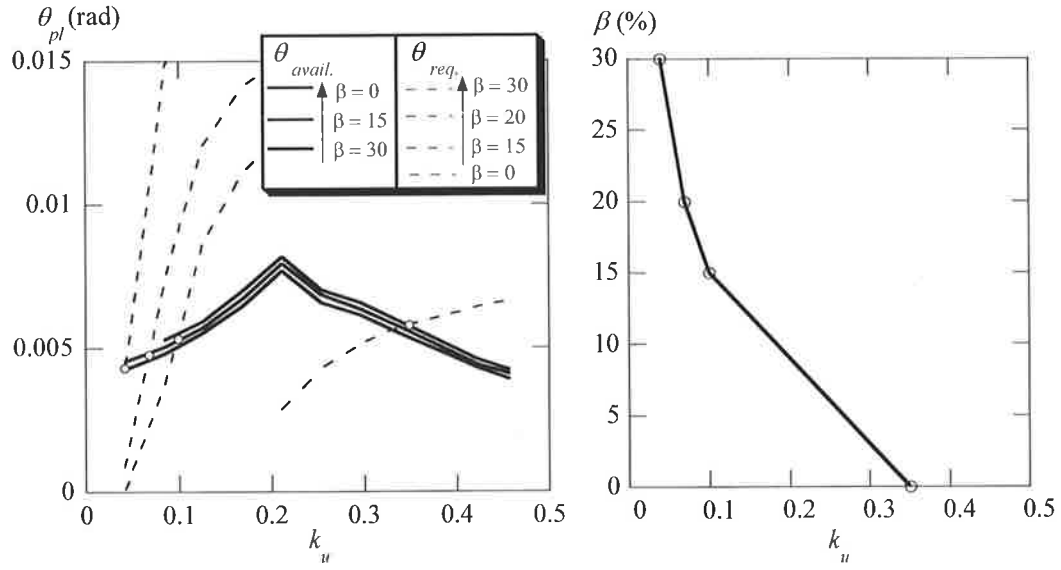

Figure C.7 Available degree of redistribution for Steel L4, ε_{su} = 2.5%, f_{su}/f_{sy} = 1.03

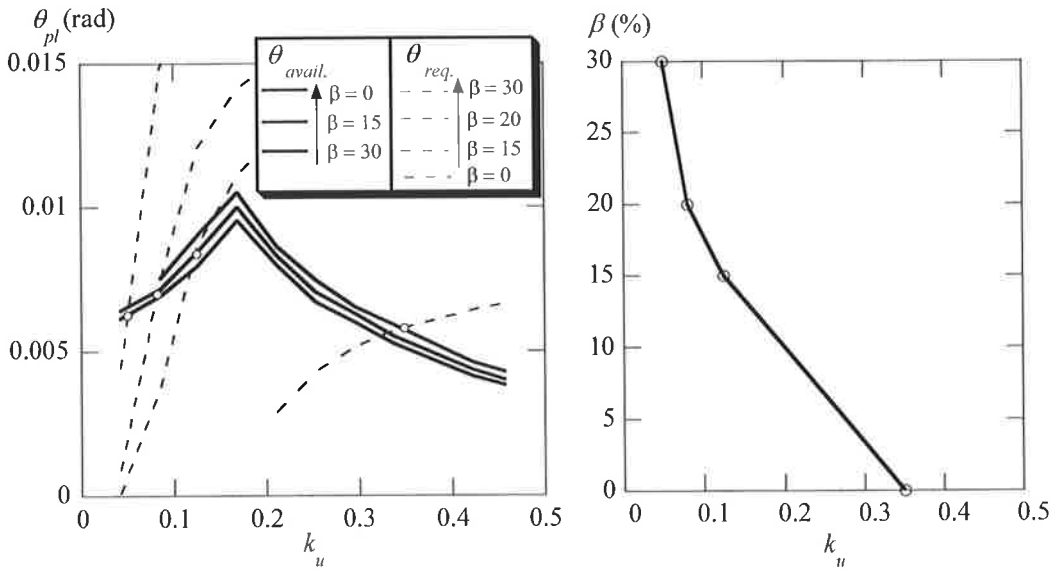

Figure C.8 Available degree of redistribution for Steel L5, ε_{su} = 3.5%, f_{su}/f_{sy} = 1.03

C.2 INFLUENCE OF SLENDERNESS RATIO

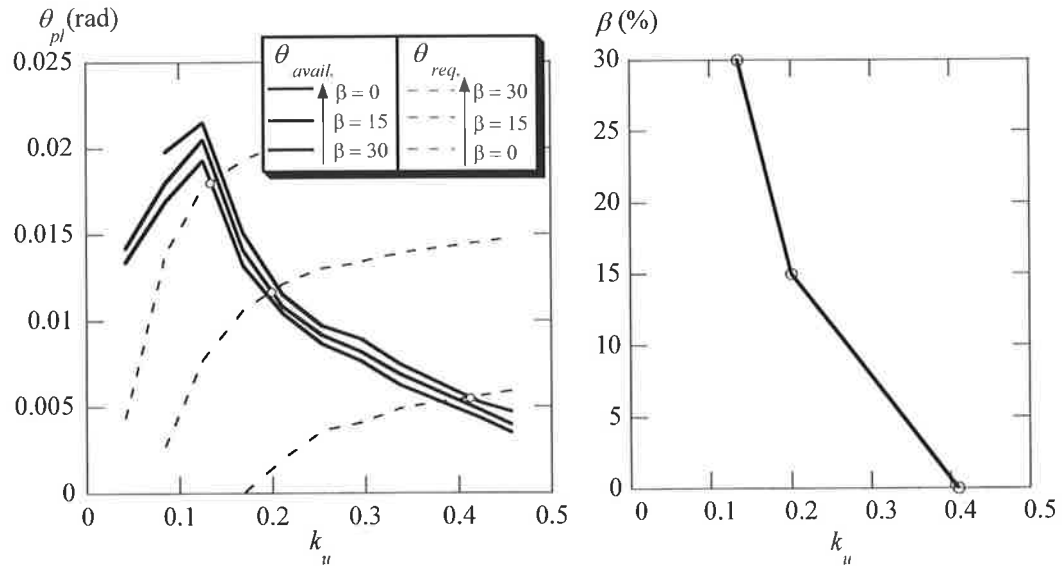

Figure C.9 Available degree of redistribution for Steel N1, one-way slab design, d = 200mm, f_{cm} = 50MPa, L/d = 35

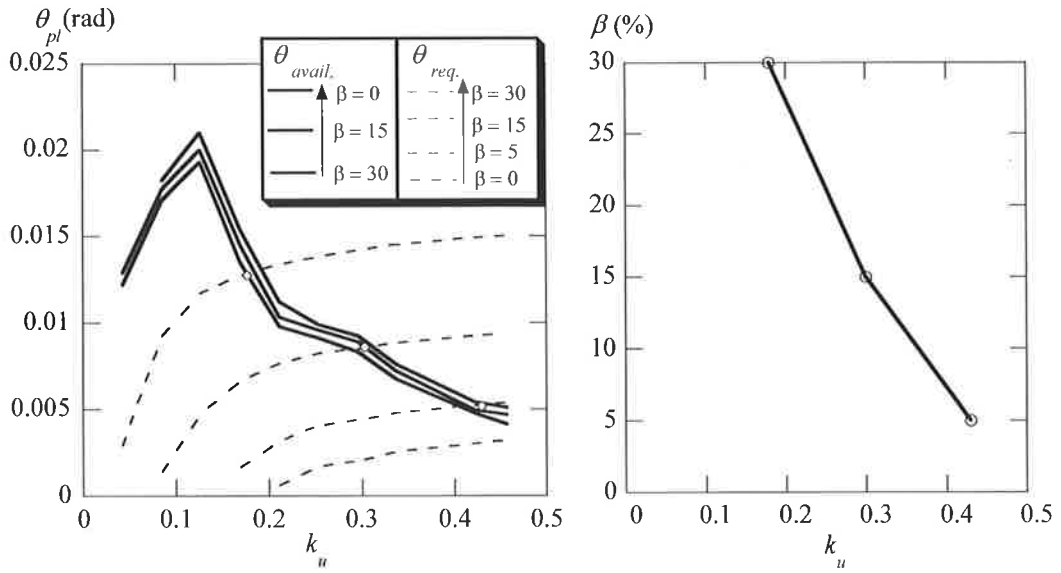

Figure C.10 Available degree of redistribution for Steel N1, one-way slab design, d = 200mm, f_{cm} = 50MPa, L/d = 25

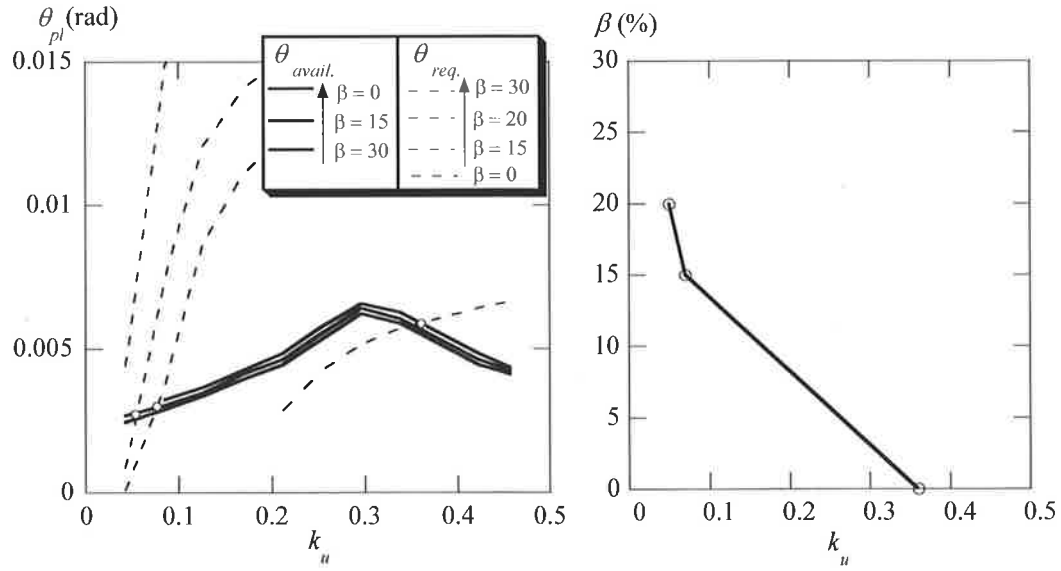

Figure C.11 Available degree of redistribution for Steel L1, one-way slab design, d = 200mm, f_{cm} = 50MPa, L/d = 35

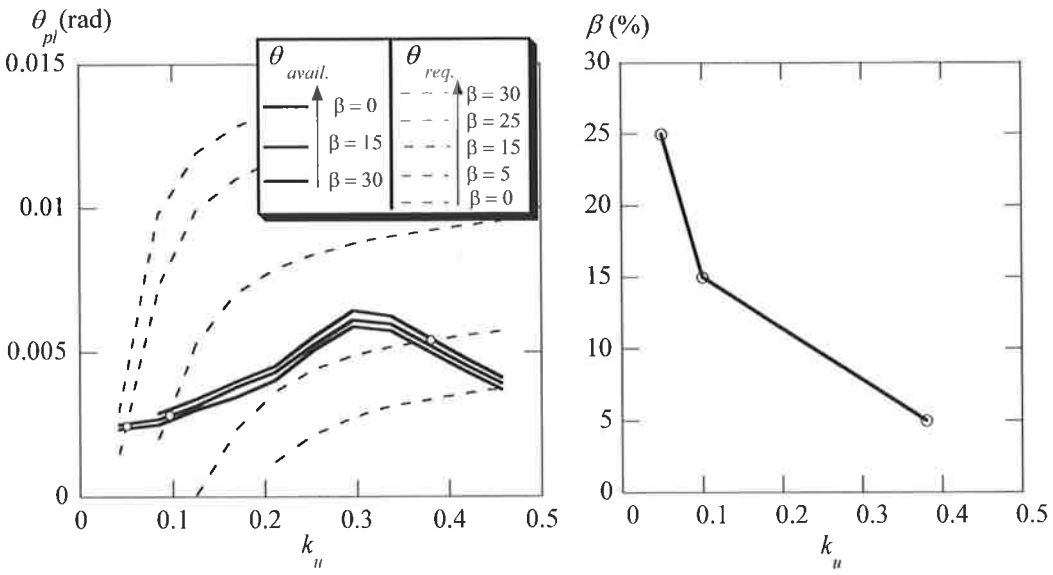

Figure C.12 Available degree of redistribution for Steel L1, one-way slab design, d = 200mm, f_{cm} = 50MPa, L/d = 25

C.3 INFLUENCE OF CONCRETE STRENGTH

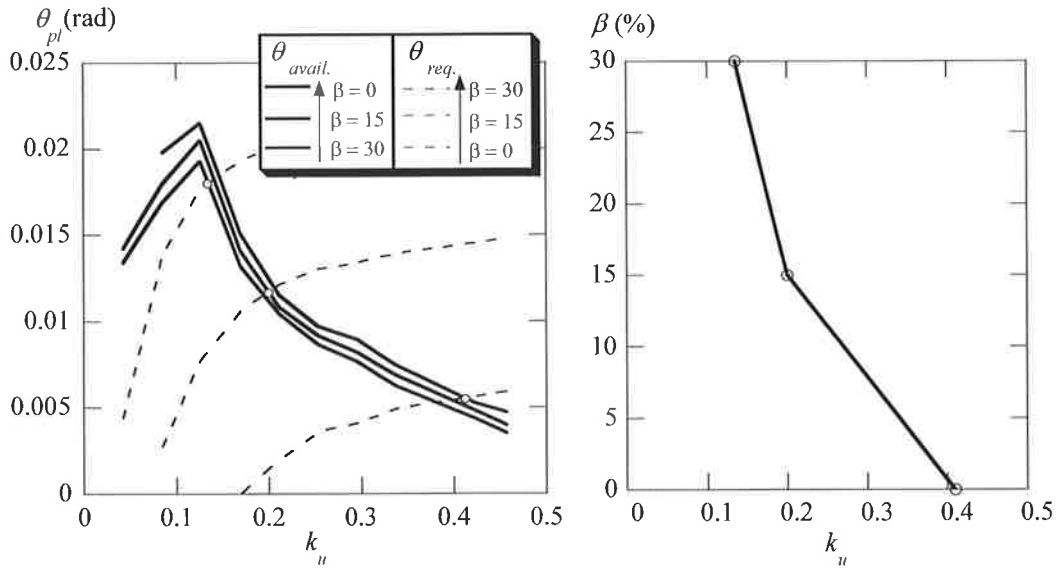

Figure C.13 Available degree of redistribution for Steel N1, one-way slab design, d = 200mm, L/d = 35, f_{cm} = 50MPa

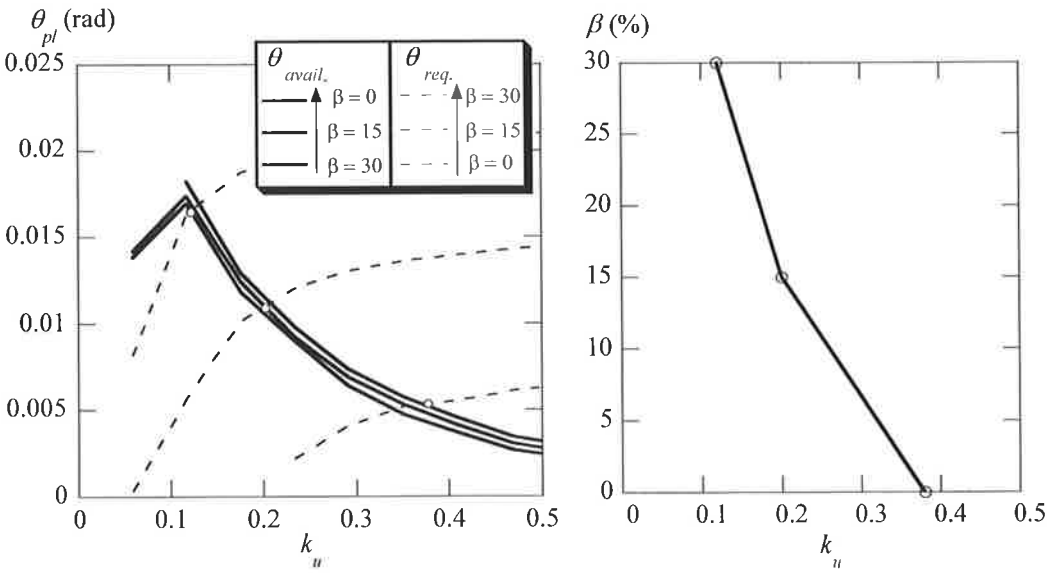

Figure C.14 Available degree of redistribution for Steel N1, one-way slab design, d = 200mm, L/d = 35, f_{cm} = 30MPa

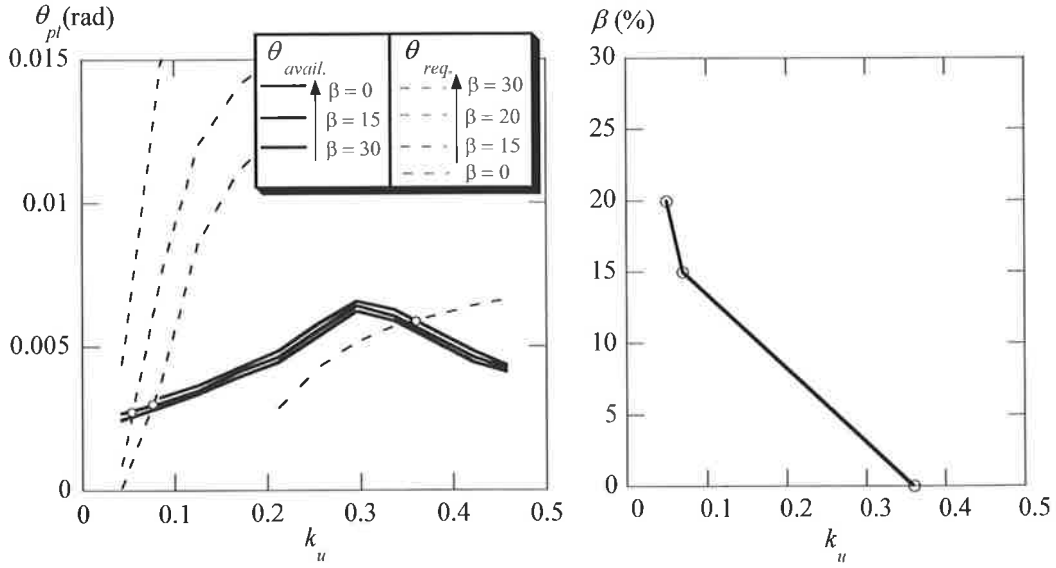

Figure C.15 Available degree of redistribution for Steel L1, one-way slab design, d = 200mm, L/d = 35, f_{cm} = 50MPa

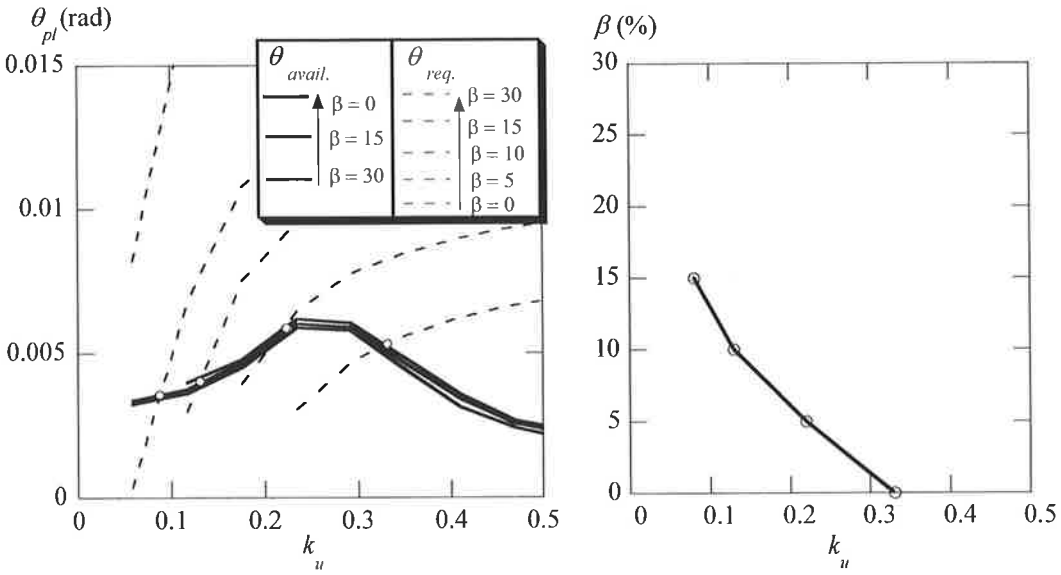

Figure C.16 Available degree of redistribution for Steel L1, one-way slab design, d = 200mm, L/d = 35, f_{cm} = 30MPa

APPENDIX D

CALCULATION OF REQUIRED ROTATION CAPACITY IN THE SUPPORT REGION OF A PROPPED CANTILEVER

For a simplified calculation of the required plastic rotation in the negative moment region of the propped cantilever in Figure D.1, we can assume that the total rotation in the negative moment region, θ_E, is made up of an elastic component and a plastic component:

$$\theta_E = \theta_{E,el} + \theta_{E,pl} \tag{D.1}$$

and the deformations in the negative moment region AE due to the negative curvature, Δ_D^-, are also made up of an elastic and plastic component:

$$\Delta_D^- = \Delta_{D,el}^- + \Delta_{D,pl}^- \tag{D.2}$$

also just prior to collapse it is assumed that the deformations due to the positive curvature, Δ_D^+, are purely elastic:

$$\Delta_D^+ = \Delta_{D,el}^+ \tag{D.3}$$

To satisfy the boundary condition of the system, the deformations due to the negative curvature and positive curvature need to be equal:

$$\Delta_D^- = \Delta_D^+ \tag{D.4}$$

Substituting Equation D.2 and Equation D.3 into Equation D.4 gives the plastic component of the negative curvature equal to:

$$\Delta_{D,pl}^{-} = \Delta_{D,el}^{+} - \Delta_{D,el}^{-} \tag{D.5}$$

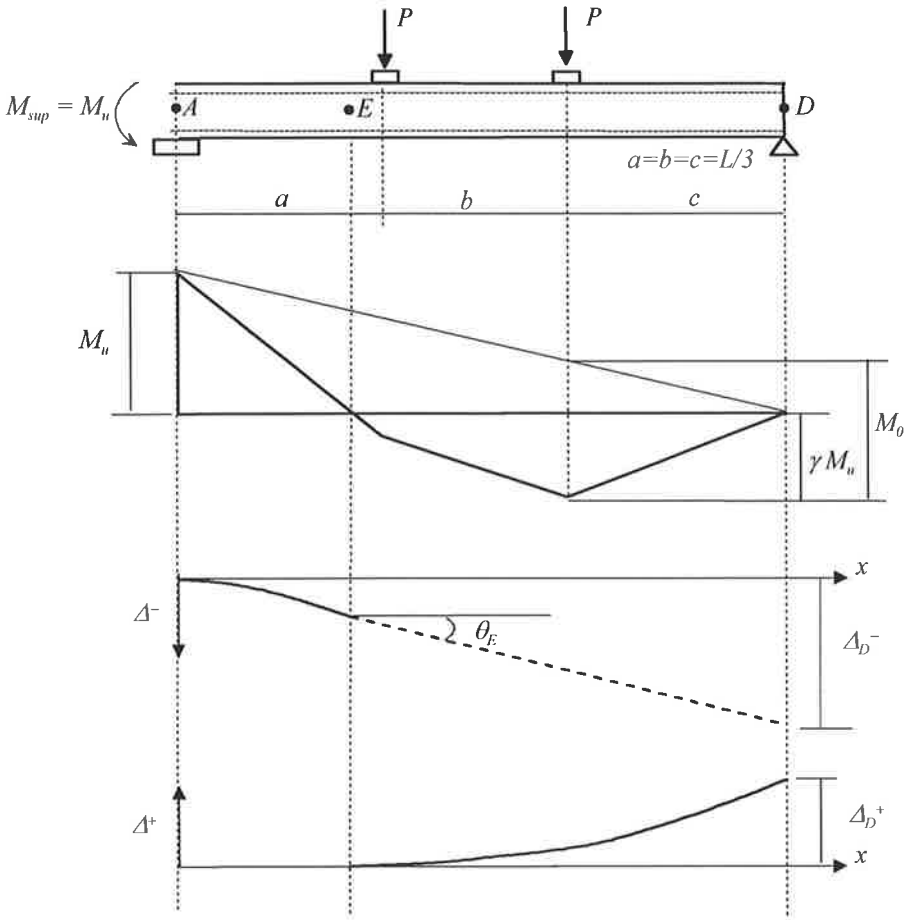

Figure D.1 Schematic of propped cantilever for calculation of required rotation capacity

The deformation due to the positive curvature, $\Delta_{D,el}^{+}$, is calculated by applying the Second Area of Moment Theorem between points *E* and *D*.

$$\Delta_{D,el}^{+} = \int_{D}^{E} \frac{M}{EI_{eff}} . \bar{x}_{ED} \tag{D.6}$$

Where $\bar{x}_{ED}$ = distance to centroid of the area of $\frac{M}{EI_{eff}}$ between points *E* and *D*, measured from point *D*, and EI_{eff} is the effective cracked stiffness calculated according to Equation 8.7 in Chapter 8.

The deformation due to negative curvature, $\Delta_{D,el}^{-}$, is also calculated by applying the Second Area of Moment Theorem but between points A and E.

$$\Delta_{D,el}^{-} = \int_{E}^{A} \frac{M}{EI_{eff}} . \bar{x}_{AE} \tag{D.7}$$

Where $\bar{x}_{AE}$ = distance to centroid of the area of $\frac{M}{EI_{eff}}$ between points A and E, measured from point E.

Having calculated $\Delta_{D,el}^{+}$ and $\Delta_{D,el}^{-}$ the plastic deformation due to the negative curvature $\Delta_{D,pl}^{-}$ can be determined from Equation D.5. However $\Delta_{D,pl}^{-}$ is made of two parts (Figure D.2).

$$\Delta_{D,pl}^{-} = \Delta_{D,pl}^{1-} + \Delta_{D,pl}^{2-} \tag{D.8}$$

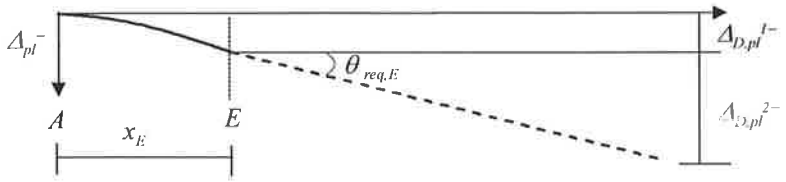

Figure D.2 Schematic of plastic deformations in negative moment region

The plastic deformation $\Delta_{D,pl}^{2-}$ can be determined from the following equation:

$$\Delta_{D,pl}^{2-} = \theta_{req,E} . (L - x_e) \tag{D.9}$$

where $\theta_{req,E}$ = total required plastic rotation between A and E.

To calculate $\Delta_{D,pl}^{1-}$ knowledge of the distribution of the plastic curvature in the region AE is required. A simplified approach is adopted that assumes that $\theta_{req,E}$ is concentrated over a distance d equal to the effective depth of the section.

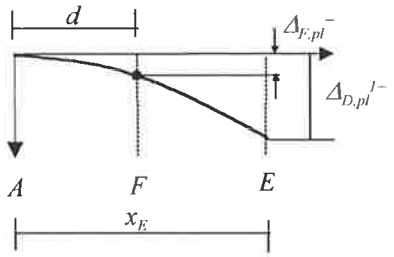

Figure D.3 Schematic of plastic deformations in negative moment region due to negative plastic curvature distribution

Using this approach part one of the plastic deformation, $\Delta_{D,pl}^{1-}$ is calculated as follows:

$$\Delta_{D,pl}^{1-} = \theta_{req,E}.(x_e - d) + \Delta_{F,pl}^{-} \tag{D.10}$$

where:

$$\Delta_{D,pl}^{1-} = \frac{d}{2}\theta_{req,E} \tag{D.11}$$

Substituting Equation D.11 into Equation D.10:

$$\Delta_{D,pl}^{1-} = \theta_{req,E}.\left(\frac{d}{2} + x_e - d\right) \tag{D.12}$$

and substituting Equation D.9 and Equation D.12 into Equation D.8 results in the following equation to calculate the plastic deformation due to the negative curvature $\Delta_{D,pl}^{-}$:

$$\Delta_{D,pl}^{-} = \theta_{req,E}.\left(L - \frac{d}{2}\right) \tag{D.13}$$

Thus the required plastic rotation in the support region of the propped cantilever can be determined from the following equation:

$$\theta_{req,E} = \frac{\Delta_{D,el}^{+} + \Delta_{D,el}^{-}}{\left(L - \frac{d}{2}\right)} \tag{D.14}$$